

博士論文

Evaluation of the clothing heat transfer coefficients

based on experiment and CFD analysis

(実験と数値解析による着衣熱伝達率に関する研究)

高 姍

Abstract

This thesis focuses on evaluating convective and radiative heat transfer coefficients and clothing insulation for a clothed human body. At the same time, it provides a database of heat transfer coefficients and clothing insulation for various types of clothing. Furthermore, how the directly measured clothing heat transfer coefficients and clothing insulation affect the prediction of thermal comfort was confirmed.

To study human thermal comfort, it is crucial to understand the heat exchange between the human body and the surrounding environment. The heat exchange characteristics of each segment of the human body can be evaluated using convective and radiative heat transfer coefficients. In recent years, experimental and numerical methods for calculating the convective and radiative heat transfer coefficients using thermal manikin or computational thermal manikin have been proposed. However, although there are numerous studies on heat transfer coefficients for naked manikins, only a few have focused on heat transfer coefficients for clothed manikins. In previous studies, clothing heat transfer coefficients have been approximated by multiplying the heat transfer coefficients of a naked human body by the clothing area factor. Thus, to accurately assess human thermal comfort, it is necessary to determine the heat transfer coefficients for a clothed human body directly. Furthermore, although substantial literature provides information on convective and radiative heat transfer coefficients for a naked human body, a considerable amount of uncertainty still exists regarding naked convective heat transfer coefficients caused by vertical airflow (Figure 1) and naked radiative heat transfer coefficients.

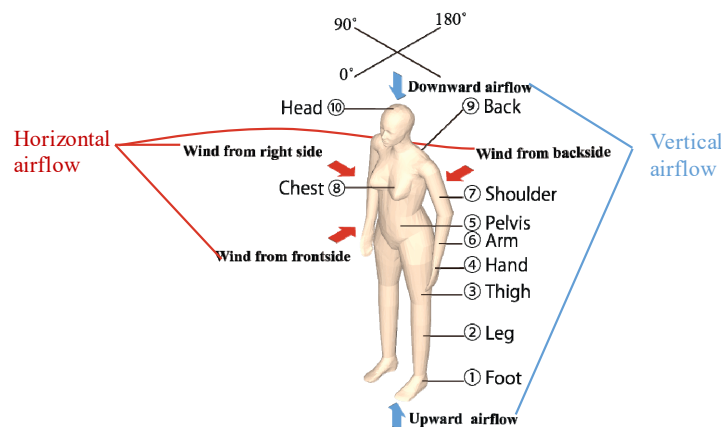


Figure 1. Thermal manikin and wind directions.

Moreover, clothing insulation is also an important parameter for evaluating human thermal comfort. Prior to the year 2000, research on clothing insulation was widely performed; however, recently, only a few studies on this subject have been carried out. In addition, owing to the advances in material engineering, clothing materials have become very diversified. For example, windbreakers and fleece coats are now made of breathable-waterproof material and raised fabric, respectively. Therefore, it is important to elucidate the thermal resistance characteristics of clothes made of such

Abstract

new materials. In addition, with the development of multi-segment thermoregulation models, there is a great demand for information on clothing insulation of different body segments.

Considering the above-mentioned context, the four themes (Chapter 4–7) shown in Figure 2 are addressed in this thesis.

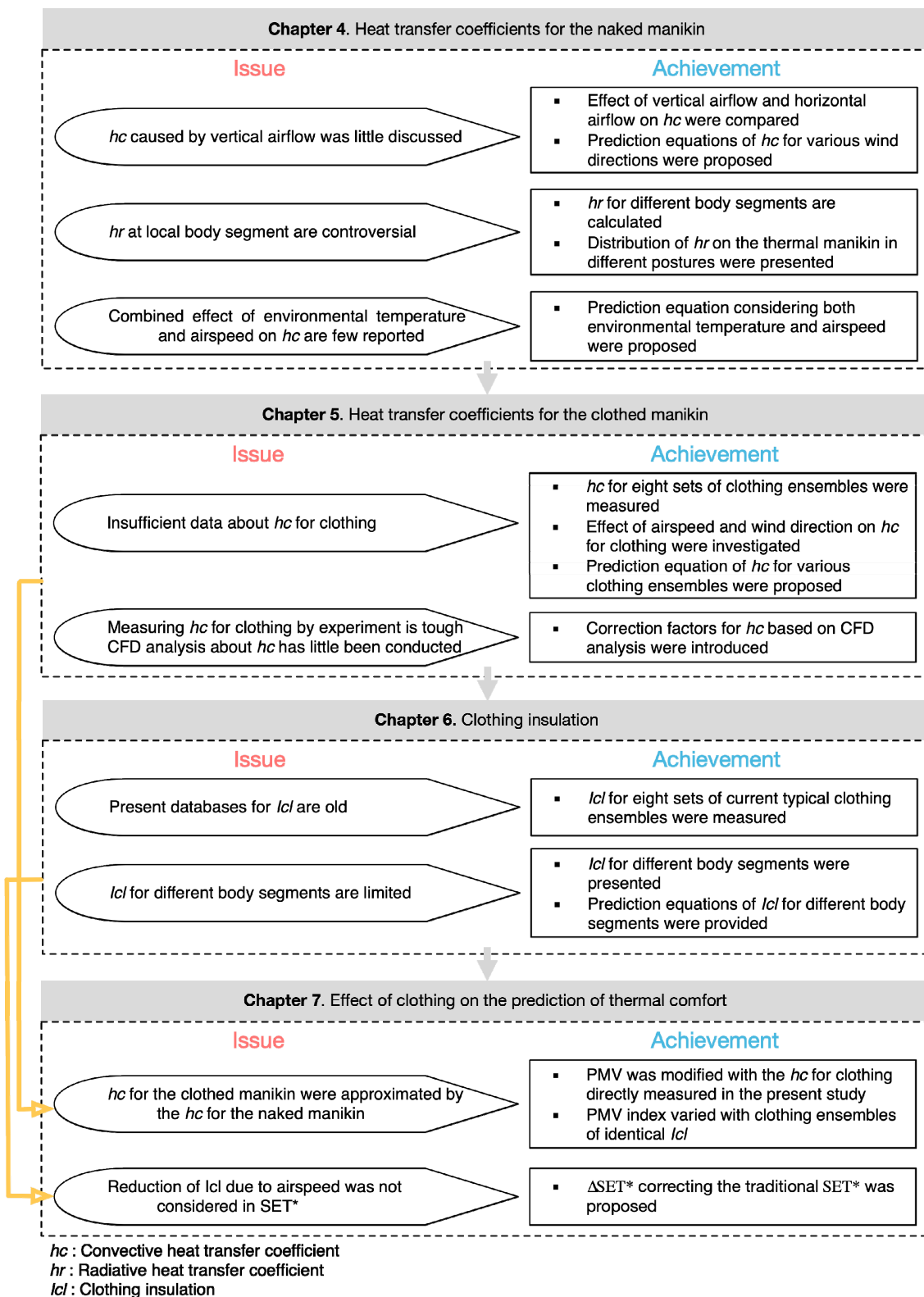


Figure 2. Main topics and results of the present thesis.

For the heat transfer coefficients for the naked manikin, the effects of vertical and horizontal airflows on convective heat transfer coefficient were compared. As there were insufficient data on

Abstract

radiative heat transfer coefficients for the different body segments, a numerical calculation was conducted to present detailed distribution of radiative heat transfer coefficients on the surface of the thermal manikin under various postures. Furthermore, prediction models for convective heat transfer coefficients based on both environmental temperature and airspeed were proposed, thus making it possible to evaluate convective heat transfer coefficients under various environmental conditions.

Concerning the heat transfer coefficients for the clothed manikin, the convective and radiative heat transfer coefficients for eight sets of clothing ensembles were measured using a thermal manikin. Experimental results indicated that convective heat transfer coefficients varied with clothing ensembles. However, the difference between the radiative heat transfer coefficients for the various clothing ensembles was negligible. Additionally, the effects of wind direction and airspeed on clothing convective heat transfer coefficients were confirmed. However, measurement of convective heat transfer coefficient is an arduous task and thermal manikin is not easily available. Thus, correction factors for clothing convective heat transfer coefficient based on (computational fluid dynamics) CFD analysis were presented.

For the clothing insulation, whole-body clothing insulation and local clothing insulation for eight sets of current typical clothing ensembles were reported. In addition, calculation for clothing insulation based on posture, wind direction, and airspeed was suggested.

Furthermore, it was necessary to examine how the different calculated clothing heat transfer coefficients and clothing insulation affect the prediction of thermal comfort. Hence, the convective heat transfer coefficient and clothing insulation directly measured in the present study were introduced to the PMV, SET*, and PET calculation program. The results indicated that the PMV and PET indices varied with clothing ensembles when clothing insulations were almost identical. Moreover, a correction factor ΔSET^* was proposed to consider the reduction of clothing insulation due to airspeed.

Clothing significantly affects human thermal comfort as it determines the heat loss from the human body to the environment. Detailed investigation on clothing convective and radiative heat transfer coefficients will lead to a better understanding of the heat transfer through clothing.

The comprehensive database for convective and radiative heat transfer coefficients and clothing insulation provides a basis for research on thermal comfort, such as personal air conditioning system, low-energy personal wearable device, and energy optimization associated with thermal comfort.

Moreover, the parameters obtained in the study can be used as input data for several thermal comfort evaluation models and indices such as the PMV index, standard effective temperature, and two-node model. These parameters will play an important role in accurately simulating the human thermal comfort.

Contents

Abstract.....	i
Contents	v
List of figures.....	ix
List of tables.....	xvii
Nomenclature.....	1
Chapter 1. Introduction.....	9
1.1 Fundamental of heat transfer from the clothed human body.....	10
1.2 Literature review	11
1.2.1 Radiative heat transfer coefficient.....	11
1.2.2 Convective heat transfer coefficient.....	12
1.2.3 Clothing insulation.....	13
1.3 Current issues.....	14
1.4 Research objective	15
1.5 Structure of this thesis.....	15
Reference.....	17
Chapter 2. Basic theory	21
2.1 Heat transfer coefficients	22
2.1.1 Heat transfer coefficients for the naked manikin	22
2.1.2 Heat transfer coefficients for the clothed manikin	22
2.2 Clothing insulation.....	23
2.2.1 Method A.....	24
2.2.2 Method B.....	24
2.2.3 Method C.....	25
2.2.4 Method D	25
2.3 Prediction of thermal comfort	26
2.3.1 PMV	26
2.3.2 SET*	28
2.3.3 PET	29
Reference.....	30
Chapter 3. Method of experiment and CFD analysis.....	33
3.1 Experimental facility.....	34
3.1.1 Thermal manikin	34
3.1.2 Climate chamber	36
3.1.3 Wind tunnel.....	37
3.2 Clothing ensembles	39
3.3 Measurement.....	40

Contents

3.3.1	Temperature.....	40
3.3.2	Airspeed	41
3.3.3	Emissivity for the clothing	42
3.3.4	Air permeability for the clothing.....	43
3.3.5	Surface friction (MIU) and surface roughness (SMD).....	45
3.4	Governing equations of fluid dynamics	49
3.4.1	Basic theory.....	49
3.4.2	Mass conservation.....	50
3.4.3	Momentum conservation.....	51
3.4.4	Energy conservation.....	54
3.5	Non-dimensionalization of the Navier–Stokes equations	57
3.6	Turbulence model.....	59
3.7	Computational thermal manikin.....	63
	Reference.....	65
	Chapter 4. Heat transfer coefficients for the naked manikin.....	67
4.1	Introduction.....	68
4.2	The effect of airspeed and wind direction	69
4.2.1	Experimental setup.....	70
4.2.2	Numerical method.....	72
4.2.3	Results.....	75
4.3	The effect of temperature	88
4.3.1	Experimental setup.....	89
4.3.2	Numerical method.....	90
4.3.3	Results.....	90
4.4	The combined effect of temperature and airspeed	95
4.4.1	Experimental setup.....	95
4.4.2	Numerical method.....	96
4.4.3	Results.....	96
4.5	Conclusions.....	100
	Reference.....	101
	Chapter 5. Heat transfer coefficients for the clothed manikin.....	105
5.1	Introduction	106
5.2	Experimental setup.....	107
5.2.1	Clothing ensembles	107
5.2.2	Environmental condition	108
5.3	Results.....	109
5.3.1	Whole-body convective heat transfer coefficient.....	109
5.3.2	Convective heat transfer coefficient for different body segments.....	114

5.3.3	Comparison of different methods for calculating convective heat transfer coefficient for the clothing	119
5.3.4	Whole-body radiative heat transfer coefficient	126
5.3.5	Radiative heat transfer coefficient for different body segments	127
5.4	Calculation of clothing heat transfer coefficients based on CFD analysis.	128
5.4.1	Method.	128
5.4.2	Results.....	130
5.5	Conclusions.....	133
	Reference.....	134
Chapter 6. Clothing insulation.....		137
6.1	Introduction.....	138
6.2	The effect of airspeed and wind direction	139
6.2.1	Experimental setup.....	139
6.2.2	Results.....	139
6.3	Conclusions.....	152
	Reference.....	153
Chapter 7. The effect of clothing on the prediction of thermal comfort		155
7.1	Introduction.....	156
7.2	The effect of clothing on PMV	156
7.2.1	The effect of convective heat transfer coefficient and clothing insulation on PMV	157
7.2.2	Comparison of PMV values for different clothing ensembles	159
7.3	The effect of clothing on SET*	161
7.3.1	The effect of accuracy for clothing insulation on SET*	161
7.3.2	The effect of reduction of clothing insulation on SET*	162
7.4	The effect of clothing insulation on PET	164
7.5	Conclusions.....	166
	Reference.....	167
Chapter 8. Conclusions and future studies		169
8.1	Conclusions.....	170
8.2	Future studies	172
Appendix A. Convective and radiative heat transfer coefficients for the clothed manikin		173
Appendix B. MaTLab code for PMV considering difference in convective heat transfer coefficients for various clothing ensembles.		177
Publications		185
Acknowledgements.....		187

Contents

List of figures

Chapter 1

Figure 1-1. The paths of heat loss from the human body	10
Figure 1-2. Conceptual diagram of I_{cl} , I_a , I_t , h_c , and h_r of the clothed human body.....	10
Figure 1-3. Structure of this thesis	16

Chapter 2

Figure 2-1. The calculation process for convective and radiative heat transfer coefficients for the naked manikin.	22
Figure 2-2. The calculation procedures for clothing heat transfer coefficients and clothing insulation (Method A).	24
Figure 2-3. The paths of heat loss from the human body.	27
Figure 2-4. The schematic for the two-node model.....	28
Figure 2-5. Calculation procedure of the two-node model and SET*	28
Figure 2-6. The schematic for the PET.....	29

Chapter 3

Figure 3-1. Thermal manikin.....	35
Figure 3-2. The control software for the thermal manikin.	36
Figure 3-3. Thermal manikin during calibration.	36
Figure 3-4. Vertical section of the climate chamber.	37
Figure 3-5. Image of the climate chamber.....	37
Figure 3-6. Image of the wind tunnel.	38
Figure 3-7. Plane view and elevation view for the second floor of the wind tunnel.	38
Figure 3-8. Traversing system.	39
Figure 3-9. Overview of tested clothing ensembles.	39
Figure 3-10. The non-woven tape and the self-made thermocouple.	41
Figure 3-11. Distribution of the temperature measurement points on the manikin surface and the clothing surface.	41
Figure 3-12. Hot-wire anemometer (Model 6542) produced by Kanomax.....	42
Figure 3-13. Miniature wire probe (55P11) produced by Dantec Dynamics.....	42
Figure 3-14. Test setup for emissivity measurement (E4).	43
Figure 3-15. Position for the thermal camera.	43
Figure 3-16. Digital frazier type air permeability tester (DAP-360) produced by Daiei Kagaku Seiki.	44
Figure 3-17. Surface friction test by the KES.	45
Figure 3-18. The variation of coefficient of friction along with the testing distance.	46
Figure 3-19. Surface roughness test by the KES.	46

List of figures

Figure 3-20. The variation of surface thickness along the testing distance.	46
Figure 3-21. The KES-FB4 surface tester.....	47
Figure 3-22. The roughness sensor and the piano-wire sensor.	48
Figure 3-23. Elemental cartesian fixed control volume showing the inlet and outlet mass flows on the x faces.....	50
Figure 3-24. Surface forces on the control volume (x -direction only).	52
Figure 3-25. Profile of the computational grid.	64
Chapter 4	
Figure 4-1. Body segments of the thermal manikin and wind directions.	69
Figure 4-2. Diagram and measurement points of wind tunnel experiments. The airspeed measurement points are 1 m before the thermal manikin; the temperature measurement points are 0.5 m before the thermal manikin (the vertical positions for the temperature measurement points are same with velocity measurement points)	71
Figure 4-3. Average airspeed and turbulence intensity profiles in the wind tunnel without presence of the thermal manikin.	72
Figure 4-4. Simulation model of the wind tunnel.....	73
Figure 4-5. Y^+ distribution for computational thermal manikin surface (Sitting posture, $U_0 = 1.4 \text{ m}\cdot\text{s}^{-1}$).....	73
Figure 4-6. Comparison of the airspeed airspeeds 1 m before the thermal manikin according to the CFD analysis and the experimental data	74
Figure 4-7. Simulation model of the climate chamber.	75
Figure 4-8. Temperature distribution for upwind and upward airflow when skin temperature was 33°C and air temperature was 27°C	76
Figure 4-9. Whole-body convective heat transfer coefficient under various wind directions (Other studies: De Dear et al. [2], Colin et al. [23], Mitchell [24], Kurazumi [7], Ono et al. [5], Yang et al. [12], Seppanen [25]).....	77
Figure 4-10. Convective heat transfer coefficients for each body segment under various airspeeds in different wind directions for standing posture according to CFD analysis ($\text{W}\cdot\text{m}^{-2}\cdot\text{K}^{-1}$).....	79
Figure 4-11. Convective heat transfer coefficients for each body segment under various airspeeds in different wind directions for sitting posture according to CFD analysis ($\text{W}\cdot\text{m}^{-2}\cdot\text{K}^{-1}$).....	80
Figure 4-12. The contour plots of temperature distribution in the climate chamber in sitting and standing postures at an airspeed of $1 \text{ m}\cdot\text{s}^{-1}$ (yz -plane).	81
Figure 4-13. Body segments of the thermal manikin and wind directions.	88
Figure 4-14. Diagram and measurement points of climate chamber experiments.	89
Figure 4-15. Convective heat transfer coefficients for each body segment under different ambient temperatures in the climate chamber an airspeed of under $0.1 \text{ m}\cdot\text{s}^{-1}$ (Left: sitting posture; Right: standing posture).	91
Figure 4-16. Air temperature distribution for an ambient temperature of 24°C in the climate	

chamber ($V = 0.1 \text{ m} \cdot \text{s}^{-1}$).....	93
Figure 4-17. Relationship between whole-body convective heat transfer coefficient and the difference between skin and ambient temperatures at an airspeed of $0.1 \text{ m} \cdot \text{s}^{-1}$ according to CFD analysis ($\Delta T = t_s - t_a$).	93
Figure 4-18. Distribution of radiative heat transfer coefficient for ambient temperatures of 20°C , 24°C , and 28°C according to numerical calculation.....	95
Figure 4-19. Radiative heat transfer coefficients and view factor.	95
Figure 4-20. Body segments of the thermal manikin and wind direction.....	96
Figure 4-21. The temperature difference between the skin surface and the air during the experiment.....	96
Figure 4-22. Comparison of convective heat transfer coefficients for sitting posture according to CFD analysis and experiment (Other studies: De Dear et al. [2], Colin et al. [23], Mitchell [24])	97
Figure 4-23. 3D plotting for the regression equation for the whole-body convective heat transfer coefficient considering both air temperature and airspeed in sitting posture according to CFD analysis.....	97
Figure 4-24. 3D plotting for the regression equation for the convective heat transfer coefficients for different body segment considering both air temperature and airspeed in sitting posture according to CFD analysis.	99
Chapter 5	
Figure 5-1. Body segments of the thermal manikin and wind directions	107
Figure 5-2. Overview of tested clothing ensembles.	108
Figure 5-3. Basic clothing insulation for various clothing ensembles under the airspeed of $0.25 \text{ m} \cdot \text{s}^{-1}$ (the average clothing insulation for three wind directions).	109
Figure 5-4. Difference between the manikin surface temperature t_{sk} and the air temperature t_a	109
Figure 5-5. Whole-body sensible heat loss of the clothed manikin under various airspeeds and wind directions.....	110
Figure 5-6. Whole-body convective heat transfer coefficient for the naked manikin and the clothed manikin under various airspeeds for standing and sitting postures (left: standing posture, right: sitting posture).	112
Figure 5-7. Whole-body convective heat transfer coefficient for the clothed manikin and the naked manikin under various wind directions (up: standing posture; down: sitting posture). ..	113
Figure 5-8. Average convective heat transfer coefficient for different clothing ensembles in standing posture (symbols represent the experimental data for different wind directions, and the line represents the regression model for the average convective heat transfer coefficient for different wind directions).	115
Figure 5-9. Average convective heat transfer coefficient for different clothing ensembles in sitting	

List of figures

posture (symbols represent the experimental data for different wind directions, and the line represents the regression model for the average convective heat transfer coefficient for different wind directions).....	116
Figure 5-10. Comparison of the average convective heat transfer coefficient for different clothing ensembles in standing and sitting postures under various airspeeds.	117
Figure 5-11. The average temperature of the wall surfaces during the experiments.	126
Figure 5-12. Whole-body radiative heat transfer coefficient for different clothing ensembles under various airspeeds for standing posture (Sorensen [17], ASHRAE [16])	126
Figure 5-13. Comparison of average radiative heat transfer coefficient of different clothing ensembles and radiative heat transfer coefficient of naked manikin at each body segment in standing posture (The results of three wind directions and four airspeeds were averaged).	127
Figure 5-14. Calculation procedure of CFD analysis.	129
Figure 5-15. The comparison of the convective heat transfer coefficients based on the CFD analysis and experiment.	131
Chapter 6	
Figure 6-1. Body segments of the thermal manikin and wind directions	139
Figure 6-2. The effect of airspeed on whole-body clothing insulation in standing and sitting postures (average value for different wind directions).	140
Figure 6-3. The reduction rate of basic insulation due to wind for various clothing ensembles under different wind directions in standing and sitting postures (W_{rr} is the reduction rate of the basic insulation due to wind, $W_{rr} = \frac{I_{cl(0.25)} - I_{cl(1.4)}}{I_{cl(0.25)}}$, where $I_{cl(0.25)}$ is the basic insulation under the airspeed of $0.25 \text{ m}\cdot\text{s}^{-1}$, $I_{cl(1.4)}$ is the basic insulation under the airspeed of $1.4 \text{ m}\cdot\text{s}^{-1}$).	140
Figure 6-4. Whole-body basic insulation for different clothing ensembles under various wind directions (up: standing posture; down: sitting posture).	141
Figure 6-5. The correction factor for posture under upwind $CFP_{cl}(CFP_{cl} = \frac{I_{cl-sit}}{I_{cl-stand}})$, I_{cl-sit} is the clothing insulation for the sitting posture, $I_{cl-stand}$ is the clothing insulation for the standing posture).....	142
Figure 6-6. The correction factor for wind direction (CFD_{cl}) in standing posture ($CFD_{cl} = [I_{cl-crosswind} \text{ or } I_{cl-downwind}] / I_{cl-upwind}$, $I_{cl-crosswind}$ is the clothing insulation caused by a crosswind, $I_{cl-downwind}$ is the clothing insulation caused by downwind, $I_{cl-upwind}$ is the clothing insulation caused by upwind).	142
Figure 6-7. The correction factor (CFD_{cl}) for wind direction in sitting posture ($CFD_{cl} = [I_{cl-crosswind} \text{ or } I_{cl-downwind}] / I_{cl-upwind}$, $I_{cl-crosswind}$ is the clothing insulation caused by the crosswind, $I_{cl-downwind}$ is the clothing insulation caused by the downwind, $I_{cl-upwind}$ is the clothing insulation caused by the upwind).	143
Figure 6-8. The calculation procedure and the determining of correction numbers for Equation	

(6-1).....	144
Figure 6-9. The effect of airspeed on local clothing insulation in standing posture (the solid black line represents the regression line of airspeed and the average clothing insulation for various clothing ensembles).....	145
Figure 6-10. The effect of airspeed on local clothing insulation in sitting posture (the solid black line represents the regression line of airspeed and the average clothing insulation for various clothing ensembles).....	146
Figure 6-11. Clothing insulation for various clothing ensembles according to Method A and Method C under different airspeeds.	151
Chapter 7	
Figure 7-1. The comparison of the PMV values calculates with the PMV MATLAB code in this study and the PMV values from ISO 7730.....	157
Figure 7-2. PMV for various clothing ensembles under different airspeeds in Case1, Case2, and Case3.....	158
Figure 7-3. PMV for various clothing ensembles under different airspeeds in Case3.	160
Figure 7-4. PMV for various clothing ensembles in different wind directions under various airspeed in Case3.....	160
Figure 7-5. The SET* calculated with clothing insulation based on Method D ($I_{cl} = 0.96$ clo) and Method A (standing posture: 0.85–1 clo, sitting posture: 0.74–0.95 clo).....	162
Figure 7-6. The comparison of SET* considering the reduction of clothing insulation and not based on $I_{cl} = 0.96$	162
Figure 7-7. The SET* calculated with measured clothing insulation of this study considering the reduction of clothing insulation caused by airspeed in standing and sitting postures.	163
Figure 7-8. The relationship between airspeed and ΔSET^* (ΔSET^* is the difference between SET* neglecting the reduction of clothing insulation and SET* considering the reduction of clothing insulation caused by airspeed).....	163
Figure 7-9. The PET value calculated with the convective heat transfer coefficient in this study compared to the results of Hoppe [11] ($t_a = 20^\circ\text{C}$, $t_{MRT} = 20^\circ\text{C}$, $V = 0.1\text{--}5\text{ m}\cdot\text{s}^{-1}$, RH = 50 %, Work metabolism = 80 W, Clo = 0.9 clo).....	165
Chapter 8	
Figure 8-1. Main results of this thesis	171

List of figures

List of tables

Chapter 1

Table 1-1. Radiative heat transfer coefficients for different body segments in standing and sitting postures based on the experimental method and numerical method ($\text{W}\cdot\text{m}^{-2}\cdot\text{K}^{-1}$).....	11
Table 1-2. Formulas for whole-body convective heat transfer coefficient.	12
Table 1-3. Convective heat transfer coefficients for different body segments in standing and sitting postures based on the experimental method and numerical method in calm condition ($\text{W}\cdot\text{m}^{-2}\cdot\text{K}^{-1}$).	13

Chapter 2

Table 2-1. Type number and thermal insulation for individual garments according to ISO 9920 (Annex B).....	25
Table 2-2. Typical insulation and permeability values for western clothing ensembles [4]..	26

Chapter 3

Table 3-1. Body segment area for the thermal manikin.	35
Table 3-2. Material information about tested clothing ensembles.	40
Table 3-3. Specifications for the thermocouple and data logger.	41
Table 3-4. Specifications for the hot-wire anemometer and split-fiber flim probe.....	42
Table 3-5. Specifications for the thermal camera.	43
Table 3-6. Specifications for the air permeability tester.	44
Table 3-7. Air permeability for each garment.	45
Table 3-8. Specification for the KES-FB4 surface tester.	48
Table 3-9. Mean coefficient for friction and surface roughness for each garment.	49
Table 3-10. Low Reynolds number $k-\varepsilon$ model in STAR CCM+ [20].	61
Table 3-11. Segment area for thermal manikin and computational thermal manikin (m^2).	63

Chapter 4

Table 4-1. The summary of environmental conditions for experiment (Exp.) and CFD analysis.	70
Table 4-2. Heights of measurement points (air temperature and velocity).	71
Table 4-3. Numerical method.	73
Table 4-4. Boundary conditions for the wind tunnel.	74
Table 4-5. Boundary conditions for the climate chamber.	75
Table 4-6. Regression models of the convective heat transfer coefficient caused by the upwind for the thermal manikin in the standing posture both for experimental and CFD results.....	81
Table 4-7. Regression models of the convective heat transfer coefficient caused by the crosswind for the thermal manikin in the standing posture both for experimental and CFD results.....	82
Table 4-8. Regression models of the convective heat transfer coefficient caused by the downwind	

List of tables

for the thermal manikin in the standing posture both for experimental and CFD results.....	83
Table 4-9. Regression models of the convective heat transfer coefficient for the thermal manikin caused by the vertical airflow in the standing posture for CFD results.....	84
Table 4-10. Regression models of the convective heat transfer coefficient for the thermal manikin caused by the upwind in the sitting posture both for experimental and CFD results.	85
Table 4-11. Regression models of the convective heat transfer coefficient caused by the crosswind for the thermal manikin in the sitting posture both for experimental and CFD results.	86
Table 4-12. Regression models of the convective heat transfer coefficient caused by the downwind for the thermal manikin in the sitting posture both for experimental and CFD results.	87
Table 4-13. Regression models of the convective heat transfer coefficient for the thermal manikin caused by the vertical airflow in the sitting posture both for experimental and CFD results.....	88
Table 4-14. The summary of environmental conditions for the experiment (Exp.) and CFD. ...	89
Table 4-15. Boundary conditions for the climate chamber (Section 4.3.2).	90
Table 4-16. Convective heat transfer coefficients for each body segment in standing posture under different ambient temperatures in the climate chamber with an airspeed of under $0.1 \text{ m}\cdot\text{s}^{-1}$ ($\text{W}\cdot\text{m}^{-2}\cdot\text{K}$).....	92
Table 4-17. Convective heat transfer coefficients for each body segment in sitting posture under different ambient temperatures in the climate chamber with an airspeed of under $0.1 \text{ m}\cdot\text{s}^{-1}$ ($\text{W}\cdot\text{m}^{-2}\cdot\text{K}$).....	92
Table 4-18. Regression models of the convective heat transfer coefficient against temperature difference between the thermal manikin and the air at an airspeed of $0.1 \text{ m}\cdot\text{s}^{-1}$ for CFD analysis	94
Table 4-19. The summary of environmental conditions for the experiment (Exp.) and CFD analysis.....	96
Table 4-20. The regression model considering both airspeed and environment temperature for the sitting posture according to CFD analysis ($\text{W}\cdot\text{m}^{-2}\cdot\text{K}^{-1}$).	99

Chapter 5

Table 5-1. The summary of environmental conditions for the experiment.....	107
Table 5-2. Material information about tested clothing ensembles.	108
Table 5-3. Regression model for the average heat transfer coefficient for different clothing ensembles in standing posture (results for three wind directions were averaged).	117
Table 5-4. Regression model for the average heat transfer coefficient for different clothing ensembles in sitting posture (results for three wind directions were averaged).	118
Table 5-5. The convective heat transfer coefficient and clothing surface temperatures for Ensemble 1 in standing posture (under an airspeed of $0.25 \text{ m}\cdot\text{s}^{-1}$ caused by the upwind).	119
Table 5-6. The convective heat transfer coefficient and clothing surface temperatures for Ensemble 2 in standing posture (under an airspeed of $0.25 \text{ m}\cdot\text{s}^{-1}$ caused by the upwind).	120

Table 5-7. The convective heat transfer coefficient and clothing surface temperatures for Ensemble 3 in standing posture (under an airspeed of $0.25 \text{ m}\cdot\text{s}^{-1}$ caused by the upwind).	121
Table 5-8. The convective heat transfer coefficient and clothing surface temperatures for Ensemble 4 in standing posture (under an airspeed of $0.25 \text{ m}\cdot\text{s}^{-1}$ caused by the upwind).	122
Table 5-9. The convective heat transfer coefficient and clothing surface temperatures for Ensemble 5 in standing posture (under an airspeed of $0.25 \text{ m}\cdot\text{s}^{-1}$ caused by the upwind).	123
Table 5-10. The convective heat transfer coefficient and clothing surface temperatures for Ensemble 6 in standing posture (under an airspeed of $0.25 \text{ m}\cdot\text{s}^{-1}$ caused by the upwind).	124
Table 5-11. The convective heat transfer coefficient and clothing surface temperatures for Ensemble 8 in standing posture (under an airspeed of $0.25 \text{ m}\cdot\text{s}^{-1}$ caused by the upwind).	125
Table 5-12. Environmental conditions for the CFD analysis of clothing.	130
Table 5-13. Boundary conditions.....	130
Table 5-14. The standard deviation of the difference between the convective heat transfer coefficient due to experiment and CFD analysis.....	131
Table 5-15. The correction factor for the CFD analysis α	131
Table 5-16. The standard deviation of the difference between the radiative heat transfer coefficient due to experiment and CFD analysis..	131
Chapter 6	
Table 6-1. The experimental conditions.....	139
Table 6-2. The correction factor for airspeed under different wind directions CFV_{cl} ($CFV_{cl} = I_{cl}/I_{cl-static}$, I_{cl} is the clothing insulation under arbitrary airspeed, $I_{cl-static}$ is the clothing insulation for under an airspeed of $0.25 \text{ m}\cdot\text{s}^{-1}$).	141
Table 6-3. The clothing insulation for Ensemble1 in standing posture under an airspeed of $0.25 \text{ m}\cdot\text{s}^{-1}$ caused by the upwind.	147
Table 6-4. The clothing insulation for Ensemble2 in standing posture under an airspeed of $0.25 \text{ m}\cdot\text{s}^{-1}$ caused by the upwind.	148
Table 6-5. The clothing insulation for Ensemble3 in standing posture under an airspeed of $0.25 \text{ m}\cdot\text{s}^{-1}$ caused by the upwind.	148
Table 6-6. The clothing insulation for Ensemble4 in standing posture under an airspeed of $0.25 \text{ m}\cdot\text{s}^{-1}$ caused by the upwind.	149
Table 6-7. The clothing insulation for Ensemble5 in standing posture under an airspeed of $0.25 \text{ m}\cdot\text{s}^{-1}$ caused by the upwind.	149
Table 6-8. The clothing insulation for Ensemble6 in standing posture under an airspeed of $0.25 \text{ m}\cdot\text{s}^{-1}$ caused by the upwind.	150
Table 6-9. The clothing insulation for Ensemble8 in standing posture under an airspeed of $0.25 \text{ m}\cdot\text{s}^{-1}$ caused by the upwind.	150
Table 6-10. The comparison of clothing insulation calculated by Method A and Method B for different clothing ensembles.	151

List of tables

Chapter 7

Table 7-1. Information on input data for PMV program for Case1, Case2, and Case3.	157
Table 7-2. Input variables for SET*	161
Table 7-3. The regression models for ΔSET^* and airspeed (ΔSET^* is the difference between SET* neglecting the reduction of clothing insulation and SET* considering the reduction of clothing insulation caused by airspeed).....	164
Table 7-4. The comparison of the results calculates with the PET calculated with the PET MATLAB code in this study and the PET values from Hoppe.	165

NOMENCLATURE

Chapter 1

Variables

h_c : Convective heat transfer coefficient for the naked manikin, $\text{W}\cdot\text{m}^{-2}\cdot\text{K}^{-1}$

I_a : Air layer insulation, clo

I_{cl} : Basic insulation, clo

I_t : Total insulation, clo

ΔT : Temperature difference between the manikin surface and the air, $^{\circ}\text{C}$

t_a : Air temperature, $^{\circ}\text{C}$

t_{cl} : Whole-body clothing surface temperature, $^{\circ}\text{C}$

V : Airspeed, $\text{m}\cdot\text{s}^{-1}$

Abbreviations

ASHRAE: American Society of Heating Refrigerating and Air-Conditioning Engineers

CFD: Computational fluid dynamics

ISO: International Organization for Standardization

Chapter 2

Variables

C : Convective heat loss from the skin, $\text{W}\cdot\text{m}^{-2}$

C_{res} : Rate of convective heat loss from respiration, $\text{W}\cdot\text{m}^{-2}$

$C + R$: Sensible heat loss from skin (total heat loss), $\text{W}\cdot\text{m}^{-2}$

CFV_{cl} : Correction factor for air velocity, dimensionless

c_b : The blood thermal capacity, $\text{J}\cdot\text{L}^{-1}\cdot\text{K}^{-1}$

E_{diff} : The latent heat flow rate from evaporation of moisture diffused through the skin, $\text{W}\cdot\text{m}^{-2}$

E_{sk} : Total rate of evaporative heat loss from the skin, $\text{W}\cdot\text{m}^{-2}$

E_{rsw} : The heat flow rate due to evaporation of the sweat, $\text{W}\cdot\text{m}^{-2}$

E_{res} : Rate of evaporative heat loss from respiration, $\text{W}\cdot\text{m}^{-2}$

F_{CS} : Heat flows from the body core to skin surface, $\text{W}\cdot\text{m}^{-2}$

F_{SC} : Heat flows from the skin surface to the clothing surface, $\text{W}\cdot\text{m}^{-2}$

f_{eff} : View factor (effective radiation area factor for each body segment), dimensionless

f_{cl} : Ratio of the surface area of the clothed body to the surface area of the naked body, dimensionless

h_c : Whole-body convective heat transfer coefficient for the naked manikin, $\text{W}\cdot\text{m}^{-2}\cdot\text{K}^{-1}$

$h_{c,cl}$: Whole-body convective heat transfer coefficient for the clothed manikin, $\text{W}\cdot\text{m}^{-2}\cdot\text{K}^{-1}$

$h_{c,i,cl}$: Convective heat transfer coefficient for the clothed manikin segment i , $\text{W}\cdot\text{m}^{-2}\cdot\text{K}^{-1}$

NOMENCLATURE

$h_{c,i(CFD)}$: Convective heat transfer coefficient for body segment i according to CFD analysis, $W \cdot m^{-2} \cdot K^{-1}$

$h_{c,i}$: Convective heat transfer coefficient for the naked manikin segment i , $W \cdot m^{-2} \cdot K^{-1}$

$h_{c,i(Exp.)}$: Convective heat transfer coefficient for body segment i according to experiment, $W \cdot m^{-2} \cdot K^{-1}$

h_r : Whole-body radiative heat transfer coefficient for the naked manikin, $W \cdot m^{-2} \cdot K^{-1}$

$h_{r,cl}$: Whole-body radiative heat transfer coefficient for the clothed manikin, $W \cdot m^{-2} \cdot K^{-1}$

$h_{r,i}$: Radiative heat transfer coefficient for the naked manikin segment i , $W \cdot m^{-2} \cdot K^{-1}$

$h_{r,i(CFD)}$: Radiative heat transfer coefficient for body segment i according to CFD analysis, $W \cdot m^{-2} \cdot K^{-1}$

$h_{r,i,cl}$: Radiative heat transfer coefficient for the clothed manikin segment i , $W \cdot m^{-2} \cdot K^{-1}$

h_e : Evaporative heat transfer coefficient, $W \cdot m^{-2} \cdot kPa^{-1}$

$h_{s,e}$: Standard evaporative heat transfer coefficient, $W \cdot m^{-2} \cdot kPa^{-1}$

$h_{s,c}$: Standard convective heat transfer coefficient, $W \cdot m^{-2} \cdot K^{-1}$

$h_{s,t}$: Standard total heat transfer coefficient, $W \cdot m^{-2} \cdot K^{-1}$

H_{C-S} : The heat transfer from core to skin, $W \cdot m^{-2}$

H_{sk} : Heat loss from the skin, $W \cdot m^{-2}$

I_{cl} : Whole-body basic insulation, clo

$I_{cl,i}$: Basic insulation for clothed manikin segment i , clo

$I_{cl,r}$: Basic insulation value in actual situations, including the effects of movements and wind, clo

I_{clu} : Basic insulations of individual garments that are available in ISO 9920, clo

I_t : Total insulation, clo

i_m : Total vapor permeation efficiency: ratio of actual evaporative heat flow capability between skin and environment to sensible heat flow capability as compared to Lewis ratio

i_{cl} : Clothing vapor permeation efficiency: ratio of actual evaporative heat flow capability through clothing to sensible heat flow capability as compared to Lewis ratio

I_a : Air insulation, clo

K : The conductance of body tissues, $K=5.28 W \cdot m^{-2} \cdot K^{-1}$

L : Thermal load on the body, $W \cdot m^{-2}$

M : Rate of metabolic heat production, $W \cdot m^{-2}$

$p_{s,sk}$: Water vapor pressure at the skin under standard environment, kPa

p_{sk} : Water vapor pressure at the skin, kPa

p_a : Ambient vapor pressure, kPa

p_{SET^*} : The saturated water vapor pressure at SET^* , kPa

$q_{c,i}$: Convective heat loss through the surface of the naked manikin segment i , $W \cdot m^{-2}$

$q_{c,i,cl}$: Convective heat loss through the surface of the clothed manikin segment i , $W \cdot m^{-2}$

$q_{c,i(CFD)}$: Convective heat loss for body segment i according to CFD analysis, $W \cdot m^{-2}$

$q_{c,i(Exp.)}$: Convective heat loss for body segment i according to experiment, $W \cdot m^{-2}$

$q_{r,i}$: Radiative heat loss through the surface of the naked manikin segment i , $W \cdot m^{-2}$
 $q_{r,i_{cl}}$: Radiative heat loss through the surface of the clothed manikin segment i , $W \cdot m^{-2}$
 $q_{r,i(CFD)}$: Radiative heat loss for body segment i according to CFD analysis, $W \cdot m^{-2}$
 $q_{t,i}$: Sensible heat loss (total heat loss) through the surface of the naked manikin segment i , $W \cdot m^{-2}$
 q_t : Whole-body sensible heat loss for the clothed manikin, $W \cdot m^{-2}$
 $q_{t,i_{cl}}$: Total heat loss through the surface of the clothed manikin segment i , $W \cdot m^{-2}$
 $q_{t,i(Exp.)}$: Total heat loss for the naked manikin segment i according to experiment, $W \cdot m^{-2}$
 R : Radiative heat loss from the skin, $W \cdot m^{-2}$
 R_{cl} : Whole-body basic insulation, $m^2 \cdot K \cdot W^{-1}$
 R_{cls} : Standard clothing for the actual activity level, $m^2 \cdot K \cdot W^{-1}$
 S_{cr} : Rate of heat storage in the core, $W \cdot m^{-2}$
 S_{sk} : Rate of heat storage in the skin, $W \cdot m^{-2}$
 S : The storage heat flow rate for heating or cooling the body mass, $W \cdot m^{-2}$
 $Skbf$: The skin blood flow, $L \cdot m^{-2} \cdot h^{-1}$
 S_j : Wall area, $j=1,2,\dots,6$, m^2
 t_a : Air temperature, $^{\circ}C$
 $t_{a(CFD)}$: Air temperature according to CFD analysis, $^{\circ}C$
 $t_{sk,i}$: Surface temperature of manikin segment i , $^{\circ}C$
 t_{sk} : Whole-body skin temperature $^{\circ}C$
 t_{co} : Core temperature, $^{\circ}C$
 \bar{t}_r : Mean radiant temperature, $^{\circ}C$
 $t_{cl,i}$: Clothing surface temperature for clothed manikin segment i , $^{\circ}C$
 t_{cl} : Whole-body clothing surface temperature, $^{\circ}C$
 $t_{w,j}$: Wall temperature, $j=1,2,\dots,6$, $^{\circ}C$
 t_r : Averaged wall temperature, $^{\circ}C$
 V : Airspeed, $m \cdot s^{-1}$
 v_b : Blood flow from body core to skin, $L \cdot s^{-1} \cdot m^{-2}$
 W : Rate of mechanical work accomplished, $W \cdot m^{-2}$
 w : Skin wetness, dimensionless

Greek letters

σ : Stefan-Boltzmann constant, $5.67 \times 10^{-8} W \cdot m^{-2} \cdot K^{-4}$
 ε : Emissivity of clothing surface, dimensionless
 α_i : Ratio of the surface area of each part of the naked manikin to the total naked manikin surface area
 ρ_b : Blood density, $kg \cdot L^{-1}$

Abbreviations

ASHRAE: American Society of Heating, Refrigerating and Air-Conditioning Engineers

NOMENCLATURE

ISO: International Organization for Standardization

PMV: Predicted mean vote

PET: Physiological equivalent temperature

RH: Relative humidity, dimensionless

SET*: Standard effective temperature, °C

Chapter 3

Variables

a: Acceleration, $\text{m}\cdot\text{s}^{-2}$

B: Any property of the fluid (mass, momentum, angular momentum, or energy), dimensionless

c_p: Heat capacity at constant pressure, $\text{kJ}\cdot\text{kg}^{-1}\cdot\text{K}^{-1}$

dE: Change in energy in the control volume, J

dA: An elemental area dA , m^2

F: Frictional force, $\text{kg}\cdot\text{m}\cdot\text{s}^{-2}$

F: External force, $\text{kg}\cdot\text{m}\cdot\text{s}^{-2}$

F_{grav}: The gravity force on the control volume, $\text{kg}\cdot\text{m}\cdot\text{s}^{-2}$

F_{surface}: The surface force on the control volume, $\text{kg}\cdot\text{m}\cdot\text{s}^{-2}$

g: Gravitational acceleration, $\text{m}\cdot\text{s}^{-2}$

I: Turbulence intensity, dimensionless

L: Movement distance of the sample, cm

m: Mass, kg

n: the unit vector normal to dA , dimensionless

p: Pressure, $\text{kg}\cdot\text{m}^{-1}\cdot\text{s}^{-2}$

P: Normal force, $\text{kg}\cdot\text{m}\cdot\text{s}^{-2}$

T: Fabric thickness measured by the sensor, μm

T̄: Mean fabric thickness, μm

t: Time, s

u': Root-mean-square of the airspeed fluctuations, $\text{m}\cdot\text{s}^{-1}$

u: *x*-direction component of instantaneous velocities, $\text{m}\cdot\text{s}^{-1}$

U: Mean airspeed, $\text{m}\cdot\text{s}^{-1}$

V: Local fluid velocity vector, $\text{m}\cdot\text{s}^{-1}$

V: Volume for the control volume, m^3

v: *y*-direction component of instantaneous velocities, $\text{m}\cdot\text{s}^{-1}$

w: *z*-direction component of instantaneous velocities, $\text{m}\cdot\text{s}^{-1}$

Greek letters

μ: Coefficient of friction, dimensionless

ρ: Local fluid density, $\text{kg}\cdot\text{m}^{-3}$

δQ : Heat added to the control volume, J
 δW : Work done by the control volume, J
 σ_{ij} : The surface stress in j direction on a face normal to i axis, $\text{N}\cdot\text{m}^{-2}$
 τ_{ij} : The viscous stress in j direction on a face normal to i axis, $\text{N}\cdot\text{m}^{-2}$

Abbreviations

KES: Kawabata-Evaluation-System
 MIU: Mean coefficient of friction, dimensionless
 SMD: Surface roughness, μm

Subscript

$\Phi_{(i,j,k)}$: A property Φ that is at the grid (i, j, k)
 Φ_{cv} : A property Φ of the control volume
 Φ_{cs} : A property Φ of the control surface

Chapter 4

Variables

h_c : Convective heat transfer coefficient for the naked manikin, $\text{W}\cdot\text{m}^{-2}\cdot\text{K}^{-1}$
 h_r : Radiative heat transfer coefficient for the naked manikin, $\text{W}\cdot\text{m}^{-2}\cdot\text{K}^{-1}$
 I_{in} : Inlet turbulence intensity, dimensionless
 k_{out} : Turbulent kinetic energy, $\text{m}^2\cdot\text{s}^{-2}$
 L_{in} : Turbulence length scale, m
 t_{wall} : Wall temperature, $^{\circ}\text{C}$
 t_a : Air temperature, $^{\circ}\text{C}$
 t_{sk} : Skin temperature, $^{\circ}\text{C}$
 ΔT : Temperature difference between the manikin surface and the air, $^{\circ}\text{C}$
 U_0 : Inlet velocity, $\text{m}\cdot\text{s}^{-1}$
 U_{out} : Outlet velocity, $\text{m}\cdot\text{s}^{-1}$
 V : Airspeed, $\text{m}\cdot\text{s}^{-1}$

Greek letters

ε_{out} : Rate of viscous dissipation, $\text{m}^2\cdot\text{s}^{-3}$

Abbreviations

CFD: Computational fluid dynamics
 SIMPLE: Semi-implicit method for pressure-linked equations

Chapter 5

Variables

NOMENCLATURE

h_c : Convective heat transfer coefficient for the clothed manikin, $\text{W}\cdot\text{m}^{-2}\cdot\text{K}^{-1}$

h_r : Radiative heat transfer coefficient for the clothed manikin, $\text{W}\cdot\text{m}^{-2}\cdot\text{K}^{-1}$

I_{cl} : Clothing insulation, clo.

t_a : Air temperature, $^{\circ}\text{C}$

t_{sk} : Skin temperature, $^{\circ}\text{C}$

ΔT : Temperature difference between the manikin surface and the air, $^{\circ}\text{C}$

Greek letters

α : The correction factor for the convective heat transfer coefficient calculated by the CFD analysis, dimensionless

Chapter 6

Variables

CFD_{cl} : Correction factor for wind direction, dimensionless

CFP_{cl} : Correction factor for posture, dimensionless

CFV_{cl} : Correction factor for airspeed, dimensionless

I_{cl} : Clothing insulation, clo

I_{cl-sit} : Clothing insulation for the sitting posture, clo

$I_{cl-stand}$: Clothing insulation for the standing posture, clo

$I_{cl(0.25)}$, $I_{cl-static}$: Clothing insulation under the airspeed of $0.25 \text{ m}\cdot\text{s}^{-1}$, clo

$I_{cl(1.4)}$: Clothing insulation under the airspeed of $1.4 \text{ m}\cdot\text{s}^{-1}$, clo

$I_{cl-crosswind}$: Clothing insulation caused by the crosswind, clo

$I_{cl-downwind}$: Clothing insulation caused by the downwind, clo

$I_{cl-upwind}$: Clothing insulation caused by the upwind, clo

W_{rr} : Reduction rate of the Clothing insulation due to the wind, dimensionless

Abbreviations

ASHRAE: American Society of Heating Refrigerating and Air-Conditioning Engineers

HVAC: Heating, ventilation, and air conditioning

ISO: International Organization for Standardization

Chapter 7

Variables

f_{cl} : Ratio of the surface area of the clothed body to the surface area of the naked body, dimensionless

h_c : Convective heat transfer coefficient for the clothed manikin, $\text{W}\cdot\text{m}^{-2}\cdot\text{K}^{-1}$

h_r : Radiative heat transfer coefficient for the clothed manikin, $\text{W}\cdot\text{m}^{-2}\cdot\text{K}^{-1}$

I_{cl} : Clothing insulation, clo

Abbreviations

ASHRAE: American Society of Heating Refrigerating and Air-Conditioning Engineers

CBE: Center for the built environment

ISO: International Organization for Standardization

M: Metabolic rate, met, $1 \text{ met} = 58 \text{ W} \cdot \text{m}^{-2}$

PET: Physiological equivalent temperature, °C

PMV: Predicted mean vote

RH: Relative humidity, dimensionless

SET*: Standard effective temperature, °C

ΔSET^* : Difference between SET* neglecting the reduction of clothing insulation and SET* considering the reduction of clothing insulation caused by airspeed, °C

NOMENCLATURE

Chapter 1.

Introduction

1.1 Fundamental of heat transfer from the clothed human body

The heat loss from the human body consists of evaporative heat loss and sensible heat loss (convective and radiative heat losses) (Figure 1-1). In this study, only sensible heat loss was considered. If the convective heat transfer coefficient and radiative heat transfer coefficient are known, the convective and radiative heat loss can be calculated, respectively.

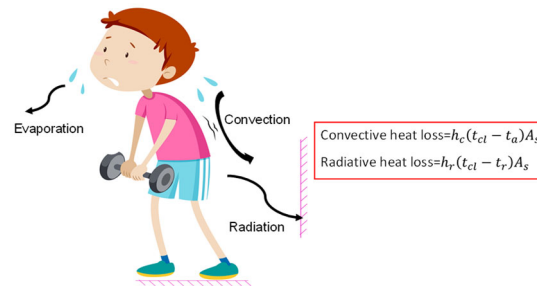


Figure 1-1. The paths of heat loss from the human body.

When it comes to the discussion of the clothed human body, the clothing affects the heat loss from the human body significantly. The sensible heat from the clothed human body flows (1) from the skin surface to the outer clothing surface through the clothing, and (2) from the outer clothing surface to the immediate surroundings (Figure 1-2).

The basic insulation I_{cl} is defined as the thermal resistance of the clothing and the air layer between the human body and the clothing surface. The air layer is affected by the posture of the human body. For example, the air layer decreases when a person sits, as the clothing on the back, thighs, and buttocks is compressed. As a result, the basic insulation for the sitting posture is smaller compared to the standing posture. The air layer is also affected by the wind. The airstream makes the air layer thinner.

Additionally, the wind affects the basic insulation by penetrating the clothing layer. I_a is defined as the thermal resistance of the air layer on the surface of clothing. Total clothing insulation I_t is the sum of I_a and I_{cl} . Convective heat transfer coefficient h_c and radiative heat transfer coefficient h_r are also illustrated in (Figure 1-2). Because the area of the clothing is larger than the area of the nude body due to the wrinkling of the clothing, the convective heat transfer coefficient for the clothed human body is higher than that of the naked human body.

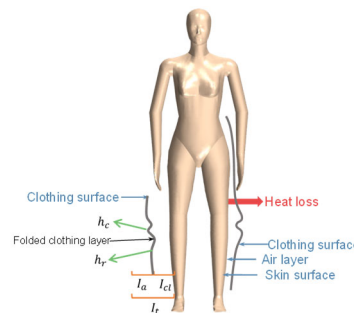


Figure 1-2. Conceptual diagram of I_{cl} , I_a , I_t , h_c , and h_r of the clothed human body.

1.2 Literature review

People play a central role in indoor environmental issues concerning air quality or thermal comfort (Licina et al. (2015b) (2015a); Murakami (2004); Voelker and Alsaad (2018)). Therefore, it is crucial to have an enhanced understanding of the relationship between the human body and surrounding environments (Gao & Niu, 2005). Additionally, the goal of thermal comfort research is to build a comprehensive model of human regulation and to predict thermal comfort through numerical algorithms. The completion of such models relies on the convective and radiative heat transfer coefficients, and clothing insulation for the whole-body or individual body segments (De Dear et al., 1997; Oguro et al., 2001).

1.2.1 Radiative heat transfer coefficient

Concerning radiative heat transfer coefficients, both experimental research and numerical research have been carried out. (Ichihara et al., 1997) measured the radiative heat transfer coefficient by setting the air temperature to the same as the thermal manikin surface temperature to isolated the radiant heat loss. (De Dear et al., 1997) determined the radiative heat transfer coefficient by applying aluminum cooking foil with a very low emissivity to the thermal manikin. Both these two methods were laborious work compared with the numerical method. (Martinho et al., 2012; Sørensen, 2002; Sørensen & Voigt, 2003) calculated the radiative heat transfer coefficient with a computational thermal manikin in sitting posture. (Najjaran et al., 2011) reported the whole-body radiative heat transfer coefficients for the computational thermal manikin in the supine posture. Some results for the radiative heat transfer coefficients are given in Table 1-1. The whole-body radiative heat transfer coefficients were similar across the studies, but the values for different body segments varied a lot.

Table 1-1. Radiative heat transfer coefficients for different body segments in standing and sitting postures based on the experimental and numerical methods ($\text{W} \cdot \text{m}^{-2} \cdot \text{K}^{-1}$).

Segment	*(Ichihara et al., 1997)		(De Dear et al., 1997)		** (Sørensen, 2002)
	Experiment		Experiment		Numerical method
	Sit	Stand	Sit	Stand	Sit
Head	4.6	4.3	3.9	4.1	5.22
Chest	3.7	3.8	3.4	4.5	4.73
Upper arm	4.6	4.0	4.8	5.2	4.63
Back	4.3	3.6	4.6	4.4	5.07
Forearm	3.9	3.9	5.2	4.9	4.30
Abdomen	3.9	3.8	4.8	4.2	5.01
Waist	4.0	4.0	4.8	4.2	5.01
Thigh	3.8	4.2	4.6	4.3	4.61
Hand	4.4	3.7	3.9	4.1	4.12
Leg	4.4	4.7	5.4	5.3	5.12
Foot	5.9	5.4	4.2	3.9	5.36
Whole-body	4.3	4.2	4.5	4.5	4.83

*Manikin surface temperature and wall temperature was 34.0 °C and 27.1 °C, respectively

**Manikin surface temperature and wall temperature was 31 °C and 19 °C, respectively

1.2.2 Convective heat transfer coefficient

Quantitative values of convective heat transfer coefficients are important, not only in estimating convection heat loss, but in evaluating operative temperature, clothing parameters, and effective temperature (“Chapter 9,” 2017). Measurement of convective heat transfer coefficients has been carried out by many researchers. (Colin & Houdas, 1967) investigated the convective heat transfer coefficient under various ambient conditions through performing experiments on subjects. Many other researchers also presented results of the convective heat transfer coefficient based on subject experiments (Mitchell, 1974; Nishi & Gagge, 1970; Seppanen, 1972). (Clark & Toy, 1975) measured the forced convective heat transfer coefficient of the human head and a heated cylinder. Later, several studies about the convective heat transfer coefficient were carried out with the thermal manikin. (Ichihara et al., 1997) reported the convective heat transfer coefficients under low airspeed in both sitting and standing postures based on the thermal manikin experiment. (De Dear et al., 1997) studied the effect of airspeed and wind direction on the convective heat transfer coefficient with a 16-segment thermal manikin. (Kurazumi et al., 2008) presented the convective heat transfer coefficient of the human body in natural convection. (J.-H. Yang et al., 2004; J. Yang et al., 2009) performed thermal manikin experiments concerning the convective heat transfer coefficients both in indoor and outdoor environments.

In recent years, computational fluid dynamics (CFD) technology has developed and makes it possible to analyze the micro-climate around a human body in detail (Gao & Niu, 2005). The heat transfer and airflow distribution around the human body were confirmed through CFD analysis in several studies (Martinho et al., 2012; Oh & Kato, 2018; Sørensen & Voigt, 2003; Topp et al., 2002). Furthermore, the approach of coupling the CFD simulation and the thermoregulation model was developed (Nilsson, 2007; Voelker & Alsaad, 2018).

Some equations of the convective heat transfer coefficients are listed in Table 1-2 and Table 1-3.

Table 1-2. Formulas for whole-body convective heat transfer coefficient.

	Range of V ($\text{m}\cdot\text{s}^{-1}$)	Wind direction	ΔT ($^{\circ}\text{C}$)	Regression equation of h_c ($\text{W}\cdot\text{m}^{-2}\cdot\text{K}^{-1}$)
Sit	< 0.2		7, 9, 13, 15, 17	$h_c = 1.222\Delta T^{0.299}$ (Kurazumi et al., 2008)
	0.2–4.0	Upwind		$h_c = 8.3V^{0.6}$ (Mitchell, 1974)
	0–1.2			$h_c = 2.7 + 8.7V^{0.67}$ (Colin & Houdas, 1967)
	0.2–5	Eight different wind azimuth angles in horizontal direction	12	$h_c = 10.1V^{0.61}$ (De Dear et al., 1997)
Stand	< 0.2		7, 9, 13, 15, 17	$h_c = 1.007\Delta T^{0.406}$ (Kurazumi et al., 2008)
	0.02–0.1			$h_c = 2.35\Delta T^{1.25}$ (Nielsen & Per, 1953)
	0.15–1.5	Upwind		$h_c = 14.8V^{0.69}$ (Seppanen, 1972)
	0.2–5	Eight different wind azimuth angles in horizontal direction	12	$h_c = 10.4V^{0.56}$ (De Dear et al., 1997)

ΔT is the temperature difference between the manikin surface and the ambient air

Table 1-3. Convective heat transfer coefficients for different body segments in standing and sitting postures based on the experimental and numerical methods in calm condition ($\text{W}\cdot\text{m}^{-2}\cdot\text{K}^{-1}$).

Segment	*(De Dear et al., 1997) Experiment		**(Oh & Kato, 2018) Numerical method		*** (Sørensen, 2002) Numerical method
	Sit	Stand	Sit	Stand	Sit
Head	3.7	3.6	2.69	2.81	3.62
Chest	3.0	3.0	2.13	2.34	2.38
Upper arm	3.4	2.9	3.04	4.94	2.71
Back	2.6	2.9	2.59	1.71	2.23
Forearm	3.8	3.7	4.41	3.43	3.82
Pelvis	2.8	3.4	3.15	2.00	2.80
Thigh	3.7	4.1	3.49	2.50	3.18
Hand	4.5	4.1	5.14	4.57	4.50
Leg	4.0	4.1	2.94	2.90	3.04
Foot	4.2	5.1	4.75	4.71	4.66
Whole-body	3.3	3.4	3.27	2.73	3.13

*Temperature difference between the manikin surface and air was 12 °C

**The air temperature was 24 °C, and the heat loss for the thermal manikin was $58 \text{ W}\cdot\text{m}^{-2}$

***Manikin surface temperature and wall temperature was 31 °C and 19 °C, respectively

The literature concerning convective and radiative heat transfer coefficients for the clothed human body is, however, limited. (Oguro et al., 2002) evaluated the convective heat transfer coefficient for a clothed manikin wearing long sleeve shirts and trousers. Their results showed that the convective heat transfer coefficients for the clothed manikin were larger than those of naked manikin. (A. Virgílio M. Oliveira et al., 2006) measured the convective heat transfer coefficient for an extremely thick clothing ensemble. (Watanabe et al., 2008) studied the effect of air velocity and wind direction on the convective heat transfer coefficient for different fitness of clothing. (Sato et al., 2011) reported that convective heat transfer coefficients for thermal manikin wearing in T-shirt, sweater, and jacket showed no difference.

1.2.3 Clothing insulation

Putting on clothing with suitable thermal insulation is one of the most crucial behavioral actions, which help humans survive in most of the climates available on Earth (Psikuta et al., 2017). (Gagge et al., 1941) suggested the concept of 'clo' to represent the thermal resistance of the clothing, which was called 'clothing insulation'. The vast majority of results about whole-body clothing insulation were reported based on subject experiments or thermal manikin experiments (G. Havenith et al., 1990; Holmer et al., 1999; McCullough & Jones, 1985; Nishi et al., 1978; Winslow et al., 1939). Besides, there are comprehensive data on clothing insulation available in international standards ("Chapter 9," 2017; ISO 7730, 2005; ISO 9920, 2007). However, the clothing insulation in these databases is based on experiments several decades ago. Furthermore, the clothing ensembles listed in these databases are not suitable for all kinds of clothing styles or types. To remedy this deficiency,

three different laboratories presented clothing insulation of non-western ensembles for use in ASHRAE Standard 55, ISO 7730, and ISO 9920 through manikin experiments (George Havenith et al., 2015). However, the efforts of completing the database on clothing insulation is far from enough. With the development of segmented thermal manikin and the need of evaluating thermal sensation at individual body segment, the clothing insulation for the different body segment was measured in several studies (Lee et al., 2013; Lu et al., 2015; Oguro et al., 2002).

There has also been a great discussion about the calculation method for clothing insulation. (Tanabe et al., 1994) compared four methods for measuring clothing insulation on the thermal manikin. (A. V. M. Oliveira et al., 2008) investigated the effect of manikin control mode on the results of clothing insulation.

Airflow always exists because of natural ventilation or air-conditioning. Besides, human activity is always changing, or sitting, or standing, or walking. Therefore, studies about the effect of airspeed, wind direction, waking etc. on clothing insulation were carried out (G. Havenith et al., 1990; Młynarczyk, 2019; Morrissey & Rossi, 2014; Watanabe et al., 2007).

1.3 *Current issues*

Under the background of the previous section, the current issues on the research of convective and radiative heat transfer coefficients, and clothing insulation for the human body are given below.

Concerning the radiative heat transfer coefficient, there is a large gap between the results of the various studies. The reason should be figured out. In addition, the radiative heat transfer coefficient for different postures at the local body segment is limited. Furthermore, there has been little research done on the radiative heat transfer coefficient for the clothed human body.

Concerning the convective heat transfer coefficient, the discussion is divided into the naked human body and the clothed human body. For the naked human body, although the effect of wind directions on the convective heat transfer coefficient was investigated a lot. Little attention has been given to the effect of vertical airflow on the convective heat transfer coefficient. Besides, there are very few reports on the prediction equation for the convective heat transfer coefficient considering both environmental temperature and airspeed. For the equation for calculating convective heat transfer coefficient provided by ASHRAE, the larger of $h_c = 2.38V(t_{cl} - t_a)^{0.25}$ and $h_c = 12.1V^{0.5}$ is selected. For the convective heat transfer coefficient for the clothed human body, limited study has been done through manikin experiments. And kinds of studied clothing ensemble were very few. The characteristics of the convective heat transfer coefficient for the clothed human body still remain controversial. Also, few studies have attempted to investigate the clothing convective heat transfer coefficient through CFD analysis.

Concerning the clothing insulation, although there are comprehensive data about clothing insulation values in the literature and standards. The measurement data on clothing insulation was extremely old. Moreover, the data for local clothing insulation (clothing insulation for different body segments) is still lacking.

1.4 Research objective

In the present study, convective and radiative heat transfer coefficients for eight sets of clothing ensembles were measured through both the manikin experiments and CFD analysis. Additionally, clothing insulations for these clothing ensembles were measured.

The present study puts its focus on points as follows.

- (1) The effect of air velocity, wind direction, and environmental temperature on convective and radiative heat transfer coefficients for the naked manikin will be investigated in detail.
- (2) The characteristics of the convective and radiative heat transfer coefficients for the clothed manikin will be discussed.
- (3) The effects of air velocity, wind direction, and posture on clothing insulation will be confirmed.
- (4) The prediction model of convective heat transfer coefficients and clothing insulations for the whole-body and different body segments will be proposed.
- (5) Confirm how the convective heat transfer coefficients and clothing insulation affect the prediction of thermal comfort.

1.5 Structure of this thesis

The structure of this thesis is presented in Figure 1-3. This thesis consists of four main parts: introduction, research methods, main body, and conclusion.

In the introduction (Chapter 1), the research background will be explained, and the research objectives will be presented.

For the description of the research methodology, firstly, the necessary knowledge about the heat transfer coefficients, clothing insulation, and thermal comfort index, will be introduced (Chapter 2). Secondly, the basic theory of numerical analysis and the experimental methods necessary for conducting this research will be described (Chapter 3).

In the main body, the core content of the thesis will be reported. Initially, convective and radiative heat transfer coefficients for the naked manikin and the clothed manikin will be described based on experiment and CFD analysis (Chapter 4 and Chapter 5). Secondly, the results of clothing insulation through manikin experiments will be detailed (Chapter 6). Thirdly, the effect of convective heat transfer coefficient and clothing insulation on several thermal comfort indexes will be discussed (Chapter 7).

In the conclusions (Chapter 8), the findings of this study will be summarized, and the remaining research issues will be indicated.

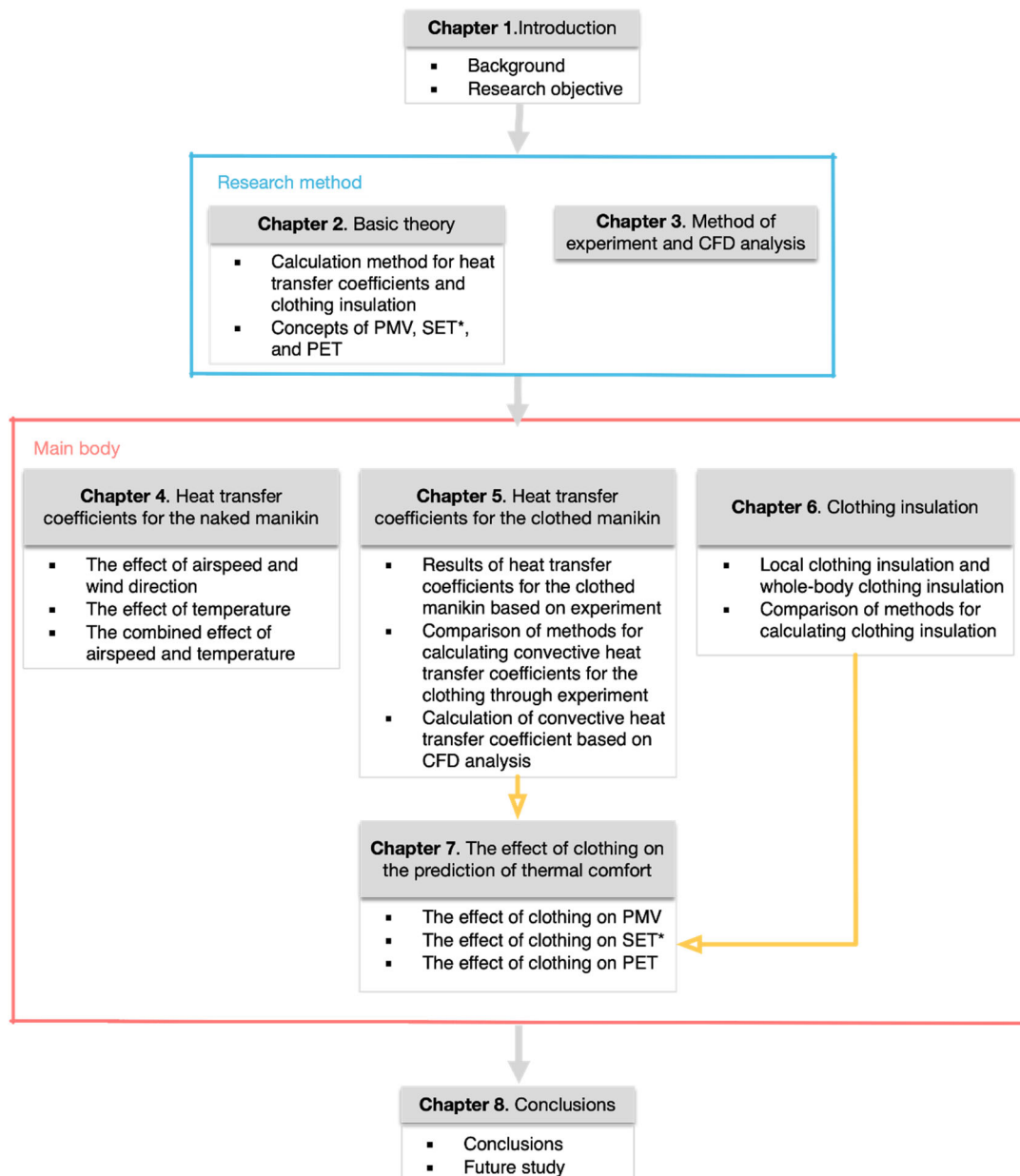


Figure 1-3. Structure of this thesis.

Reference

- Chapter 9. (2017). In *ASHRAE handbook Fundamentals* (pp. 9.1-9.30).
<https://www.ashrae.org/technical-resources/ashrae-handbook/description-2017-ashrae-handbook-fundamentals>
- Clark, R. P., & Toy, N. (1975). Forced convection around the human head. *The Journal of Physiology*, 244(2), 295–302. <https://doi.org/10.1113/jphysiol.1975.sp010798>
- Colin, J., & Houdas, Y. (1967). Experimental determination of coefficient of heat exchanges by convection of human body. *Journal of Applied Physiology*, 22(1), 31–38.
<https://doi.org/10.1152/jappl.1967.22.1.31>
- De Dear, R. J., Arens, E., Hui, Z., & Oguero, M. (1997). Convective and radiative heat transfer coefficients for individual human body segments. *International Journal of Biometeorology*, 40(3), 141–156. <https://doi.org/10.1007/s004840050035>
- Gagge, A. P., Burton, A. C., & Bazett, H. C. (1941). A practical system of units for the description of the heat exchange of man with his environment. *Science*, 94(2445), 428–430.
<https://doi.org/10.1126/science.94.2445.428>
- Gao, N. P., & Niu, J. L. (2005). CFD study of the thermal environment around a human body: A Review. *Indoor and Built Environment*, 14(1), 5–16. <https://doi.org/10.1177/1420326X05050132>
- Havenith, G., HEUS, R., & Lotens, W. A. (1990). Resultant clothing insulation: a function of body movement, posture, wind, clothing fit and ensemble thickness. *Ergonomics*, 33(1), 67–84.
<https://doi.org/10.1080/00140139008927094>
- Havenith, George, Lundgren, K., Fan, J., Hodder, S., Loveday, D., Ouzzahra, Y., Kuklane, K., Lundgren, K., Fan, J., Au, Y., Hodder, S., & Loveday, D. (2015). A database of static clothing thermal insulation and vapor permeability values of non-western ensembles for use in ASHRAE Standard 55, ISO 7730, and ISO 9920. *ASHRAE Transactions*, 121, 197–215.
- Holmer, I., Nilsson, H., Havenith, G., & Parsons, K. (1999). Clothing convective heat exchange—proposal for improved prediction in standards and models. *The Annals of Occupational Hygiene*, 43(5), 329–337. <https://doi.org/10.1093/annhyg/43.5.329>
- Ichihara, M., Saitou, M., Nishimura, M., & Tanabe, S. (1997). Measurement of convective and radiative heat transfer coefficients of standing and sitting human body by using a thermal manikin (in Japanese). *Journal of Architecture and Planning (Transactions of AIJ)*, 62(501), 45–51. https://doi.org/10.3130/aija.62.45_5
- ISO 7730. (2005). *Ergonomics of the thermal environment — Analytical determination and interpretation of thermal comfort using calculation of the PMV and PPD indices and local thermal comfort criteria*. <https://www.iso.org/standard/39155.html>
- ISO 9920. (2007). *Ergonomics of the thermal environment — Estimation of thermal insulation and water vapour resistance of a clothing ensemble*. <https://www.iso.org/standard/39257.html>
- Kurazumi, Y., Tsuchikawa, T., Ishii, J., Fukagawa, K., Yamato, Y., & Matsubara, N. (2008). Radiative and convective heat transfer coefficients of the human body in natural convection. *Building and*

- Environment*, 43(12), 2142–2153. <https://doi.org/10.1016/j.buildenv.2007.12.012>
- Lee, J., Zhang, H., & Arens, E. (2013). Typical clothing ensemble insulation levels for sixteen body parts. *CLIMA Conference 2013*. <https://escholarship.org/uc/item/18f0r375>
- Licina, D., Melikov, A., Pantelic, J., Sekhar, C., & Tham, K. W. (2015). Human convection flow in spaces with and without ventilation: Personal exposure to floor-released particles and cough-released droplets. *Indoor Air*, 25(6), 672–682. <https://doi.org/10.1111/ina.12177>
- Licina, D., Melikov, A., Sekhar, C., & Tham, K. W. (2015). Human convective boundary layer and its interaction with room ventilation flow. *Indoor Air*, 25(1), 21–35. <https://doi.org/10.1111/ina.12120>
- Lu, Y., Wang, F., Wan, X., Song, G., Zhang, C., Shi, W., & Zhang, C. (2015). Clothing resultant thermal insulation determined on a movable thermal manikin. Part II: effects of wind and body movement on local insulation. *International Journal of Biometeorology*, 59(10), 1487–1498. <https://doi.org/10.1007/s00484-015-0959-0>
- Martinho, N., Lopes, A., & Gameiro da Silva, M. (2012). Evaluation of errors on the CFD computation of air flow and heat transfer around the human body. *Building and Environment*, 58, 58–69. <https://doi.org/10.1016/j.buildenv.2012.06.018>
- McCullough, E. A., & Jones, B. W. (1985). A comprehensive data base for estimating clothing insulation. *ASHRAE Transactions*, 91, 29–47.
- Mitchell, D. (1974). Convective heat transfer from man and other animals. In J. L. Monteith & L. E. Mount (Eds.), *Heat Loss from Animals and Man* (pp. 59–76). Elsevier. <https://linkinghub.elsevier.com/retrieve/pii/B978040870652050010X>
- Młynarczyk, M. (2019). Influence of air velocity on the total thermal insulation of different types of clothing. *Fibres and Textiles in Eastern Europe*, 27(6), 75–80. <https://doi.org/10.5604/01.3001.0013.4470>
- Morrissey, M. P., & Rossi, R. M. (2014). The effect of wind, body movement and garment adjustments on the effective thermal resistance of clothing with low and high air permeability insulation. *Textile Research Journal*, 84(6), 583–592. <https://doi.org/10.1177/0040517513499431>
- Murakami, S. (2004). Analysis and design of micro-climate around the human body with respiration by CFD. *Indoor Air*, 14(s7), 144–156. <https://doi.org/10.1111/j.1600-0668.2004.00283.x>
- Najjaran, A., Tahavvor, A. R., Najjaran, A., & Ahmadvard, M. A. (2011). Numerical simulation of radiation heat transfer of the human body for determining its radiation coefficient. *Volume 10: Heat and Mass Transport Processes, Parts A and B, January 2015*, 1149–1154. <https://doi.org/10.1115/IMECE2011-65353>
- Nielsen, M., & Per, L. (1953). Studies on the heat loss by radiation and convection from the clothed human body. *Acta Physiologica Scandinavica*, 27(2–3), 272–294. <https://doi.org/10.1111/j.1748-1716.1953.tb00943.x>
- Nilsson, H. O. (2007). Thermal comfort evaluation with virtual manikin methods. *Building and Environment*, 42(12), 4000–4005. <https://doi.org/10.1016/j.buildenv.2006.04.027>

- Nishi, Y., & Gagge, A. P. (1970). Direct evaluation of convective heat transfer coefficient by naphthalene sublimation. *Journal of Applied Physiology*, 29(6), 830–838.
<https://doi.org/10.1152/jappl.1970.29.6.830>
- Nishi, Y., Gonzalez, R. R., & Gagge, A. P. (1978). Clothing insulation as a biometeorological parameter during rest and exercise. *International Journal of Biometeorology*, 22(3), 177–189.
<https://doi.org/10.1007/BF01555396>
- Oguro, M., Arens, E., de Dear, R., Zhang, H., & Katayama, T. (2002). Convective heat transfer coefficients and clothing insulation for parts of the clothed human body under airflow conditions. *Journal of Architecture and Planning (Transactions of AIJ)*, 67(561), 21–29.
https://doi.org/10.3130/aija.67.21_5
- Oguro, M., Arenz, E., De Dear, R., Zhang, H., & Katayama, T. (2001). Evaluation of the effect of air flow on clothing insulation and on dry heat transfer coefficients for each part of the clothed human body. *Journal of Architecture and Planning (Transactions of AIJ)*, 66(549), 13–21.
<https://doi.org/10.3130/aija.66.13>
- Oh, W., & Kato, S. (2018). The effect of airspeed and wind direction on human's thermal conditions and air distribution around the body. *Building and Environment*, 141(May), 103–116.
<https://doi.org/10.1016/j.buildenv.2018.05.052>
- Oliveira, A. V. M., Branco, V. J., Gaspar, A. R., & Quintela, D. A. (2008). Measuring thermal insulation of clothing with different manikin control methods. *7th International Thermal Manikin and Modelling Meeting*.
- Oliveira, A. Virgilio M., Gaspar, A. R., & Quintela, D. A. (2006). Convective heat transfer from a clothed manikin. *Windsor International Conference - Comfort and Energy Use in Buildings: Getting Them Right*. <https://www.researchgate.net/publication/237778232>
- Psikuta, A., Allegrini, J., Koelblen, B., Bogdan, A., Annaheim, S., Martínez, N., Derome, D., Carmeliet, J., & Rossi, R. M. (2017). Thermal manikins controlled by human thermoregulation models for energy efficiency and thermal comfort research – A review. *Renewable and Sustainable Energy Reviews*, 78(April), 1315–1330. <https://doi.org/10.1016/j.rser.2017.04.115>
- Sato, K., Kurabuchi, T., Ogasawara, T., Ohba, M., Iwamoto, S., Sahashi, N., & Ikehara, S. (2011). A study on the convective heat transfer coefficient and thermal resistance of clothing under cross ventilation. *International Journal of Ventilation*, 10(2), 155–162.
<https://doi.org/10.1080/14733315.2011.11683944>
- Seppanen, O. (1972). Thermal insulating values for typical indoor clothing ensembles. *ASHRAE Trans.*, 78(1), 120–130.
- Sørensen, D. N. (2002). Radiation between segments of the seated human body. *Roomvent 2002- 8th International Conference on Air Distribution in Rooms: Individually Controlled Environment*.
<https://orbit.dtu.dk/en/publications/radiation-between-segments-of-the-seated-human-body>
- Sørensen, D. N., & Voigt, L. K. (2003). Modelling flow and heat transfer around a seated human body by computational fluid dynamics. *Building and Environment*, 38(6), 753–762.

- [https://doi.org/10.1016/S0360-1323\(03\)00027-1](https://doi.org/10.1016/S0360-1323(03)00027-1)
- Tanabe, S., Hasebe, Y., & Nishimura, M. (1994). Comparison of calculation methods for basic clothing insulation with a thermal manikin (in Japanese). *Sen'i Gakkaishi*, 50(4), 180–187.
https://doi.org/10.2115/fiber.50.4_180
- Topp, C., Nielsen, P. V., & Sørensen, D. N. (2002). Application of computer simulated persons in indoor environmental modeling. *ASHRAE Transactions*, 108(2), 1084–1089.
- Voelker, C., & Alsaad, H. (2018). Simulating the human body's microclimate using automatic coupling of CFD and an advanced thermoregulation model. *Indoor Air*, 28(3), 415–425.
<https://doi.org/10.1111/ina.12451>
- Watanabe, S., Horikoshi, T., Ishii, J., Uno, Y., Kaneko, T., & Tomita, A. (2008). Effect of wind velocities and wind directions on forced convective heat transfer coefficients for human body bu using thermal manikin (in Japanese). *Journal of Environmental Engineering (Transactions of AIJ)*, 73(629), 887–893. <https://doi.org/10.3130/aije.73.887>
- Watanabe, S., Horikoshi, T., Kaneko, T., Uno, Y., Ishii, J., & Tomita, A. (2007). Effect of wind velocity and wind direction on thermal insulation values of clothing ensembles by using thermal manikin. *Journal of Environmental Engineering (Transactions of AIJ)*, 72(621), 23–28.
https://doi.org/10.3130/aije.72.23_4
- Winslow, C.-E. A., Gagge, A. P., & Herrington, L. P. (1939). The influence of air movement upon heat losses from the clothed human body. *American Journal of Physiology*, 127(3), 505–518.
- Yang, J.-H., Kato, S., Hayashi, T., & Murakami, S. (2004). Measurement of convective heat transfer coefficients with using an experimental and computational thermal manikin in indoor environments (in Japanese). *Journal of Environmental Engineering (Transactions of AIJ)*, 69(584), 33–40. https://doi.org/10.3130/aije.69.33_3
- Yang, J., Kato, S., & Seo, J. (2009). Evaluation of the convective heat transfer coefficient of the human body using the wind tunnel and thermal manikin. *Journal of Asian Architecture and Building Engineering*, 8(2), 563–569. <https://doi.org/10.3130/jaabe.8.563>

Chapter 2.

Basic theory

2.1 Heat transfer coefficients

2.1.1 Heat transfer coefficients for the naked manikin

Heat dissipates from the human body to the immediate surroundings through several models of heat exchange can be expressed by Equation (2-1).

$$M - W = (C + R + E_{sk}) + (C_{res} + E_{res}) + (S_{sk} + S_{cr}) \quad (2-1)$$

In the present research, only sensible heat transfer was taken into consideration (2-2).

$$q_{t,i} = q_{c,i} + q_{r,i} \quad (2-2)$$

Therefore, the convective heat transfer coefficient and radiative heat transfer coefficient can respectively be calculated using Equation (2-3) and (2-4).

$$q_{c,i} = h_{c,i}(t_{sk,i} - t_a) \quad (2-3)$$

and

$$q_{r,i} = h_{r,i}(t_{sk,i} - t_r) \quad (2-4)$$

The average wall temperature t_r is calculated using Equation (2-5).

$$t_r = \frac{\sum_{j=1}^6 S_j \cdot t_{w,j}}{\sum_{j=1}^6 S_j} \quad (2-5)$$

The calculation process for convective and radiative heat transfer coefficients for the naked manikin is shown in Figure 2-1.

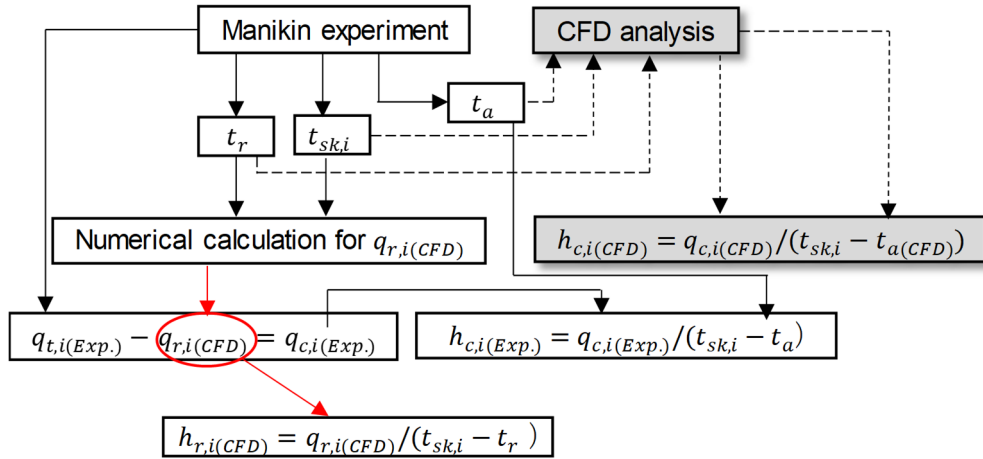


Figure 2-1. The calculation process for convective and radiative heat transfer coefficients for the naked manikin.

2.1.2 Heat transfer coefficients for the clothed manikin

2.1.2.1 Method 1

The sensible heat loss can be divided into convective heat loss and radiative heat loss similar to the naked manikin (Equation (2-6)).

$$q_{t,i_{cl}} = q_{c,i_{cl}} + q_{r,i_{cl}} \quad (2-6)$$

$q_{t,i_{cl}}$ was recorded through the control software of the thermal manikin. $q_{r,i_{cl}}$ was calculated

using Equation (2-7).

$$q_{r,i_cl} = \sigma \varepsilon f_{eff} \left[(t_{cl,i} + 273.15)^4 - (t_r + 273.15)^4 \right] \quad (2-7)$$

where, f_{eff} is the view factor (effective radiation area factor for each body segment) [1]. The view factor was calculated using the surface-to-surface radiation model of commercial CFD code STAR-CCM+ ver. 12.02, based on the geometry of the thermal manikin and the wind tunnel or the climate chamber.

Therefore, the convective heat transfer coefficient and radiative heat transfer coefficient for the clothed manikin were calculated with Equation (2-8) and Equation (2-9), respectively.

$$h_{c,i_cl} = \frac{q_{t,i_cl} - q_{r,i_cl}}{(t_{cl,i} - t_a)} \quad (2-8)$$

$$h_{r,i_cl} = \sigma \varepsilon f_{eff} \left[(t_{cl,i} + 273.15)^2 + (t_r + 273.15)^2 \right] \left[(t_{cl,i} + 273.15) + (t_r + 273.15) \right] \quad (2-9)$$

The whole-body convective and radiative heat transfer coefficients were calculated using Equation (2-10) and Equation (2-11), respectively.

$$h_{c_cl} = \sum \alpha_i \cdot h_{c,i_cl} \quad (2-10)$$

$$h_{r_cl} = \sum \alpha_i \cdot h_{r,i_cl} \quad (2-11)$$

2.1.2.2 Method 2

In method 1, the surface temperature of the clothing was directly measured with thermocouples. The surface temperature of the clothing can also be predicted by the sensible heat loss and clothing insulation (Equation (2-12)) [2]. q_t was based on experiment.

$$t_{cl} = t_{sk} - q_t I_{cl} \quad (2-12)$$

2.1.2.3 Method 3

In ISO 7730, the convective heat transfer coefficients for different clothing ensembles are assumed to be the same and are calculated using Equation (2-13) [3].

$$h_{c_cl} = \begin{cases} f_{cl} \cdot 2.38 \cdot |t_{cl} - t_a|^{0.25} & \text{for } 2.38 \cdot |t_{cl} - t_a|^{0.25} > 12.1V^{0.5} \\ f_{cl} \cdot 12.1V^{0.5} & \text{for } 2.38 \cdot |t_{cl} - t_a|^{0.25} < 12.1V^{0.5} \end{cases} \quad (2-13)$$

2.2 Clothing insulation

In the present study, four methods for calculating the clothing insulation were compared.

Method A, the basic clothing insulation was directly calculated with the measured clothing surface temperature (Equation (2-14)).

Method B, the basic clothing insulation I_{cl} was calculated by subtracting the air insulation I_a from the total insulation I_t (Equation (2-16)).

Method C, the basic clothing insulation I_{cl} was calculated by referring to the thermal insulation for individual garments provided by ISO 9920 (Equation (2-17)).

Method D, the basic clothing insulation, was defined by finding similar clothing ensembles in ASHRAE Handbook [4].

2.2.1 Method A

The basic insulation for clothing segment i was calculated using Equation (2-14) [5].

$$I_{cl,i} = \frac{t_{sk,i} - t_{cl,i}}{q_{t,i,cl} \cdot 0.155} \quad (2-14)$$

The whole-body basic clothing insulation was calculated using (2-15) [5].

$$\frac{1}{I_{cl}} = \sum \frac{\alpha_i}{I_{cl,i}} \quad (2-15)$$

The calculation procedures for clothing heat transfer coefficients and clothing insulation (Method A) are shown in Figure 2-2.

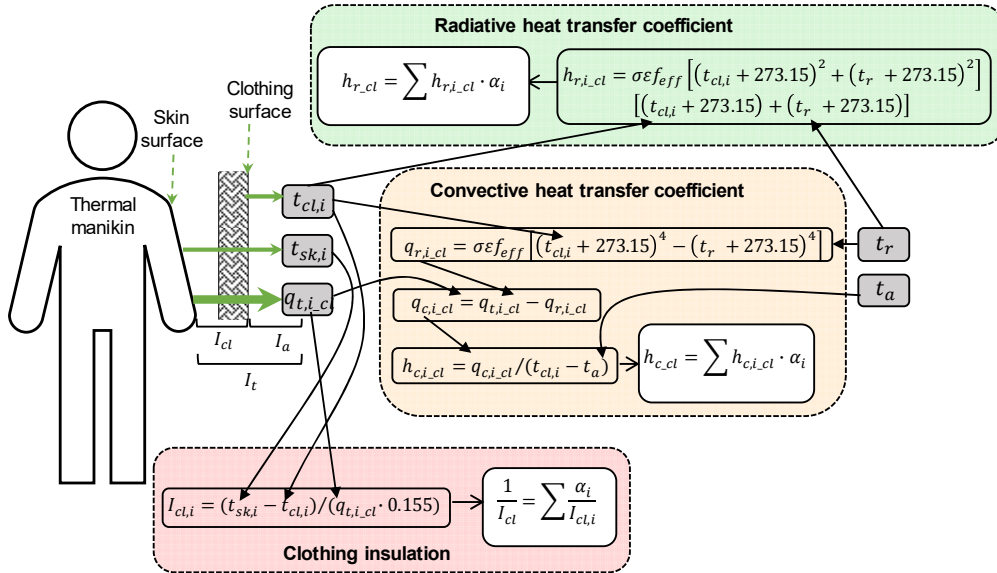


Figure 2-2. The calculation procedures for clothing heat transfer coefficients and clothing insulation (Method A).

2.2.2 Method B

The basic insulation I_{cl} can also be calculated using Equation (2-16), where I_t is the total

insulation, I_a is the air insulation. I_a is measured with the naked manikin under the same condition used while measuring I_t . However, when there is a significant temperature difference between the naked and clothed surface, the air insulation I_a from the naked manikin should not be used for the clothed manikin [6]. Therefore, to attain a more precise result of basic insulation, the direct method was used in this study (Equation (2-14)).

$$I_{cl} = I_t - \frac{I_a}{f_{cl}} \quad (2-16)$$

2.2.3 Method C

When the manikin experiment cannot be performed, ISO 9920 provides the database of the basic insulation for various individual garments (I_{clu}). Table 2-1 lists the type number and basic insulation for individual garments measured in this study by referring to Annex B of ISO 9920 [5].

Table 2-1. Type number and thermal insulation for individual garments according to ISO 9920 (Annex B).

	Socks		Shoes		Panty		Bra		Shirt		Trousers		Jacket	
	No.	I_{clu} (clo)	No.	I_{clu} (clo)	No.	I_{clu} (clo)	No.	I_{clu} (clo)	No.	I_{clu} (clo)	No.	I_{clu} (clo)	No.	I_{clu} (clo)
E1	252	0.11	262	0.02	1	0.03	2	0.01	30	0.08	106	0.19	152	0.21
E2	252	0.11	262	0.02	1	0.03	2	0.01	30	0.08	90	0.24	172	0.46
E3	252	0.11	262	0.02	1	0.03	2	0.01	30	0.08	90	0.24	142	0.36
E4	252	0.11	262	0.02	1	0.03	2	0.01	30	0.08	90	0.24	152	0.21
E5	252	0.11	262	0.02	1	0.03	2	0.01	30	0.08	90	0.24	151	0.26
E6	252	0.11	262	0.02	1	0.03	2	0.01	30	0.08	90	0.24	152	0.21
E7	252	0.11	262	0.02	1	0.03	2	0.01	30	0.08	90	0.24	151	0.26
E8	252	0.11	262	0.02	1	0.03	2	0.01	30	0.08	90	0.24	151	0.26

The basic insulation for the whole-body could be estimated with Equation (2-17) [5].

$$I_{cl} = 0.161 + 0.835 \sum I_{clu} \quad (2-17)$$

When there is the wind, corrections for air velocity shall be applied (Equation (2-18)).

$$I_{cl,r} = CFV_{cl} \cdot I_{cl} \quad (2-18)$$

2.2.4 Method D

A more simplified way to define clothing insulation is to utilize the clothing insulation (comparable to the ones in question) provided by clothing insulation database. Several databases of clothing insulation provide clothing insulation for typical clothing ensembles [4,5]. The clothing ensembles in this study consisted of trousers, shirts, and coats. Through comparing to the clothing ensembles listed in ASHRAE Handbook, the clothing insulation was assumed to 0.96 clo shown in Table 2-2 in blue.

Table 2-2. Typical insulation and permeability values for western clothing ensembles [4].

Ensemble description ^a	I_{cl} (clo)	I_t^b (clo)	f_{cl}	i_{cl}	i_m^b
Walking shorts, short-sleeved shirt	0.36	1.02	1.10	0.34	0.42
Trousers, short-sleeved shirt	0.57	1.20	1.15	0.36	0.43
Trousers, long-sleeved shirt	0.61	1.21	1.20	0.41	0.45
Same as above, plus suit jacket	0.96	1.54	1.23		
Same as above, plus vest and T-shirt	1.14	1.69	1.32	0.32	0.37
Trousers, long-sleeved shirt, long-sleeved sweater, T-shirt	1.01	1.56	1.28		
Same as above, plus suit jacket and long underwear bottoms	1.30	1.83	1.33		
Sweat pants, sweat shirt	0.74	1.35	1.19	0.41	0.45
Long-sleeved pajama top, long pajama trousers, short 3/4 sleeved robe, slippers (no socks)	0.96	1.50	1.32	0.37	0.41
Knee-length skirt, short-sleeved shirt, panty hose, sandals	0.54	1.10	1.26		
Knee-length skirt, long-sleeved shirt, full slip, panty hose	0.67	1.22	1.29		
Knee-length skirt, long-sleeved shirt, half slip, panty hose, long-sleeved sweater	1.10	1.59	1.46		
Same as above, replace sweater with suit jacket	1.04	1.60	1.30	0.35	0.40
Ankle-length skirt, long-sleeved shirt, suit jacket, panty hose	1.10	1.59	1.46		
Long-sleeved coveralls, T-shirt	0.72	1.30	1.23		
Overalls, long-sleeved shirt, T-shirt	0.89	1.46	1.27	0.35	0.40
Insulated coveralls, long-sleeved thermal underwear, long underwear bottoms	1.37	1.94	1.26	0.35	0.39

Source: From McCullough and Jones (1984) [7] and McCullough et al. (1989) [8].

^aAll ensembles include shoes and briefs or panties. All ensembles except those with panty hose include socks unless otherwise noted.

^bFor $t_r = t_a$ and air velocity less than $0.2 \text{ m}\cdot\text{s}^{-1}$ ($I_a = 0.72 \text{ clo}$ and $I_m = 0.48$ when nude).
1 clo = $0.155 \text{ W}\cdot\text{m}^{-2}\cdot\text{K}^{-1}$.

2.3 Prediction of thermal comfort

2.3.1 PMV

The (predicted mean vote) PMV index predicts the average response of a large group of people according to the ASHRAE seven points thermal sensation scale [4]. PMV is calculated based on the heat balance equation (Equation (2-1) listed in Section 2.1.1). The PMV index is limited to a steady-state. Hence, no heat storage occurs. In other words, $S_{sk} + S_{cr} = 0$.

The paths of heat loss from the human body are shown in Figure 2-3.

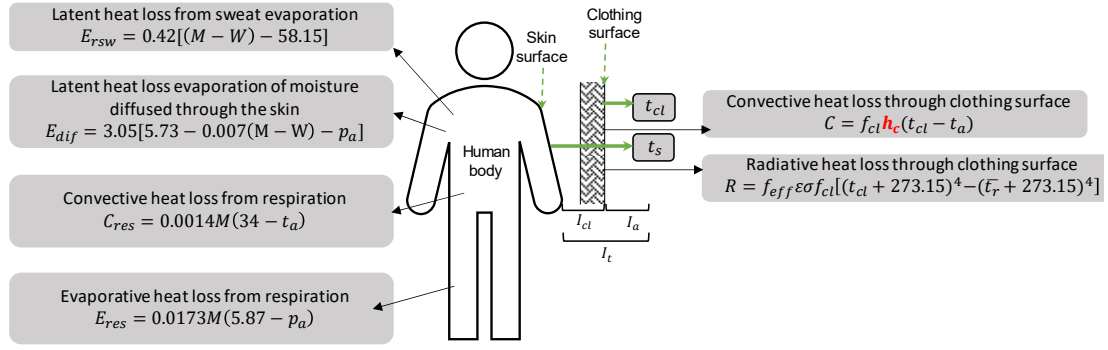


Figure 2-3. The paths of heat loss from the human body.

By substituting equations shown in Figure 2-3 to Equation (2-1), the equation combining the environmental and personal variables can be expressed as follows [4]:

$$M - W = 3.96 \times 10^{-8} f_{cl} [(t_{cl} + 273)^4 - (\bar{t}_r + 273)^4] + f_{cl} h_c (t_{cl} - t_a) + 3.05 [5.73 - 0.007(M - W) - p_a] + 0.42 [(M - W) - 58.15] + 0.0173M(5.87 - p_a) + 0.0014M(34 - t_a) \quad (2-19)$$

When calculating the PMV index, t_{cl} is predicted with equation (2-20).

$$t_{cl} = 35.7 - 0.0275(M - W) - R_{cl} \{ 39.6 \times 10^{-9} f_{cl} [(t_{cl} + 273)^4 - (\bar{t}_r + 273)^4] + f_{cl} h_c (t_{cl} - t_a) \} \quad (2-20)$$

$$h_c = \begin{cases} 2.38(t_{cl} - t_a)^{0.25} & \text{for } 2.38(t_{cl} - t_a)^{0.25} > 12.1\sqrt{V} \\ 12.1\sqrt{V} & \text{for } 2.38(t_{cl} - t_a)^{0.25} < 12.1\sqrt{V} \end{cases} \quad (2-21)$$

$$f_{cl} = \begin{cases} 1.0 + 0.2I_{cl} & I_{cl} < 0.5 \text{ clo} \\ 1.05 + 0.1I_{cl} & I_{cl} > 0.5 \text{ clo} \end{cases} \quad (2-22)$$

Fanger related PMV to the imbalance between the actual heat flow from the body in a given environment (the right side of Equation (2-19)) and the heat flow required for optimum comfort at the specified activity (the left side of Equation (2-19)) through a large number of experiments.

The relationship between the imbalance and PMV value is concluded by equation (2-23).

$$PMV = [0.303 \exp(-0.036M) + 0.028]L \quad (2-23)$$

where, $L = \text{Left side of Equation (2-19)} - \text{Right side of Equation (2-19)}$.

2.3.2 SET*

The new standard effective temperature (SET*) converts the air temperature, mean radiant temperature, airspeed, and relative humidity of a real environment into a theoretical dry-bulb temperature considering the clothing and metabolic heat production. SET* is termed as the equivalent air temperature of an standard environment at a relative humidity (RH) 50% in which a subject, wearing clothing standardized for the activity concerned, has the same heat stress (skin temperature) and thermoregulatory strain (skin wettedness) as in the actual environment [9]. The SET* was developed based on two-node model of thermal regulation shown in Figure 2-4 [4,10,11]. Figure 2-5 illustrates the calculation procedure for the two-node model and the SET*.

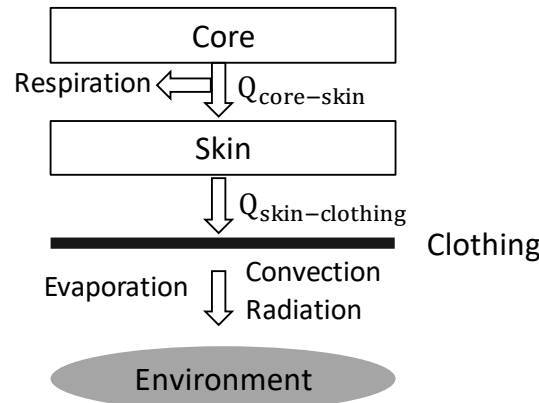


Figure 2-4. The schematic for two-node model.

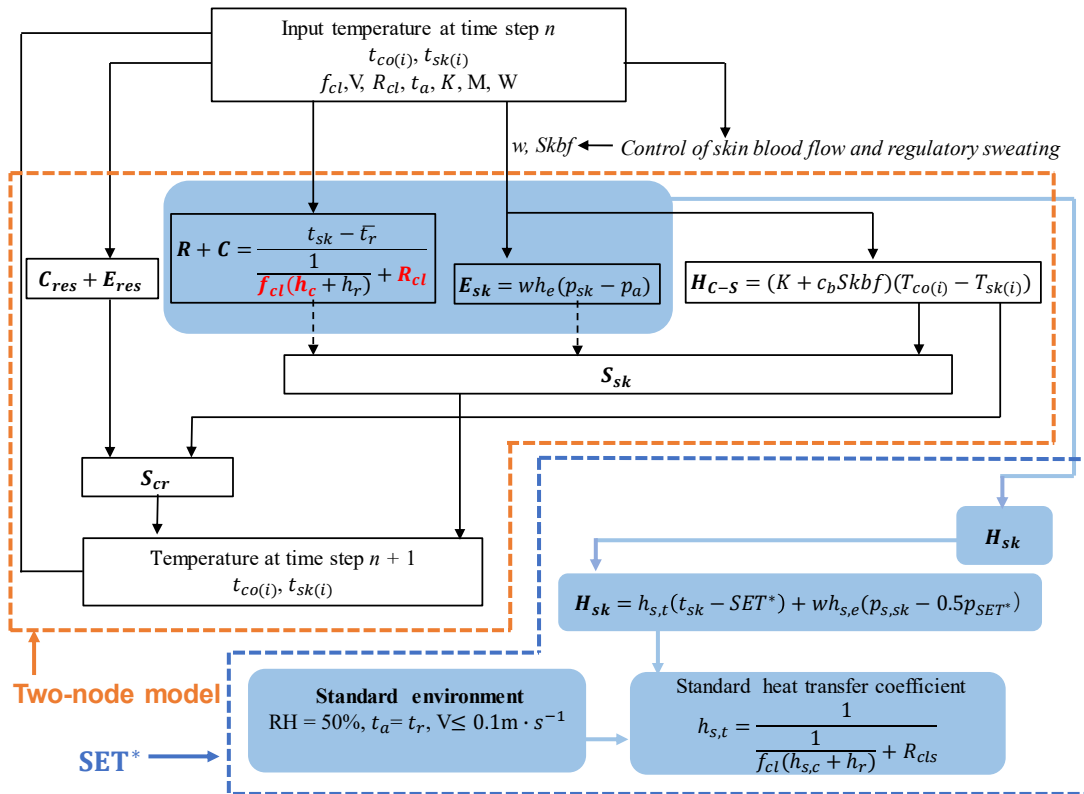


Figure 2-5. Calculation procedure of the two-node model and SET*.

2.3.3 PET

The physiological equivalent temperature (PET) is defined as the air temperature at which, in a typical indoor environment (free of wind and solar radiation), core temperature and skin temperature are same with those in the complex outdoor environments to be assessed [12]. Therefore, a layperson can compare the thermal condition of outdoor with his own experience indoors. The PET was proposed by Hoppe and Mayer, and modified by Walther and Goestchel, and usually, be used to evaluate the outdoor environment [13–15].

The prediction of PET is mainly based on Equation (2-24), Equation (2-25) and Equation (2-26) [12]. T_{co} and T_{sk} resulting from the studied environment are calculated with Equation (2-24), Equation (2-25) and Equation (2-26). The calculated T_{co} and T_{sk} are inserted to the equation system for T_a (with $V = 0.1 \text{ m}\cdot\text{s}^{-1}$, $\text{RH}=50\%$, $T_{MRT} = T_a$). The air temperature T_a obtained is PET.

$$M + W + R + C + E_{diff} + E_{rsw} + Q_{resp} + S = 0 \quad (2-24)$$

$$F_{CS} = v_b \rho_b c_b (t_{co} - t_{sk}) \quad (2-25)$$

$$F_{SC} = (1/I_{cl}) / (t_{sk} - t_{cl}) \quad (2-26)$$

The PET is also developed based on two-node model, and the schematic is shown in Figure 2-6 [15].

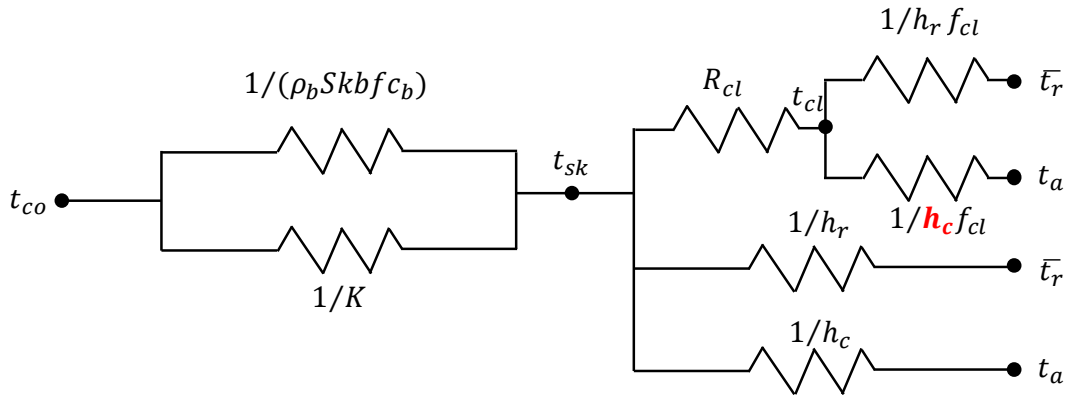


Figure 2-6. The schematic for the PET.

Reference

- [1] D.N. Sørensen, Radiation between segments of the seated human body, in: Roomvent 2002-8th International Conference on Air Distribution in Rooms: Individually Controlled Environment, Denmark, 2002. <https://orbit.dtu.dk/en/publications/radiation-between-segments-of-the-seated-human-body>.
- [2] K. Sato, T. Kurabuchi, T. Ogasawara, M. Ohba, S. Iwamoto, N. Sahashi, S. Ikehara, A study on the convective heat transfer coefficient and thermal resistance of clothing under cross ventilation, *International Journal of Ventilation*. 10 (2011) 155–162. doi:10.1080/14733315.2011.11683944.
- [3] ISO 7730, Ergonomics of the thermal environment — Analytical determination and interpretation of thermal comfort using calculation of the PMV and PPD indices and local thermal comfort criteria, (2005). <https://www.iso.org/standard/39155.html>.
- [4] Chapter 9, in: ASHRAE Handbook Fundamentals, 2017: pp. 9.1-9.30. <https://www.ashrae.org/technical-resources/ashrae-handbook/description-2017-ashrae-handbook-fundamentals>.
- [5] ISO 9920, Ergonomics of the thermal environment — Estimation of thermal insulation and water vapour resistance of a clothing ensemble, (2007). <https://www.iso.org/standard/39257.html>.
- [6] M. Oguro, E. Arens, R. de Dear, H. Zhang, T. Katayama, Convective heat transfer coefficients and clothing insulation for parts of the clothed human body under airflow conditions, *Journal of Architecture and Planning (Transactions of AIJ)*. 67 (2002) 21–29. doi:10.3130/aija.67.21_5.
- [7] E.A. McCullough, B.W. Jones, A comprehensive data base for estimating clothing insulation, *ASHRAE Transactions*. 91 (1985) 29–47.
- [8] E.A. McCullough, B.W. Jones, Tamura Tomaoki, A database for determining the evaporative resistance of clothing, *ASHRAE Transactions*. 95 (1989) 316–328.
- [9] ASHRAE Standard 55-2013: Thermal environmental conditions for human occupancy, 2013. <https://www.ashrae.org/technical-resources/bookstore/standard-55-thermal-environmental-conditions-for-human-occupancy>.
- [10] G. Ye, C. Yang, Y. Chen, Y. Li, A new approach for measuring predicted mean vote (PMV) and standard effective temperature (SET), *Building and Environment*. 38 (2003) 33–44. doi:10.1016/S0360-1323(02)00027-6.
- [11] L.G. Gagge, A. P., Fobelets, A. P. and Berglund, A standard predictive index of human response to thermal environment, *American Society of Heating, Refrigerating and Air-Conditioning Engineers*. 92(2B) (1986) 709–731.
- [12] P. Hoppe, The physiological equivalent temperature - a universal index for the biometeorological assessment of the thermal environment., *International Journal of Biometeorology*. 43 (1999) 71–75.
- [13] C. Deb, R. Alur, The significance of physiological equivalent temperature (PET) in outdoor

- thermal comfort studies, *International Journal of Engineering Science and Technology*. 2 (2010) 2825–2828.
- [14] H. Mayer, P. Höppe, Thermal comfort of man in different urban environments, *Theoretical and Applied Climatology*. 38 (1987) 43–49. doi:10.1007/BF00866252.
- [15] E. Walther, Q. Goestchel, The P.E.T. comfort index: Questioning the model, *Building and Environment*. 137 (2018) 1–10. doi:10.1016/j.buildenv.2018.03.054.

Chapter 3.

Method of experiment and CFD analysis

3.1 *Experimental facility*

3.1.1 *Thermal manikin*

A thermal manikin produced by PT Teknik was occupied in the present study (Figure 3-1) [1]. The height of the manikin is 1.66 m in standing posture, while 1.21 m in sitting posture. The skin surface area is 1.48 m². The shape of the thermal manikin was designed according to the shape of an ordinary female body. There are joints between the leg and the thigh, which can make the leg bend 90°. The cutting heaps of the thighs and the pelvis are carefully chosen to make the thighs move naturally. There are also joints between the shoulder and central body, the hand and arm, the central body and head. All these devices make it easy to change the posture of the manikin.

Pure nickel is placed with a distance of 2.2 mm over each body segment of the thermal manikin and embedded in heat-conducting polyester. Then the heat-conducting polyester is covered by glass fiber and painted with a dull color. The painting of the manikin surface has a similar emissivity with human skin.

The thermal manikin has 16 independent body segments (Table 3-1). There is a control system for each body segment of the thermal manikin. The surface temperature of the thermal manikin can be measured by recording the resistance of the nickel wire. Then the needed power for heat can be calculated according to the surface temperature. The surface temperature is measured 40 times one second. The heat loss of the manikin is updated eight times, based on the average temperature of five times. A connector board connects the control system of each body segment, and this connector board can be connected to the PC (Figure 3-2).

The thermal manikin was well calibrated before the experiments. During the calibration, the manikin was placed in a climate chamber where the temperature can be precisely controlled. The manikin was situated on a mesh chair with very little insulation. And the feet were lifted to avoid air stratification (Figure 3-3). Three fans were placed around the thermal manikin to make the temperature distribution around the manikin much more uniform. For the control mode, the thermal manikin was set to no heat mode. Firstly, the temperature inside the climate chamber was regulated to 20 °C. When the surface temperature for the thermal manikin became the same with the air temperature and stabled, temperature A in the manikin software was set to 20 °C. The manikin was calibrated at the low temperature. Secondly, the air temperature of the climate chamber was set to 33 °C. When the surface temperature for the thermal manikin became the same with the air temperature and stabled again, temperature B in the manikin software was set to 33 °C. In this way, the thermal manikin was calibrated.



Figure 3-1. Thermal manikin.

Table 3-1. Body segment area for the thermal manikin.

Segment	Area (m ²)
10. Head	0.130
9. Back	0.130
8. Chest	0.140
7. Shoulder (L)	0.073
(R)	0.078
6. Arm (L)	0.050
(R)	0.050
5. Pelvis	0.165
4. Hand (L)	0.038
(R)	0.037
3. Thigh (L)	0.165
(R)	0.160
2. Leg (L)	0.090
(R)	0.090
1. Foot (L)	0.043
(R)	0.043
Whole-body	1.483

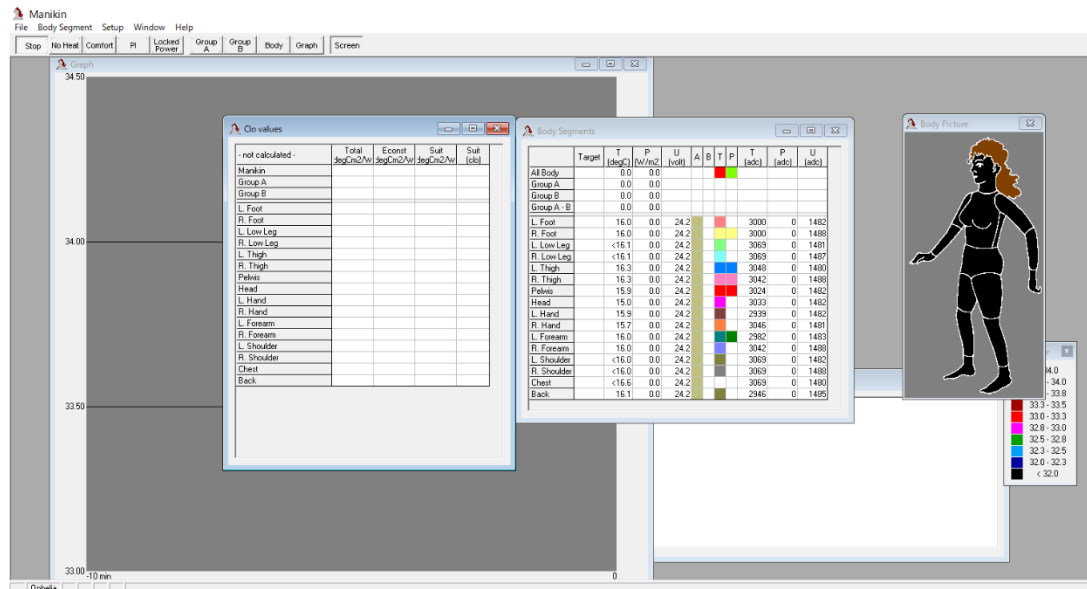


Figure 3-2. The control software for the thermal manikin.



Figure 3-3. Thermal manikin during calibration.

3.1.2 Climate chamber

The climate chamber has a double structure in which an outer chamber of 6.75 m × 4.25 m × 2.9 m has an inner chamber of 3.0 m × 3.5 m × 2.5 m (Figure 3-4 and Figure 3-5). Two unit coolers (for cooling) and one cooling unit for heating are mounted to the ceiling of the outer chamber. The air

blows in through the entire floor surface and blows out through the whole ceiling. The air temperature of the climate chamber can be controlled from $-30\text{ }^{\circ}\text{C}$ to $40\text{ }^{\circ}\text{C}$, with a precision of $0.1\text{ }^{\circ}\text{C}$. The floor of the inner chamber is a perforated stainless sheet covered by carpet. Thus the airflow from the floor is very uniform.

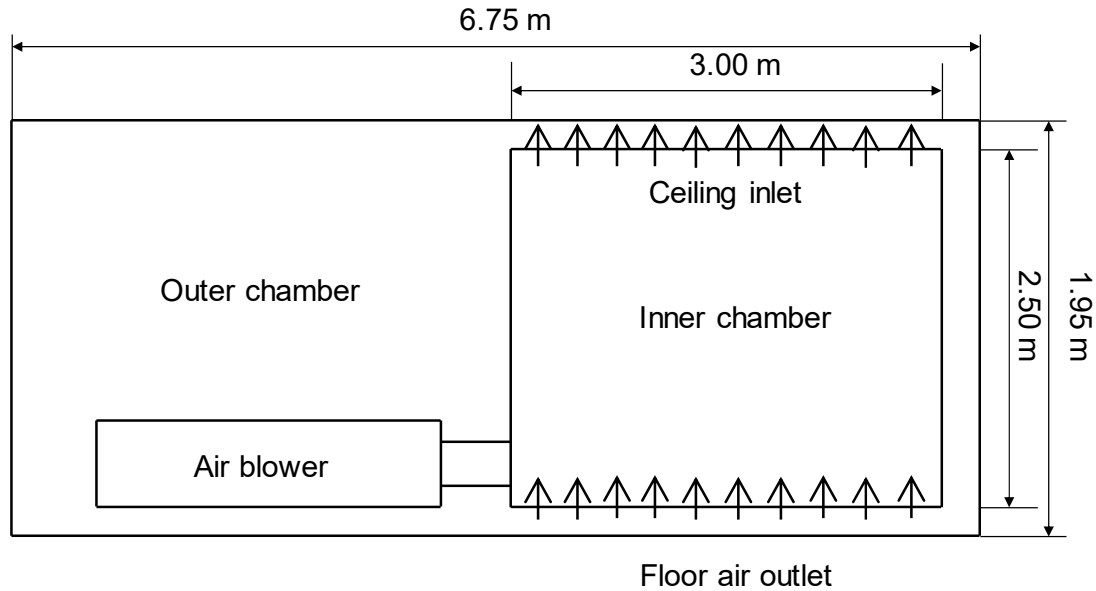


Figure 3-4. Vertical section of the climate chamber.



Figure 3-5. Image of the climate chamber.

3.1.3 Wind tunnel

Figure 3-6 and Figure 3-7 show the overview of the wind tunnel located in Institute of Industrial Science, the University of Tokyo [2]. The fetch length of the wind tunnel is 16 m. The width of the test section is 2.2 m, and the height of the test section is 1.8 m. There are vanes at each corner to eliminate the disturbance factors such as pressure fluctuations during measurement. The wind tunnel is capable of reproducing a wide range of wind speeds from 0.2 to $20\text{ m}\cdot\text{s}^{-1}$.

A 4-axis remote automatic stop type traverse system is installed on the ceiling of the test section (Figure 3-8). The smallest movement is 1 mm. A shaft for attaching a measuring device is attached to the tip of the traverse system. The movement of the traverse system can be controlled by

controlling software.

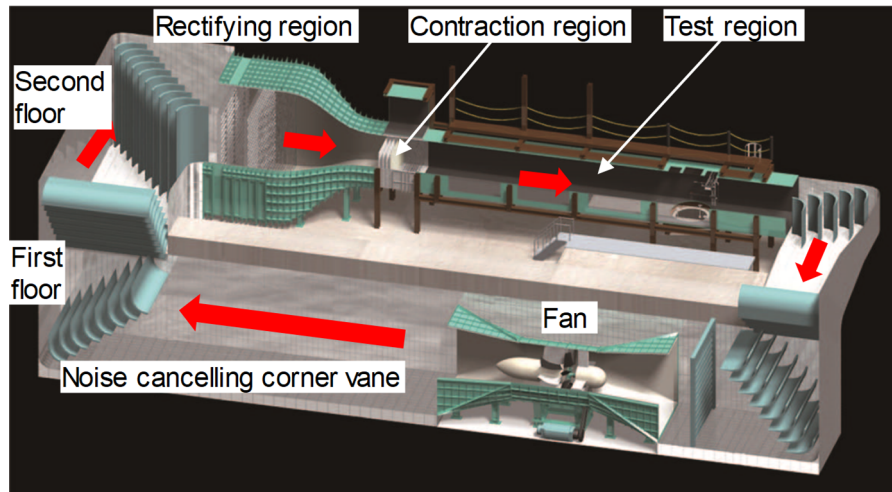


Figure 3-6. Image of the wind tunnel.

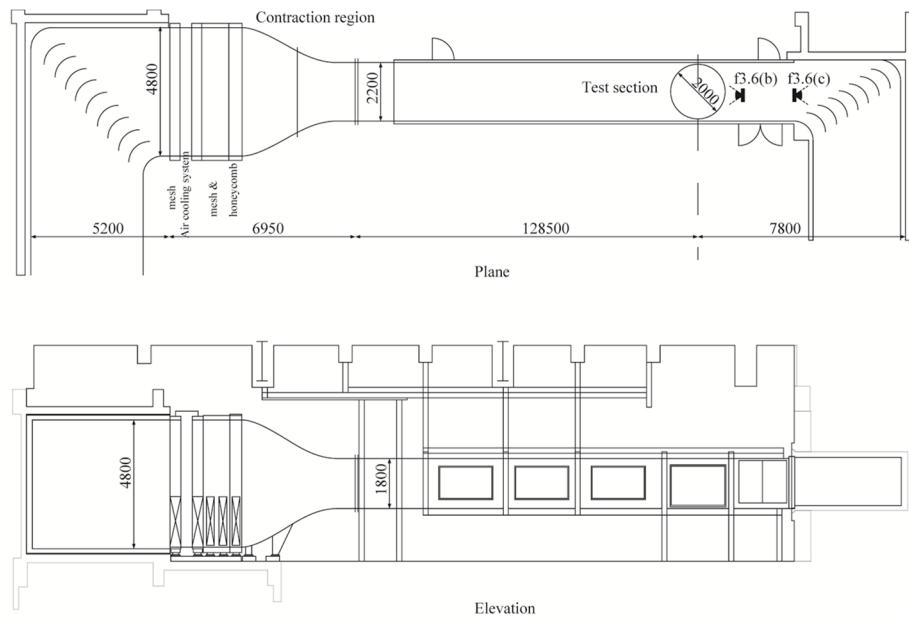


Figure 3-7. Plane view and elevation view for the second floor of the wind tunnel.

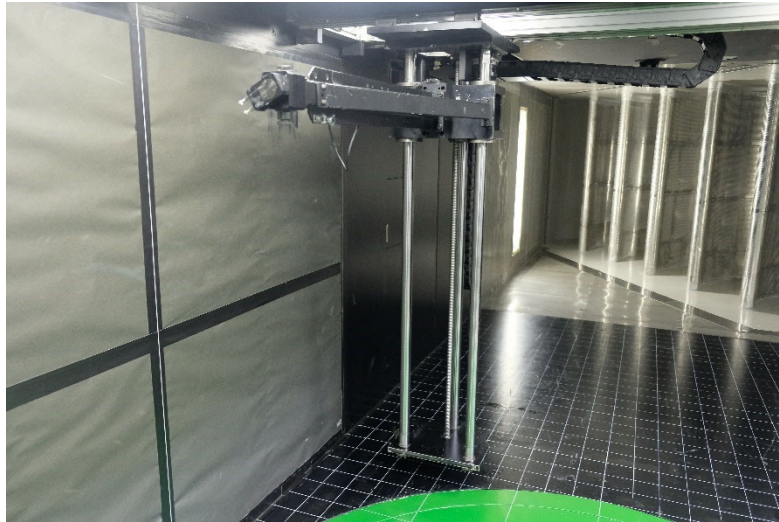


Figure 3-8. Traversing system.

3.2 Clothing ensembles

In this study, eight sets of clothing ensembles were selected (Figure 3-9 and Table 3-2). For the standing posture, all the ensembles were tested. For the sitting posture, E8 was not tested. The underwear (bra and panty), shirt, and shoes in each clothing ensemble were the same. The material of the underwear and the shirt are both 100% cotton. The material of the shoes are 100 % cotton for the upper, rubber for the sole.



Figure 3-9. Overview of tested clothing ensembles.

Table 3-2. Material information on tested clothing ensembles.

Ensemble code	Catalogue	Components
E1	Tops	Wind blast jacket: the outer material was 100% nylon, the inner material (mesh) was 100% polyester
	Bottoms	Windbreaker trousers: same with tops
E2	Tops	Suit jacket: 100% polyester
	Bottoms	Work trousers: 90% polyester, 10% cotton
E3	Tops	Sweater: 85% acrylic fiber, 15% wool
	Bottoms	Work trousers: 90% polyester, 10% cotton
E4	Tops	Work jacket: 90% polyester, 10% cotton
	Bottoms	Work trousers: 90% polyester, 10% cotton
E5	Tops	Fleece jacket: 100% polyester
	Bottoms	Work trousers: 90% polyester, 10% cotton
E6	Tops	Sports jacket: 35% polyester, 65% cotton
	Bottoms	Work trousers: 90% polyester, 10% cotton
E7	Tops	Raincoat: 100% PVC coated nylon
	Bottoms	
E8	Tops	Mountain jacket: 2-layer GORE-TEX Shell (exterior: 100% nylon, interior: 100% polyester)
	Bottoms	Work trousers: 90% polyester, 10% cotton

3.3 Measurement

3.3.1 Temperature

The air temperature, wall temperature, manikin surface temperature, and the clothing surface temperature were all measured with T-type thermocouple. The temperatures were recorded over 10 min at 10 s intervals with data logger, which were then averaged. The recording started after the ambient temperature and the manikin surface temperature had stabilized. The information for the thermocouple and the data logger are listed in Table 3-3.

For the measurement of the manikin surface temperature and the clothing surface temperature, the thermocouple was soldered onto a 0.1 mm-thick copper disk with a diameter of 6 mm. The self-made thermocouples were attached to the manikin surface or the clothing surface with non-woven tape (Figure 3-10). Distribution of the temperature measurement points on the manikin surface and the clothing surface are presented in

Table 3-3. Specifications for the thermocouple and data logger.

Thermocouple	T-type, 0.32 mm diameter Valid range: −40–125 °C Accuracy: ±0.5 °C
Data logger	Graphtec GL800

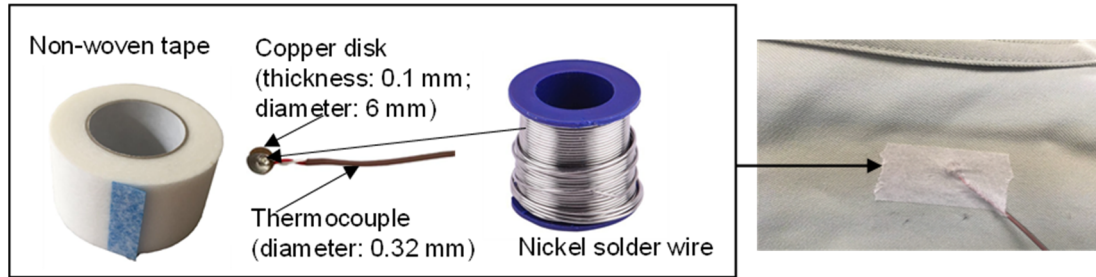


Figure 3-10. The non-woven tape and the self-made thermocouple.

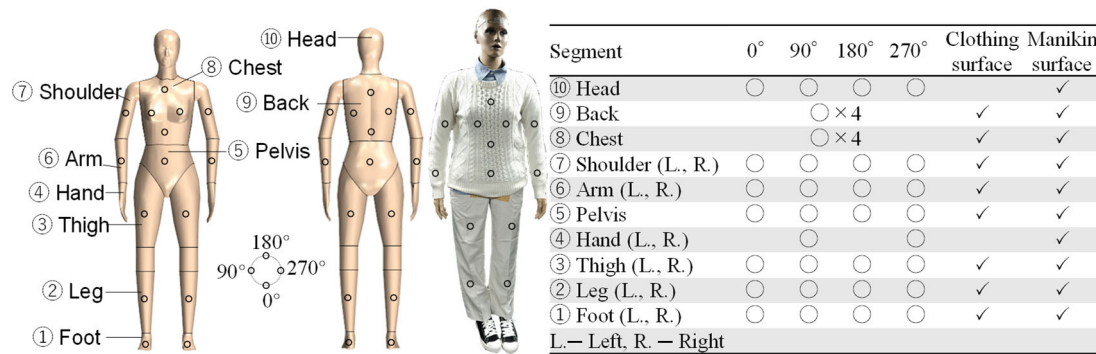


Figure 3-11. Distribution of the temperature measurement points on the manikin surface and the clothing surface.

3.3.2 Airspeed

For the experiments in the climate chamber, the airspeed was measured with hot-wire anemometer (Model 6542) produced by Kanomax (Figure 3-12 and Table 3-4). For the experiments in the wind tunnel, the airspeed was measured with miniature wire probe (55P11) produced by Dantec Dynamics (Figure 3-13 and Table 3-4). During the experiment, the probe was suspended in the air stream by a programmable traverse system, enabling automatic airspeed profiles. The traverse system was programmed to stop for 90 s at equally spaced heights, and 1000 airspeed data were recorded in 1 s. To avoid the influence of the movement of the probe and traversing system, data recording was started 10 s after reaching the specified height. The turbulence intensity was calculated as follows:

$$I = \frac{u'}{U} \quad (3-1)$$



Figure 3-12. Hot-wire anemometer (Model 6542) produced by Kanomax.



Figure 3-13. Miniature wire probe (55P11) produced by Dantec Dynamics.

Table 3-4. Specifications for the hot-wire anemometer and split-fiber film probe.

Instrument	Valid range	Accuracy
Hot-wire anemometer (Model 6542)	$0.01\text{--}30 \text{ m}^{-1}\cdot\text{s}$	$\pm 2\%$ of reading or $\pm 0.015 \text{ m}\cdot\text{s}^{-1}$, whichever is greater
Split-fiber film probe (55P11)	$0.05\text{--}500 \text{ m}^{-1}\cdot\text{s}$	Depending on the quality of calibration

3.3.3 Emissivity for the clothing

The emissivity of E2, E3, and E4 was measured according to the ASTM E1933 standard [3]. The results showed that the emissivity of E2, E3, and E4 was 0.95. According to Fanger, most types of clothing have an emissivity of 0.95 [4]. Therefore, the emissivities of clothing in this study were assumed to 0.95. The measuring procedures are as follows:

- (1) The thermal manikin was heated.
- (2) The thermal manikin was dressed in the studied clothing, the manikin and clothing were pasted with double-sided tape at the target measuring point, to make full contact between the manikin and the clothing.
- (3) A thermocouple was applied to the clothing surface where the emissivity was to be measured.

The temperature of the clothing surface was recorded after it became stable (Figure 3-14).

(4) The thermal camera was placed on the tripod at the desired distance from the thermal manikin, and then the thermal camera was focused on the portion of the clothing where the emissivity is to be measured (the same with the portion of Step (2) (Figure 3-15). The detailed specifications for the thermal camera is listed in Table 3-5.

(5) The temperature of the target part was measured without moving the thermal camera. The emissivity was adjusted in the settings panel of the thermal camera until the same temperature recorded in (2) was reached. The indicated emissivity value was the measured emissivity of the clothing.

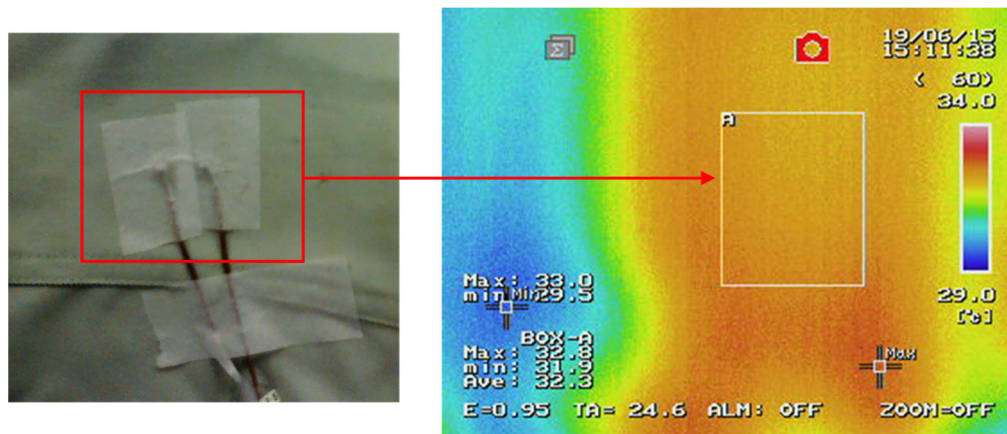


Figure 3-14. Test setup for emissivity measurement (E4).



Figure 3-15. Position for the thermal camera.

Table 3-5. Specifications for the thermal camera.

Type	R300SR produced by Nippon avionocs
Measuring range	-40–500 °C
Sensitivity	0.003 °C at 30 °C
Accuracy	±1 °C at a range of (10–40 °C)

3.3.4 Air permeability for the clothing

Air permeability is an expression describing the properties of a fabric that permit the passage of air through the fabric's interstices [5]. In this research, the air permeability for the clothing ensembles were measured with digital frazier type air permeability tester (DAP-360) produced by Daiei Kagaku Seiki shown in Figure 3-16. The specifications for the air permeability tester are listed in Table 3-6. Both the tester and the experiment procedure followed ISO 9073–15 and ISO 9237 [6,7]. The air temperature during the experiment was 21.2 °C. The humidity was 63%. The measuring procedures are as follows:

- (1) 20 cm × 20 cm sample was cut from each garment.
- (2) Each test specimen was placed on the test head of the air permeability tester, and the guard ring device was sealed with adequate tension to prevent distortion or side leakage while the test was being performed. The diameter for the guard ring was 75 mm. Therefore the test area was 44 cm².
- (3) The permeability tester was started. The result was recorded after the value of permeability stabilized.
- (4) Steps (1)–(3) were repeated five times, and the five results were averaged.

The air permeability for each garment is shown in Table 3-7.

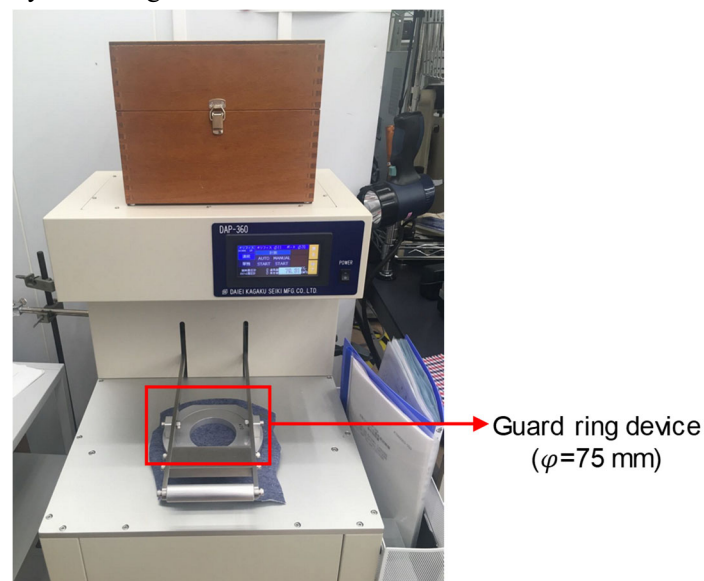


Figure 3-16. Digital frazier type air permeability tester (DAP-360) produced by Daiei Kagaku Seiki.

Table 3-6. Specifications for the air permeability tester.

Measuring range	0.3–300 cm ³ ·cm ⁻² ·s ⁻¹
Accuracy	±2%
Range of pressure drop	50–450 Pa

Table 3-7. Air permeability for each garment.

Garment	Air permeability ($\text{cm}^3 \cdot \text{cm}^2 \cdot \text{s}^{-1}$)
Coat and trousers for E1	1.13
Coat for E2	29.19
Coat for E3	121.81
Coat for E4	19.39
Coat for E5	39.82
Coat for E6	80.74
Coat and trousers for E7	$< 0.3^*$
Coat for E8	0.244^{**}
Trousers for E2, E3, E4, E5, E6, and E8	40.87
Shirt for all clothing ensembles	13.90

*E7 consisted of raincoats and rain trousers, which had minimal air permeability exceeded the measuring range of the air permeability tester.

**Since this value was lower than the minimum measurement range of the air permeability tester, it could only be used as a reference.

3.3.5 Surface friction (MIU) and surface roughness (SMD)

The Kawabata-Evaluation-System (KES) method was established by Professor Kawabata and his colleagues at Kyoto University to quantify the texture of fabrics [8]. The KES method has been used in the wide spread for the fabric assessment.

3.3.5.1 Coefficient of friction, MIU

Press the surface of the sample with a sensing element with a force of 50 g, as shown in Figure 3-17. The sample moves with a speed of $0.1 \text{ cm} \cdot \text{s}^{-1}$. The force required to pull the sample passing the contactor is measured [9]. Therefore, the coefficient of friction can be calculated (Equation (3-2)).

$$\mu = \frac{\text{frictional force (F)}}{\text{normal force (P)}} \quad (3-2)$$

Therefore, the mean value of the coefficient of friction for the sample can be calculated with Equation (3-3) (Figure 3-18).

$$MIU = \frac{1}{L} \int_0^L \mu dl \quad (3-3)$$

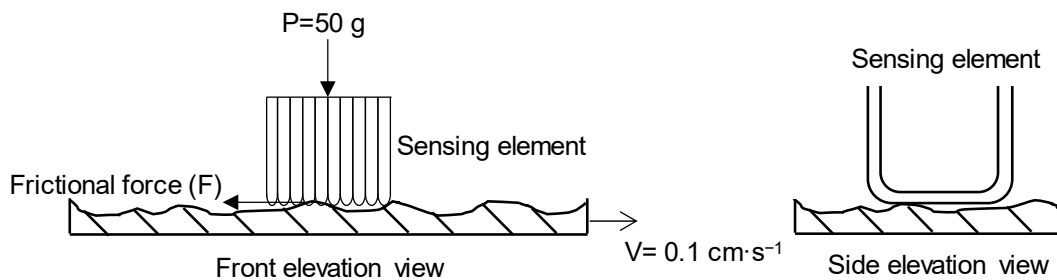


Figure 3-17. Surface friction test by KES.

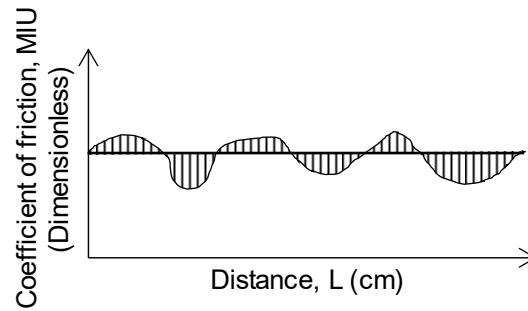


Figure 3-18. The variation of coefficient of friction along with the testing distance.

3.3.5.2 Surface roughness, SMD

The surface roughness is measured using sensing element with a U shape (Figure 3-19). Press the sample with a force of 10 g. The same with measuring the coefficient of friction, the sample moves with a speed of $0.1 \text{ cm} \cdot \text{s}^{-1}$. The mean deviation of surface thickness can be calculated through Figure 3-20 with Equation (3-4) [9].

$$\text{SMD} = \frac{\text{hatched area}}{L} = \frac{1}{L} \int_0^L (T - \bar{T}) dl \quad (3-4)$$

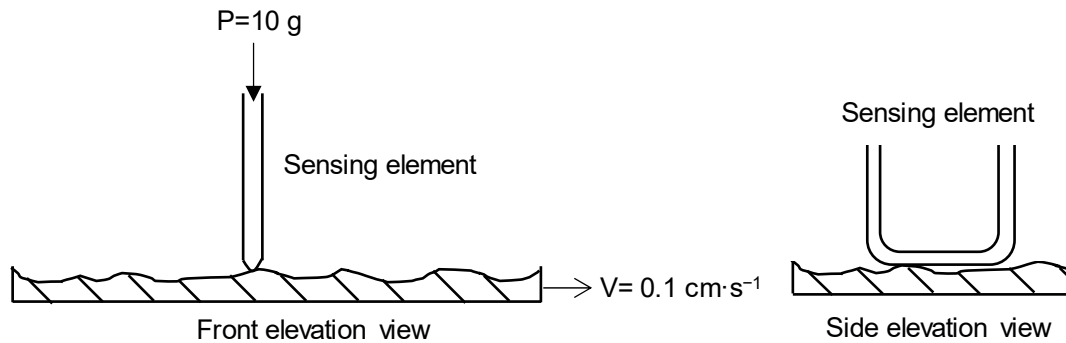


Figure 3-19. Surface roughness test by KES.

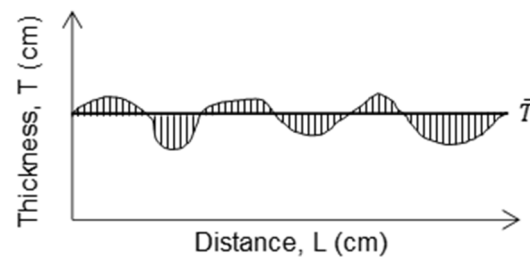


Figure 3-20. The variation of surface thickness along the testing distance.

The surface friction MIU and surface roughness SMD were measured with the KES-FB4 surface tester shown in Figure 3-21. The specification for the KES-FB4 surface tester are listed in Table 3-8. Figure 3-22 illustrates the image during the measurement. The details for the roughness sensor and the piano-wire sensor were also presented. The air temperature during the experiment was 21.2 °C. The humidity was 63%. The measuring procedures are as follows:

- (1) 20 cm × 20 cm sample was cut from each garment.
- (2) The surface friction for the weft direction of the sample were measured three times. The three surface friction values were averaged.
- (3) The sample was rotated 90°. The surface friction for the warp direction of the sample were measured three times. The three surface friction values were averaged.
- (4) The surface friction for the weft direction and warp direction were averaged. The measuring procedures for the surface roughness were the same as surface friction.

The results for the coefficient of friction and surface roughness for each garment are listed in Table 3-9.

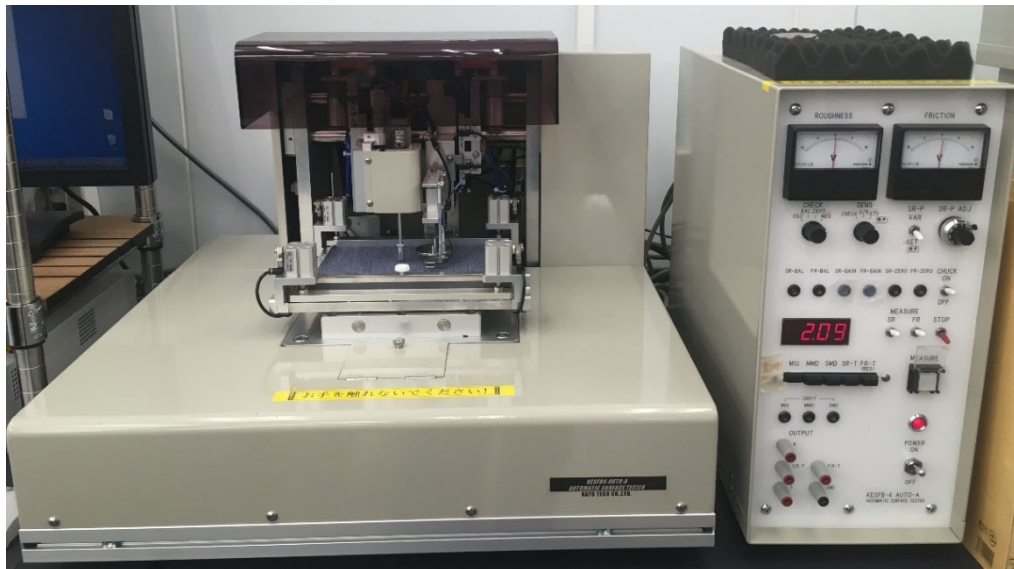


Figure 3-21. The KES-FB4 surface tester.

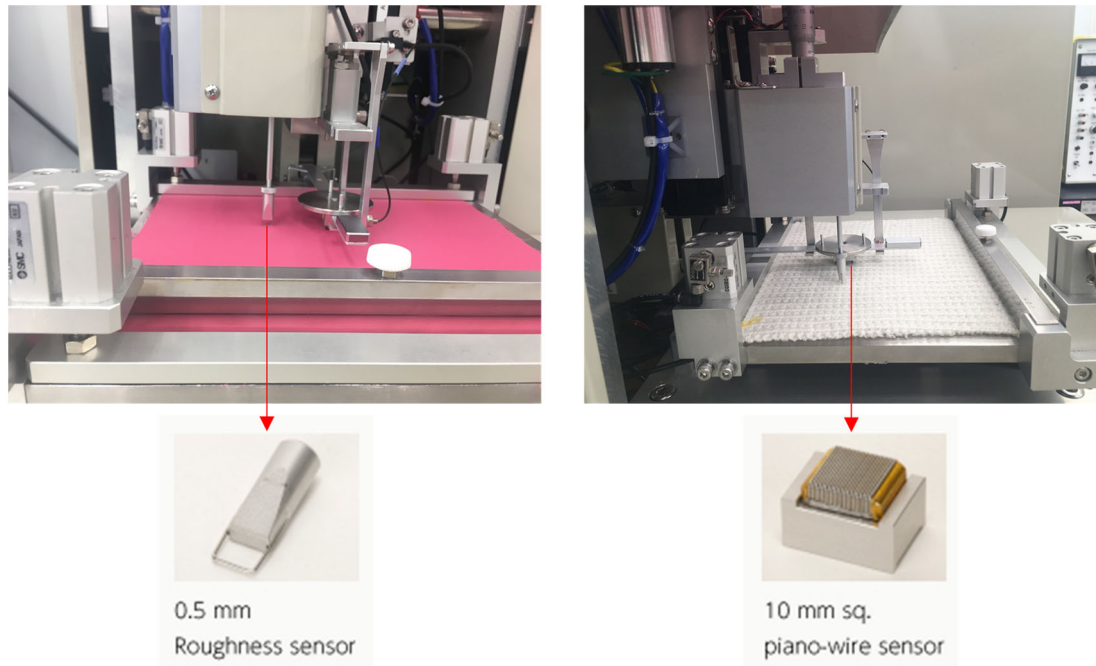


Figure 3-22. The roughness sensor and the piano-wire sensor.

Table 3-8. Specification for the KES-FB4 surface tester.

Sample size	20 cm × 20 cm Thickness: 2 mm (max.)
Surface friction detection	Detector: Ring-type detector with differential transformer Load (full scale): 200 gf (with standard measurement) Accuracy: ±0.5% or less of full scale
Surface roughness detection	Detector: Differential transformer Displacement (full scale): 0.4 mm Accuracy: ±1.0% or less of full scale
Detection of surface measurement movement	Detector: Potentiometer Travel distance: 30 mm (Range of effective measurement distance: 20 mm) Accuracy: ±0.5% or less of full scale
Sensor size	Friction contactor: 10 mm × 10 mm Roughness contactor: 0.5 mm diameter single wire (contact surface width: 5 mm)
Velocity of sample movement	1 mm·sec ⁻¹ (standard)

Table 3-9. Mean coefficient for friction and surface roughness for each garment.

	Coefficient of friction (MIU)	Surface roughness (SMD) μm
Coat and trousers for E1	0.16	2.14
Coat for E2	0.21	3.42
Coat for E3	0.31	7.20
Coat for E4	0.20	3.18
Coat for E5	0.33	3.66
Coat for E6	0.21	3.12
Coat for E7	0.15	0.28
Shirt for all clothing ensembles	0.17	2.02

3.4 Governing equations of fluid dynamics

3.4.1 Basic theory

(1) Conversion of mass:

$$m_{cv} = \text{constant} \quad (3-5)$$

(2) Newton's second law:

$$\mathbf{F} = m\mathbf{a} = m \frac{d\mathbf{V}}{dt} = \frac{d}{dt}(m\mathbf{V}) \quad (3-6)$$

(3) The first law of thermodynamics:

$$\delta Q - \delta W = dE \quad (3-7)$$

(4) The Reynolds transport theorem [10]:

$$\begin{aligned} \frac{d}{dt}(B_{cv}) &= \frac{d}{dt} \left(\int_{cv} \beta \rho dV \right) + \int_{cs} \beta \rho V_n dA_{out} - \int_{cs} \beta \rho V_n dA_{in} \\ &= \frac{d}{dt} \left(\int_{cv} \beta \rho dV \right) + \int_{cs} \beta \rho (\mathbf{V} \cdot \mathbf{n}) dA \end{aligned} \quad (3-8)$$

$$\beta = \frac{dB}{dm}$$

A system derivative equals the rate of change of B within the control volume plus the flow of B out of the control surface minus the flow of B into the control surface.

$$\text{Mass conservation} \quad B = m$$

$$\text{Momentum conservation} \quad B = m\mathbf{V}$$

$$\text{Energy conservation} \quad B = E$$

(5) The total time derivative of the velocity vector:

$$\mathbf{a} = \frac{d\mathbf{V}}{dt} = \frac{\partial \mathbf{V}}{\partial t} + \left(u \frac{\partial \mathbf{V}}{\partial x} + v \frac{\partial \mathbf{V}}{\partial y} + w \frac{\partial \mathbf{V}}{\partial z} \right) = \frac{\partial \mathbf{V}}{\partial t} + (\mathbf{V} \cdot \nabla) \mathbf{V} \quad (3-9)$$

3.4.2 Mass conservation

We assume that the fluid flows through an elemental cartesian fixed control volume (dx, dy, dz) with a fixed spatial position shown in Figure 3-23. The time rate of mass change in the control volume is equal to the net mass flow of the control volume (Equation (3-10)).

$$\left(\frac{dm}{dt}\right)_{cv} = 0 = \int_{cv} \frac{\partial \rho}{\partial t} dV + \sum_i (\rho_i A_i V_i)_{out} - \sum_i (\rho_i A_i V_i)_{in} \quad (3-10)$$

The control volume is so small that the volume integral simply is taken as a differential term:

$$\int_{cv} \frac{\partial \rho}{\partial t} dV \approx \frac{\partial \rho}{\partial t} dx dy dz \quad (3-11)$$

Mass change due to inflow and outflow for x -direction is

$$\left[\rho u + \frac{\partial}{\partial x}(\rho u) dx \right] dy dz - \rho u dy dz \quad (3-12)$$

Mass change due to inflow and outflow for y -direction is

$$\left[\rho v + \frac{\partial}{\partial y}(\rho v) dy \right] dx dz - \rho v dx dz \quad (3-13)$$

Mass change due to inflow and outflow for z -direction is

$$\left[\rho w + \frac{\partial}{\partial z}(\rho w) dz \right] dx dy - \rho w dx dy \quad (3-14)$$

Introduce Equation (3-11), (3-12), (3-13), and (3-14) into Equation (3-10), and we have

$$\left(\frac{\partial \rho}{\partial t} + \frac{\partial}{\partial x}(\rho u) + \frac{\partial}{\partial y}(\rho v) + \frac{\partial}{\partial z}(\rho w) \right) dx dy dz = 0 \quad (3-15)$$

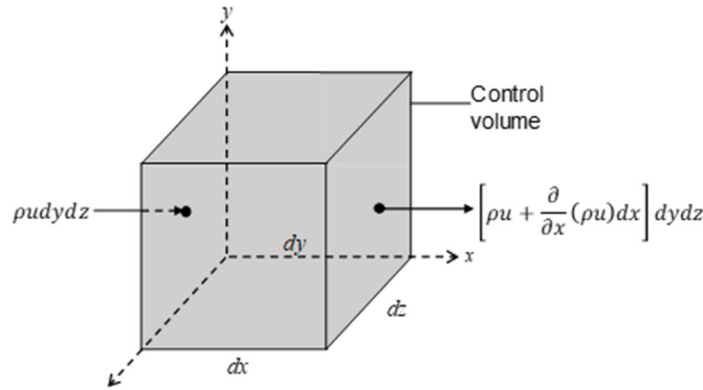


Figure 3-23. Elemental cartesian fixed control volume showing the inlet and outlet mass flows on the x faces.

Namely:

$$\frac{\partial \rho}{\partial t} + \frac{\partial}{\partial x}(\rho u) + \frac{\partial}{\partial y}(\rho v) + \frac{\partial}{\partial z}(\rho w) = 0 \quad (3-16)$$

Introduce the definition of the del operator in the cartesian coordinate system:

$$\nabla = \mathbf{i} \frac{\partial}{\partial x} + \mathbf{j} \frac{\partial}{\partial y} + \mathbf{k} \frac{\partial}{\partial z} \quad (3-17)$$

Equation (3-16) can be written as

$$\frac{\partial \rho}{\partial t} + \nabla \cdot (\rho \mathbf{V}) = 0 \quad (3-18)$$

For the incompressible flow, density changes are negligible, so Equation (3-18) can be written as

$$\nabla \cdot \mathbf{V} = 0 \quad (3-19)$$

Namely:

$$\frac{\partial u}{\partial x} + \frac{\partial v}{\partial y} + \frac{\partial w}{\partial z} = 0 \quad (3-20)$$

3.4.3 Momentum conservation

In this part, we apply a basic physics principle to the fluid control volume, Newton's second law:

$$\frac{d(m\mathbf{V})}{dt} = \sum \mathbf{F} = \frac{\partial}{\partial t} \left(\int_{CV} \rho \mathbf{V} dV \right) + \sum (m_i \mathbf{V}_i)_{out} - \sum (m_i \mathbf{V}_i)_{in} \quad (3-21)$$

The net momentum flux in the x -direction:

$$\left[\rho u + \frac{\partial}{\partial x} (\rho u) dx \right] \mathbf{V} dy dz - \rho u \mathbf{V} dy dz \quad (3-22)$$

The net momentum flux in the y -direction:

$$\left[\rho v + \frac{\partial}{\partial y} (\rho v) dy \right] \mathbf{V} dx dz - \rho v \mathbf{V} dx dz \quad (3-23)$$

The net momentum flux in the z -direction:

$$\left[\rho w + \frac{\partial}{\partial z} (\rho w) dz \right] \mathbf{V} dx dy - \rho w \mathbf{V} dx dy \quad (3-24)$$

Introduce Equation (3-22), (3-23), and (3-24) into Equation (3-21):

$$\begin{aligned} \sum \mathbf{F} &= \left(\frac{\partial (\rho \mathbf{V})}{\partial t} + \frac{\partial}{\partial x} (\rho u) \mathbf{V} + \frac{\partial}{\partial y} (\rho v) \mathbf{V} + \frac{\partial}{\partial z} (\rho w) \mathbf{V} \right) dx dy dz \\ &= \left[\left(\mathbf{V} \frac{\partial \rho}{\partial t} + \rho \frac{\partial \mathbf{V}}{\partial t} \right) + \left(\mathbf{V} \frac{\partial \rho u}{\partial x} + \rho u \frac{\partial \mathbf{V}}{\partial x} \right) + \left(\mathbf{V} \frac{\partial \rho v}{\partial y} + \rho v \frac{\partial \mathbf{V}}{\partial y} \right) + \left(\mathbf{V} \frac{\partial \rho w}{\partial z} + \rho w \frac{\partial \mathbf{V}}{\partial z} \right) \right] dx dy dz \\ &= \left[\left(\mathbf{V} \frac{\partial \rho}{\partial t} + \mathbf{V} \frac{\partial \rho u}{\partial x} + \mathbf{V} \frac{\partial \rho v}{\partial y} + \mathbf{V} \frac{\partial \rho w}{\partial z} \right) + \left(\rho \frac{\partial \mathbf{V}}{\partial t} + \rho u \frac{\partial \mathbf{V}}{\partial x} + \rho v \frac{\partial \mathbf{V}}{\partial y} + \rho w \frac{\partial \mathbf{V}}{\partial z} \right) \right] dx dy dz \\ &= \left\{ \mathbf{V} \left[\frac{\partial \rho}{\partial t} + \nabla \cdot (\rho \mathbf{V}) \right] + \rho \left(\frac{\partial \mathbf{V}}{\partial t} + u \frac{\partial \mathbf{V}}{\partial x} + v \frac{\partial \mathbf{V}}{\partial y} + w \frac{\partial \mathbf{V}}{\partial z} \right) \right\} dx dy dz \end{aligned} \quad (3-25)$$

According to Equation (3-18), $\frac{\partial \rho}{\partial t} + \nabla \cdot (\rho \mathbf{V}) = 0$

$$\sum \mathbf{F} = \rho \frac{d\mathbf{V}}{dt} dx dy dz \quad (3-26)$$

The main source of $\sum \mathbf{F}$ on the control volume consists of two parts:

- (1) Body forces. The body forces directly act on the control volume. For example, gravity, magnetism, electric potential. Here, we only consider gravity. The gravity force on the control volume is

$$d\mathbf{F}_{grav} = \rho \mathbf{g} dx dy dz \quad (3-27)$$

- (2) Surface forces. The surface forces are divided into two parts

- Pressure distribution acting on the surface of the control volume by a fluid entrained outside the control volume.
- The shear stress and normal stress distribution acting on the surface in a frictional manner due to the external fluid pushing and pulling the control volume.

The total surface forces acting in the x -direction of the control volume is as shown in Figure 3-24 [11].

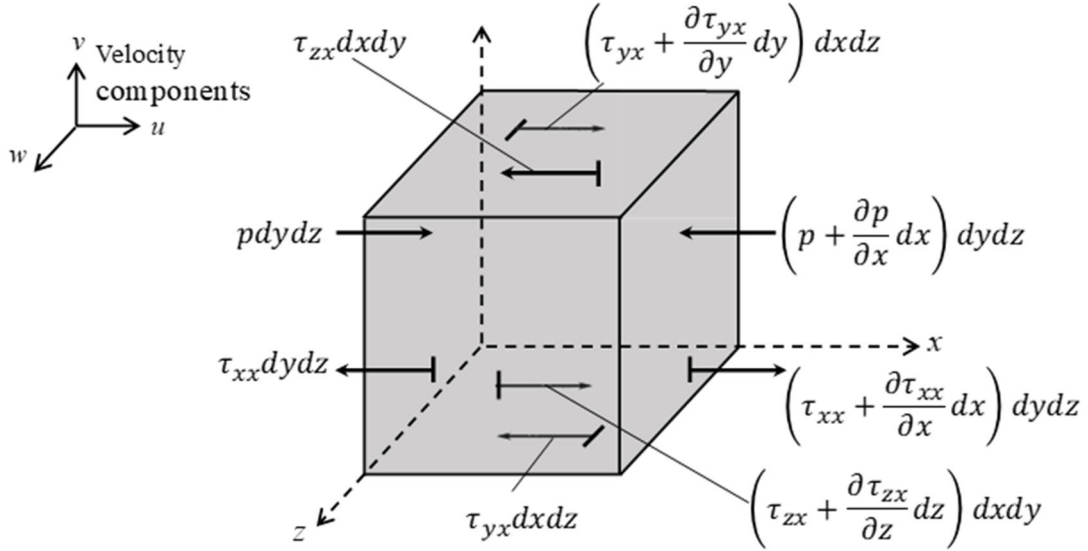


Figure 3-24. Surface forces on the control volume (x -direction only).

The surface forces for different directions are consisted of hydrostatic pressure and viscous stress, shown in Equation (3-28).

$$d\mathbf{F}_{\text{surface}} = \sigma_{ij} = \begin{bmatrix} \sigma_{xx} & \sigma_{yx} & \sigma_{zx} \\ \sigma_{xy} & \sigma_{yy} & \sigma_{zy} \\ \sigma_{xz} & \sigma_{yz} & \sigma_{zz} \end{bmatrix} = \begin{bmatrix} -p + \tau_{xx} & \tau_{yx} & \tau_{zx} \\ \tau_{xy} & -p + \tau_{yy} & \tau_{zy} \\ \tau_{xz} & \tau_{yz} & -p + \tau_{zz} \end{bmatrix} \quad (3-28)$$

σ_{ij} denotes the force in the j direction acting on the surface perpendicular to the i direction.

Surface forces acting on the surface perpendicular to the x -axis in the x -direction:

$$\begin{aligned} \sigma_{xx} &= \left[p - \left(p + \frac{\partial p}{\partial x} dx \right) \right] dydz + \left[-\tau_{xx} + \left(\tau_{xx} + \frac{\partial \tau_{xx}}{\partial x} dx \right) \right] dydz \\ &= \frac{\partial(-p + \tau_{xx})}{\partial x} dx dydz \end{aligned} \quad (3-29)$$

Surface forces acting on the surface perpendicular to the y -axis in the x -direction:

$$\sigma_{yx} = -\tau_{yx} + \left(\tau_{yx} + \frac{\partial \tau_{yx}}{\partial y} dy \right) dx dz = \frac{\partial \tau_{yx}}{\partial y} dx dy dz \quad (3-30)$$

Surface forces acting on the surface perpendicular to the z -axis in the x -direction:

$$\sigma_{zx} = -\tau_{zx} + \left(\tau_{zx} + \frac{\partial \tau_{zx}}{\partial z} dz \right) dx dy = \frac{\partial \tau_{zx}}{\partial z} dx dy dz \quad (3-31)$$

Therefore, the net surface force in the x -direction is

$$dF_{x,surface} = \left[-\frac{\partial p}{\partial x} + \frac{\partial \tau_{xx}}{\partial x} + \frac{\partial \tau_{yx}}{\partial y} + \frac{\partial \tau_{zx}}{\partial z} \right] dxdydz \quad (3-32)$$

Similarly, the net surface force in the y -direction is

$$dF_{y,surface} = \left[-\frac{\partial p}{\partial y} + \frac{\partial \tau_{xy}}{\partial x} + \frac{\partial \tau_{yy}}{\partial y} + \frac{\partial \tau_{zy}}{\partial z} \right] dxdydz \quad (3-33)$$

The net surface force in the z -direction is

$$dF_{z,surface} = \left[-\frac{\partial p}{\partial z} + \frac{\partial \tau_{xz}}{\partial x} + \frac{\partial \tau_{yz}}{\partial y} + \frac{\partial \tau_{zz}}{\partial z} \right] dxdydz \quad (3-34)$$

Equation (3-32), (3-33), and (3-34) can be rewritten as:

$$\frac{dF_{x,surface}}{dV} = -\frac{\partial p}{\partial x} + \frac{\partial \tau_{xx}}{\partial x} + \frac{\partial \tau_{yx}}{\partial y} + \frac{\partial \tau_{zx}}{\partial z} \quad (3-35)$$

$$\frac{dF_{y,surface}}{dV} = -\frac{\partial p}{\partial y} + \frac{\partial \tau_{xy}}{\partial x} + \frac{\partial \tau_{yy}}{\partial y} + \frac{\partial \tau_{zy}}{\partial z} \quad (3-36)$$

$$\frac{dF_{z,surface}}{dV} = -\frac{\partial p}{\partial z} + \frac{\partial \tau_{xz}}{\partial x} + \frac{\partial \tau_{yz}}{\partial y} + \frac{\partial \tau_{zz}}{\partial z} \quad (3-37)$$

Transform Equation (3-35), (3-36), and (3-37) into divergence form:

$$\left(\frac{d\mathbf{F}}{dV} \right)_{surface} = -\nabla p + \left(\frac{d\mathbf{F}}{dV} \right)_{viscous} = -\nabla p + \nabla \cdot \boldsymbol{\tau}_{ij} \quad (3-38)$$

Introduce Equation (3-26), (3-27), and (3-38) into Equation (3-21):

$$\rho \frac{d\mathbf{V}}{dt} = \rho \mathbf{g} - \nabla p + \nabla \cdot \boldsymbol{\tau}_{ij} \quad (3-39)$$

Equation (3-39) can be explained as:

Gravity force per unit volume + pressure force per unit volume + viscous force per unit volume = density \times acceleration

Write out the component equations for Equation (3-39) in full:

$$\begin{aligned} \rho \frac{du}{dt} &= \rho g_x - \frac{\partial p}{\partial x} + \frac{\partial \tau_{xx}}{\partial x} + \frac{\partial \tau_{yx}}{\partial y} + \frac{\partial \tau_{zx}}{\partial z} \\ \rho \frac{dv}{dt} &= \rho g_y - \frac{\partial p}{\partial y} + \frac{\partial \tau_{xy}}{\partial x} + \frac{\partial \tau_{yy}}{\partial y} + \frac{\partial \tau_{zy}}{\partial z} \\ \rho \frac{dw}{dt} &= \rho g_z - \frac{\partial p}{\partial z} + \frac{\partial \tau_{xz}}{\partial x} + \frac{\partial \tau_{yz}}{\partial y} + \frac{\partial \tau_{zz}}{\partial z} \end{aligned} \quad (3-40)$$

Stokes assumes that the relationship between shear stress and velocity gradient is

$$\tau_{ij} = \begin{bmatrix} \lambda(\nabla \cdot \mathbf{V}) + 2\mu \frac{\partial u}{\partial x} & \mu(\frac{\partial v}{\partial x} + \frac{\partial u}{\partial y}) & \mu(\frac{\partial u}{\partial z} + \frac{\partial w}{\partial x}) \\ \mu(\frac{\partial v}{\partial x} + \frac{\partial u}{\partial y}) & \lambda(\nabla \cdot \mathbf{V}) + 2\mu \frac{\partial v}{\partial y} & \mu(\frac{\partial w}{\partial y} + \frac{\partial v}{\partial z}) \\ \mu(\frac{\partial u}{\partial z} + \frac{\partial w}{\partial x}) & \mu(\frac{\partial w}{\partial y} + \frac{\partial v}{\partial z}) & \lambda(\nabla \cdot \mathbf{V}) + 2\mu \frac{\partial w}{\partial z} \end{bmatrix} \quad (3-41)$$

For the incompressible fluid, $\lambda(\nabla \cdot \mathbf{V})=0$

μ : viscosity ν : Kinematic viscosity, $\nu = \frac{\mu}{\rho}$

Introduce Equation (3-41) into Equation (3-40):

$$\begin{aligned} \rho \frac{du}{dt} &= \rho g_x - \frac{\partial p}{\partial x} + \frac{\partial}{\partial x} \left(2\mu \frac{\partial u}{\partial x} \right) + \frac{\partial}{\partial y} \left[\mu \left(\frac{\partial v}{\partial x} + \frac{\partial u}{\partial y} \right) \right] + \frac{\partial}{\partial z} \left[\mu \left(\frac{\partial u}{\partial z} + \frac{\partial w}{\partial x} \right) \right] \\ \rho \frac{dv}{dt} &= \rho g_y - \frac{\partial p}{\partial y} + \frac{\partial}{\partial x} \left[\mu \left(\frac{\partial v}{\partial x} + \frac{\partial u}{\partial y} \right) \right] + \frac{\partial}{\partial y} \left(2\mu \frac{\partial v}{\partial y} \right) + \frac{\partial}{\partial z} \left[\mu \left(\frac{\partial w}{\partial y} + \frac{\partial v}{\partial z} \right) \right] \\ \rho \frac{dw}{dt} &= \rho g_z - \frac{\partial p}{\partial z} + \frac{\partial}{\partial x} \left[\mu \left(\frac{\partial u}{\partial z} + \frac{\partial w}{\partial x} \right) \right] + \frac{\partial}{\partial y} \left[\mu \left(\frac{\partial w}{\partial y} + \frac{\partial v}{\partial z} \right) \right] + \frac{\partial}{\partial z} \left(2\mu \frac{\partial w}{\partial z} \right) \end{aligned} \quad (3-42)$$

Simply Equation (3-42) for x direction:

$$\begin{aligned} \rho \frac{du}{dt} &= \rho g_x - \frac{\partial p}{\partial x} + 2\mu \frac{\partial^2 u}{\partial x^2} + \mu \frac{\partial^2 v}{\partial x \partial y} + \mu \frac{\partial^2 u}{\partial y^2} + \mu \frac{\partial^2 u}{\partial z^2} + \mu \frac{\partial^2 w}{\partial x \partial z} \\ &= \rho g_x - \frac{\partial p}{\partial x} + \left(\mu \frac{\partial^2 u}{\partial x^2} + \mu \frac{\partial^2 u}{\partial y^2} + \mu \frac{\partial^2 u}{\partial z^2} \right) + \left(\mu \frac{\partial^2 v}{\partial x \partial y} + \mu \frac{\partial^2 w}{\partial x \partial z} \right) \\ &= \rho g_x - \frac{\partial p}{\partial x} + \mu \left(\frac{\partial^2 u}{\partial x^2} + \frac{\partial^2 u}{\partial y^2} + \frac{\partial^2 u}{\partial z^2} \right) + \mu \frac{\partial}{\partial x} \left(\frac{\partial u}{\partial x} + \frac{\partial v}{\partial y} + \frac{\partial w}{\partial z} \right) \end{aligned} \quad (3-43)$$

Similarly, the momentum equation for x, y, z directions are

$$\begin{aligned} \frac{\partial u}{\partial t} + \frac{\partial u}{\partial x} + \frac{\partial u}{\partial y} + \frac{\partial u}{\partial z} &= g_x - \frac{1}{\rho} \frac{\partial p}{\partial x} + \nu \left(\frac{\partial^2 u}{\partial x^2} + \frac{\partial^2 u}{\partial y^2} + \frac{\partial^2 u}{\partial z^2} \right) \\ \frac{\partial v}{\partial t} + \frac{\partial v}{\partial x} + \frac{\partial v}{\partial y} + \frac{\partial v}{\partial z} &= g_y - \frac{1}{\rho} \frac{\partial p}{\partial y} + \nu \left(\frac{\partial^2 v}{\partial x^2} + \frac{\partial^2 v}{\partial y^2} + \frac{\partial^2 v}{\partial z^2} \right) \\ \frac{\partial w}{\partial t} + \frac{\partial w}{\partial x} + \frac{\partial w}{\partial y} + \frac{\partial w}{\partial z} &= g_z - \frac{1}{\rho} \frac{\partial p}{\partial z} + \nu \left(\frac{\partial^2 w}{\partial x^2} + \frac{\partial^2 w}{\partial y^2} + \frac{\partial^2 w}{\partial z^2} \right) \end{aligned} \quad (3-44)$$

Tensor form for the momentum equation is

$$\frac{d\mathbf{V}}{dt} = \mathbf{g} + \frac{\nabla p}{\rho} + \nu \nabla^2 \cdot \mathbf{V} \quad (3-45)$$

3.4.4 Energy conservation

In this part, we apply the first law of thermodynamics to the fluid control volume

$$\dot{Q} - \dot{W}_s - \dot{W}_V - \dot{W}_p = \frac{dE}{dt} = \frac{\partial}{\partial t} \left(\int_{CV} e \rho dV \right) + \int_{CS} (e \rho + p) (\mathbf{V} \cdot \mathbf{n}) dA \quad (3-46)$$

where, $\dot{W}_s = 0$

The shaft work isolates the portion of the work that is deliberately done by a machine (pump impeller, fan blade, piston, or the like) protruding through the control surface into the control volume.

(1) \dot{W}_v , Shear work due to viscous stresses

For x -direction

$$\dot{W}_{v,xx} = \left[-u\tau_{xx} + \left(u\tau_{xx} + \frac{\partial u\tau_{xx}}{\partial x} dx \right) \right] dydz = \frac{\partial(-\tau_{xx})}{\partial x} dx dy dz \quad (3-47)$$

$$\dot{W}_{v,yx} = \left[-u\tau_{yx} + \left(u\tau_{yx} + \frac{\partial u\tau_{yx}}{\partial y} dy \right) \right] dx dz = \frac{\partial(-\tau_{yx})}{\partial y} dx dy dz \quad (3-48)$$

$$\dot{W}_{v,zx} = \left[-u\tau_{zx} + \left(u\tau_{zx} + \frac{\partial u\tau_{zx}}{\partial z} dz \right) \right] dx dy = \frac{\partial(-\tau_{zx})}{\partial z} dx dy dz \quad (3-49)$$

Viscous work for the surface force in x -direction on the control volume

$$\dot{W}_{v,x} = \left[\frac{\partial(-\tau_{xx})}{\partial x} + \frac{\partial(-\tau_{yx})}{\partial y} + \frac{\partial(-\tau_{zx})}{\partial z} \right] dx dy dz \quad (3-50)$$

Viscous work for the surface force in x, y, z -direction on the control volume

$$\begin{aligned} \dot{W}_v &= \left[\frac{\partial(-\tau_{xx})}{\partial x} + \frac{\partial(-\tau_{yx})}{\partial y} + \frac{\partial(-\tau_{zx})}{\partial z} \right] dx dy dz \\ &= \left[\frac{\partial(-\tau_{xy})}{\partial x} + \frac{\partial(-\tau_{yy})}{\partial y} + \frac{\partial(-\tau_{zy})}{\partial z} \right] dx dy dz \\ &= \left[\frac{\partial(-\tau_{xz})}{\partial x} + \frac{\partial(-\tau_{yz})}{\partial y} + \frac{\partial(-\tau_{zz})}{\partial z} \right] dx dy dz \\ &= -\nabla \cdot (\mathbf{V} \cdot \boldsymbol{\tau}_{ij}) dx dy dz \end{aligned} \quad (3-51)$$

(2) \dot{W}_p , work done by pressure forces

For x -direction

$$\left[up - \left(up + \frac{\partial(up)}{\partial x} dx \right) \right] dydz = -\frac{\partial(up)}{\partial x} dx dy dz \quad (3-52)$$

For the whole control volume

$$\dot{W}_p = - \left[\frac{\partial(up)}{\partial x} + \frac{\partial(vp)}{\partial y} + \frac{\partial(wp)}{\partial z} \right] = -\nabla \cdot (p\mathbf{V}) dx dy dz \quad (3-53)$$

(3) \dot{Q} , total heat flow into the control volume

$$\begin{aligned} \dot{Q} &= \left[- \left(q_x + \frac{\partial}{\partial x} q_x dx \right) dydz + q_x dydz \right] + \left[- \left(q_y + \frac{\partial}{\partial y} q_y dy \right) dx dz + q_y dx dz \right] \\ &+ \left[- \left(q_z + \frac{\partial}{\partial z} q_z dz \right) dx dy + q_z dx dy \right] \\ &= - \left(\frac{\partial}{\partial x} q_x + \frac{\partial}{\partial y} q_y + \frac{\partial}{\partial z} q_z \right) dx dy dz \\ &= -\nabla \cdot \mathbf{q} dx dy dz \end{aligned} \quad (3-54)$$

According to Fourier's law of conduction,

$$\mathbf{q} = -k\nabla T \quad (3-55)$$

Therefore,

$$\dot{Q} = \nabla \cdot (k \nabla T) dx dy dz \quad (3-56)$$

Refer to Equation (3-25),

$$\begin{aligned} \frac{dE}{dt} &= e \frac{\partial \rho}{\partial t} + \rho \frac{\partial e}{\partial t} + \frac{\partial}{\partial x} u \rho e + \frac{\partial}{\partial x} u p + \frac{\partial}{\partial y} v \rho e + \frac{\partial}{\partial y} v p + \frac{\partial}{\partial z} w \rho e + \frac{\partial}{\partial z} w p \\ &= e \frac{\partial \rho}{\partial t} + \rho \frac{\partial e}{\partial t} + e \frac{\partial}{\partial x} (\rho u) + (\rho u) \frac{\partial e}{\partial x} + e \frac{\partial}{\partial y} (\rho v) + (\rho v) \frac{\partial e}{\partial y} + e \frac{\partial}{\partial z} (\rho w) \\ &\quad + (\rho w) \frac{\partial e}{\partial z} + \left(\frac{\partial}{\partial x} u p + \frac{\partial}{\partial y} v p + \frac{\partial}{\partial z} w p \right) \\ &= e \left[\frac{\partial \rho}{\partial t} + \frac{\partial}{\partial x} (\rho u) + \frac{\partial}{\partial y} (\rho v) + \frac{\partial}{\partial z} (\rho w) \right] \\ &\quad + \left[\rho \frac{\partial e}{\partial t} + (\rho u) \frac{\partial e}{\partial x} + (\rho v) \frac{\partial e}{\partial y} + (\rho w) \frac{\partial e}{\partial z} \right] + \left(\frac{\partial}{\partial x} u p + \frac{\partial}{\partial y} v p + \frac{\partial}{\partial z} w p \right) \\ &= \rho \frac{de}{dt} + u \frac{\partial p}{\partial x} + p \frac{\partial u}{\partial x} + v \frac{\partial p}{\partial y} + p \frac{\partial v}{\partial y} + w \frac{\partial p}{\partial z} + p \frac{\partial w}{\partial z} = \rho \frac{de}{dt} + \mathbf{V} \cdot \nabla p + p \nabla \cdot \mathbf{V} \end{aligned} \quad (3-57)$$

Introduce Equation (3-51), (3-53), (3-56) and (3-57) to Equation (3-46), we get

$$\rho \frac{de}{dt} + \mathbf{V} \cdot \nabla p + p \nabla \cdot \mathbf{V} = \nabla \cdot (k \nabla T) - \nabla \cdot (\mathbf{V} \cdot \boldsymbol{\tau}_{ij}) - \nabla \cdot (p \mathbf{V}) \quad (3-58)$$

$$e = \hat{u} + \frac{1}{2} u^2 + gz$$

$$\rho c_p \frac{dT}{dt} = k \nabla^2 T + \Phi \quad (3-59)$$

$$\begin{aligned} \Phi &= \mu \left[2 \left(\frac{\partial u}{\partial x} \right)^2 + 2 \left(\frac{\partial v}{\partial y} \right)^2 + 2 \left(\frac{\partial w}{\partial z} \right)^2 + \left(\frac{\partial v}{\partial x} + \frac{\partial u}{\partial y} \right)^2 + \left(\frac{\partial w}{\partial y} + \frac{\partial v}{\partial z} \right)^2 \right. \\ &\quad \left. + \left(\frac{\partial u}{\partial z} + \frac{\partial w}{\partial x} \right)^2 \right] \end{aligned} \quad (3-60)$$

For incompressible flow with constant properties

Continuity:

$$\nabla \cdot \mathbf{V} = 0 \quad (3-61)$$

Momentum:

$$\rho \frac{d\mathbf{V}}{dt} = \rho \mathbf{g} - \nabla p + \mu \nabla^2 \cdot \mathbf{V} \quad (3-62)$$

Energy:

$$\rho c_p \frac{dT}{dt} = k \nabla^2 T + \Phi \quad (3-63)$$

3.5 *Non-dimensionalization of the Navier–Stokes equations*

$$\mathbf{V}^* = \frac{\mathbf{V}}{U} \quad (3-64)$$

$$\nabla^* = L \nabla \quad (3-65)$$

$$x^* = \frac{x}{L} \quad (3-66)$$

$$y^* = \frac{y}{L} \quad (3-67)$$

$$z^* = \frac{z}{L} \quad (3-68)$$

$$t^* = \frac{t}{L/U} \quad (3-69)$$

$$p^* = \frac{p}{\rho U^2} \quad (3-70)$$

$$T^* = \frac{T}{T_0} \quad (3-71)$$

$$\frac{\nu}{UL} = \frac{1}{Re} \quad (3-72)$$

Froude number

$$Fr = \frac{U^2}{gL} \quad (3-73)$$

Reynolds number

$$Re = \frac{\rho UL}{\mu} \quad (3-74)$$

Prandtl number

$$Pr = \frac{\mu c_p}{k} \quad (3-75)$$

Eckert number

$$E_c = \frac{U^2}{c_p T_0} \quad (3-76)$$

(1) Continuity

$$\nabla \cdot \mathbf{V} = 0 \quad (3-77)$$

$$\frac{\nabla^*}{L} \cdot \mathbf{V}^* U = 0 \quad (3-78)$$

$$\nabla^* \cdot \mathbf{V}^* = 0 \quad (3-79)$$

(2) Momentum

$$\rho \frac{d\mathbf{V}}{dt} = \rho \mathbf{g} + \nabla p + \mu \nabla^2 \cdot \mathbf{V} \quad (3-80)$$

$$\rho \frac{d\mathbf{V}}{dt} = \rho \mathbf{g} + \nabla p + \mu \nabla^2 \cdot \mathbf{V} \quad (3-81)$$

$$\rho \frac{U^2}{L} \frac{d\mathbf{V}^*}{dt^*} = \rho g + \frac{\rho U^2}{L} p^* \nabla^* + \mu \frac{U}{L^2} \nabla^{*2} \mathbf{V}^* \quad (3-82)$$

$$\frac{d\mathbf{V}^*}{dt^*} = \frac{gL}{U^2} + p^* \nabla^* + \frac{\mu}{\rho UL} (\nabla^*)^2 \mathbf{V}^* \quad (3-83)$$

$$\frac{d\mathbf{V}^*}{dt^*} = -p^* \nabla^* + \frac{1}{Re} (\nabla^*)^2 \mathbf{V}^* + \frac{1}{Fr} \quad (3-84)$$

(3) Energy

$$\rho c_p \frac{dT}{dt} = k \nabla^2 T + \Phi \quad (3-85)$$

$$\rho c_p \frac{d(T^* \cdot T_0)}{d(t^* \cdot \frac{L}{U})} = k \left(\frac{\nabla^*}{L} \right)^2 \cdot (T^* \cdot T_0) + \Phi \quad (3-86)$$

$$\frac{T_0}{\left(\frac{L}{U} \right)} \rho c_p \frac{dT^*}{dt^*} = \frac{k T_0}{L^2} (\nabla^*)^2 T^* + \Phi \quad (3-87)$$

$$\Phi = \frac{\rho UL}{Re} \cdot \frac{U^2}{L^2} \Phi^* = \frac{\rho U^3}{Re L} \Phi^* \quad (3-88)$$

$$\frac{dT^*}{dt^*} = \frac{k}{LU\rho c_p} (\nabla^*)^2 T^* + \frac{U^2}{ReT_0 c_p} \Phi^* \quad (3-89)$$

$$\frac{dT^*}{dt^*} = \frac{1}{PrRe} (\nabla^*)^2 T^* + \frac{1}{ReE_c} \Phi^* \quad (3-90)$$

3.6 Turbulence model

Here, we introduce the Reynolds decomposition of the instantaneous flow variables to model the random feature of turbulence flows [12].

$$\varphi(t) = \bar{\varphi} + \varphi(t)' \quad (3-91)$$

$$\overline{\varphi(t)'} = 0$$

For example:

$$u = \bar{u} + u' \quad (3-92)$$

To make it easier to understand, we introduce Reynolds decomposition into the two-dimension N-S equation:

$$\frac{\partial \bar{u}}{\partial t} + \bar{u} \frac{\partial \bar{u}}{\partial x} + \bar{v} \frac{\partial \bar{u}}{\partial y} = -\frac{1}{\rho} \frac{\partial \bar{p}}{\partial x} + \frac{\partial}{\partial x} \left(\bar{v} \frac{\partial \bar{u}}{\partial x} - \overline{u'v'} \right) + \frac{\partial}{\partial y} \left(\bar{v} \frac{\partial \bar{u}}{\partial y} - \overline{u'v'} \right) \quad (3-93)$$

$$\frac{\partial \bar{v}}{\partial t} + \bar{u} \frac{\partial \bar{v}}{\partial x} + \bar{v} \frac{\partial \bar{v}}{\partial y} = -\frac{1}{\rho} \frac{\partial \bar{p}}{\partial y} + \frac{\partial}{\partial x} \left(\bar{v} \frac{\partial \bar{v}}{\partial x} - \overline{u'v'} \right) + \frac{\partial}{\partial y} \left(\bar{v} \frac{\partial \bar{v}}{\partial y} - \overline{v'v'} \right) \quad (3-94)$$

The unknowns are \bar{u} , \bar{v} , \bar{p} , $\overline{u'u'}$, $\overline{u'v'}$, $\overline{v'v'}$. Equations are not enough to calculate the unknowns. Closure hypotheses are needed to solve the equations [12]. There are two primary methods to close these equations: eddy-viscosity models and Reynolds-stress models [13]. In these, we utilized eddy-viscosity models:

$$-\overline{u'_i u'_j} = \nu_t \left(\frac{\partial \bar{u}_i}{\partial x_j} + \frac{\partial \bar{u}_j}{\partial x_i} \right) - \frac{2}{3} \rho k \delta_{ij} = 2\nu_t S_{ij} - \frac{2}{3} \rho k \delta_{ij} \quad (3-95)$$

δ_{ij} is the Kronecker delta, $\delta_{ij}=1$ if $i=j$, and $\delta_{ij}=0$, otherwise. S_{ij} is the rate of the strain tensor. ν_t is the turbulent viscosity.

There are kinds of eddy-viscosity models based on how to formulate the turbulence viscosity.

Zero-equation eddy-viscosity model [14].

$$\nu_t = 0.03874UL \quad (3-96)$$

U is the local mean velocity, and L is the distance to the nearest wall.

One-equation eddy-viscosity model [13]:

$$\nu_t = Ck^{\frac{1}{2}}l \quad (3-97)$$

$k = \frac{1}{2}(\overline{u^2} + \overline{v^2} + \overline{w^2})$, C is a constant, and l is the turbulence length scale.

Two-equation eddy-viscosity model (k - ε) [15]:

$$\mu_t = \rho C_\mu \frac{k^2}{\varepsilon} \quad (3-98)$$

C_μ is a constant, k is the turbulence kinetic energy, ε is the dissipation rate of turbulence energy.

Transport equation for k

$$\frac{\partial(\rho k)}{\partial t} + \nabla(\rho k \mathbf{V}) = \nabla \left(\frac{\mu_t}{\sigma_k} \nabla k \right) + 2\mu_t S_{ij} \cdot S_{ij} - \rho \varepsilon \quad (3-99)$$

Transport equation for ε

$$\frac{\partial(\rho \varepsilon)}{\partial t} + \nabla(\rho \varepsilon \mathbf{V}) = \nabla \left(\frac{\mu_t}{\sigma_\varepsilon} \nabla \varepsilon \right) + C_{1\varepsilon} 2\mu_t S_{ij} \cdot S_{ij} - C_{2\varepsilon} \rho \frac{\varepsilon^2}{k} \quad (3-100)$$

Where, $C_\mu=0.09$, $\sigma_k=1.00$, $\sigma_\varepsilon=1.30$, $C_{1\varepsilon}=1.44$, $C_{2\varepsilon}=1.92$.

Terms in the equation from left to right represent rate of change of k and ε , transport of k and ε by convection, transport of k and ε by diffusion, rate of production of k and ε , and rate of destruction of k and ε [16]. The k - ε model described above is called the standard k - ε model. The standard k - ε model has been applied to many relatively simple flow fields and yielded corrective results. However, in a complicated flow field, a correct solution cannot be obtained using standard k - ε model. Various improvements have been attempted. Among the weakness of the standard k - ε model, there are the following two major points:

- (1) The eddy-viscosity $-\overline{u'_i u'_j}$ is modeled assuming that the eddy viscosity is isotropic. However, for the complicated flow field, the eddy-viscosity is significantly anisotropy. At this moment, the prediction accuracy is limited.
- (2) Since the model was developed for sufficiently turbulent flow fields, the wall damping effect near the wall and the flow field with a viscous effect (low Reynolds number flow field) cannot be predicted with high precision.
- (3) As for (1), various anisotropic k - ε models that take account of anisotropy have been proposed, but they are not explained here. Regarding the problem (2), many low-Reynolds number-type k - ε models have been proposed, and the Launder-Sharma-type low Reynolds-number k - ε model is generally utilized [17].

The standard k - ε model does not solve the region near the wall but assumes a wall function that describes the turbulent characteristics near the wall, thereby giving the wall boundary condition. For the adhering boundary layer, appropriate wall functions have been proposed based on the log law and power law. However, the wall functions ignore the diversity of near-wall flow fields for complex turbulent flow fields other than the adhering boundary layer; therefore, do not give a highly accurate prediction in this region. In particular, it is difficult to obtain a correct solution for problems of the flow field, including separation and adhesion, temperature boundary layer problem related to heat transfer.

The following improvements are generally made in the low Reynolds number type model proposed to solve the above problems.

- (1) When calculating the eddy viscosity, a damping function f_μ is introduced.
- (2) Introduce function f_1 and f_2 to the production term and destruction term of the transport equation for ε .

- (3) Trough applying sufficiently fine mesh to the region near the wall and setting no-slip boundary condition, the turbulent flow behavior near the wall and the low Reynolds number effect are reproduced correctly.

The equations of the low Reynolds number k - ε model are given below [18]:

$$\mu_t = \rho C_\mu f_\mu \frac{k^2}{\varepsilon} \quad (3-101)$$

$$\frac{\partial(\rho k)}{\partial t} + \nabla(\rho k \mathbf{V}) = \nabla \left[\left(\mu + \frac{\mu_t}{\sigma_k} \right) \nabla k \right] + 2\mu_t S_{ij} \cdot S_{ij} - \rho \varepsilon \quad (3-102)$$

$$\frac{\partial(\rho \varepsilon)}{\partial t} + \nabla(\rho \varepsilon \mathbf{V}) = \nabla \left[\left(\mu + \frac{\mu_t}{\sigma_\varepsilon} \right) \nabla \varepsilon \right] + C_{\varepsilon 1} f_1 \frac{\varepsilon}{k} 2\mu_t S_{ij} \cdot S_{ij} - C_{\varepsilon 2} f_2 \rho \frac{\varepsilon^2}{k} \quad (3-103)$$

Many types of model have been proposed for the low Reynolds number k - ε model. Model constants, additional terms, and model functions have been proposed for each model, but details are not mentioned here. In this study, Star-CCM+ is used, and the low Reynolds number k - ε model in Star-CCM+ are proposed by Lien et al. given in Table 3-10 [19].

Table 3-10. Low Reynolds number k - ε model in STAR CCM+ [20].

- (1) The mean mass transport equation

$$\frac{\partial \rho}{\partial t} + \nabla[\rho \bar{\mathbf{V}}] = 0 \quad (3-104)$$

- (2) The mean momentum transport equation

$$\frac{d\bar{\mathbf{V}}}{dt} = \mathbf{g} + \frac{\nabla p}{\rho} + \nu \nabla^2 \cdot \bar{\mathbf{V}} \quad (3-105)$$

- (3) The energy transport equation

$$\rho c_p \frac{d\bar{T}}{dt} = k \nabla^2 \bar{T} + \Phi \quad (3-106)$$

- (4) The k transport equation

$$\frac{\partial(\rho k)}{\partial t} + \nabla(\rho k \bar{\mathbf{V}}) = \nabla \left[\left(\mu + \frac{\mu_t}{\sigma_k} \right) \nabla k \right] + P_k - \rho \varepsilon \quad (3-107)$$

- (5) The ε transport equation

$$\frac{\partial(\rho \varepsilon)}{\partial t} + \nabla(\rho \varepsilon \bar{\mathbf{V}}) = \nabla \left[\left(\mu + \frac{\mu_t}{\sigma_\varepsilon} \right) \nabla \varepsilon \right] + C_{\varepsilon 1} \frac{\varepsilon}{k} P_\varepsilon - C_{\varepsilon 2} f_2 \rho \frac{\varepsilon^2}{k} \quad (3-108)$$

- (6) The Reynolds stress

$$T_t = 2\nu_t S_{ij} - \frac{2}{3} \rho k \delta_{ij} \quad (3-109)$$

- (7) The eddy viscosity

$$\mu_t = \rho C_\mu f_\mu \frac{k^2}{\varepsilon} \quad (3-110)$$

(8) The production term of k

$$P_k = G_k + G_b + \gamma_M \quad (3-111)$$

where

$$\text{Turbulent production } G_k = \mu_t S^2 - \frac{2}{3} \rho k \nabla \bar{\mathbf{V}} - \frac{2}{3} \mu_t (\nabla \cdot \bar{\mathbf{V}})^2, S = \sqrt{2 S_{ij} S_{ij}}$$

$$\text{Buoyancy production } G_b = \frac{\mu_t}{Pr_t} (\nabla \bar{T} \cdot \mathbf{g}), Pr_t \text{ is the turbulent Prandtl number}$$

$$\text{Compressibility modification } \gamma_M = \frac{C_M k \varepsilon}{c^2}, c \text{ is the speed of sound, } C_M \text{ is a model coefficient}$$

(9) The production term of ε

$$P_k = G_k + G_{nl} + G' + C_{\varepsilon 3} G_b + \frac{\rho}{C_{\varepsilon 1}} \gamma_y \quad ((3-112)$$

Non-linear production $G_{nl} = \nabla \cdot \bar{\mathbf{V}}: (T_{t,NL}), T_{t,NL}$ is the non-linear contribution to the contribution to the constitutive relationship

$$\text{Additional production } Df_2 \left(G_k + 2\mu \frac{k}{d^2} \right) \exp(-E Re_d^2)$$

$$\text{Yap correction } \gamma_y = C_w \frac{\varepsilon^2}{k} \max \left[\left(\frac{l}{l_\varepsilon} - 1 \right) \left(\frac{l}{l_\varepsilon} \right)^2, 0 \right]$$

C_w is a model coefficient, l and l_ε are length scales defined as $l = \frac{k^{\frac{3}{2}}}{\varepsilon}$ and $l_\varepsilon = C_l d$, where C_l

is a model coefficient

(10) Damping functions

$$f_\mu = 1 - \exp[-(C_{d0} \sqrt{Re_d} + C_{d1} Re_d + C_{d2} Re_d^2)] \quad (3-113)$$

where

$$\text{Wall-distance Reynolds number } Re_d = \frac{\sqrt{k} d}{\nu},$$

k is the turbulent kinetic energy, d is the distance to the wall, ν is the kinematic viscosity

$$f_2 = 1 - C \exp(-Re_t^2) \quad (3-114)$$

where

$$\text{Turbulent Reynolds number } Re_t = \frac{k^2}{\nu \varepsilon}$$

ε is the turbulent dissipation rate

$$C = 0.3, C_{d0} = 0.091, C_{d1} = 0.0042, C_{d2} = 0.00011, C_l = 2.55, C_M = 2, C_T = 0.6, \\ C_t = 1, C_w = 0.83, C_{\varepsilon 1} = 1.44, C_{\varepsilon 1} = 1.92, C_\mu = 0.09, D = 1, E = 0.00375, \sigma_\varepsilon = 1.3, \\ \sigma_k = 1$$

3.7 Computational thermal manikin

A computational thermal manikin was created according to the shape of the thermal manikin used in experiments (Figure 3-1). The total and segment skin areas of the computational thermal manikin and thermal manikin were almost identical (Table 3-11). To resolve the complex geometry of the manikin, the unstructured grid was utilized [21]. For hands, feet, and face, the smallest grid size was 5 mm. For the other parts, the mesh size was 20 mm. 20 layers of prisms with a growth rate of 1.13 and a thickness of 20 mm were created at the manikin surface [12]. For other regions, tetrahedral cells were utilized [22,23]. The computational grid system is shown in Figure 3-25. Although there are many kinds of turbulence models, no one model can solve all the problems. In the simulation analysis around the human body, the Low Reynolds number $k-\epsilon$ model is the most frequently used [22]. As stated in Section 3.6, in this study, Low Reynolds number $k-\epsilon$ model (Lien-Chen type) was utilized.

Table 3-11. Segment area for thermal manikin and computational thermal manikin (m²).

Segment	Exp. (Sitting/Standing)	CFD (Standing)	CFD (Sitting)
10. Head	0.130	0.116	0.117
9. Back	0.130	0.115	0.136
8. Chest	0.140	0.149	0.144
7. Shoulder (L)	0.073	0.072	0.068
(R)	0.078	0.072	0.068
6. Arm (L)	0.050	0.047	0.047
(R)	0.050	0.048	0.047
5. Pelvis	0.165	0.146	0.161
4. Hand (L)	0.038	0.030	0.031
(R)	0.037	0.030	0.031
3. Thigh (L)	0.165	0.146	0.161
(R)	0.160	0.163	0.163
2. Leg (L)	0.090	0.082	0.083
(R)	0.090	0.082	0.083
1. Foot (L)	0.043	0.042	0.043
(R)	0.043	0.041	0.043
Overall	1.483	1.399	1.427

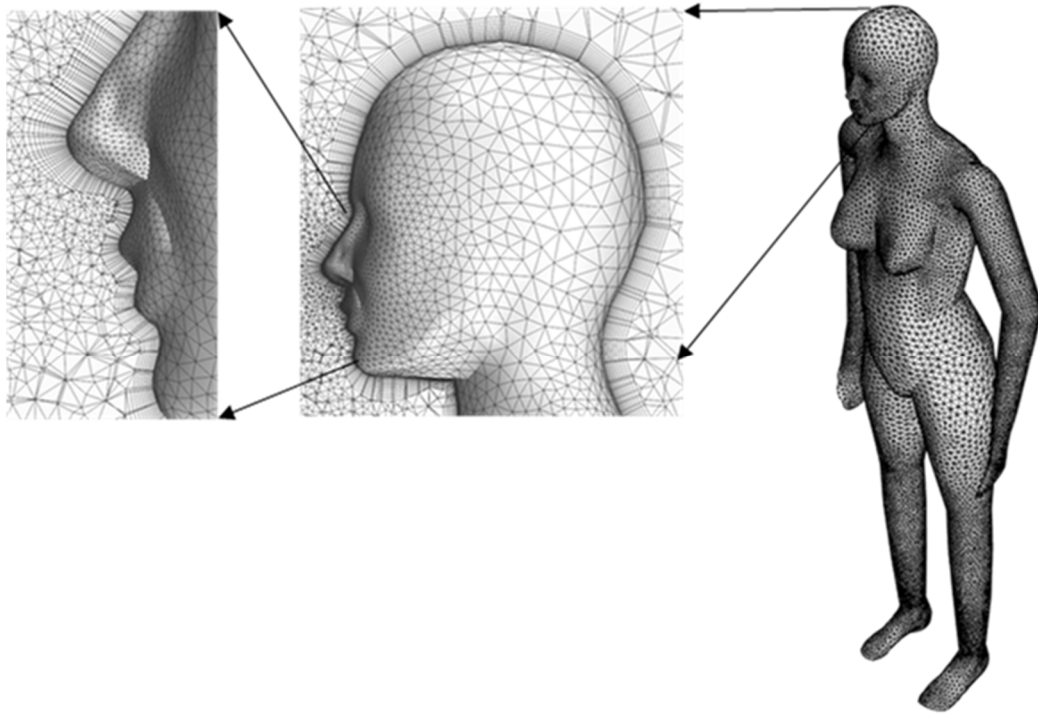


Figure 3-25. Profile of the computational grid.

Reference

- [1] PT TEKNIK, (n.d.). <https://pt-teknik.dk/> (accessed April 17, 2020).
- [2] K. Nakao, Wind tunnel experiments and numerical analysis on higher-order statistics for hazard assessment of hazardous substances generated in urban areas (Japanese), PhD thesis, The University of Tokyo, 2013.
- [3] Standard practice for measuring and compensating for emissivity using infrared imaging radiometers, ASTM E1933-14. (n.d.). <http://www.astm.org/Standards/E1862.htm>.
- [4] P.O. Fanger, Conditions for thermal comfort, in: *Thermal Comfort: Analysis and Applications in Environmental Engineering*, Copenhagen: Danish Technical Press, 1970: pp. 19–64.
- [5] K. Stevens, M. Fuller, Chapter9, in: *Textile-Led Design for the Active Ageing Population*, Elsevier, 2015: pp. 117–138. <https://doi.org/10.1016/B978-0-85709-538-1.00009-2>.
- [6] ISO 9073-15, Textiles-Test methods for nonwovens-Part 15: Determination of air permeability, (2007). <https://www.iso.org/standard/42093.html>.
- [7] ISO 9237, Textiles-Determination of the permeability of facrics to air, (1995). <https://www.iso.org/standard/16869.html>.
- [8] S. Kawabata, The standardization and analysis of hand evaluation, Textile Machinery Society of Japan, 1980.
- [9] Y. Li, X.-Q. Dai, Fabrics, in: Y. Li, X.-Q. Dai (Eds.), *Biomechanical Engineering of Textiles and Clothing*, Elsevier, 2006: pp. 199–222. <https://doi.org/10.1533/9781845691486.3.199>.
- [10] F. White, Fluid mechanics (Chapter 4), McGraw-Hill Education, 2016.
- [11] H.K. Versteeg, W. Malalasekera, An introduction to computational fluid dynamics (Chapter 2), 2nd ed., Prentice Hall, 2007. <https://books.google.co.jp/books?id=RvBZ-UMpGzIC>.
- [12] P. V. Nielsen, F. Allard, H.B. Awbi, L. Davidson, A. Schälin, L. B. Awbi, A. Schalin, Computational fluid dynamics in ventilation design REHVA guidebook No 10, International Journal of Ventilation. 6 (2007) 291–294. <https://doi.org/10.1080/14733315.2007.11683784>.
- [13] Z.J. Zhai, Z. Zhang, W. Zhang, Q.Y. Chen, Evaluation of various turbulence models in predicting airflow and turbulence in enclosed environments by CFD: Part 1—Summary of prevalent turbulence models, HVAC&R Research. 13 (2007) 853–870. <https://doi.org/10.1080/10789669.2007.10391459>.
- [14] Q. Chen, W. Xu, A zero-equation turbulence model for indoor airflow simulation, Energy and Buildings. 28 (1998) 137–144. [https://doi.org/10.1016/S0378-7788\(98\)00020-6](https://doi.org/10.1016/S0378-7788(98)00020-6).
- [15] B.E. Launder, D.B. Spalding, The numerical computation of turbulent flows, Computer Methods in Applied Mechanics and Engineering. 3 (1974) 269–289. [https://doi.org/10.1016/0045-7825\(74\)90029-2](https://doi.org/10.1016/0045-7825(74)90029-2).
- [16] H.K. Versteeg, W. Malalasekera, An introduction to computational fluid dynamics (Chapter 3), Prentice Hall, 2007. <https://books.google.co.jp/books?id=RvBZ-UMpGzIC>.
- [17] B.E.E. Launder, B.I.I. Sharma, Application of the energy-dissipation model of turbulence to the calculation of flow near a spinning disc, Letters in Heat and Mass Transfer. 1 (1974) 131–137. [https://doi.org/10.1016/0094-4548\(74\)90150-7](https://doi.org/10.1016/0094-4548(74)90150-7).

- [18] V.C. Patel, W. Rodi, G. Scheuerer, Turbulence models for near-wall and low Reynolds number flows - A review, *AIAA Journal*. 23 (1985) 1308–1319. <https://doi.org/10.2514/3.9086>.
- [19] F.S. Lien, W.L. Chen, M.A. Leschziner, Low-Reynolds-Number eddy-viscosity modelling based on non-linear stress-strain/vorticity relations, in: *Engineering Turbulence Modelling and Experiments*, Elsevier, 1996: pp. 91–100. <https://doi.org/10.1016/B978-0-444-82463-9.50015-0>.
- [20] STAR-CCM+ User Guide - version 12.02, (2017).
<https://mdx.plm.automation.siemens.com/star-ccm-plus>.
- [21] D.N. Sørensen, L.K. Voigt, Modelling flow and heat transfer around a seated human body by computational fluid dynamics, *Building and Environment*. 38 (2003) 753–762.
[https://doi.org/10.1016/S0360-1323\(03\)00027-1](https://doi.org/10.1016/S0360-1323(03)00027-1).
- [22] N.P. Gao, J.L. Niu, CFD study of the thermal environment around a human body: A Review, *Indoor and Built Environment*. 14 (2005) 5–16. <https://doi.org/10.1177/1420326X05050132>.
- [23] W. Oh, S. Kato, The effect of airspeed and wind direction on human's thermal conditions and air distribution around the body, *Building and Environment*. 141 (2018) 103–116.
<https://doi.org/10.1016/j.buildenv.2018.05.052>.

Chapter 4.

Heat transfer coefficients for the naked manikin

4.1 Introduction

The development of realistic-looking thermal manikin makes it possible to acquire the heat transfer coefficients for the human body precisely. Ichihara et al. conducted an experiment to measure the convective and radiative heat transfer coefficients for each segment of thermal manikin both in sitting and standing postures [1]. De Dear et al. calculated the convective and radiative heat transfer coefficients of different body parts using a 16-segment thermal manikin under a wide range of airspeeds and wind directions [2]. Ozeki et al. investigated the heat transfer coefficients for the thermal manikin under solar radiation [3].

Computational fluid dynamics (CFD) has become an essential tool to predict thermal comfort in recent years. The CFD method can predict temperature and velocity fields cheaply and quickly compared to experiment work [4]. Besides, distributions of heat transfer coefficients, skin temperature, etc. can be acquired rather than the mean value of each segment through manikin experiments. Ono et al. conducted both the manikin experiment and the CFD analysis and verified the accuracy of CFD analysis in simulating the heat transfer around the human body [5]. However, in their research, only standing posture was adopted, and only upwind with airspeeds of 0.5–2.0 $\text{m}\cdot\text{s}^{-1}$ was reproduced. Sorensen et al. reported the airflow distribution and temperature distribution around a computational thermal manikin in a clam condition. Also, the convective and radiative heat transfer coefficients for the computational thermal manikin were presented [6].

In these researches, airflow blew only from the horizontal direction (e.g., from the front side, back side, right side, and left side of the thermal manikin). However, in traditional air condition systems, supply air from the ceiling is familiar [7]. Moreover, much attention has been paid to task ambient air conditioning systems during recent years. Ceiling-mounted and floor-based personalized ventilation system were mentioned in the literature [8,9]. Yang et al. evaluated the thermal environment and air environment of a ceiling-mounted ventilation system [8]. Lim et al. confirmed the performance of floor air outlets through CFD analysis. They found that task ambient air conditioning systems with floor air outlets can guarantee a comfortable thermal environment [10]. Therefore, the effect of upward airflow and downward airflow on the convective heat transfer coefficients are indispensable for thermal comfort studies.

The convective and radiative heat transfer coefficients are also affected by ambient temperature [11]. Yang et al. developed regression equations for the convective heat transfer coefficients based on the temperature difference between the skin and the ambient air [12]. Fanger's PMV model (i.e., $h_c = 2.38(t_{cl} - t_a)^{0.25}$) provides a widely accepted regression equation for the convective heat transfer coefficient based on the temperature difference between clothing surface and the ambient air, but this equation is at the whole-body level [13]. Kurazumi et al. measured the convective and radiative heat transfer coefficients for the human body under different ambient temperatures (16–26 °C) through a manikin experiment [14]. However, the heat transfer coefficients were also revealed at the whole-body level.

The aforementioned studies investigated the effect of airspeed on the convective heat transfer coefficient or the effect of temperature on the convective heat transfer coefficient. And they provided equations about airspeeds and the convective heat transfer coefficients ($h_c = aV^x$) or equations about the temperature differences and the convective heat transfer coefficients ($h_c = a\Delta T^x$). If the airspeed or temperature difference is known, the convective heat transfer coefficient can be calculated. However, if the temperature condition changes, the constants for equation $h_c = aV^x$ will be different. If the airspeed condition changes, the constants for equation $h_c = a\Delta T^x$ will also be different. Therefore, an equation both considering the effect of airspeed and temperature difference is essential.

In this chapter, firstly, the effect of wind from different directions on the convective heat transfer coefficient was discussed in Section 4.2. Secondly, how the temperature difference between the thermal manikin and the ambient air affected the convective and radiative heat transfer coefficients was confirmed in Section 4.3. Lastly, equations considering both the effect of airspeed and temperature difference were proposed in Section 4.4.

4.2 The effect of airspeed and wind direction

How the horizontal airflow and vertical airflow affects the convective heat transfer coefficient for the naked manikin was confirmed in this section (Figure 4-1). Both experiments and simulations were carried out. The summary of environmental conditions for experiment and CFD analysis is listed in Table 4-1. The detail in information will be described in 4.2.1 and 4.2.2.

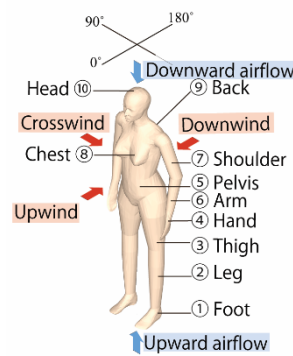


Figure 4-1. Body segments of the thermal manikin and wind directions.

Table 4-1. The summary of environmental conditions for experiment (Exp.) and CFD analysis.

Environmental conditions			Posture	Exp.	CFD
Horizontal airflow	Upwind	$t_a = 27.1\text{ }^{\circ}\text{C}$ (standing)	Standing Sitting	○	○
	Crosswind	$t_a = 27.5\text{ }^{\circ}\text{C}$ (sitting)			
	Downwind	$V = 0.25, 0.75, 1.1, 1.4\text{ m}\cdot\text{s}^{-1}$ $t_{sk} = 33.0\text{ }^{\circ}\text{C}$			
Vertical airflow	Upward	$0.05\text{--}1.4\text{ m}\cdot\text{s}^{-1}$			○
	Downward	$t_a = 27\text{ }^{\circ}\text{C}$ (standing, sitting)			
		$t_{sk} = 33.0\text{ }^{\circ}\text{C}$			

4.2.1 Experimental setup

Figure 4-2 shows a diagram of the temperature stratification wind tunnel ($16.5\text{ m} \times 2.2\text{ m} \times 1.8\text{ m}$). This study aims to discuss the indoor environment. ISO 7730 recommends indoor airspeed in the range of $0.1\text{--}0.3\text{ m}\cdot\text{s}^{-1}$ [15]. It was mentioned by Schiavon et al. that a hurricane stand fan could generate airspeeds of $0.05\text{--}1.3\text{ m}\cdot\text{s}^{-1}$ at 2 m distance [16]. However, this wind tunnel can only reproduce stable wind at a minimum airspeed of $0.25\text{ m}\cdot\text{s}^{-1}$. Therefore, wind speeds of $0.25\text{ m}\cdot\text{s}^{-1}$, $0.75\text{ m}\cdot\text{s}^{-1}$, $1.1\text{ m}\cdot\text{s}^{-1}$, and $1.4\text{ m}\cdot\text{s}^{-1}$ were reproduced, which are in the range of expected indoor wind speeds. The thermal manikin was rotated between three directions such that the wind flowed from the front side, back side, and right side of the thermal manikin (Figure 4-1).

The air temperature in the wind tunnel cannot be precisely controlled. However, the natural temperature in the wind tunnel was stable during the experiment. For the sitting posture, the mean air temperature in the wind tunnel was $27.5\text{ }^{\circ}\text{C}$, and the wall temperature was the same. For the standing posture, the mean air temperature in the wind tunnel was $27.1\text{ }^{\circ}\text{C}$ and the mean wall temperature was $27.0\text{ }^{\circ}\text{C}$. The distribution of radiation was made uniform by pasting black paper to styrene board placed 0.01 m from the sidewalls of the wind tunnel. The ceiling was also pasted by black paper, and the lights were turned off during the experiments.

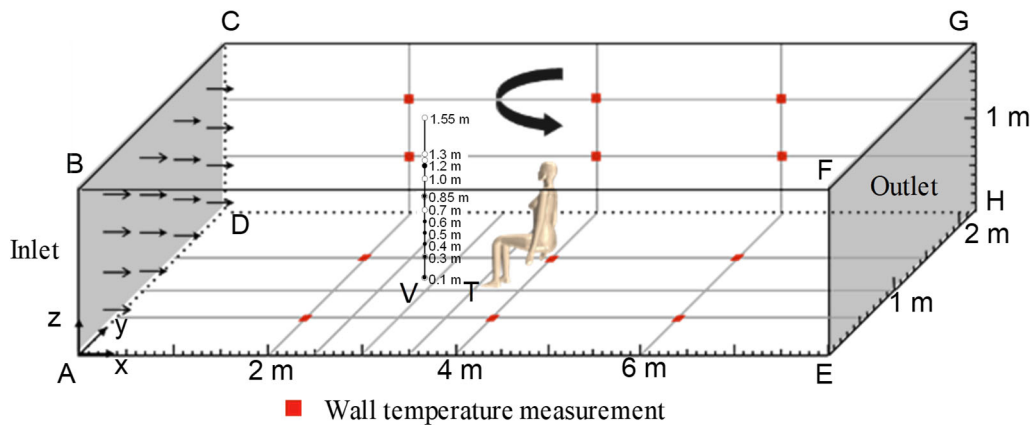


Figure 4-2. Diagram and measurement points of wind tunnel experiments. The airspeed measurement points are 1 m before the thermal manikin; the temperature measurement points are 0.5 m before the thermal manikin (the vertical positions for the temperature measurement points are same with velocity measurement points).

There were six temperature measurement points on each wall other than the inlet and outlet (Figure 4-2). The positions of measurement points on wall AEFB were the same as those wall DHGC, and the positions of the measurement points of wall BFGC (i.e., the ceiling) were the same as wall AEHD (i.e., the floor). The air temperature and airspeed were separately measured 0.5 m and 1 m before the manikin at heights of 0.05 m, 0.1 m, 0.3 m, 0.4 m, 0.5 m, 0.6 m, 0.7 m, 0.85 m, 1.0 m, 1.2 m, 1.25 m, and 1.55 m, which are the heights of each segment of the thermal manikin during sitting and standing postures, as listed in Table 4-2.

Table 4-2. Heights of measurement points (air temperature and velocity).

i	Segment (i)	Sitting (m)	Standing (m)
10	Head	1.2	1.55
9	Back	0.85	1.25
8	Chest	0.85	1.25
7 L / 7 R	Left shoulder / Right shoulder	0.85	1.3
6 L / 6 R	Left arm / Right arm	0.6	1.0
5	Pelvis	0.6	1.0
4 L / 4 R	Left hand / Right hand	0.4	0.7
3 L / 3 R	Left thigh / Right thigh	0.5	0.7
2 L / 2 R	Left leg / Right leg	0.3	0.3
1 L / 1 R	Left foot / Right foot	0.1	0.1

Note: For the body segments which have left and right side, for example, the leg and the hand, the segment number i for the right and left side are the same.

The average airspeed and turbulence intensity profiles in the wind tunnel are shown in Figure 4-3. The airspeeds below 0.3 m and above 1.2 m from the floor were smaller than other heights owing

to the roughness of the floor and ceiling surface, underlining the importance of utilizing the actual airspeed profile near the different segments of the manikin. As for the turbulence intensity, smaller airspeeds resulted in higher turbulence intensity. The turbulence intensity near the ceiling and floor was much higher at all airspeeds. Except for the minimum airspeed of $0.25 \text{ m} \cdot \text{s}^{-1}$ —whose turbulence intensity was much higher, i.e., 4–14%—the difference between the turbulence intensities of the airspeeds was small.

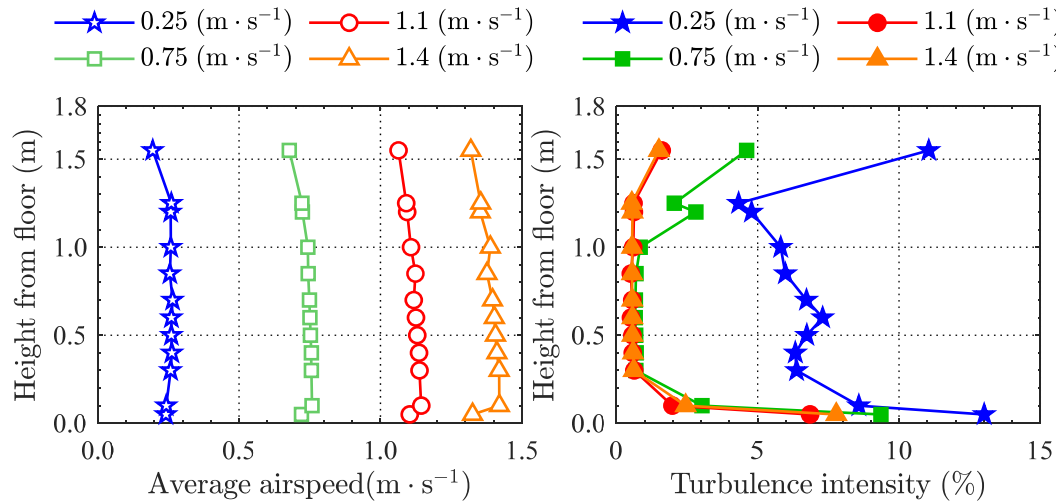


Figure 4-3. Average airspeed and turbulence intensity profiles in the wind tunnel without presence of the thermal manikin.

4.2.2 Numerical method

4.2.2.1 Wind tunnel

A geometry model was created referring to the shape of the wind tunnel and thermal manikin (Figure 4-4). As reserve flow happened, volume mesh of the outlet (i.e., surface EFGH) was extended to surface IJKL to make the flow fully develop with a low cell count—three million. The y^+ was below one everywhere on the manikin surface and wall surface (Figure 4-5). For the grid system for the wind tunnel and the climate chamber, we both did the mesh independence study. The mesh independence study was carried out by running additional CFD analysis with the same simulation model and boundary conditions but with different grid systems (coarse, medium, and fine mesh). The convective heat transfer coefficients calculated by the fine grid system were approximately the same with the present grid system. Therefore, a finer grid system had no considerable effects on the results. In the simulation of airflow around the human body, one of the most often utilized turbulence models is the low Reynolds-number $k-\varepsilon$ model [17]. Low Reynolds number $k-\varepsilon$ model was verified to analyze accurately convective heat transfer around complicated geometry [18]. In this study, the flow and heat transfer were calculated with the Reynolds-averaged Navier–Stokes equations closed by a Lien-Chen low Reynolds number $k-\varepsilon$ model [19]. For the finite volume method, the second-order upwind difference scheme was utilized. The SIMPLE algorithm was used for the pressure–velocity coupling. The numerical method is shown in Table 4-3.

The boundary conditions of the CFD analysis were set from the experiment. Table 4-4 details these boundary conditions. The inlet velocity boundary conditions were set from the airspeeds measured

1 m before the thermal manikin (Figure 4-3). The airspeeds 1 m before the thermal manikin according to the CFD analysis were consistent with the experimental data (Figure 4-6). The other boundary conditions of the CFD analysis are given in Table 4-4.



Figure 4-4. Simulation model of the wind tunnel.

Table 4-3. Numerical method.

Computational grid	Cell types: tetrahedral mesh, prism layer Number of cells: approximately 20 million
Turbulence model	Low Reynolds number $k-\varepsilon$ model (Lien-Chen type)
Difference scheme	Convection term: second-order upwind
Algorithm	SIMPLE
Radiation	Surface-to-surface model [20]

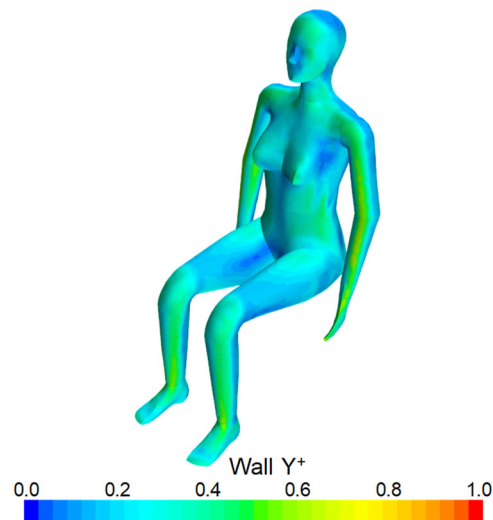


Figure 4-5. Y^+ distribution for computational thermal manikin surface (Sitting posture, $U_0 = 1.4 \text{ m}\cdot\text{s}^{-1}$).

Table 4-4. Boundary conditions for the wind tunnel.

Inlet (ABCD)	Velocity: U_0 , results of the experiment (Figure 4-3) Turbulence intensity: I_{in} , results of the experiment (Figure 4-3) Turbulence length scale: $*L_{in} = 0.14$ m Temperature: results of the experiment (stand, 27.1 °C, sit, 27.5 °C)
Outlet (EFGH)	U_{out} : depends on the law of mass conservation [21] k_{out} , ε_{out} : free slip
Wall	Surface temperature: t_{wall} , results of the experiment (stand, 27.0 °C, sit, 27.5 °C) Velocity: no slip
Thermal manikin	Surface temperature: 33 °C Velocity: no slip Emissivity: 0.95 Direction: front side (upwind), back side (crosswind), right side (downwind)

* $L_{in} = 0.07 L$ [22], L : characteristic length of inlet

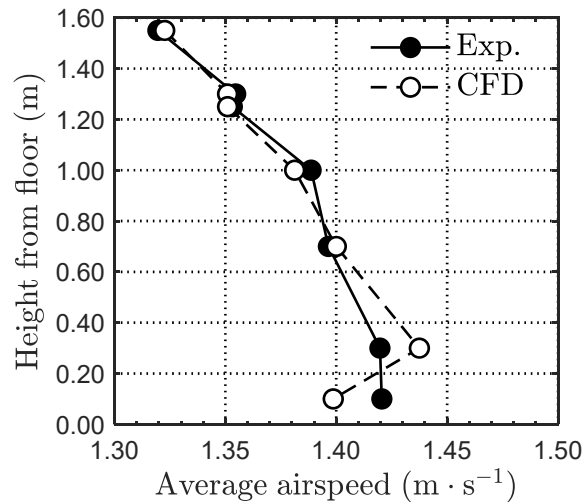


Figure 4-6. Comparison of the airspeed 1 m before the thermal manikin according to the CFD analysis and the experimental data.

4.2.2.2 Climate chamber

A geometry model was created referring to the shape of the climate chamber and the thermal manikin (Figure 4-7). To confirm how the airflows in the vertical direction affect heat transfer around the human body, the downward airflow condition and upward airflow condition with inlet airspeeds of 0.05–1.4 m · s⁻¹ at an ambient temperature of 27 °C were simulated. With respect to the upward airflow condition, the airflow flowed in from the whole floor and flowed out through the whole ceiling. With respect to the downward airflow condition, the airflow flowed in through the

ceiling and flowed out through the floor. The numerical method for the climate chamber was the same as that for the wind tunnel (Table 4-3), except that the number of cells was approximately 10 million. The boundary conditions are listed in Table 4-5.

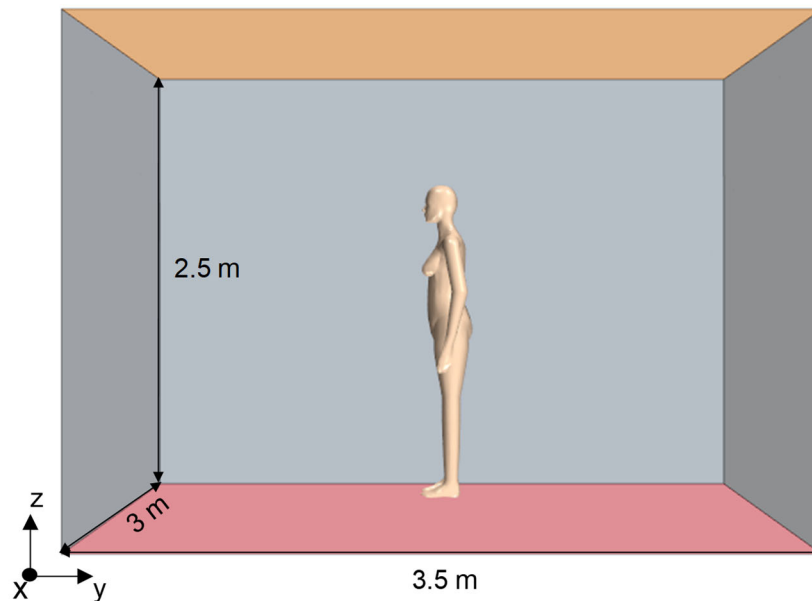


Figure 4-7. Simulation model of the climate chamber.

Table 4-5. Boundary conditions for the climate chamber.

Inlet (floor/ceiling)	Velocity: U_0 (results of experiment) Temperature: 27 °C Turbulence intensity: $I_{in} = 10\%$ Turbulence length scale: $L_{in} = 0.2$ m
Outlet (ceiling/floor)	Pressure outlet: static pressure, $P = 0$
Wall	Surface temperature: adiabatic Velocity: no slip Emissivity: 0.9
Thermal manikin	Surface temperature: 33 °C Velocity: no slip Emissivity: 0.95

4.2.3 Results

4.2.3.1 Whole-body convective heat transfer coefficient

(1) Horizontal airflow

There was no significant difference in the whole-body convective heat transfer coefficients caused by wind from the horizontal directions for the sitting posture (Figure 4-9). However, the whole-body convective heat transfer coefficient for the standing posture caused by wind from the right side of the thermal manikin was smallest owing to the lower surface area facing the wind. Additionally,

for standing posture, the whole-body convective heat transfer coefficient of downwind was the largest.

The convective heat transfer coefficient for the whole body in the sitting posture was smaller than the standing posture because some body segments shielded others from the flow.

As it is illustrated in Figure 4-9, the results of convective heat transfer coefficients fell in the middle of the results from other studies. Moreover, the whole-body convective heat transfer coefficients according to the experiment and CFD analysis were consistent. Hence, about convective heat transfer coefficients for different body segments, only results of CFD analysis were listed in Section 4.2.3.2.

(2) Vertical airflow

The convective heat transfer coefficients caused by the upward airflow were larger than those caused by downward airflow both in the standing and sitting posture (Figure 4-9). The reason is that upward plume resulted from natural convection and upward airflow representing forced convection worked together, the convective heat transfer between the manikin and surrounding air was enhanced.

The convective heat transfer coefficients for sitting posture were larger than those of standing posture. This is because the body area facing the airflow was larger in the sitting posture with the thighs facing the wind.

(3) Comparison of horizontal airflow and vertical airflow

Concerning the sitting posture, convective heat transfer coefficients caused by the vertical airflow were larger. This is because the body area facing the wind was larger for the sitting posture. Concerning the standing posture, the convective heat transfer coefficients caused by the horizontal wind were larger. A potential explanation for this finding is that the horizontal airflow is easier to break the thermal plume (Figure 4-8).

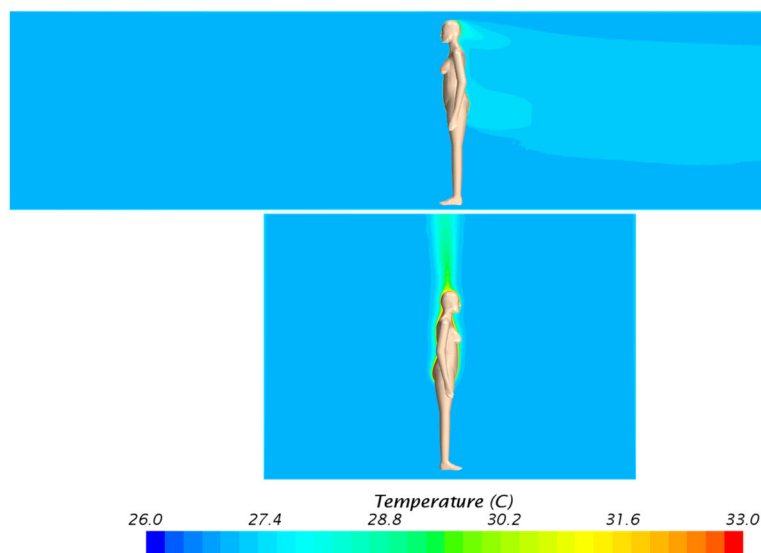


Figure 4-8. Temperature distribution for upwind and upward airflow when skin temperature was 33 °C and air temperature was 27 °C.

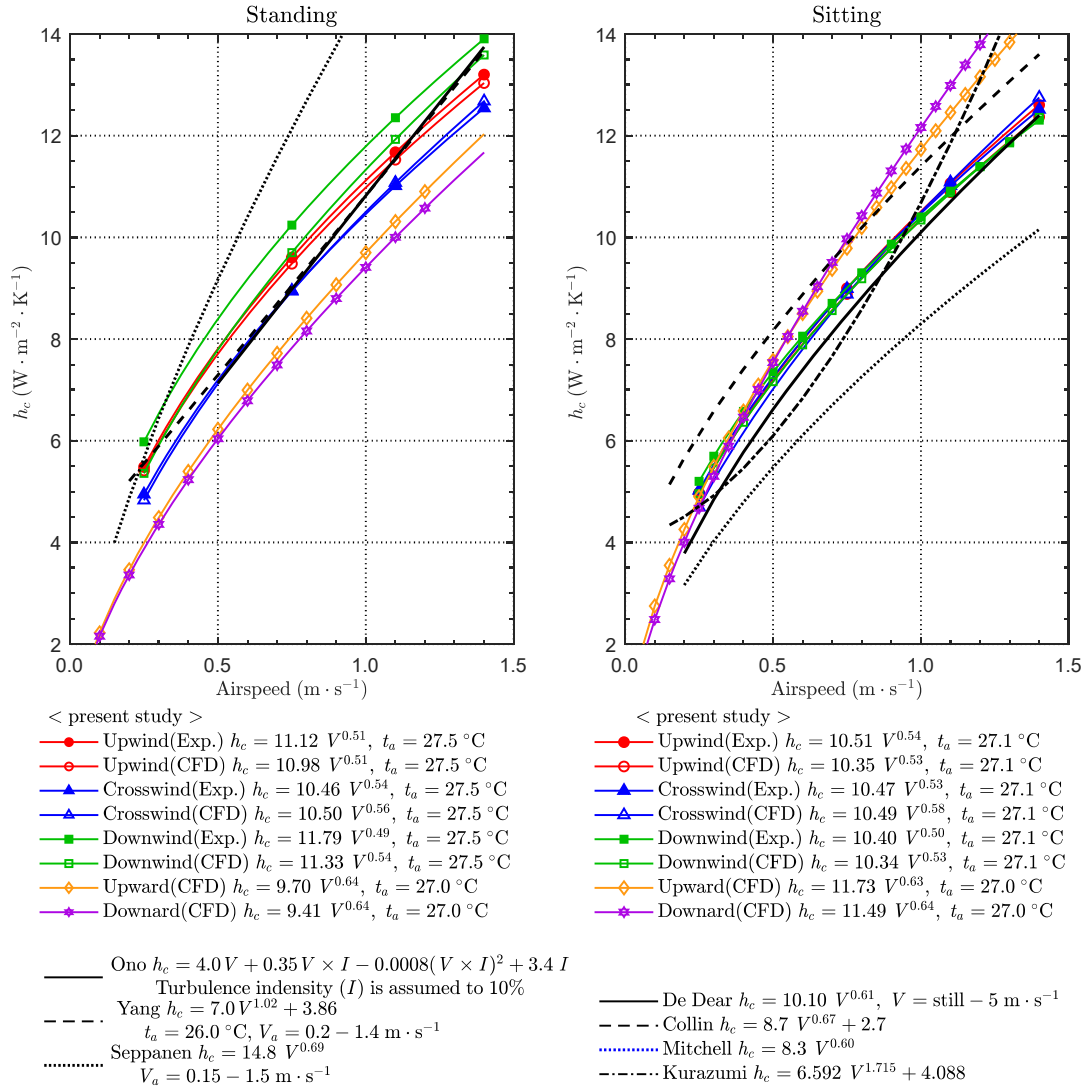


Figure 4-9. Whole-body convective heat transfer coefficient under various wind directions (Other studies: De Dear et al. [2], Colin et al. [23], Mitchell [24], Kurazumi [7], Ono et al. [5], Yang et al. [12], Seppanen [25]).

4.2.3.2 Convective heat transfer coefficients for different body segments

Figure 4-10 shows the convective heat transfer coefficients for different body segments of various wind direction in standing posture.

Convective heat transfer coefficients for the feet, hands, and arms were larger than other body segments. The reason is that these segments had thin boundary layer.

Concerning the head, there were no significant differences in convective heat transfer coefficients between different wind directions except for the downward airflow. Concerning the back, the results for the downwind and downward airflow were larger than other wind directions. The higher value for downwind is because the wind was blowing directly on the back. The higher value for downward airflow is because the back was near the ceiling inlet. Hence, the airspeed near the back was higher. Concerning the chest, as it is also seen for the back, the convective heat transfer coefficients caused by the downward airflow were the largest. Concerning the pelvis, there were no significant differences in convective heat transfer coefficients between different wind directions. This is

because the pelvis was in the central part of the body. Hence, it was hard for the airflow to reach the pelvis.

Concerning the shoulders, the convective heat transfer coefficients caused by the upward airflow were smaller than other wind directions. A potential reason is that the shoulders had a long distance from the floor inlet, and the velocity was reduced when the airflow hit the shoulder. Moreover, the airflow velocity hitting the shoulders was decreased due to the resistance of body surface. It is also indicated that when the wind blew from the right side of the thermal manikin, the convective heat transfer coefficient for the right shoulder was larger than that of the left shoulder.

Concerning the arms, the results for the horizontal airflow were larger. The thermal boundary layer for the arms was thin. Additionally, the horizontal airflow disturbed the thermal boundary layer easily. Thus, the convective heat transfer coefficients for the arms caused by the horizontal wind were larger.

Concerning the hands, the results for the horizontal airflow were also larger. The reason is the same as that of the arms.

Concerning the thighs, the results for the horizontal airflow were slightly larger.

Concerning the legs and feet, the convective heat transfer coefficients caused by the upward airflow were larger than those of the downward airflow because the upward airflow was blowing directly on the feet and legs.

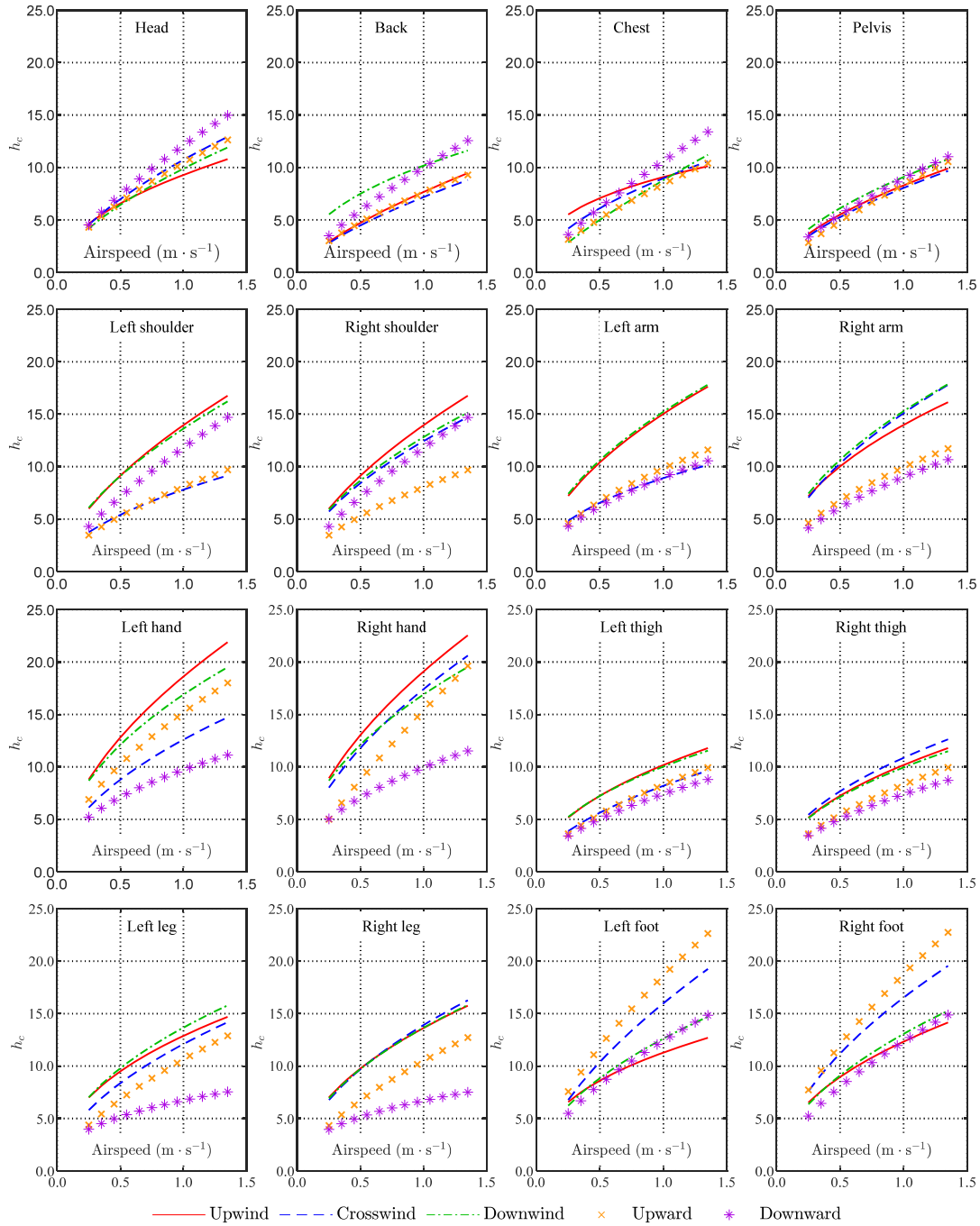


Figure 4-10. Convective heat transfer coefficients for each body segment under various airspeeds in different wind directions for standing posture according to CFD analysis ($\text{W} \cdot \text{m}^{-2} \cdot \text{K}^{-1}$).

Figure 4-11 shows the convective heat transfer coefficients for different body segments caused by various wind direction in sitting posture. As also seen in the standing posture, the convective heat transfer coefficients for the feet, hands, and arms were larger than other body segments. The effect of wind of various directions on convective heat transfer coefficients for sitting posture were similar to the standing posture except for the thighs and pelvis.

Concerning the thighs, the convective heat transfer coefficients caused by the vertical airflow were larger than those caused by horizontal airflow. The reason is that the thighs were facing vertical

airflow while sitting.

Concerning the pelvis, in the vertical airflow, the convective heat transfer coefficients were larger than the standing posture. This is because the thermal boundary layer for the standing position was thinner than the sitting position due to the geometry shape (Figure 4-12).

The regression models for convective heat transfer coefficients against airspeed for standing posture and sitting posture are shown from Table 4-6 to Table 4-13.

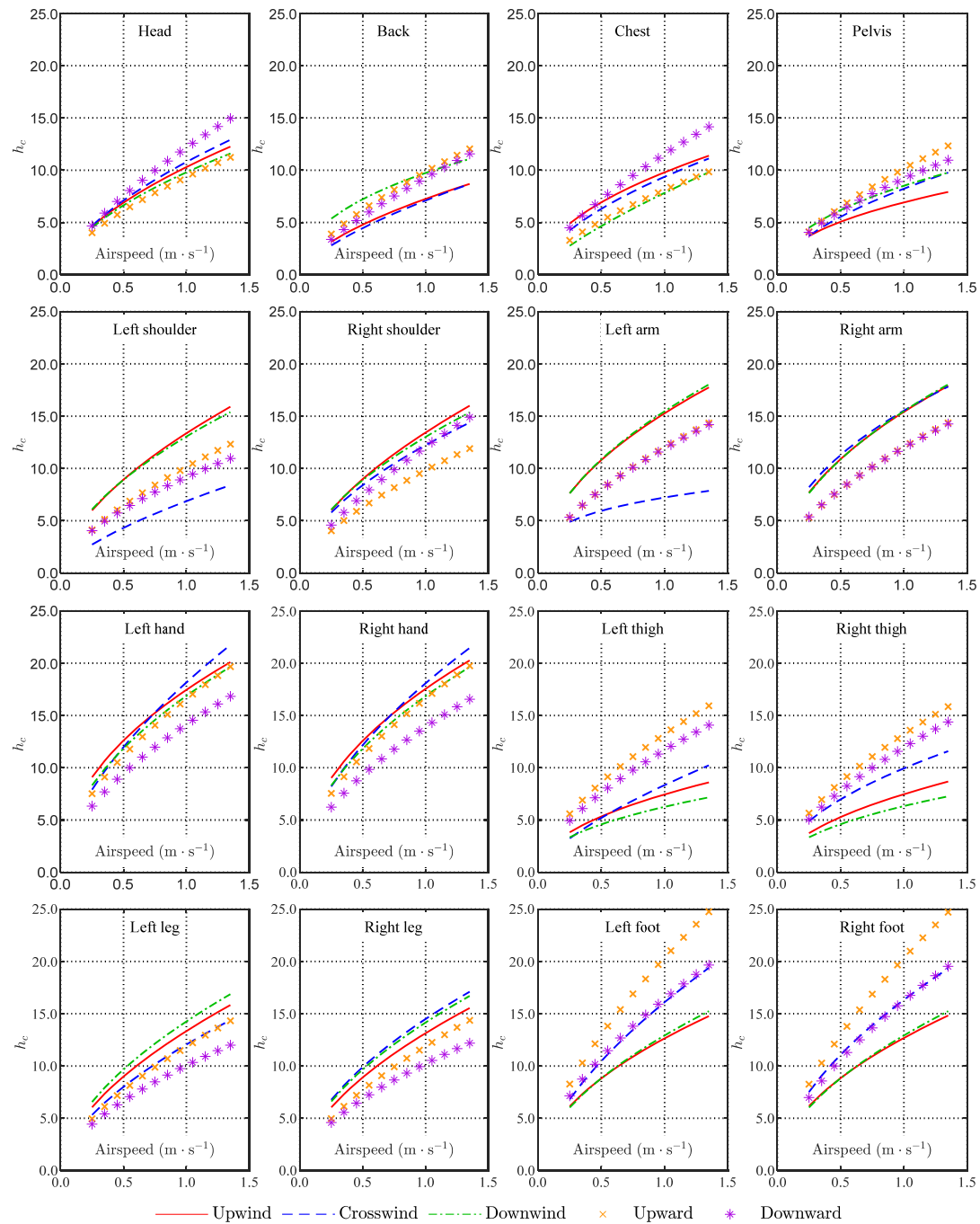


Figure 4-11. Convective heat transfer coefficients for each body segment under various airspeeds in different wind directions for sitting posture based on CFD analysis ($\text{W} \cdot \text{m}^{-2} \cdot \text{K}^{-1}$).

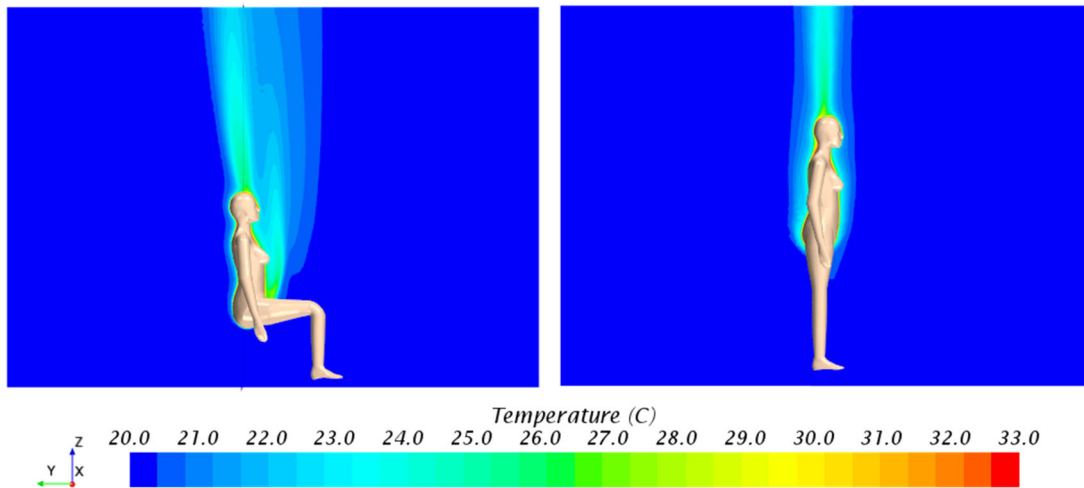


Figure 4-12. The contour plots of temperature distribution in the climate chamber in sitting and standing postures at an airspeed of $1 \text{ m}\cdot\text{s}^{-1}$ (yz-plane).

Table 4-6. Regression models of the convective heat transfer coefficient caused by the upwind for the thermal manikin in the standing posture both for experimental and CFD results.

$$h_c = aV^b \text{ (W}\cdot\text{m}^{-2}\cdot\text{K}^{-1}\text{)}$$

Segment	Upwind					
	Exp.			CFD		
	a	b	R ²	a	b	R ²
10. Head	9.78	0.67	0.996	9.29	0.50	0.996
9. Back	7.55	0.84	0.989	7.67	0.70	0.998
8. Chest	12.23	0.45	0.995	8.09	0.36	0.993
7. Shoulder (R)	13.12	0.67	0.997	12.50	0.52	0.996
(L)	12.10	0.56	0.999	13.96	0.61	0.999
6. Arm (R)	12.68	0.48	0.993	13.98	0.48	0.996
(L)	12.18	0.47	0.990	15.04	0.53	0.996
5. Pelvis	8.30	0.44	0.971	8.30	0.59	0.999
4. Hand (R)	17.08	0.58	0.971	19.11	0.55	0.988
(L)	15.83	0.52	0.999	18.62	0.54	0.990
3. Thigh (R)	10.19	0.47	0.945	10.18	0.49	0.991
(L)	9.48	0.34	0.960	10.58	0.54	0.983
2. Leg (R)	11.71	0.40	0.955	13.64	0.48	0.989
(L)	12.77	0.39	0.961	12.88	0.44	0.986
1. Foot (R)	14.25	0.55	0.999	12.33	0.46	0.997
(L)	16.65	0.58	0.994	11.29	0.39	0.997
Whole-body	11.12	0.51	0.985	10.98	0.51	0.997

Table 4-7. Regression models of the convective heat transfer coefficient caused by the crosswind for the thermal manikin in the standing posture both for experimental and CFD results.

$$h_c = aV^b \text{ (W}\cdot\text{m}^{-2}\cdot\text{K}^{-1}\text{)}$$

Segment	Crosswind					
	Exp.			CFD		
	a	b	R ²	a	b	R ²
10. Head	7.95	0.62	0.988	10.73	0.62	0.996
9. Back	7.84	0.74	0.987	7.18	0.68	0.999
8. Chest	8.64	0.52	0.948	8.97	0.55	0.999
7. Shoulder (R)	12.15	0.54	0.995	12.44	0.56	0.999
(L)	6.33	0.41	0.828	7.81	0.53	0.864
6. Arm (R)	13.88	0.51	0.996	15.10	0.55	0.999
(L)	8.19	0.43	0.930	8.91	0.44	0.768
5. Pelvis	10.36	0.67	0.993	8.05	0.61	0.986
4. Hand (R)	16.11	0.60	0.997	17.42	0.56	0.998
(L)	12.03	0.44	0.970	12.60	0.52	0.951
3. Thigh (R)	10.35	0.43	0.991	10.87	0.50	0.993
(L)	9.56	0.43	0.954	8.20	0.54	0.914
2. Leg (R)	13.77	0.52	0.999	13.92	0.52	0.999
(L)	12.64	0.49	0.999	12.10	0.53	0.998
1. Foot (R)	17.00	0.65	0.997	16.53	0.56	0.999
(L)	13.58	0.58	0.996	15.99	0.62	0.999
Whole-body	10.46	0.54	0.987	10.50	0.56	0.993

Table 4-8. Regression models of the convective heat transfer coefficient caused by the downwind for the thermal manikin in the standing posture both for experimental and CFD results.

$$h_c = aV^b \text{ (W}\cdot\text{m}^{-2}\cdot\text{K}^{-1}\text{)}$$

Segment	Downwind					
	Exp.			CFD		
	a	b	R ²	a	b	R ²
10. Head	9.28	0.75	0.998	9.89	0.62	0.999
9. Back	16.58	0.43	0.997	10.18	0.44	0.997
8. Chest	8.36	0.67	0.998	8.79	0.81	0.996
7. Shoulder (R)	12.18	0.58	0.996	12.82	0.56	0.999
(L)	13.63	0.58	0.995	12.84	0.56	0.999
6. Arm (R)	13.49	0.60	0.992	15.29	0.52	0.997
(L)	12.75	0.52	0.982	15.24	0.52	0.997
5. Pelvis	9.78	0.45	0.946	9.09	0.57	0.999
4. Hand (R)	25.08	0.45	0.983	16.91	0.48	0.996
(L)	23.08	0.47	0.951	16.89	0.48	0.996
3. Thigh (R)	10.58	0.41	0.944	9.95	0.48	0.988
(L)	9.77	0.44	0.935	10.03	0.47	0.989
2. Leg (R)	11.11	0.37	0.939	13.66	0.49	0.988
(L)	12.27	0.43	0.947	13.67	0.48	0.988
1. Foot (R)	12.73	0.46	0.989	13.07	0.52	0.989
(L)	12.54	0.51	0.979	12.62	0.51	0.989
Whole-body	11.79	0.49	0.981	11.33	0.54	0.998

Table 4-9. Regression models of the convective heat transfer coefficient for the thermal manikin caused by the vertical airflow in the standing posture for CFD results.

$h_c = aV^b$ ($\text{W}\cdot\text{m}^{-2}\cdot\text{K}^{-1}$)

Segment	Upward			Downward		
	CFD			CFD		
	a	b	R ²	a	b	R ²
10. Head	10.42	0.64	0.989	12.10	0.71	0.979
9. Back	7.60	0.67	0.994	10.00	0.76	0.985
8. Chest	8.41	0.71	0.985	10.60	0.78	0.986
7. Shoulder (R)	8.06	0.61	0.975	11.80	0.73	0.983
(L)	8.08	0.61	0.975	11.81	0.73	0.978
6. Arm (R)	9.83	0.55	0.978	9.02	0.56	0.921
(L)	9.83	0.55	0.978	9.00	0.53	0.879
5. Pelvis	8.35	0.78	0.986	8.94	0.70	0.979
4. Hand (R)	15.39	0.81	0.988	9.94	0.49	0.897
(L)	15.18	0.57	0.988	9.72	0.45	0.817
3. Thigh (R)	8.30	0.60	0.969	7.39	0.55	0.875
(L)	8.29	0.60	0.969	7.43	0.56	0.880
2. Leg (R)	10.50	0.64	0.989	6.70	0.38	0.819
(L)	10.63	0.64	0.989	6.73	0.38	0.872
1. Foot (R)	18.77	0.64	0.992	12.35	0.62	0.957
(L)	18.63	0.65	0.992	12.43	0.59	0.966
Whole-body	9.70	0.64	0.985	9.41	0.64	0.958

Table 4-10. Regression models of the convective heat transfer coefficient for the thermal manikin caused by the upwind in the sitting posture both for experimental and CFD results.

$$h_c = aV^b \text{ (W}\cdot\text{m}^{-2}\cdot\text{K}^{-1}\text{)}$$

Segment	Upwind					
	Exp.			CFD		
	a	b	R ²	a	b	R ²
10. Head	9.25	0.72	0.998	10.30	0.58	0.998
9. Back	6.86	0.66	0.964	7.26	0.60	0.986
8. Chest	12.34	0.53	0.995	9.80	0.50	0.996
7. Shoulder (R)	10.80	0.50	0.999	13.44	0.58	0.999
(L)	12.23	0.60	0.986	13.36	0.58	0.999
6. Arm (R)	12.14	0.44	0.981	15.41	0.50	0.995
(L)	12.00	0.46	0.982	15.28	0.50	0.995
5. Pelvis	9.12	0.51	0.991	6.92	0.45	0.988
4. Hand (R)	14.27	0.55	0.961	17.55	0.48	0.993
(L)	15.37	0.47	0.992	17.45	0.47	0.995
3. Thigh (R)	10.28	0.55	0.999	7.47	0.50	0.999
(L)	9.04	0.53	0.998	7.45	0.48	0.999
2. Leg (R)	10.74	0.46	0.992	13.14	0.56	0.998
(L)	11.75	0.51	0.994	13.34	0.57	0.998
1. Foot (R)	12.40	0.50	0.995	12.68	0.52	0.996
(L)	12.44	0.55	0.984	12.64	0.52	0.997
Whole-body	10.51	0.54	0.994	10.35	0.53	0.997

Table 4-11. Regression models of the convective heat transfer coefficient caused by the crosswind for the thermal manikin in the sitting posture both for experimental and CFD results.

$$h_c = aV^b \text{ (W}\cdot\text{m}^{-2}\cdot\text{K}^{-1}\text{)}$$

Segment	Crosswind					
	Exp.			CFD		
	a	b	R ²	a	b	R ²
10. Head	8.12	0.60	0.987	10.78	0.60	1.000
9. Back	9.81	0.67	0.997	7.10	0.67	0.965
8. Chest	9.01	0.59	0.892	9.37	0.57	0.994
7. Shoulder (R)	11.68	0.61	0.975	12.23	0.54	0.993
(L)	9.40	0.53	0.790	6.87	0.67	0.968
6. Arm (R)	13.52	0.46	0.977	15.53	0.46	0.994
(L)	8.15	0.33	0.934	7.22	0.28	0.788
5. Pelvis	9.18	0.43	0.998	8.23	0.57	0.981
4. Hand (R)	16.92	0.60	1.000	18.09	0.57	0.991
(L)	13.29	0.53	0.960	18.16	0.60	0.999
3. Thigh (R)	11.21	0.55	0.991	9.94	0.51	0.994
(L)	9.46	0.64	0.996	8.34	0.68	0.997
2. Leg (R)	13.67	0.47	0.997	14.50	0.55	0.999
(L)	11.23	0.41	0.996	12.05	0.59	0.995
1. Foot (R)	14.90	0.46	0.980	16.33	0.56	0.998
(L)	11.32	0.42	0.991	16.10	0.62	0.998
Whole-body	10.47	0.53	0.993	10.49	0.58	0.993

Table 4-12. Regression models of the convective heat transfer coefficient caused by the downwind for the thermal manikin in the sitting posture both for experimental and CFD results.

$$h_c = aV^b \text{ (W}\cdot\text{m}^{-2}\cdot\text{K}^{-1}\text{)}$$

Segment	Downwind					
	Exp.			CFD		
	a	b	R ²	a	b	R ²
10. Head	8.33	0.72	0.998	9.80	0.56	0.999
9. Back	11.92	0.45	0.993	9.74	0.43	0.990
8. Chest	7.15	0.59	0.997	7.83	0.75	0.995
7. Shoulder (R)	12.00	0.58	0.998	13.02	0.55	0.997
(L)	11.98	0.58	0.993	13.05	0.55	0.998
6. Arm (R)	13.19	0.43	0.984	15.48	0.51	0.994
(L)	13.33	0.47	0.993	15.47	0.51	0.994
5. Pelvis	9.07	0.48	0.981	8.51	0.46	0.984
4. Hand (R)	13.72	0.45	0.953	16.85	0.51	0.995
(L)	12.70	0.47	0.972	16.87	0.51	0.996
3. Thigh (R)	8.96	0.35	0.896	6.33	0.46	0.935
(L)	8.04	0.35	0.930	6.26	0.45	0.925
2. Leg (R)	11.33	0.54	0.995	14.16	0.55	0.999
(L)	11.54	0.61	0.991	14.26	0.56	0.999
1. Foot (R)	12.63	0.52	0.991	12.92	0.55	0.992
(L)	12.98	0.49	0.990	12.92	0.55	0.993
Whole-body	10.40	0.50	0.992	10.34	0.52	0.992

Table 4-13. Regression models of the convective heat transfer coefficient for the thermal manikin caused by the vertical airflow in the sitting posture both for experimental and CFD results.

$$h_c = aV^b \text{ (W} \cdot \text{m}^{-2} \cdot \text{K}^{-1}\text{)}$$

Segment	Upward			Downward		
	CFD			CFD		
	a	b	R ²	a	b	R ²
10. Head	9.35	0.61	0.985	12.16	0.69	0.986
9. Back	9.85	0.67	0.994	9.29	0.73	0.981
8. Chest	8.10	0.65	0.987	11.54	0.68	0.996
7. Shoulder (R)	9.82	0.64	0.985	12.08	0.70	0.992
(L)	9.87	0.64	0.985	12.16	0.70	0.991
6. Arm (R)	12.03	0.59	0.980	11.98	0.58	0.989
(L)	12.01	0.59	0.979	11.92	0.58	0.987
5. Pelvis	10.14	0.65	0.980	9.18	0.59	0.979
4. Hand (R)	16.64	0.57	0.991	13.91	0.58	0.979
(L)	16.57	0.57	0.991	14.14	0.58	0.982
3. Thigh (R)	13.19	0.61	0.992	11.94	0.62	0.984
(L)	13.22	0.62	0.991	11.68	0.62	0.981
2. Leg (R)	11.89	0.63	0.994	10.24	0.58	0.944
(L)	11.85	0.63	0.994	10.05	0.59	0.947
1. Foot (R)	20.33	0.65	0.994	16.26	0.61	0.965
(L)	20.37	0.65	0.994	16.41	0.60	0.975
Whole-body	11.73	0.63	0.990	11.49	0.64	0.983

4.3 The effect of temperature

A thermal manikin with fixed surface temperature (33 °C) was placed in a climate chamber with ambient temperatures of 20 °C, 24 °C, and 28 °C, at airspeeds of under 0.1 m·s⁻¹ to confirm the effects of ambient temperature on convective and radiative heat transfer coefficients (Figure 4-13). CFD analysis was performed with conditions matching those of the experiment by using a computational thermal manikin with the same shape as that used in the experiment.

The summary of environmental conditions for experiment and CFD analysis is listed in Table 4-14.

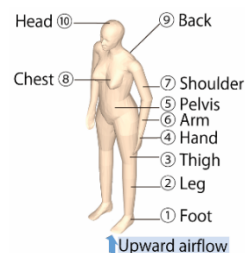


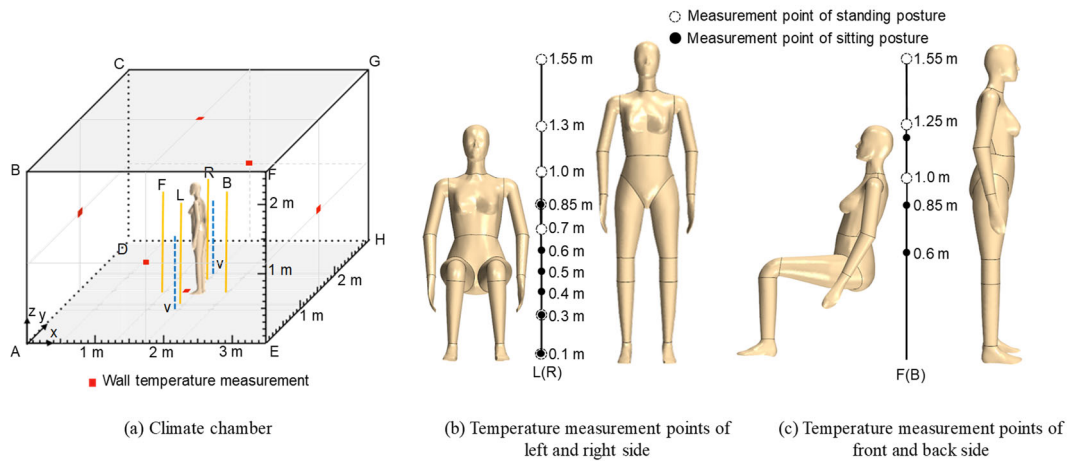
Figure 4-13. Body segments of the thermal manikin and wind directions.

Table 4-14. The summary of environmental conditions for the experiment (Exp.) and CFD analysis.

Temperature	Velocity	Wind direction	Posture	Exp.	CFD
$t_{in} = 20\text{ }^{\circ}\text{C}, 24\text{ }^{\circ}\text{C}, 28\text{ }^{\circ}\text{C}$ $t_{sk} = 33\text{ }^{\circ}\text{C}$	$0.1\text{ m}\cdot\text{s}^{-1}$	Upward	Standing Sitting	○	○

4.3.1 Experimental setup

Figure 4-14 shows a diagram and measurement points of the climate chamber ($3.0\text{ m} \times 3.5\text{ m} \times 2.5\text{ m}$). The thermal manikin was placed in the center of the climate chamber. The air temperature was set to $20\text{ }^{\circ}\text{C}$, $24\text{ }^{\circ}\text{C}$, and $28\text{ }^{\circ}\text{C}$ in order to confirm the effect of ambient temperature on the convective and radiative heat transfer coefficients. The conditioned air was supplied to the chamber from the entire floor and was removed from the ceiling. The inlet velocity was very difficult to control at different levels. Therefore, a uniform upward airflow velocity of under $0.1\text{ m}\cdot\text{s}^{-1}$ was set in the chamber. Air temperature (t_a) near each body segment was measured (Figure 4-14 (b) and (c)). The positions of measurement points of t_a are shown in Figure 4-14. Wall temperature was measured at the center of each wall (Figure 4-14 (a)). It turned out that in all experiments in the climate chamber wall temperature was nearly consistent with air temperature. Airspeed was measured on the left and right sides of thermal manikin at the heights of 0.1 m , 0.6 m , 1.1 m , to confirm the uniformity of the air environment (Figure 4-14 (a)).



(a) The solid lines in yellow present the air temperature measurement points. The dotted lines in the blue present the airspeed measurement points (the heights of the airspeed measurement points on both left and right sides are 0.1 m , 0.6 m , and 1.1 m). The square point in red presents the wall temperature measurement point, for the other walls, the temperature measurement points are in the same position of each wall);

(b) The vertical positions for the air temperature measurement points on the right and left sides of the thermal manikin;

(c) The vertical positions for the air temperature measurement points on the front and back sides of the thermal manikin.

Figure 4-14. Diagram and measurement points of climate chamber experiments.

4.3.2 Numerical method

The simulation model for the climate chamber was the same as that in Section 4.2.2.2 (Figure 4-7). The numerical method was also the same as that in Section 4.2.2.2. The boundary condition was set up from the experiment (Table 4-15).

Table 4-15. Boundary conditions for the climate chamber (Section 4.3.2).

Inlet (floor)	Velocity: U_0 (results of experiment)
	Temperature: t_{in} (results of experiment)
	Turbulence intensity: $I_{in} = 10\%$
	Turbulence length scale: $L_{in} = 0.2$ m
Outlet (ceiling)	Pressure outlet: static pressure, $P = 0$
Wall	Surface temperature: t_{wall} (results of the experiment)
	Velocity: no slip
	Emissivity: 0.9
Thermal manikin	Surface temperature: 33 °C
	Velocity: no slip
	Emissivity: 0.95

$L_{in} = 0.07 L$, L : characteristic length of inlet

4.3.3 Results

4.3.3.1 Convective heat transfer coefficient

The results of the convective heat transfer coefficient for different ambient temperatures are summarized in Figure 4-15, Table 4-16, and Table 4-17. The convective and radiative heat transfer coefficient for the right and left sides of each body segment were averaged because the air environment was uniform. The convective heat transfer coefficients for limbs (i.e., feet, hands, and arms) were larger than those of trunk (i.e., pelvis, shoulders, back, and chest). This is because thermal boundary layers of limbs were much thinner, and were exposed in cold upward flow where the thermal plume was not fully developed (Figure 4-16) [17]. The much thicker thermal boundary layer of the trunk yielded much smaller convective heat transfer coefficients than other body segments. The convective heat transfer coefficient of the head was relatively low because it was in the fully developed thermal plume [26]. As the relative error between the experimental data with CFD analysis for sitting and standing posture was respectively 10 % and 13%. The overall convective heat transfer coefficient obtained by CFD analysis was consistent with the experimental one, but this was not what happened for the head and some limbs. Although a considerable effort was taken to make the boundary condition of CFD analysis consistent with the experiment condition, it was very tough to make the fluid field of CFD analysis the same with the experiment. Besides, the low Reynolds-number $k-\varepsilon$ model over-predicted the velocity of the thermal plume, which led to a larger convective heat transfer coefficient for the head [27]. Furthermore, in other research, the peak velocity simulated by CFD analysis was slightly higher than that of the experiment [6,28].

Another possible reason is that the surface temperature of the manikin head did not reach 33 °C in the experiment, as it was at the end of the body, and it was difficult to reach the target temperature. Therefore, in the following experiments, the surface manikin of the thermal temperature was also confirmed by the thermocouple.

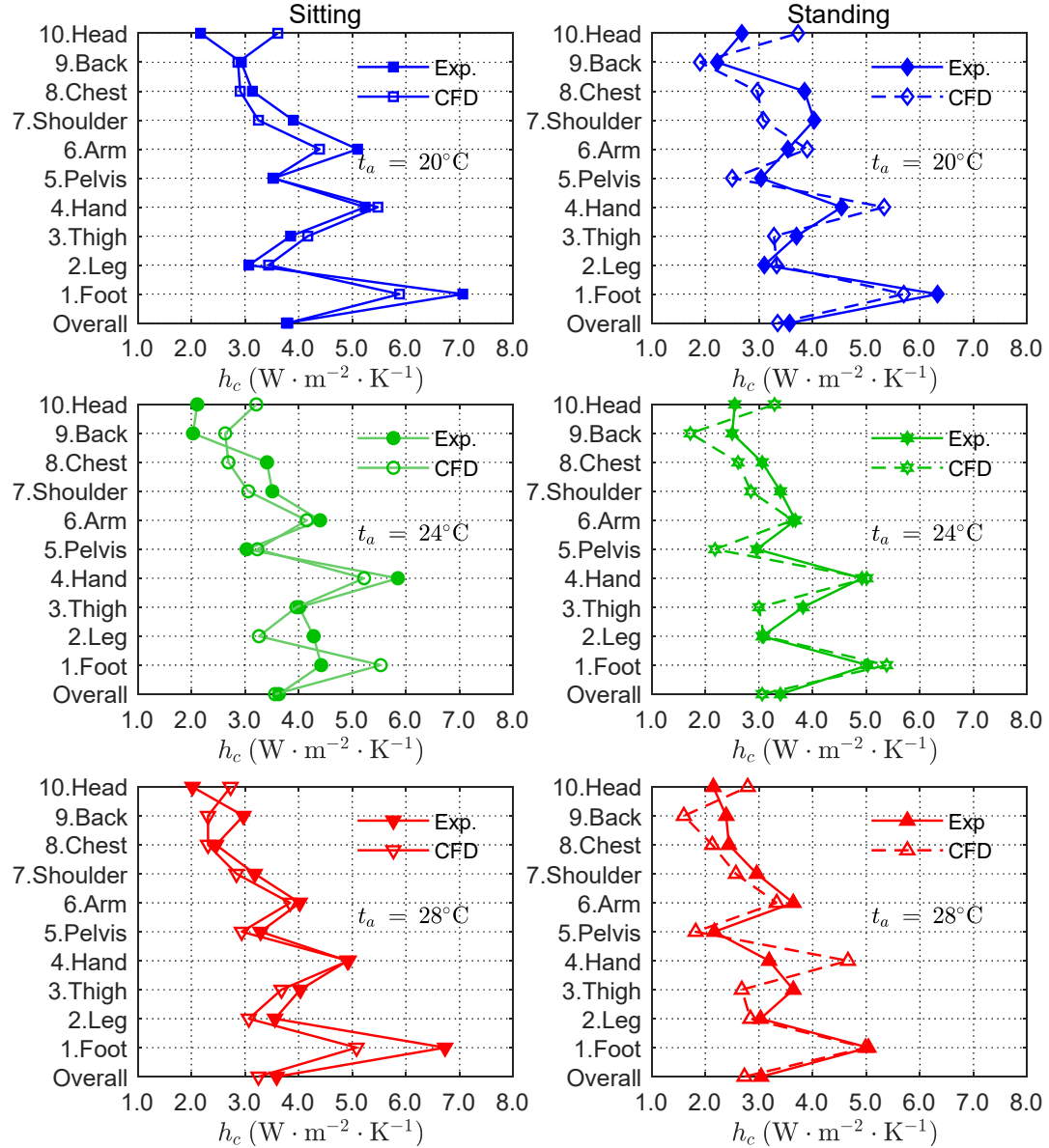


Figure 4-15. Convective heat transfer coefficients for each body segment under different ambient temperatures in the climate chamber at an airspeed of under 0.1 m·s⁻¹ (left: sitting posture; right: standing posture).

Table 4-16. Convective heat transfer coefficients for each body segment in standing posture under different ambient temperatures in the climate chamber with an airspeed of under $0.1 \text{ m}\cdot\text{s}^{-1}$ ($\text{W}\cdot\text{m}^{-2}\cdot\text{K}^{-1}$).

	20 °C		24 °C		28 °C	
Segment	Exp.	CFD	Exp.	CFD	Exp.	CFD
10.Head	2.68	3.73	2.55	3.29	2.15	2.79
9.Back	2.22	1.90	2.50	1.72	2.39	1.60
8.Chest	3.85	2.97	3.06	2.61	2.44	2.13
7.Shoulder	4.03	3.08	3.40	2.85	2.96	2.57
6.Arm	3.54	3.90	3.68	3.63	3.64	3.33
5.Pelvis	3.04	2.50	2.96	2.18	2.17	1.82
4.Hand	4.54	5.33	4.92	5.01	3.19	4.66
3.Thigh	3.70	3.28	3.82	3.00	3.64	2.68
2.Leg	3.10	3.33	3.06	3.09	3.03	2.84
1.Foot	6.33	5.70	5.03	5.38	5.04	4.99
Whole-body	3.57	3.35	3.40	3.06	3.04	2.73

Table 4-17. Convective heat transfer coefficients for each body segment in sitting posture under different ambient temperatures in the climate chamber with an airspeed of under $0.1 \text{ m}\cdot\text{s}^{-1}$ ($\text{W}\cdot\text{m}^{-2}\cdot\text{K}^{-1}$).

	20 °C		24 °C		28 °C	
Segment	Exp.	CFD	Exp.	CFD	Exp.	CFD
10.Head	2.17	3.61	2.11	3.21	2.02	2.73
9.Back	2.93	2.87	2.03	2.63	2.97	2.31
8.Chest	3.14	2.91	3.41	2.69	2.46	2.31
7.Shoulder	3.90	3.25	3.51	3.06	3.18	2.84
6.Arm	5.10	4.39	4.40	4.15	4.02	3.84
5.Pelvis	3.53	3.52	3.03	3.23	3.29	2.94
4.Hand	5.24	5.48	5.85	5.22	4.91	4.93
3.Thigh	3.85	4.17	4.01	3.96	4.03	3.68
2.Leg	3.07	3.44	4.28	3.26	3.56	3.07
1.Foot	7.06	5.88	4.42	5.53	6.73	5.08
Whole-body	3.77	3.80	3.63	3.56	3.59	3.25

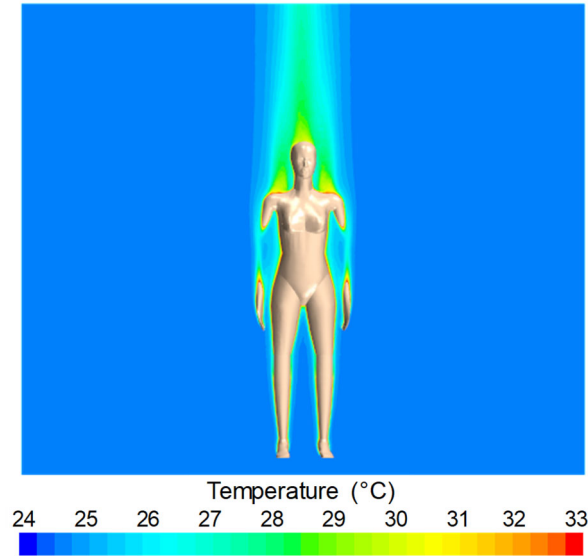


Figure 4-16. Air temperature distribution for an ambient temperature of 24 °C in the climate chamber ($V = 0.1 \text{ m} \cdot \text{s}^{-1}$).

Figure 4-17 lists the relationship between the whole-body convective heat transfer coefficient and the difference between skin and ambient temperature at an airspeed of $0.1 \text{ m} \cdot \text{s}^{-1}$, according to CFD analysis. The convective heat transfer coefficient tended to increase with the difference between skin temperature and air temperature. The whole-body convective heat transfer coefficient for the sitting posture was larger than that of standing posture because the body area facing the wind was larger. Table 4-18 shows the regression models of the convective heat transfer coefficient against temperature difference between the thermal manikin and the air at an airspeed of $0.1 \text{ m} \cdot \text{s}^{-1}$ for CFD analysis.

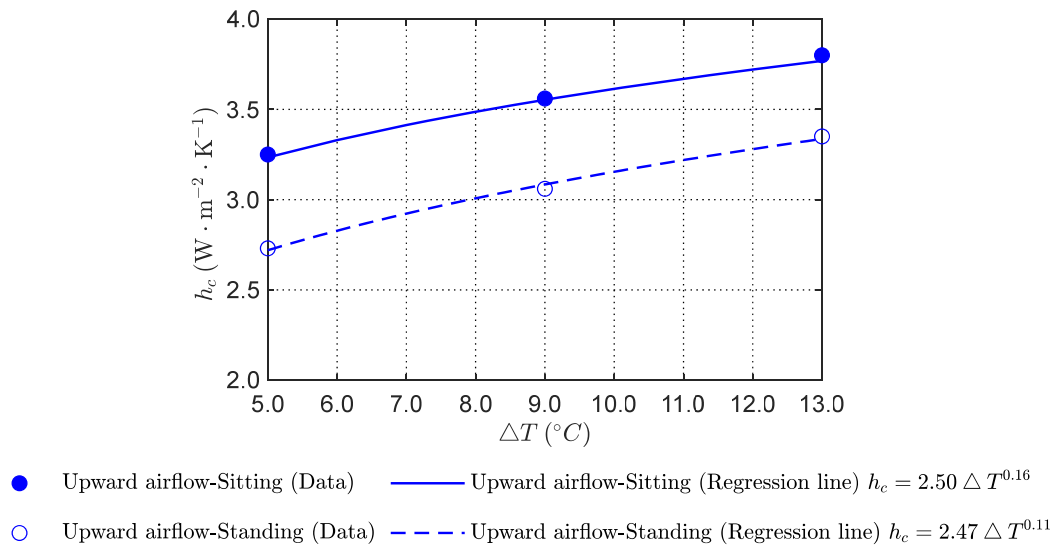


Figure 4-17. Relationship between whole-body convective heat transfer coefficient and the difference between skin and ambient temperatures at an airspeed of $0.1 \text{ m} \cdot \text{s}^{-1}$ according to CFD analysis ($\Delta T = t_s - t_a$).

Table 4-18. Regression models of the convective heat transfer coefficient against temperature difference between the thermal manikin and the air at an airspeed of $0.1 \text{ m}\cdot\text{s}^{-1}$ for CFD analysis.

$$y = a\Delta T^b \text{ (W}\cdot\text{m}^{-2}\cdot\text{K}^{-1}\text{)}$$

Segment	Standing			Sitting		
	a	b	R ²	a	b	R ²
10.Head	1.71	0.30	0.997	1.70	0.29	0.998
9.Back	1.20	0.17	0.951	1.60	0.23	1
8.Chest	1.22	0.35	1	1.57	0.24	0.997
7.Shoulder	1.89	0.18	0.998	2.26	0.14	0.995
6.Arm	2.55	0.16	0.994	3.06	0.14	0.998
5.Pelvis	1.06	0.33	0.997	2.17	0.18	0.989
4.Hand	3.71	0.14	0.992	4.13	0.11	0.993
3.Thigh	1.91	0.21	0.996	2.98	0.13	0.999
2.Leg	2.17	0.16	0.991	2.53	0.12	0.990
1.Foot	4.00	0.14	0.997	3.97	0.15	0.998
Whole-body	1.93	0.21	0.996	2.50	0.16	0.999

4.3.3.2 Radiative heat transfer coefficient

The distribution of radiative heat transfer coefficients for an ambient temperature of 20 °C, 24 °C, and 28 °C according to numerical calculation is given in Figure 4-18. Radiative heat transfer coefficients between the arm and the torso were relatively small; likewise, the radiative heat transfer coefficients for the inner parts of the left and right thighs were lower than other parts. This occurred because the view factors between these parts became smaller due to being shielded from other body segments. The radiative heat transfer coefficients for the pelvis, back, and chest were larger than those for hands, arms, and thighs (Figure 4-19, left), because view factors for the pelvis, back, and chest were larger than those for hands, arms and thighs (Figure 4-19, right). Figure 4-19 also indicates that the view factors for each body segment of standing posture were larger than those of sitting posture except hands. Therefore, the radiative heat transfer coefficient for each body segment of standing posture were larger than that of sitting posture except hands. The whole-body radiative heat transfer coefficient for the standing posture was larger than that of the sitting posture. It is clear from Figure 4-19 that higher ambient temperatures (i.e., average wall temperature) led to an increase in the radiative heat transfer coefficient.

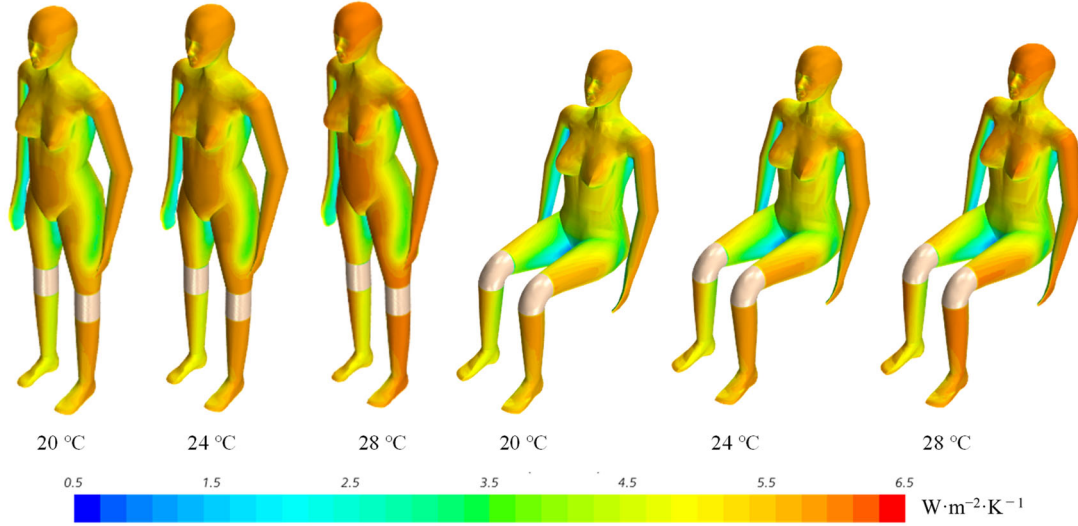


Figure 4-18. Distribution of radiative heat transfer coefficient for ambient temperatures of 20 °C, 24 °C, and 28 °C according to numerical calculation.

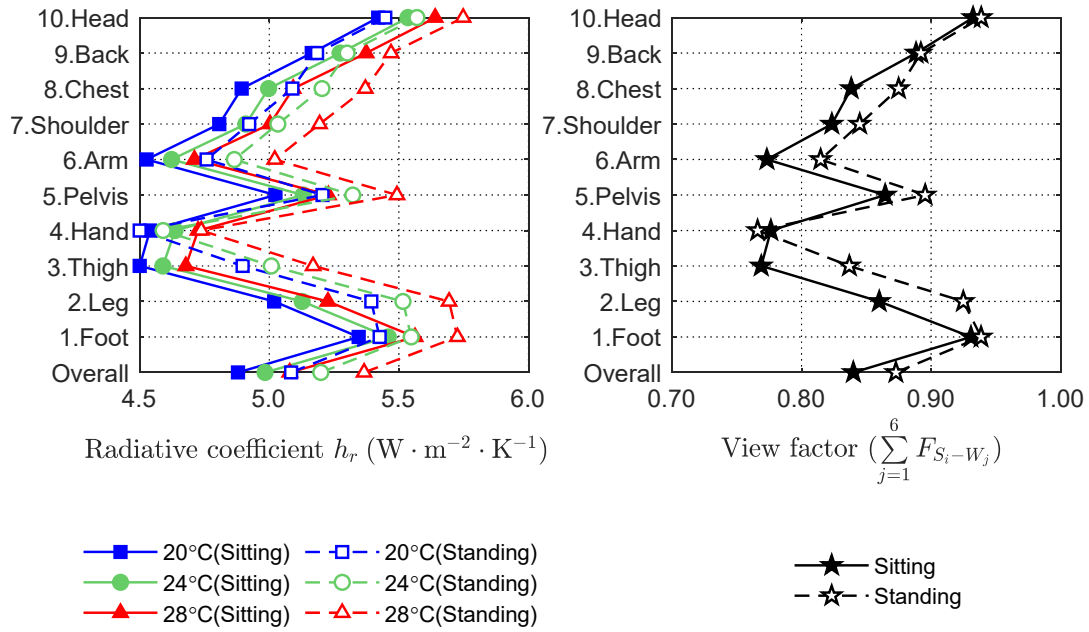


Figure 4-19. Radiative heat transfer coefficients and view factor.

4.4 The combined effect of temperature and airspeed

4.4.1 Experimental setup

The same thermal manikin was placed in the wind tunnel already shown in Figure 4-2 in Section 4.2.1. Airspeeds of $0.25 \text{ m}\cdot\text{s}^{-1}$, $0.75 \text{ m}\cdot\text{s}^{-1}$, $1.1 \text{ m}\cdot\text{s}^{-1}$, and $1.4 \text{ m}\cdot\text{s}^{-1}$ were reproduced, same with that in Section 4.2.1. And the wind direction was upwind only (Figure 4-20). The surface temperatures of the thermal manikin were set at 4°C , 7°C , and 10°C higher than the air temperature, respectively.

The environmental conditions for the experiment and CFD analysis are listed in Table 4-19.

Table 4-19. The summary of environmental conditions for the experiment (Exp.) and CFD analysis.

Temperature difference (ΔT)	Airspeed	Wind direction	Posture	Exp.	CFD
4 °C, 7 °C, 10 °C	0.25 m·s ⁻¹ , 0.75 m·s ⁻¹ , 1.1 m·s ⁻¹ , and 1.4 m·s ⁻¹	Upwind	Sitting	○	○

* ΔT is the difference between the skin temperature and the air temperature.

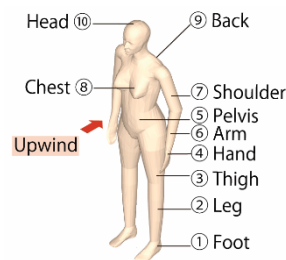


Figure 4-20. Body segments of the thermal manikin and wind direction.

4.4.2 Numerical method

The boundary conditions for the CFD analysis were set up from the experiments. The numerical method was the same with that listed in Table 4-3.

4.4.3 Results

The temperature difference between the manikin surface and the air is shown in Figure 4-21.

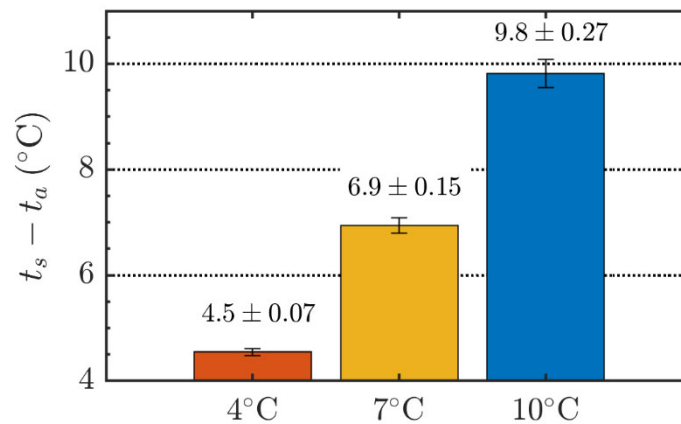


Figure 4-21. The temperature difference between the skin surface and the air during the experiment.

4.4.3.1 Whole-body

Figure 4-22 shows the results of convective heat transfer coefficients according to CFD analysis and experiments for sitting posture. The results based on the CFD analysis were consistent with the results based on the experiments. Additionally, both the results based on CFD analysis and experiments were in the range of the results of other studies.

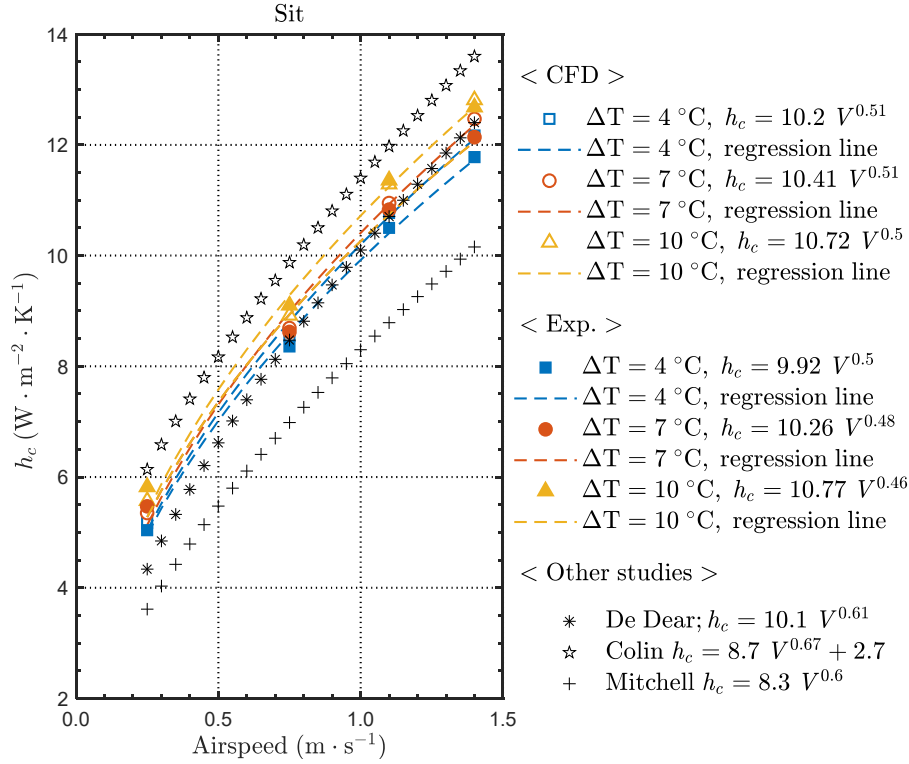


Figure 4-22. Comparison of convective heat transfer coefficients for sitting posture according to CFD analysis and experiment (Other studies: De Dear et al. [2], Colin et al. [23], Mitchell [24])

As convective heat transfer coefficients under different temperatures and airspeeds were measured, regression equations considering both the effect of airspeed and the temperature were concluded. The results of the CFD analysis were consistent with experiments. Therefore, the combination formulas are based on the results of CFD analysis (Figure 4-23).

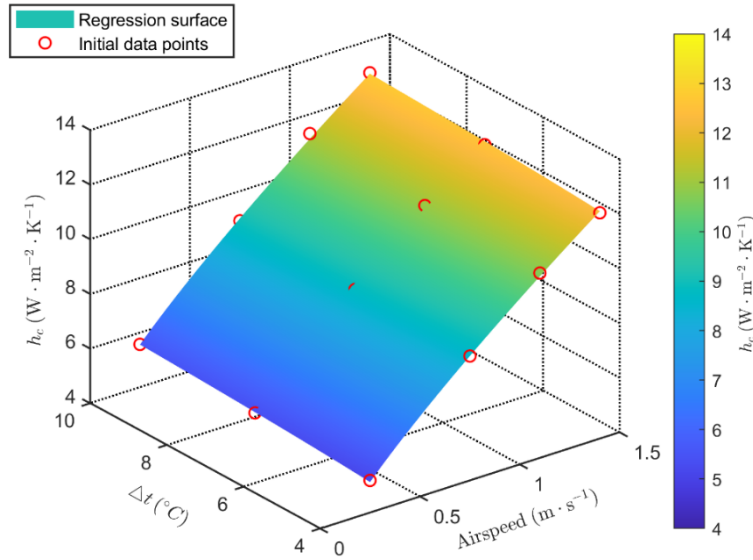
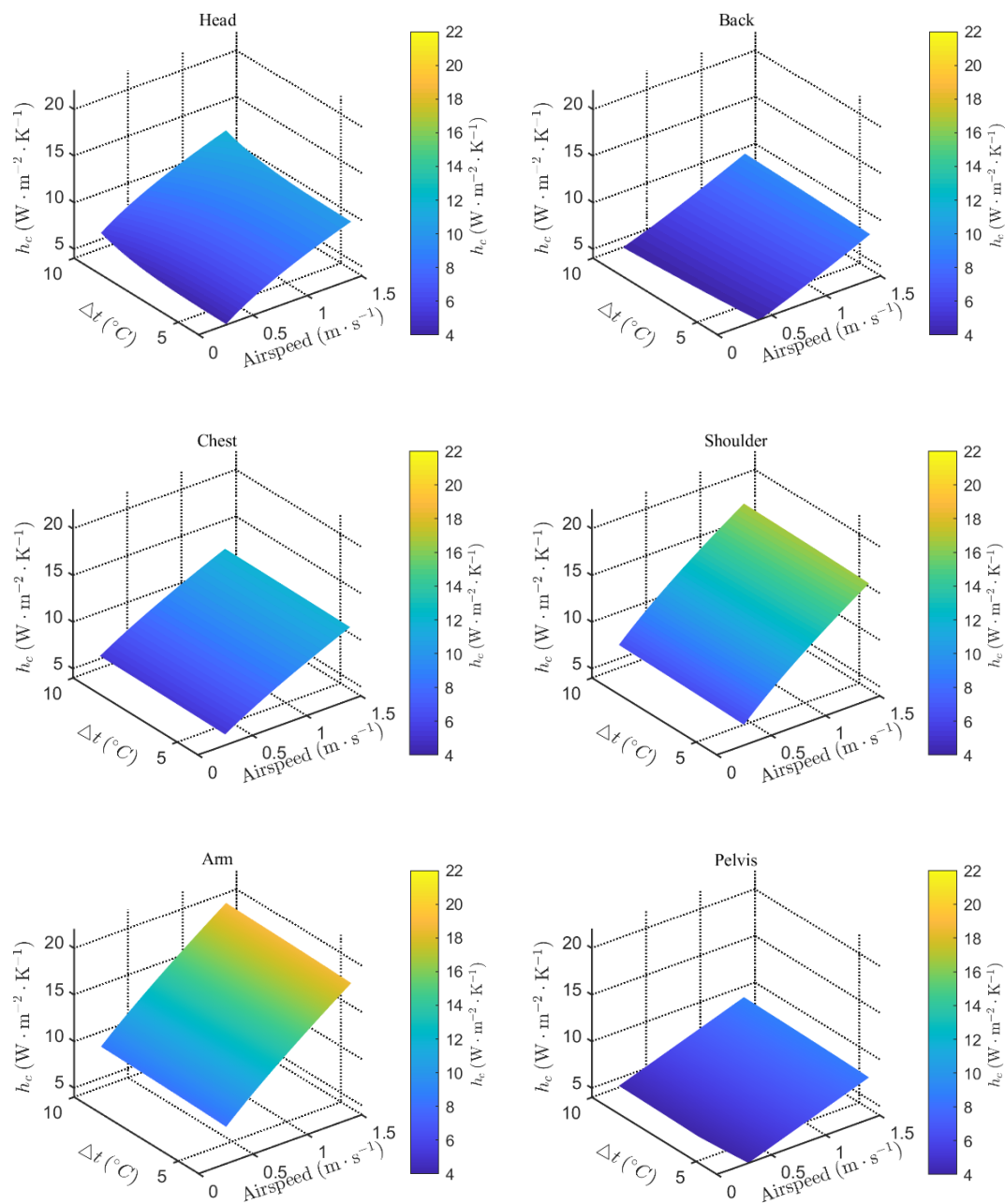


Figure 4-23. 3D plotting for the regression equation for the whole-body convective heat transfer coefficient considering both air temperature and airspeed in sitting posture according to CFD analysis.

$$(h_c = 2.05\Delta T^{0.17} + 7.46V^{0.78})$$

4.4.3.2 Convective heat transfer coefficients for different body segments

The regression models for different body segments considering both airspeed and environment temperature are shown in Figure 4-24 and Table 4-20.



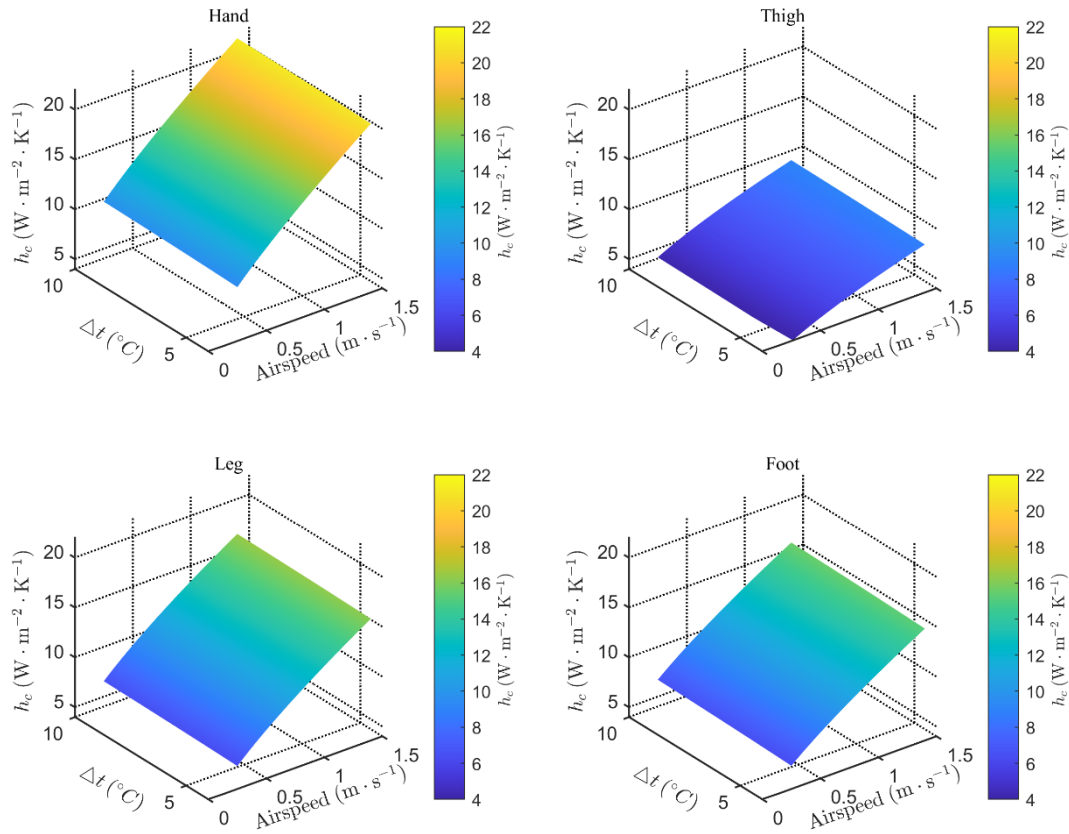


Figure 4-24. 3D plotting for the regression equation for the convective heat transfer coefficients for different body segments considering both air temperature and airspeed in sitting posture according to CFD analysis.

Table 4-20. The regression model considering both airspeed and environment temperature for the sitting posture according to CFD analysis ($\text{W} \cdot \text{m}^{-2} \cdot \text{K}^{-1}$).

Segment	Regression model	R^2
10.Head	$h_c = 8.59V^{0.53}$	0.953
9.Back	$h_c = 2.13\Delta T^{0.16} + 4.21V^{1.17}$	0.996
8.Chest	$h_c = 2.54\Delta T^{0.06} + 6.96V^{0.77}$	0.999
7.Shoulder	$h_c = 1.94\Delta T^{0.13} + 10.97V^{0.76}$	0.999
6.Arm	$h_c = 4.23\Delta T^{0.08} + 10.45V^{0.84}$	0.999
5.Pelvis	$h_c = 2.35\Delta T^{0.13} + 4.04V^1$	0.995
4.Hand	$h_c = 5.06\Delta T^{0.06} + 11.75V^{0.8}$	0.995
3.Thigh	$h_c = 1.27\Delta T^{0.14} + 5.82V^{0.65}$	0.999
2.Leg	$h_c = 2.10\Delta T^{0.11} + 10.65V^{0.75}$	0.999
1.Foot	$h_c = 2.52\Delta T^{0.13} + 9.44V^{0.76}$	0.999
Whole-body	$h_c = 2.05\Delta T^{0.17} + 7.46V^{0.78}$	0.999

4.5 Conclusions

In this chapter, the effect of airspeed, wind direction, and the temperature difference between the thermal manikin and the air on convective heat transfer coefficients were confirmed through both experiments and CFD analysis.

The main conclusions arising from this chapter are as follows:

The effect of airspeed and wind direction:

- (1) For the convective heat transfer coefficient caused by the horizontal airflow, the results for the standing posture were higher than those of the sitting posture. Conversely, for the convective heat transfer coefficient caused by the vertical airflow, the results for the sitting posture were larger than those of the standing posture.
- (2) Concerning the results for the horizontal airflow, there was no significant difference between the convective heat transfer coefficients caused by various wind directions. However, in the standing posture, the convective heat transfer coefficient caused by the crosswind was the lowest, and that caused by the downwind was the highest.
- (3) Concerning the results for the vertical airflow, the convective heat transfer coefficient caused by the upward airflow was larger than that caused by downward airflow.

The effect of environmental temperature:

- (4) Higher ambient temperatures led to a decrease in the convective heat transfer coefficient. In contrast, the radiative heat transfer coefficients increased with average wall temperature.
- (5) Convective heat transfer coefficients for trunks were smaller than those for limbs. Radiative heat transfer coefficients for the pelvis, legs, and feet were larger than other body segments.

The combined effect of airspeed and environmental temperature:

- (6) The regression models of convective heat transfer coefficient considering both the airspeed and the environmental temperature were proposed. They made the calculation of convective heat transfer coefficient under arbitrary airspeed and environmental temperature possible.

The convective and radiative heat transfer coefficients under various airspeeds, wind directions, and environmental temperatures were listed in this chapter. The comprehensive database for convective and radiative heat transfer coefficients provides a basis for the research about thermal comfort, such as the personal air conditioning system.

Reference

- [1] M. Ichihara, M. Saitou, M. Nishimura, S. Tanabe, Measurement of convective and radiative heat transfer coefficients of standing and sitting human body by using a thermal manikin (in Japanese), *Journal of Architecture and Planning (Transactions of AIJ)*. 62 (1997) 45–51. doi:10.3130/aija.62.45_5.
- [2] R.J. de Dear, E. Arens, Z. Hui, M. Oguro, Convective and radiative heat transfer coefficients for individual human body segments, *International Journal of Biometeorology*. 40 (1997) 141–156. doi:10.1007/s004840050035.
- [3] Y. Ozeki, T. Hira, M. Konishi, J. Nakano, S. Tanabe, Convective heat transfer coefficient at skin surface of thermal manikin under solar radiation (in Japanese), *Journal of Architecture and Planning (Transactions of AIJ)*. 67 (2002) 29–36. doi:10.3130/aija.67.29_4.
- [4] H.O. Nilsson, Thermal comfort evaluation with virtual manikin methods, *Building and Environment*. 42 (2007) 4000–4005. doi:10.1016/j.buildenv.2006.04.027.
- [5] T. Ono, S. Murakami, R. Ooka, T. Omori, Numerical and experimental study on convective heat transfer of the human body in the outdoor environment, *Journal of Wind Engineering and Industrial Aerodynamics*. 96 (2008) 1719–1732. doi:10.1016/j.jweia.2008.02.007.
- [6] D.N. Sørensen, L.K. Voigt, Modelling flow and heat transfer around a seated human body by computational fluid dynamics, *Building and Environment*. 38 (2003) 753–762. doi:10.1016/S0360-1323(03)00027-1.
- [7] Y. Kurazumi, L. Rezgals, Convective heat transfer coefficients of the human body under forced convection from ceiling, *Journal of Ergonomics*. 04 (2014) 1–6. doi:10.4172/2165-7556.1000126.
- [8] B. Yang, S.C. Sekhar, A.K. Melikov, Ceiling-mounted personalized ventilation system integrated with a secondary air distribution system - a human response study in hot and humid climate, *Indoor Air*. 20 (2010) 309–319. doi:10.1111/j.1600-0668.2010.00655.x.
- [9] F.S.S. Bauman, E.A.A. Arens, S. Tanabe, H. Zhang, A. Baharloo, Testing and optimizing the performance of a floor-based task conditioning system, *Energy and Buildings*. 22 (1995) 173–186. doi:10.1016/0378-7788(95)91161-J.
- [10] E. Lim, K. Sagara, T. Yamanaka, H. Kotani, N. Mishima, S. Horikawa, T. Ushio, CFD analysis of airflow characteristics in office room with task air-conditioning and natural ventilation, in: *Proceedings of Indoor Air Quality. Ventilation & Energy Conservation in Buildings (IAQVEC)*, 2007: pp. 508–515.
https://scholar.google.co.jp/scholar?hl=en&as_sdt=0%2C5&q=%2C+CFD+analysis+of+airflow+characteristics+in+office+room+with+task+air-conditioning+and+natural+ventilation&btnG=.
- [11] S. Murakami, S. Kato, J. Zeng, Flow and temperature fields around human body with various room air distribution, Part 1 - CFD study on computational thermal manikin, in: *ASHRAE Transactions*, 1997: pp. 3–15. <https://www.scopus.com/inward/record.uri?eid=2-s2.0-0030704102&partnerID=40&md5=a46d35ac10d9a911c2d3288f741d5965>.

- [12] J. Yang, S. Kato, J. Seo, Evaluation of the convective heat transfer coefficient of the human body using the wind tunnel and thermal manikin, *Journal of Asian Architecture and Building Engineering*. 8 (2009) 563–569. doi:10.3130/jaabe.8.563.
- [13] P.O. Fanger, *Thermal comfort: analysis and applications in environmental engineering*, Copenhagen: Danish Technical Press, 1970.
- [14] Y. Kurazumi, T. Tsuchikawa, J. Ishii, K. Fukagawa, Y. Yamato, N. Matsubara, Radiative and convective heat transfer coefficients of the human body in natural convection, *Building and Environment*. 43 (2008) 2142–2153. doi:10.1016/j.buildenv.2007.12.012.
- [15] ISO 9920, *Ergonomics of the thermal environment — Estimation of thermal insulation and water vapour resistance of a clothing ensemble*, (2007).
<https://www.iso.org/standard/39257.html>.
- [16] S. Schiavon, B. Yang, Y. Donner, V.W.C. Chang, W.W. Nazaroff, Thermal comfort, perceived air quality, and cognitive performance when personally controlled air movement is used by tropically acclimatized persons, *Indoor Air*. 27 (2017) 690–702. doi:10.1111/ina.12352.
- [17] N.P. Gao, J.L. Niu, CFD study of the thermal environment around a human body: A Review, *Indoor and Built Environment*. 14 (2005) 5–16. doi:10.1177/1420326X05050132.
- [18] S. Murakami, S. Kato, J. Zeng, Combined simulation of airflow, radiation and moisture transport for heat release from a human body, *Building and Environment*. 35 (2000) 489–500. doi:10.1016/S0360-1323(99)00033-5.
- [19] F.S. Lien, W.L. Chen, M.A. Leschziner, Low-Reynolds-Number eddy-viscosity modelling based on non-linear stress-strain/vorticity relations, in: *Engineering Turbulence Modelling and Experiments*, Elsevier, 1996: pp. 91–100. doi:10.1016/B978-0-444-82463-9.50015-0.
- [20] STAR-CCM+ User Guide - version 12.02, (2017).
<https://mdx.plm.automation.siemens.com/star-ccm-plus>.
- [21] W. Zhang, K. Hiyama, S. Kato, Y. Ishida, Building energy simulation considering spatial temperature distribution for nonuniform indoor environment, *Building and Environment*. 63 (2013) 89–96. doi:10.1016/j.buildenv.2013.02.007.
- [22] H.K. Versteeg, W. Malalasekera, *An introduction to computational fluid dynamics: (Chapter 3)*, Prentice Hall, 2007. <https://books.google.co.jp/books?id=RvBZ-UMpGzIC>.
- [23] J. Colin, Y. Houdas, Experimental determination of coefficient of heat exchanges by convection of human body., *Journal of Applied Physiology*. 22 (1967) 31–38. doi:10.1152/jappl.1967.22.1.31.
- [24] D. Mitchell, Convective heat transfer from man and other animals, in: J.L. Monteith, L.E. Mount (Eds.), *Heat Loss from Animals and Man*, Elsevier, London, 1974: pp. 59–76.
<https://linkinghub.elsevier.com/retrieve/pii/B978040870652050010X>.
- [25] O. Seppanen, Thermal insulating values for typical indoor clothing ensembles, *ASHRAE Trans*. 78 (1972) 120–130.
- [26] C. Voelker, H. Alsaad, Simulating the human body’s microclimate using automatic coupling of

- CFD and an advanced thermoregulation model, *Indoor Air*. 28 (2018) 415–425. doi:10.1111/ina.12451.
- [27] F. Liu, J.X. Wen, The effect of turbulence modelling on the CFD simulation of buoyant diffusion flames, *Fire Safety Journal*. 37 (2002) 125–150. doi:10.1016/S0379-7112(01)00022-4.
- [28] S. Murakami, Analysis and design of micro-climate around the human body with respiration by CFD, *Indoor Air*. 14 (2004) 144–156. doi:10.1111/j.1600-0668.2004.00283.x.

Chapter 5.

Heat transfer coefficients for the clothed manikin

5.1 Introduction

Many studies have looked at heat transfer coefficients for the naked human body through experiments and numerical simulations, as stated in Chapter 4 [1–4]. However, heat transfer coefficients for the clothed human body have rarely been investigated because measuring them is generally difficult. The heat transfer coefficients for clothing was estimated through multiplying the heat transfer coefficients of the naked human body by the clothing area factor [5]. The clothing area factor is defined as the ratio of the clothing surface area to the body surface area. However, not only does the increase in the area due to clothing cause an increased heat transfer coefficients, but also other factors, such as the properties of the clothing surface material, affect the heat transfer coefficients of clothing.

Ciesielska-Wrobel et al. measured the roughness of three types of textiles and then assessed the thermal haptic properties of these textiles. They found that the rougher the fabric, the warmer the feeling it induced when touched, mainly due to the air stored in the gaps between the surfaces of the textiles [6]. Sun et al. reported that increasing the roughness of the fabric could help improve the warmth-keeping property [7]. Oliveria et al. measured the clothing convective heat transfer coefficient for an extremely thick clothing ensemble with clothing insulation of 1.75 clo [8]. Their results indicated that for the most body parts, the convective heat transfer coefficient for the naked manikin was higher than that of the clothed manikin. They also pointed out that comprehensive factors such as air and vapor permeability of clothing, fitness of clothing, air infiltrations, body movement affected the clothing convective heat transfer coefficient. Oguro et al. conducted an experiment on a thermal manikin with a clothing ensemble with clothing insulation of 0.8 clo [9]. They observed that the convective heat transfer coefficient for the clothed manikin was larger than that of the naked manikin at most of the body segments when the airspeed exceeded $0.8 \text{ m}\cdot\text{s}^{-1}$. While, in the low airspeed range, there was a small difference between the results of the naked manikin and clothed manikin. Kuwabara et al. measured the convective heat transfer coefficients for two sets of clothing ensembles [10]. The clothing insulation was 0.8 clo, and 1.6 clo, respectively. They found that the clothing insulation did not affect the convective heat transfer coefficient for the clothing. In a word, the effect of clothing on the convective heat transfer coefficient remains controversial. It is necessary to increase the types of clothing to verify.

Investigation concerning clothing convective heat transfer coefficient with CFD analysis is challenging because it is difficult to build the geometry shape of the clothed manikin. Tian et al. simplified the clothing layer at the waist and the leg into two pieces [11]. Takada et al. built the three-dimensional shape of a clothed manikin with a laser scanner [12]. However, these methods are tough to achieve or with high demanding of equipment.

Therefore, in this chapter, the convective heat transfer coefficient, radiative heat transfer coefficient for eight sets of clothing ensembles were measured through the manikin experiment. The impacts of wind and posture on the parameters mentioned above were also assessed. The correction factor

for the convective heat transfer coefficient calculated by the CFD analysis was presented.

The environmental conditions for the experiments of measuring clothing heat transfer coefficients are listed in Table 5-1 and Figure 5-1.

Table 5-1. The summary of environmental conditions for the experiment.

Temperature difference (ΔT)	Airspeed	Wind direction	Posture	Exp.
10 °C	0.25 m·s ⁻¹ , 0.75 m·s ⁻¹ , 1.1 m·s ⁻¹ , and 1.4 m·s ⁻¹	Upwind, crosswind, downwind	Standing, sitting	○

* ΔT is the difference between the skin temperature and the air temperature.

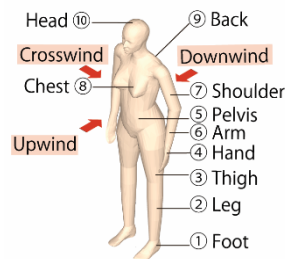


Figure 5-1. Body segments of the thermal manikin and wind directions

5.2 Experimental setup

5.2.1 Clothing ensembles

The clothing ensembles and their information are shown in Section 3.2 in Figure 3-9 and Table 3-2. To make it easier to refer to, they are listed here again (Figure 5-2 and Table 5-2).

To compare the influence of the surface feature of clothing on the convective and radiative heat transfer coefficients, clothing ensembles with almost the same basic insulation, approximately 1 clo, were selected. The surface emissivity of clothing was assumed to be 0.95 for all clothing ensembles. For very loose clothing, a chimney effect will occur—where ventilation of the trapped air layer will remove the heat through openings such as collars, cuffs, and the hem [13,14]. Therefore, all the clothing ensembles were tightly fit. The zippers were zipped up to the neck, and the buttons were buttoned up to the neck to avoid the chimney effect. Tightly fit here means the clothing ensembles were just fine for the thermal manikin, not too large or too small. If the size of the garment is too large, the thickness of the air layer between the manikin and the surface of the garment will be thicker, so the movement of air under the clothing will become complicated. This complicated movement thereby affects the heat transfer coefficient of the garment. Therefore, to avoid the effect of size, clothing of almost identical fit size was selected.



Figure 5-2. Overview of tested clothing ensembles.

Table 5-2. Material information about tested clothing ensembles.

Ensemble code	Catalog	Components
E1	Tops	Wind blast jacket: the outer material was 100% nylon, the inner material (mesh) was 100% polyester
	Bottoms	Windbreaker trousers: same with tops
E2	Tops	Suit jacket: 100% polyester
	Bottoms	Work trousers: 90% polyester, 10% cotton
E3	Tops	Sweater: 85% acrylic fiber, 15% wool
	Bottoms	Work trousers: 90% polyester, 10% cotton
E4	Tops	Work jacket: 90% polyester, 10% cotton
	Bottoms	Work trousers: 90% polyester, 10% cotton
E5	Tops	Fleece jacket: 100% polyester
	Bottoms	Work trousers: 90% polyester, 10% cotton
E6	Tops	Sports jacket: 35% polyester, 65% cotton
	Bottoms	Work trousers: 90% polyester, 10% cotton
E7	Tops	Raincoat: 100% PVC coated nylon
	Bottoms	
E8	Tops	Mountain jacket: 2-layer GORE-TEX Shell (exterior: 100% nylon, interior: 100% polyester)
	Bottoms	Work trousers: 90% polyester, 10% cotton

5.2.2 Environmental condition

The surface temperature of the thermal manikin was set at 10 °C higher than the air temperature. Other experimental conditions have already listed in Table 5-1. The thermal manikin was situated in the wind tunnel shown in Figure 4-2 in Section 4.2.1.

5.3 Results

The insulation values for the clothing ensembles are shown in Figure 5-3. Although it is tough to select clothing ensembles with identical insulation, it was confirmed that the clothing insulation (I_{cl}) for each clothing ensemble was approximately 1 clo. The clothing insulation for the standing posture was 1.0 ± 0.1 clo, while it was 0.8 ± 0.1 clo for the sitting posture. Sato et al. reported that the convective heat transfer coefficient for thermal manikin wearing in T-shirt (0.22 clo), sweater (0.74 clo), and suit (0.9 clo) showed no difference [15]. Therefore, the small difference between the clothing ensembles measured in this study was considered not to affect the convective heat transfer coefficient.

The difference between the manikin surface temperature and the air temperature was well controlled. The temperature difference for the standing posture was 10.5 ± 0.2 °C, and for the sitting posture, the temperature difference was 10.6 ± 0.5 °C (Figure 5-4).

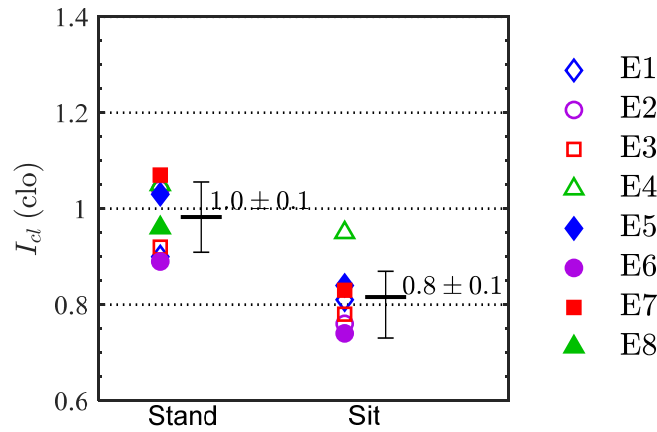


Figure 5-3. Basic clothing insulation for various clothing ensembles under the airspeed of $0.25 \text{ m}\cdot\text{s}^{-1}$ (the average clothing insulation for three wind directions).

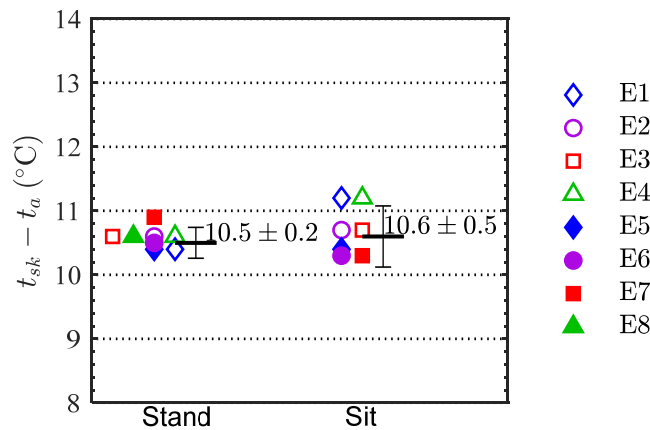


Figure 5-4. Difference between the manikin surface temperature t_{sk} and the air temperature t_a .

5.3.1 Whole-body convective heat transfer coefficient

The sensible heat loss of the clothed thermal manikin caused by different wind directions under

various airspeeds is presented in Figure 5-5. In the standing posture, the sensible heat loss for clothing ensembles with clothing insulation of approximately 1 clo was in the range of $35 \text{ W} \cdot \text{m}^{-2}$ to $45 \text{ W} \cdot \text{m}^{-2}$ when the temperature difference between the manikin and air was 10°C (at an airspeed of $0.25 \text{ m} \cdot \text{s}^{-1}$). The sensible heat loss was the lowest for E5. The potential reason is that the fleece coat was an excellent insulator because the surface structure of the fleece had an air-trapping ability. Additionally, the sensible heat loss caused by the crosswind was the least due to the smaller body area facing the wind.

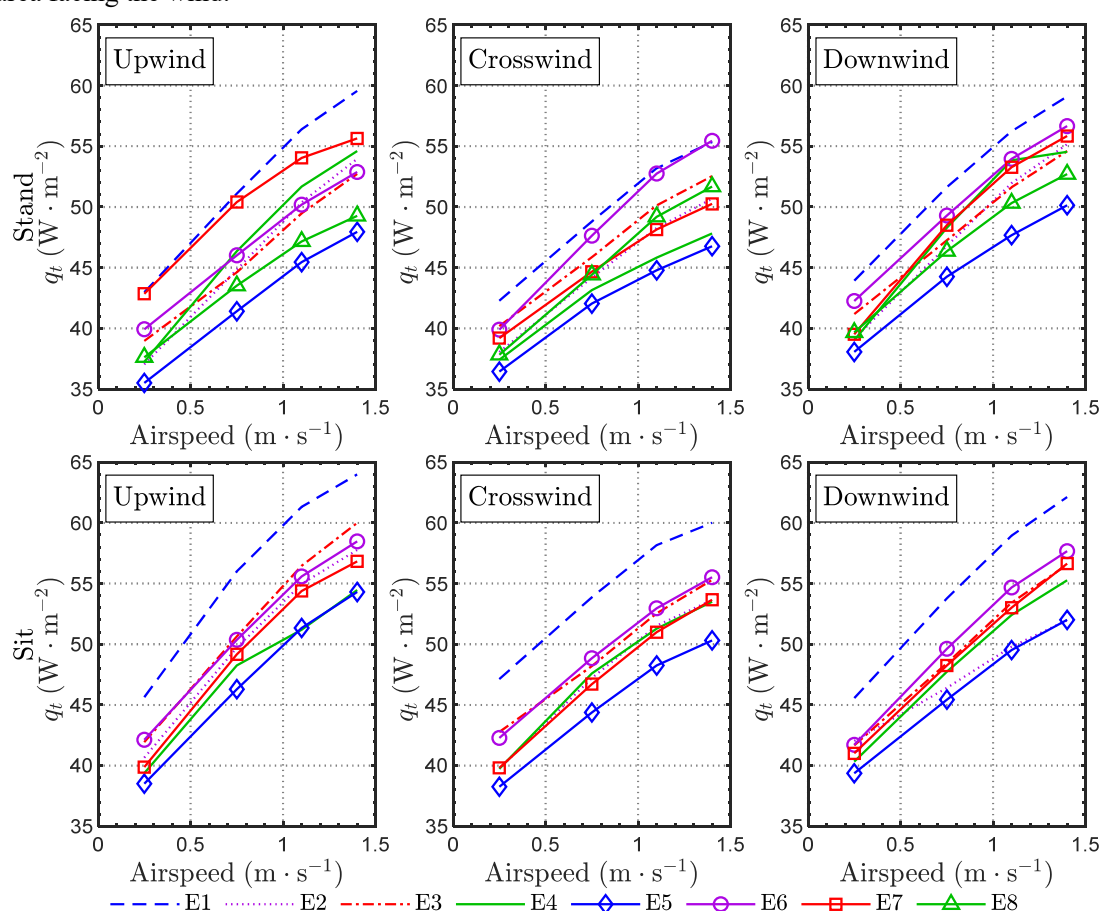


Figure 5-5. Whole-body sensible heat loss of the clothed manikin under various airspeeds and wind directions.

Figure 5-6 shows the whole-body convective heat transfer coefficient for the naked manikin and the clothed manikin under various airspeeds. Results for the three wind directions were averaged. The shoes were the same for each clothing ensemble. As the head and hands were not covered by any clothing, the clothing heat transfer coefficients for the shoes, head, and hands were not included while calculating the whole-body clothing heat transfer coefficients. Thus, only the legs (left and right), thighs (left and right), arms (left and right), pelvis, shoulders (left and right), chest, and back were taken into consideration while calculating the whole-body heat transfer coefficients. The whole-body convective heat transfer coefficients including head, hands, and feet are listed in Table B-1–Table B-4 in Appendix A.

When looking at the results of standing posture, the convective heat transfer coefficients (h_c) for the clothed manikin were higher than those for the naked manikin, except in the low airspeed range

($V < 0.5 \text{ m}\cdot\text{s}^{-1}$). The clothing convective heat transfer coefficient for E7 was the largest, 35% higher than the convective heat transfer coefficient for the naked manikin under an airspeed of $1.4 \text{ m}\cdot\text{s}^{-1}$. Additionally, the convective heat transfer coefficients for various clothing ensembles were different. The convective heat transfer coefficients for E1 and E7 were significantly higher than those of other clothing ensembles. The largest clothing convective heat transfer coefficient (E7) was 32% higher than the smallest clothing convective heat transfer coefficient (E5) under an airspeed of $1.4 \text{ m}\cdot\text{s}^{-1}$. One of the potential causes for this result was the difference in the surface features of clothing, i.e., E1 consisted of a wind blast jacket and trousers, and E7 consisted a raincoat, both of which are very smooth surfaces compared to ordinary clothing. Comparatively, E3 consists of a sweater, and E5 a fleece coat, both of which have rough surfaces compared to ordinary clothing. The fluid resistance and convective heat transfer coefficients are larger in the case of a rough pipe than in a smooth pipe. However, the current results are contrary to this finding. In the case of an obstacle placed in a moving fluid, the unevenness on the surface of the obstacle can control the size of vortices generated on the surface. It has been reported that the surface resistance becomes smaller when the surface has a moderate amount of unevenness [16,17]. The dimples on the surface of a golf ball can be a perfect example of this phenomenon [18]. With respect to the results of this study, the large convective heat transfer coefficients for E1 and E7, and the small convective heat transfer coefficient for E3 and E5 may also be related to this reason. However, further studies are needed to clarify this phenomenon.

In addition, the air was stopped in the fiber of the surface and heated by the warm human body. y, it has been reported that hairy fabrics carry a greater volume of air on the fabric surface than smooth surfaces [36]. Therefore, the stored air on the surface of the textile provides an insulating barrier.

In the low airspeed range, there was a small difference among different clothing ensembles. A possible reason is that the effect of the permeability of clothing was not significant, and the consequence of air infiltration was negligible in the low airspeed range. This indicates that in the low airspeed range, the convective heat transfer coefficient for naked manikin can be used as the clothing convective heat transfer coefficient. It is also clear from Figure 5-6 that the difference in convective heat transfer coefficients between clothing ensembles increased with an increase in airspeed.

When looking at the results for the manikin in sitting posture, the convective heat transfer coefficients for the clothed manikin were found to be higher than those of the naked manikin when the airspeed exceeded $0.5 \text{ m}\cdot\text{s}^{-1}$ as already seen in the standing posture, except for the coefficients of E5 and E6. The convective heat transfer coefficient for E6 was lower than that of the naked manikin until the airspeed exceeded $1.0 \text{ m}\cdot\text{s}^{-1}$. The convective heat transfer coefficient for E5 was lower than that of the naked manikin for all airspeeds. In the sitting posture, the air layer between the manikin surface and the clothing was very thin. Thus, the heat loss due to the breakup of the air layer was low. Additionally, Kamata et al. conducted an experiment to investigate the effect of fabric on heat transfer [19]. In their research, a heated cylinder was covered with a cloth with no

gap. They found that the convective heat transfer coefficient for the clothed cylinder with a roughness surface was lower than that of the naked cylinder, which was consistent with the results in this study.

Similar to the standing posture, the convective heat transfer coefficient for E1 was significantly higher than that of other clothing ensembles. However, there was no significant difference between the results for E2, E3, E4, and E7.

The convective heat transfer coefficients of the standing posture were higher than those of the sitting posture. This is because certain body segments shielded other body segments from the airflow during the sitting posture. Hence, the airspeed near certain body segments was reduced, which in turn reduced the effect of airspeed. The results presented by Oguro et al., Kuwabara et al., and the ASHRAE handbook are also listed in Figure 5-6 [9,10,20]. However, there was a lack of sufficient information regarding the surface temperature of the naked manikin in these studies.

Figure 5-7 shows the convective heat transfer coefficient for different clothing ensembles caused by various wind directions for standing and sitting postures. The convective heat transfer coefficient caused by the crosswind was the lowest, as the body area facing the wind was smaller for the crosswind.

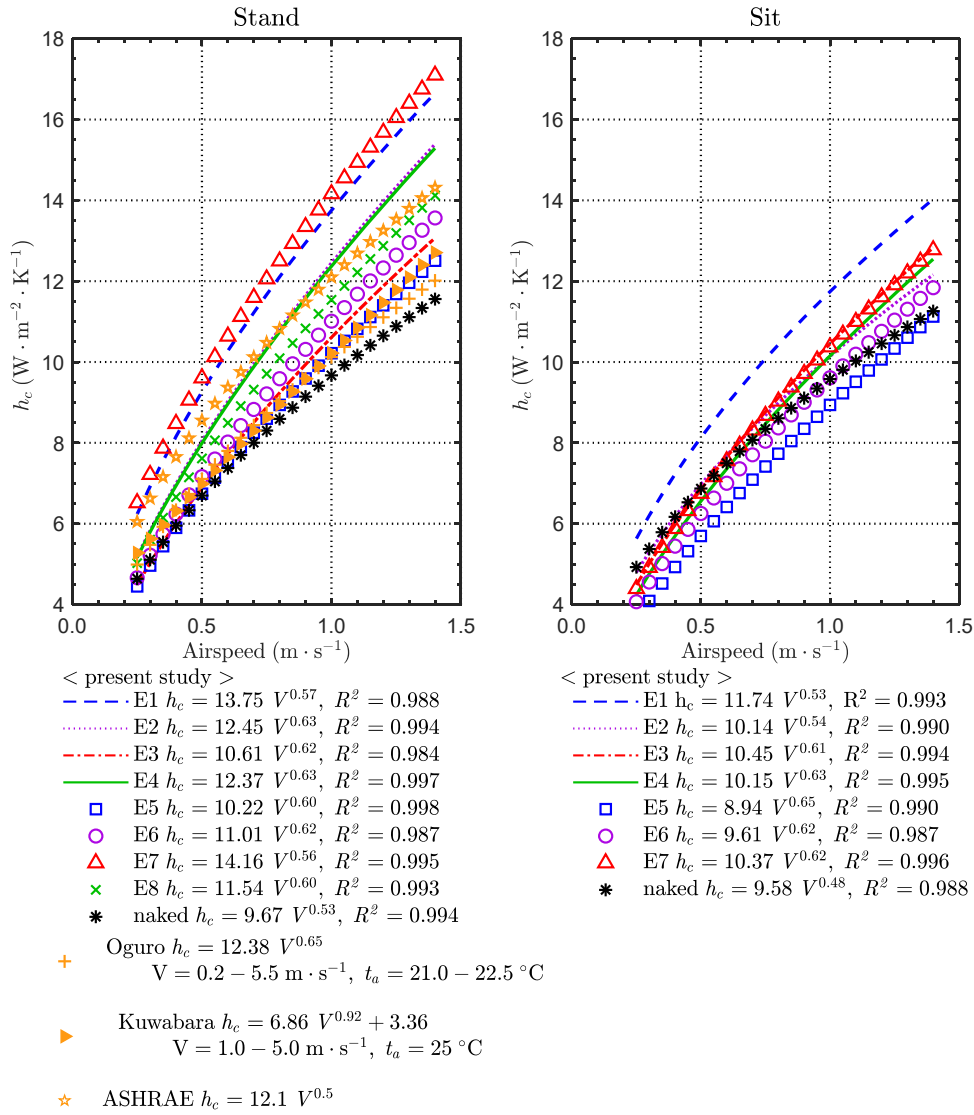


Figure 5-6. Whole-body convective heat transfer coefficient for the naked manikin and the clothed manikin under various airspeeds for standing and sitting postures (left: standing posture, right: sitting posture).

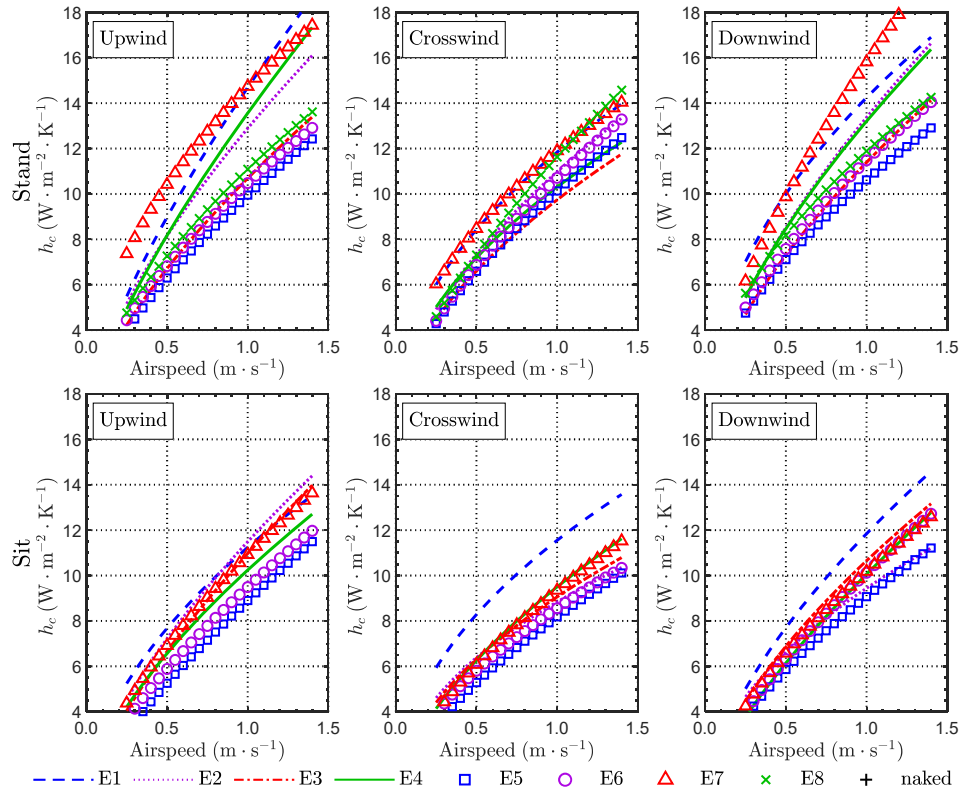


Figure 5-7. Whole-body convective heat transfer coefficient for the clothed manikin and the naked manikin under various wind directions (up: standing posture; down: sitting posture).

5.3.2 Convective heat transfer coefficient for different body segments

Figure 5-8 shows the average convective heat transfer coefficient for different clothing ensembles under various airspeeds and wind directions in standing posture. Because the sequence of the convective heat transfer coefficients of various clothing ensembles at each body segment was different, the average of various clothing ensembles was taken.

For the back, the convective heat transfer coefficient caused by the downwind was larger than that caused by the upwind. For the chest and the pelvis, the results were the opposite.

In the discussion of the convective heat transfer coefficients for the naked manikin, the convective heat transfer coefficient for the right parts of the manikin were higher than the left part while the thermal manikin was facing the crosswind (i.e., wind from the right side of the thermal manikin). However, Figure 5-8 presents that when the wind blew from the right side of the manikin, the convective heat transfer coefficients for body segments of the right side were not the highest. The different shapes of the clothing of the right and left parts of the manikin were attributed to this circumstance. There was a difference between the right and left sides for the convective heat transfer coefficients caused by the upwind or the downwind. The reason is that the fitness and shape of the clothing were different [9].

Figure 5-9 shows the average convective heat transfer coefficient for different clothing ensembles under various airspeeds and wind directions in the sitting posture. The results for different body segments for the sitting posture had a similar characteristic with that of standing posture. However, the results for legs and thighs in sitting posture were significantly lower than those of standing

posture, which is much more clearly shown in Figure 5-10. The convective heat transfer coefficient for thighs in sitting posture was smaller than that in standing posture because the thighs did not face the wind directly in sitting posture. The convective heat transfer coefficient for the legs in the standing posture was larger than that for sitting posture due to the loose fit at the legs in the standing posture. It can also be seen from Figure 5-10 that the convective heat transfer coefficients for the legs were the highest among all the body segments. The back had the lowest convective heat transfer coefficient.

The regression models for the average convective heat transfer coefficient for different clothing ensembles are given in Table 5-3 and Table 5-4 (the results for three wind directions were averaged).

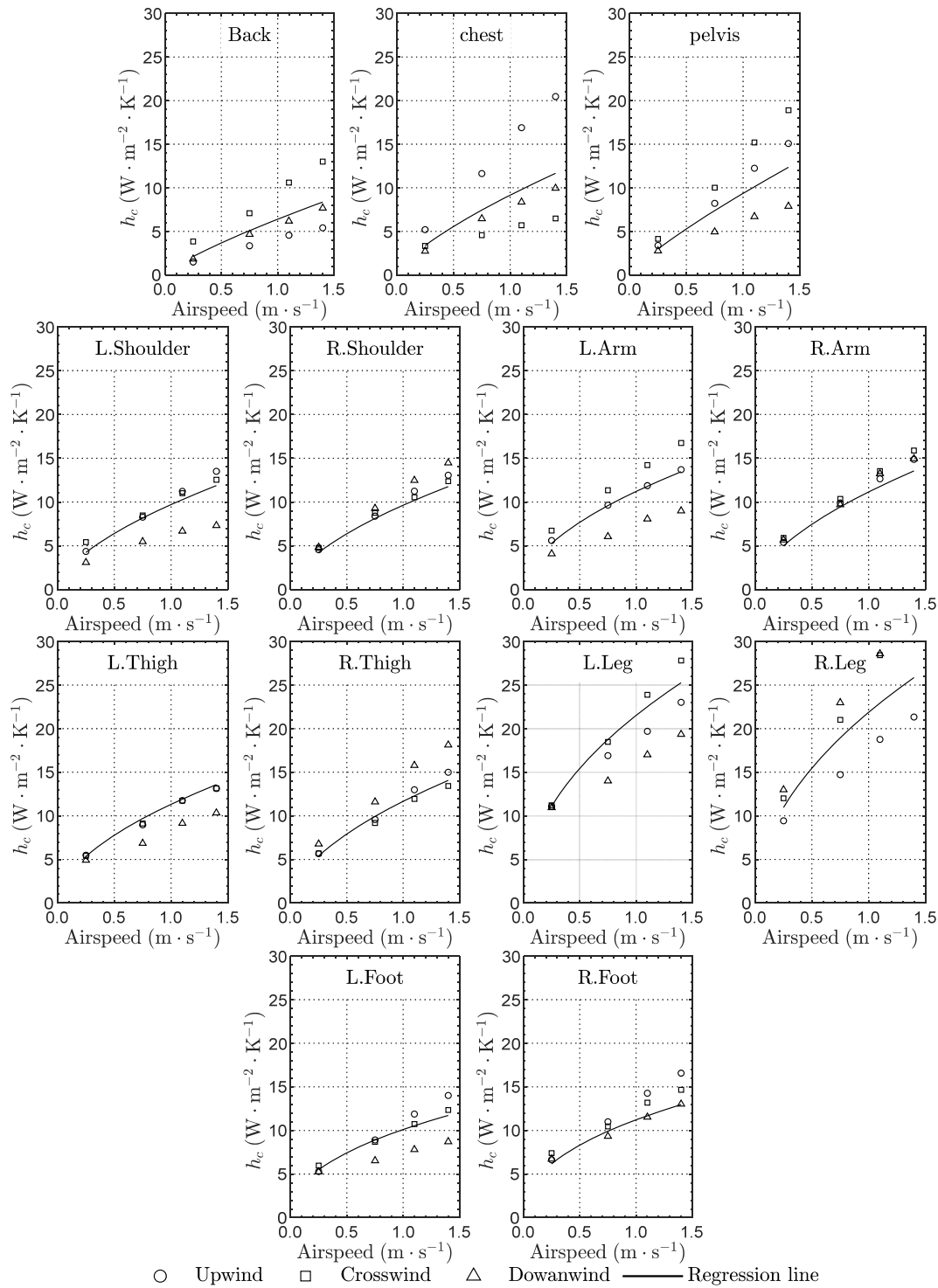


Figure 5-8. Average convective heat transfer coefficient for different clothing ensembles in standing posture (symbols represent the experimental data for different wind directions, and the line represents the regression model for the average convective heat transfer coefficient for different wind directions).

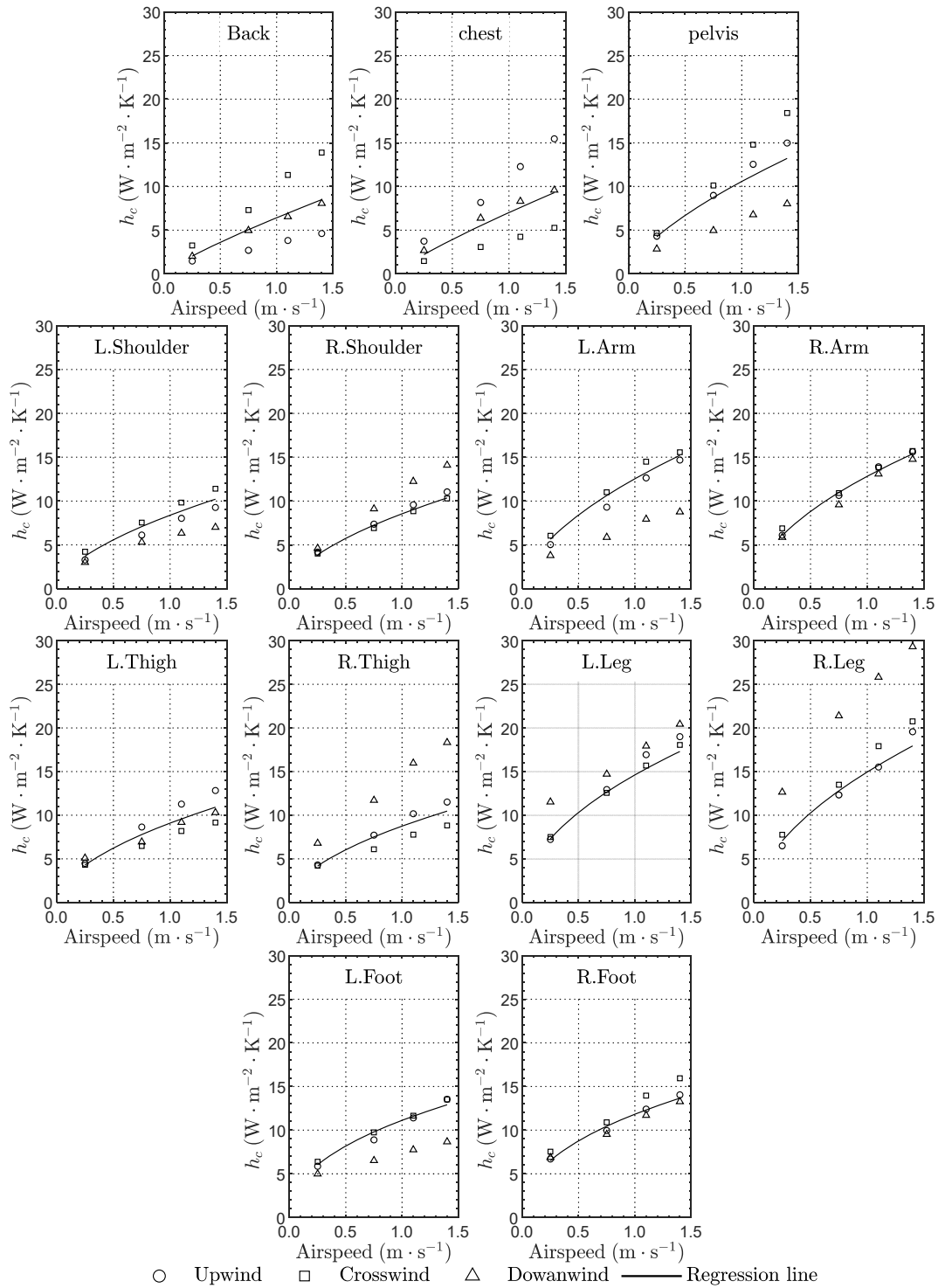


Figure 5-9. Average convective heat transfer coefficient for different clothing ensembles in sitting posture (symbols represent the experimental data for different wind directions, and the line represents the regression model for the average convective heat transfer coefficient for different wind directions).

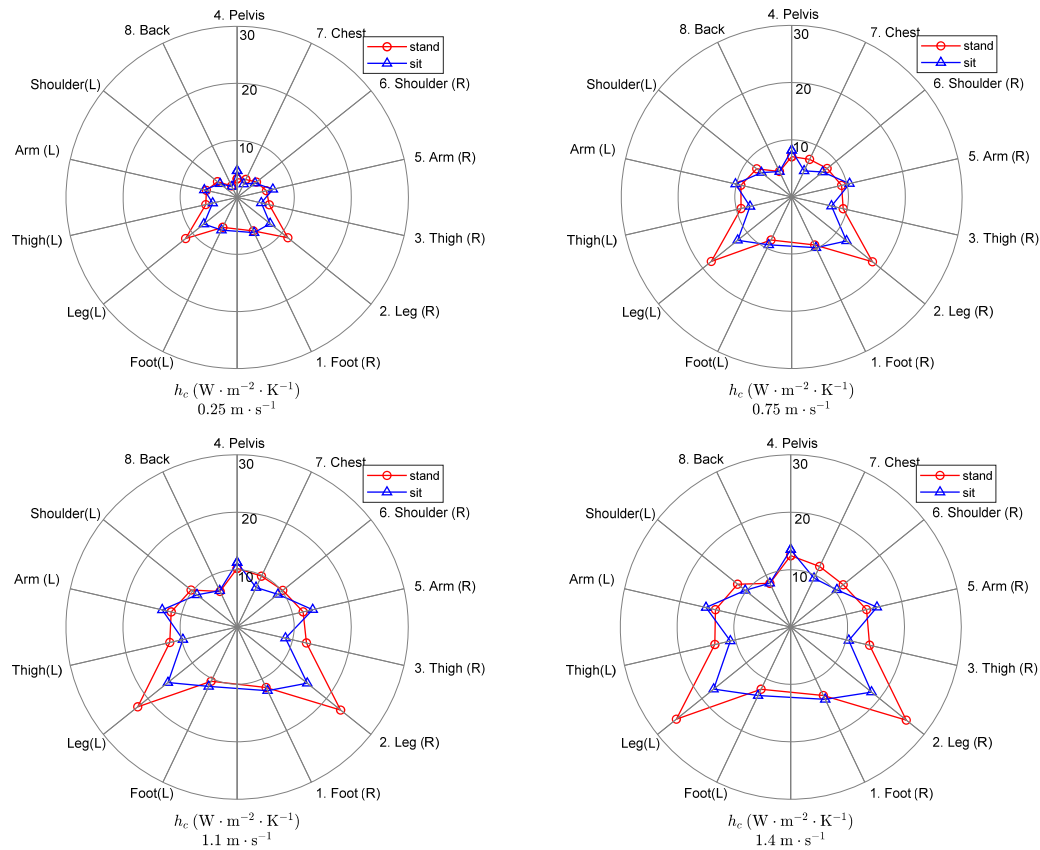


Figure 5-10. Comparison of the average convective heat transfer coefficient for different clothing ensembles in standing and sitting postures under various airspeeds.

Table 5-3. Regression model for the average heat transfer coefficient for different clothing ensembles in standing posture (results for three wind directions were averaged).

$h_c = aV^b \text{ (W} \cdot \text{m}^{-2} \cdot \text{K}^{-1})$			
Segments	a	b	R ²
9. Back	6.40	0.80	0.998
8. Chest	9.16	0.72	0.999
7. Shoulder (R)	9.63	0.59	0.999
(L)	9.71	0.60	0.996
6. Arm (R)	11.15	0.58	0.993
(L)	11.20	0.54	0.993
4. Pelvis	9.36	0.82	0.995
3. Thigh (R)	11.66	0.56	0.986
(L)	11.32	0.54	0.988
2. Leg (R)	21.87	0.50	0.993
(L)	21.51	0.48	0.992
1. Foot (R)	11.22	0.43	0.980
(L)	10.11	0.44	0.997
Whole-body	11.33	0.58	0.994

Table 5-4. Regression model for the average heat transfer coefficient for different clothing ensembles in sitting posture (results for three wind directions were averaged).

$$h_c = aV^b \text{ (W}\cdot\text{m}^{-2}\cdot\text{K}^{-1}\text{)}$$

Segments	a	b	R ²
9. Back	6.42	0.83	0.999
8. Chest	7.02	0.84	0.985
7. Shoulder (R)	8.55	0.57	0.995
(L)	8.39	0.59	0.996
6. Arm (R)	12.83	0.54	0.991
(L)	12.54	0.57	0.993
4. Pelvis	10.58	0.66	0.986
3. Thigh (R)	8.75	0.53	0.993
(L)	9.10	0.54	0.995
2. Leg (R)	14.95	0.54	0.994
(L)	14.62	0.50	0.996
1. Foot (R)	11.83	0.43	0.980
(L)	11.13	0.44	0.981
Whole-body	9.80	0.58	0.993

The clothing convective heat transfer coefficients for different body segments cause by various wind directions are listed in Table B-5– Table B-8.

5.3.3 Comparison of different methods for calculating convective heat transfer coefficient for the clothing

As it was stated in Section 2.1.2, there are three methods to calculate the convective heat transfer coefficient for the clothing. The difference between Method 1 and Method 2 is the acquisition of the surface temperature of the clothing. In Method 1, the clothing surface temperature was measured directly. In Method 2, the clothing insulation was approximated from the skin temperature using the clothing insulation. In Method 3, the heat transfer coefficients for clothing was estimated through multiplying the heat transfer coefficients of the naked human body by the clothing area factor. The comparison of the convective heat transfer coefficients calculated by these three methods is summarized from Table 5-5 to Table 5-11. With regards to the whole-body convective heat transfer coefficient, the results calculated with Method 2 were 1.3–1.8 times of that calculated with Method 1. The results calculated with Method 3 were similar to those calculated with Method 3. With regards to the convective heat transfer coefficients for different body segments, the results calculated with Method 2 was 0.5–20 times of that calculated with Method 1.

Table 5-5. The convective heat transfer coefficients and clothing surface temperatures for Ensemble 1 in standing posture (under an airspeed of $0.25 \text{ m}\cdot\text{s}^{-1}$ caused by the upwind).

Segments	t_{cl} ($^{\circ}\text{C}$)		h_c ($\text{W}\cdot\text{m}^{-2}\cdot\text{K}^{-1}$)		
	$t_{cl-\text{Method1}}$	$t_{cl-\text{Method2}}$	$h_{c-\text{Method1}}$	$h_{c-\text{Method2}}$	$h_{c-\text{Method3}}$
9. Back	29.2	26.9	2.03	8.96	3.56
8 Chest	27.5	28.3	5.15	3.24	5.15
7.Shoulder (L)	28.5	28.7	4.77	4.24	5.82
(R)	28.8	29.4	4.27	3.22	5.82
6.Arm (L)	28.2	27.1	5.47	8.94	6.54
(R)	28.2	27.6	6.01	7.65	6.54
4.Pelvis	27.3	27.3	3.05	3.13	4.47
3.Thigh (L)	29.3	29.0	5.35	4.82	5.66
(R)	28.3	28.7	6.82	6.07	5.74
2.Leg (L)	27.5	29.4	11.73	5.94	8.11
(R)	27.4	29.0	11.76	6.53	7.74
1.Foot (L)	28.9	28.0	5.34	7.50	7.24
(R)	28.6	28.8	5.70	5.41	7.88
Whole-body	28.2	28.3	5.73	7.69	5.67

$t_{cl-\text{Method1}}$: the clothing surface temperature for Method 1 (measured directly)

$t_{cl-\text{Method2}}$: the clothing surface temperature for Method 2

$h_{c-\text{Method1}}$: the convective heat transfer coefficient calculated by Method 1

$h_{c-\text{Method2}}$: the convective heat transfer coefficient calculated by Method 2

$h_{c-\text{Method3}}$: the convective heat transfer coefficient calculated by Method 3

Table 5-6. The convective heat transfer coefficients and clothing surface temperatures for Ensemble 2 in standing posture (under an airspeed of $0.25 \text{ m}\cdot\text{s}^{-1}$ caused by the upwind).

Segments	t_{cl} ($^{\circ}\text{C}$)		h_c ($\text{W}\cdot\text{m}^{-2}\cdot\text{K}^{-1}$)		
	$t_{cl-\text{Method1}}$	$t_{cl-\text{Method2}}$	$h_{c-\text{Method1}}$	$h_{c-\text{Method2}}$	$h_{c-\text{Method3}}$
9. Back	27.6	25.4	1.77	7.82	3.68
8 Chest	25.7	26.4	5.80	4.67	5.40
7.Shoulder (L)	26.8	27.3	3.83	2.83	6.17
(R)	26.6	27.7	4.71	2.57	6.17
6.Arm (L)	26.4	25.9	6.51	8.27	6.89
(R)	27.2	26.4	4.91	7.16	6.65
4.Pelvis	27.0	25.8	1.72	4.75	4.38
3.Thigh (L)	27.7	27.2	5.35	6.44	5.77
(R)	27.6	27.3	5.99	6.71	5.74
2.Leg (L)	26.6	28.5	10.67	5.37	8.19
(R)	26.2	28.1	13.28	6.57	7.79
1.Foot (L)	28.4	26.6	4.67	9.58	7.18
(R)	28.5	27.4	5.20	7.77	7.71
Whole-body	27.0	26.9	5.46	7.82	5.74

$t_{cl-\text{Method1}}$: the clothing surface temperature for Method 1 (measured directly)

$t_{cl-\text{Method2}}$: the clothing surface temperature for Method 2

$h_{c-\text{Method1}}$: the convective heat transfer coefficient calculated by Method 1

$h_{c-\text{Method2}}$: the convective heat transfer coefficient calculated by Method 2

$h_{c-\text{Method3}}$: the convective heat transfer coefficient calculated by Method 3

Table 5-7. The convective heat transfer coefficients and clothing surface temperatures for Ensemble 3 in standing posture (under an airspeed of $0.25 \text{ m}\cdot\text{s}^{-1}$ caused by the upwind).

Segments	t_{cl} ($^{\circ}\text{C}$)		h_c ($\text{W}\cdot\text{m}^{-2}\cdot\text{K}^{-1}$)		
	$t_{cl-\text{Method1}}$	$t_{cl-\text{Method2}}$	$h_{c-\text{Method1}}$	$h_{c-\text{Method2}}$	$h_{c-\text{Method3}}$
9. Back	29.2	27.1	1.63	6.58	3.65
8 Chest	27.4	28.4	5.01	2.63	5.30
7.Shoulder (L)	28.2	29.1	4.85	3.10	6.03
(R)	29.4	29.9	3.26	2.65	5.86
6.Arm (L)	28.7	27.8	5.05	7.45	6.70
(R)	28.5	28.3	5.99	6.55	6.59
4.Pelvis	27.4	27.4	3.78	3.94	4.46
3.Thigh (L)	30.2	28.9	3.45	5.88	5.66
(R)	29.1	28.4	5.17	6.77	5.72
2.Leg (L)	28.0	29.7	9.99	5.53	7.71
(R)	29.0	30.0	7.47	5.32	5.66
1.Foot (L)	29.4	28.3	5.63	8.67	7.21
(R)	28.7	29.3	7.19	5.97	7.87
Whole-body	28.7	28.5	4.87	7.22	5.70

$t_{cl-\text{Method1}}$: the clothing surface temperature for Method 1 (measured directly)

$t_{cl-\text{Method2}}$: the clothing surface temperature for Method 2

$h_{c-\text{Method1}}$: the convective heat transfer coefficient calculated by Method 1

$h_{c-\text{Method2}}$: the convective heat transfer coefficient calculated by Method 2

$h_{c-\text{Method3}}$: the convective heat transfer coefficient calculated by Method 3

Table 5-8. The convective heat transfer coefficients and clothing surface temperatures for Ensemble 4 in standing posture (under an airspeed of $0.25 \text{ m}\cdot\text{s}^{-1}$ caused by the upwind).

Segments	t_{cl} ($^{\circ}\text{C}$)		h_c ($\text{W}\cdot\text{m}^{-2}\cdot\text{K}^{-1}$)		
	$t_{cl-\text{Method1}}$	$t_{cl-\text{Method2}}$	$h_{c-\text{Method1}}$	$h_{c-\text{Method2}}$	$h_{c-\text{Method3}}$
9. Back	27.4	25.8	2.07	5.89	3.74
8 Chest	26.0	26.6	4.51	2.94	5.42
7.Shoulder (L)	28.2	27.7	3.24	4.04	5.82
(R)	27.3	28.3	4.54	2.71	5.99
6.Arm (L)	27.3	26.1	4.79	8.57	6.72
(R)	26.9	26.4	5.07	6.49	6.74
4.Pelvis	26.5	25.6	2.39	4.76	4.49
3.Thigh (L)	27.3	27.1	6.61	7.04	5.76
(R)	27.6	27.0	5.41	6.86	5.76
2.Leg (L)	26.6	23.2	11.04	6.06	8.16
(R)	26.9	23.4	9.40	6.18	7.77
1.Foot (L)	28.3	27.2	4.44	6.98	7.27
(R)	28.1	27.5	5.20	6.59	7.83
Whole-body	27.1	26.9	5.16	7.64	5.75

$t_{cl-\text{Method1}}$: the clothing surface temperature for Method 1 (measured directly)

$t_{cl-\text{Method2}}$: the clothing surface temperature for Method 2

$h_{c-\text{Method1}}$: the convective heat transfer coefficient calculated by Method 1

$h_{c-\text{Method2}}$: the convective heat transfer coefficient calculated by Method 2

$h_{c-\text{Method3}}$: the convective heat transfer coefficient calculated by Method 3

Table 5-9. The convective heat transfer coefficients and clothing surface temperatures for Ensemble 5 in standing posture (under an airspeed of $0.25 \text{ m}\cdot\text{s}^{-1}$ caused by the upwind).

Segments	t_{cl} ($^{\circ}\text{C}$)		h_c ($\text{W}\cdot\text{m}^{-2}\cdot\text{K}^{-1}$)		
	$t_{cl-\text{Method1}}$	$t_{cl-\text{Method2}}$	$h_{c-\text{Method1}}$	$h_{c-\text{Method2}}$	$h_{c-\text{Method3}}$
9. Back	27.7	25.6	1.14	6.20	3.77
8 Chest	26.5	26.8	3.83	3.12	5.33
7.Shoulder (L)	27.3	27.3	3.80	3.72	6.01
(R)	27.6	27.5	2.92	3.01	6.03
6.Arm (L)	26.9	25.6	4.25	8.71	6.90
(R)	27.0	26.1	4.43	7.28	6.77
4.Pelvis	26.7	25.5	2.41	7.74	4.43
3.Thigh (L)	28.3	27.6	4.42	5.94	5.73
(R)	28.2	26.9	4.38	7.41	5.70
2.Leg (L)	26.4	28.3	11.96	5.93	8.18
(R)	27.5	28.0	7.25	5.91	7.77
1.Foot (L)	28.6	26.9	4.46	8.85	7.18
(R)	27.2	27.7	7.83	6.38	7.91
Whole-body	27.4	26.9	4.47	7.94	5.74

$t_{cl-\text{Method1}}$: the clothing surface temperature for Method 1 (measured directly)

$t_{cl-\text{Method2}}$: the clothing surface temperature for Method 2

$h_{c-\text{Method1}}$: the convective heat transfer coefficient calculated by Method 1

$h_{c-\text{Method2}}$: the convective heat transfer coefficient calculated by Method 2

$h_{c-\text{Method3}}$: the convective heat transfer coefficient calculated by Method 3

Table 5-10. The convective heat transfer coefficients and clothing surface temperatures for Ensemble 6 in standing posture (under an airspeed of $0.25 \text{ m}\cdot\text{s}^{-1}$ caused by the upwind).

Segments	t_{cl} ($^{\circ}\text{C}$)		h_c ($\text{W}\cdot\text{m}^{-2}\cdot\text{K}^{-1}$)		
	$t_{cl-\text{Method1}}$	$t_{cl-\text{Method2}}$	$h_{c-\text{Method1}}$	$h_{c-\text{Method2}}$	$h_{c-\text{Method3}}$
9. Back	28.7	25.9	0.52	6.40	3.66
8 Chest	26.7	27.4	4.81	3.24	5.22
7.Shoulder (L)	27.8	28.1	4.80	4.31	5.83
(R)	28.6	28.6	3.84	3.83	5.77
6.Arm (L)	28.4	26.8	4.16	8.12	6.60
(R)	27.7	27.1	5.76	7.35	6.55
4.Pelvis	27.5	26.7	2.87	4.67	4.24
3.Thigh (L)	28.8	28.2	4.75	5.94	5.68
(R)	28.1	27.7	5.14	6.03	5.75
2.Leg (L)	26.6	28.4	11.80	5.87	8.21
(R)	27.7	28.3	7.65	6.04	7.74
1.Foot (L)	28.9	27.0	4.42	9.37	7.16
(R)	28.2	27.8	6.09	6.98	7.81
Whole-body	27.0	27.5	4.83	7.95	5.68

$t_{cl-\text{Method1}}$: the clothing surface temperature for Method 1 (measured directly)

$t_{cl-\text{Method2}}$: the clothing surface temperature for Method 2

$h_{c-\text{Method1}}$: the convective heat transfer coefficient calculated by Method 1

$h_{c-\text{Method2}}$: the convective heat transfer coefficient calculated by Method 2

$h_{c-\text{Method3}}$: the convective heat transfer coefficient calculated by Method 3

Table 5-11. The convective heat transfer coefficients and clothing surface temperatures for Ensemble 8 in standing posture (under an airspeed of $0.25 \text{ m}\cdot\text{s}^{-1}$ caused by the upwind).

Segments	t_{cl} ($^{\circ}\text{C}$)		h_c ($\text{W}\cdot\text{m}^{-2}\cdot\text{K}^{-1}$)		
	$t_{cl-\text{Method1}}$	$t_{cl-\text{Method2}}$	$h_{c-\text{Method1}}$	$h_{c-\text{Method2}}$	$h_{c-\text{Method3}}$
9. Back	29.0	26.6	0.25	5.30	3.78
8 Chest	26.4	27.6	6.60	2.84	5.50
7.Shoulder (L)	28.0	28.4	5.15	4.23	5.94
(R)	27.7	29.4	6.88	3.19	5.95
6.Arm (L)	27.6	26.7	5.84	9.29	6.83
(R)	28.4	27.4	4.81	7.37	6.61
4.Pelvis	27.5	27.1	2.76	3.61	4.49
3.Thigh (L)	29.3	28.9	4.83	5.69	5.70
(R)	29.1	28.4	5.10	6.82	5.68
2.Leg (L)	28.5	29.3	7.68	5.92	8.09
(R)	27.5	29.0	10.69	6.01	7.81
1.Foot (L)	28.1	27.8	8.04	8.97	7.29
(R)	28.4	28.6	6.88	6.56	7.87
Whole-body	28.2	28.1	5.30	7.71	5.73

$t_{cl-\text{Method1}}$: the clothing surface temperature for Method 1 (measured directly)

$t_{cl-\text{Method2}}$: the clothing surface temperature for Method 2

$h_{c-\text{Method1}}$: the convective heat transfer coefficient calculated by Method 1

$h_{c-\text{Method2}}$: the convective heat transfer coefficient calculated by Method 2

$h_{c-\text{Method3}}$: the convective heat transfer coefficient calculated by Method 3

5.3.4 Whole-body radiative heat transfer coefficient

There was a large difference in the wall temperature among the experiments for different clothing ensembles in sitting posture (Figure 5-11). Therefore, it is difficult to compare the radiative heat transfer coefficient for different clothing ensembles in the sitting posture. Only the results in the standing posture for radiative heat transfer coefficients are shown in Figure 5-12.

The radiative heat transfer coefficient for the clothed manikin was 2%–4% smaller than that of the naked manikin. The reason is that the surface temperature of the clothing was lower than the surface temperature of the thermal manikin. The maximum difference between the convective heat transfer coefficient for the clothed manikin and the naked manikin was 35%. Hence, the radiative heat transfer coefficient for the naked manikin and the clothed manikin could be considered to be the same.

The radiative heat transfer coefficients for different clothing ensembles were also marginally different. The largest clothing radiative heat transfer coefficient (for E3) was 2% higher than the lowest clothing radiative heat transfer coefficient (for E2) at an airspeed of $1.4 \text{ m}\cdot\text{s}^{-1}$. The difference in the radiative heat transfer coefficients between various clothing ensembles was negligible.

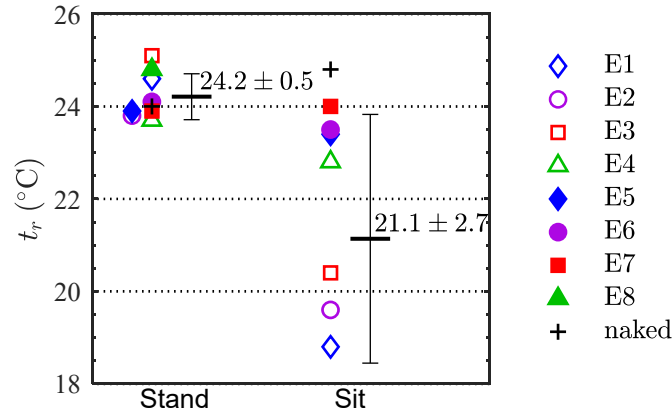


Figure 5-11. The average temperature of the wall surfaces during the experiments.

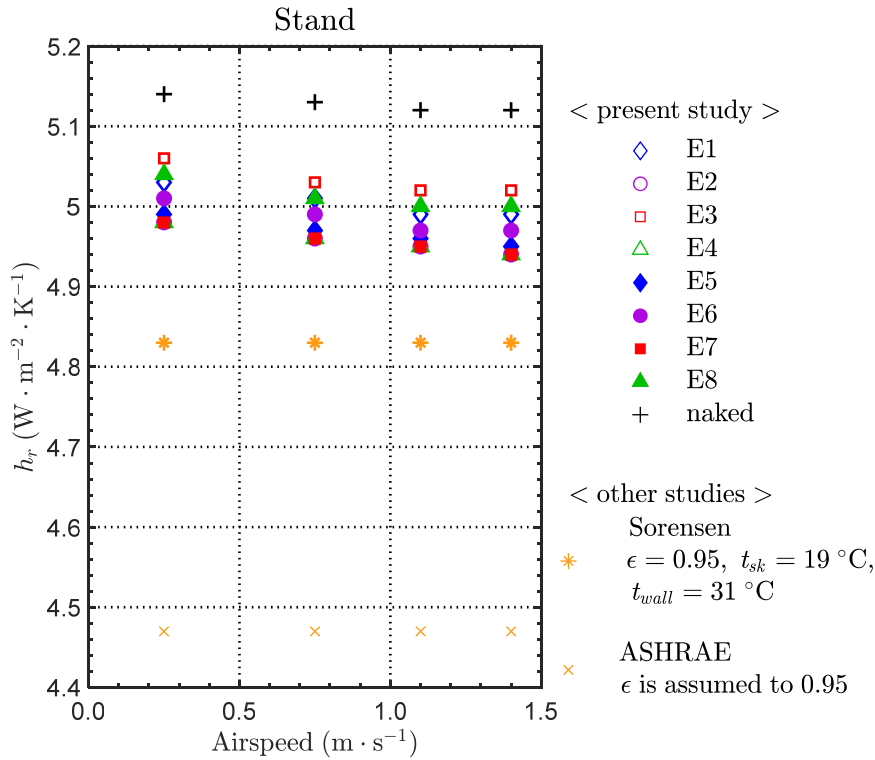


Figure 5-12. Whole-body radiative heat transfer coefficient for different clothing ensembles under various airspeeds for standing posture (Sorensen [21], ASHRAE [20]).

5.3.5 Radiative heat transfer coefficient for different body segments

Figure 5-13 shows the radiative heat transfer coefficient for each body segment. As there was no difference in the radiative heat transfer coefficients between different wind directions, results for the three wind directions were averaged. Radiative heat transfer coefficient almost unaffected by airspeed (Figure 5-12). Hence, the results for various airspeeds were averaged. Figure 5-13 reveals that the radiative heat transfer coefficient for the clothed manikin was smaller than that of the naked manikin at each body segment. The reason is that the temperature for the clothing surface was lower than the naked manikin surface. Hence, the radiative heat loss from the clothing surface was less than the naked manikin. The average radiative heat transfer coefficients for different clothing

ensembles including the head, hands, and feet are listed in Table B-9 in Appendix A.

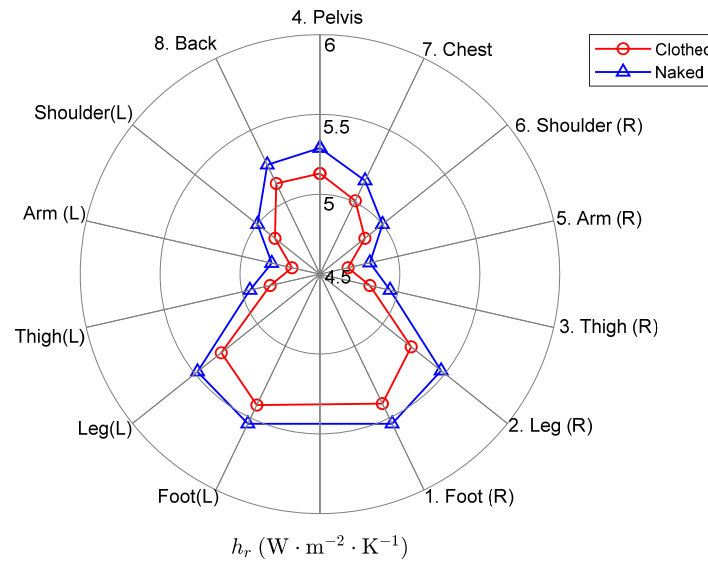


Figure 5-13. Comparison of average radiative heat transfer coefficient of different clothing ensembles and radiative heat transfer coefficient of naked manikin at each body segment in standing posture (the results of three wind directions and four airspeeds were averaged).

5.4 Calculation of clothing heat transfer coefficients based on CFD analysis.

In section 5.2 and 5.3, the experimental results were presented. In this section, the CFD analysis method to calculate the heat transfer coefficients for the clothing ensembles were proposed. It is very laborious and time-consuming to measure the heat transfer coefficient of clothing by experiment. Also, the thermal manikin is not very universal equipment. Therefore, CFD simulations would be useful when experiments are not possible. Also, if CFD simulations is possible, convective heat transfer coefficients for various environmental conditions can be calculated. In addition, CFD and energy coupling analysis are often used. Hence, CFD simulation methodology is needed.

5.4.1 Method

The numerical method was the same as that listed in Table 4-3 in Chapter 4. The environmental conditions for the CFD analysis are summarized in Table 5-12. The boundary conditions for the CFD analysis were set from the experiments (Table 5-13).

For the segments covered by clothing, the clothing surface temperature was set as the boundary condition for the thermal manikin indicated as Equation (5.1). I_{cl} is the whole-body clothing insulation, which will be presented in Chapter 6. t_{sk} is the surface temperature for the naked thermal manikin.

$$t_{cl} = t_{sk} - q_t I_{cl} \quad (5.1)$$

For the segments not covered by clothing, the surface temperature for the naked manikin was set according to the experimental results. The calculation procedure of CFD analysis is shown in Figure 5-14. Although there are two unknowns in Equation (5.1), t_{cl} and q_t . As t_a and t_r are known

from the experiment, q_t can be predicted if t_{cl} is assumed to an arbitrary value (Equation (5.2)).

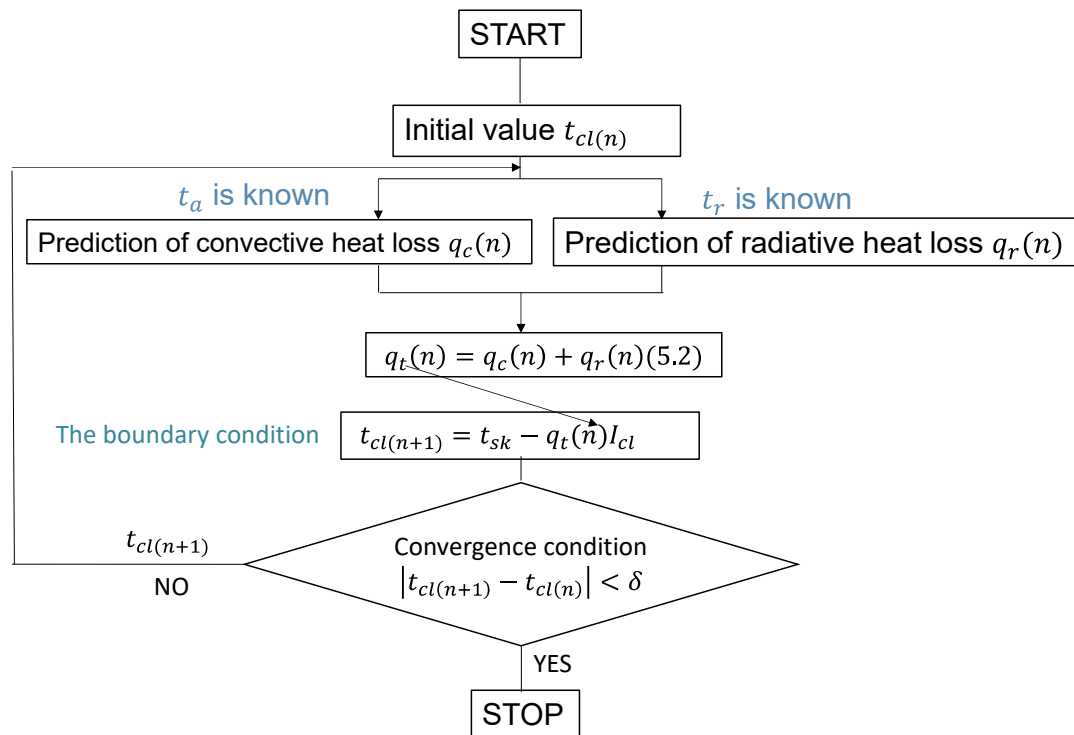


Figure 5-14. Calculation procedure of CFD analysis.

Table 5-12. Environmental conditions for the CFD analysis of clothing.

Wind direction	Upwind
Airspeed	0.25 0.75 1.1 1.4 m·s ⁻¹
Posture	Standing
Manikin surface temperature	10 °C higher than the air temperature
Clothing ensembles	E1, E2, E3, E4, E5, E6, E7, E8

Table 5-13. Boundary conditions.

Inlet (ABCD)	Velocity: U_0 , results of the experiment (Figure 4-3 in Chapter 4) Turbulence intensity: I_{in} , results of the experiment (Figure 4-3 in Chapter 4) Turbulence length scale: $*L_{in} = 0.14$ m Temperature: results of the experiment
Outlet (EFGH)	U_{out} : depends on the law of mass conservation [22] k_{out} , ε_{out} : free slip
Wall	Surface temperature: t_{wall} , results of the experiment Velocity: no slip
Computational thermal manikin	For the body segments covered by clothing, sensible q_t was set For the body segments not covered by the clothing, surface temperature for the naked manikin was set Velocity: no slip Emissivity: 0.95 (the emissivity for the clothing ensembles were all 0.95) Direction: upwind

* $L_{in} = 0.07 L$ [23], L : characteristic length of inlet

5.4.2 Results

The comparison of the convective heat transfer coefficients based on the CFD analysis and experiment is shown in Figure 5-14. The standard deviation of the difference between the convective heat transfer coefficient due to the experiment and CFD analysis is listed in Table 5-14. It is clear from Figure 5-14 and Table 5-14 that the difference between the results of the experiment and the CFD analysis increased with airspeed. There are many factors influencing the convective heat transfer coefficient for the clothing, such as the air permeability of clothing, fit of clothing, the geometry shape of the clothing, and the roughness of the clothing surface [8,9,24]. To explain the individual influencing factor will be very challenging. Therefore the correction factor for the CFD analysis α was introduced by comparing the results of experiment and the CFD analysis (Table 5-15). The air permeability and surface roughness for different clothing ensembles are summarized in Section 3.3 in Table 3-7 and Table 3-9. If the experiment is not possible, the convective heat transfer coefficient due to the CFD analysis can be corrected by the correction factor α by looking for an identical or similar ensemble in the present study.

Table 5-14. The standard deviation of the difference between the convective heat transfer coefficient due to experiment and CFD analysis.

	$0.25 \text{ m}\cdot\text{s}^{-1}$	$0.75 \text{ m}\cdot\text{s}^{-1}$	$1.1 \text{ m}\cdot\text{s}^{-1}$	$1.4 \text{ m}\cdot\text{s}^{-1}$
Standard deviation	0.52	0.97	0.98	1.11

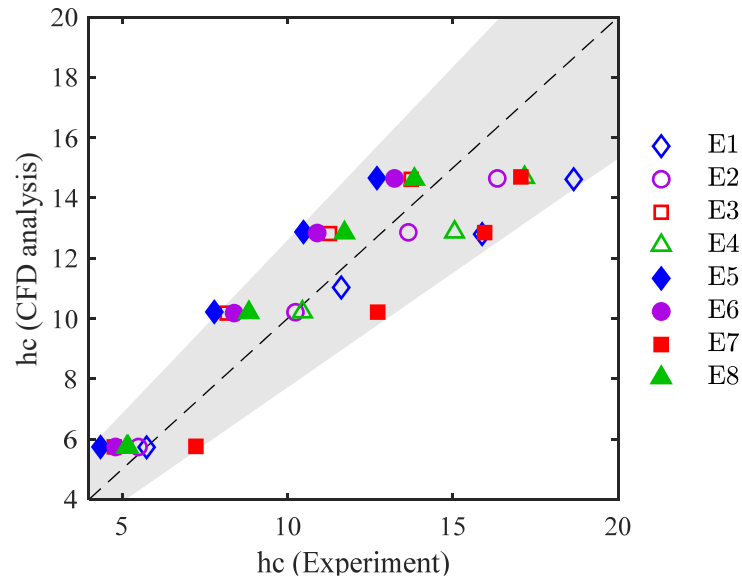


Figure 5-15. The comparison of the convective heat transfer coefficients based on the CFD analysis and experiment.

Table 5-15. The correction factor for the CFD analysis α .

$\alpha = aV + b$			
	a	b	R^2
E1	0.10	0.89	0.924
E2	0.05	0.90	0.998
E3	0.04	0.76	0.761
E4	0.05	0.90	0.998
E5	0.04	0.70	0.913
E6	0.02	0.80	0.689
E7	-0.03	1.30	0.716
E8	0.02	0.86	0.562

The comparison of radiative heat transfer coefficients based on the CFD analysis and experiment is shown in Figure 5-14 and Table 5-16. The results based on CFD analysis agreed with the results based on experiments.

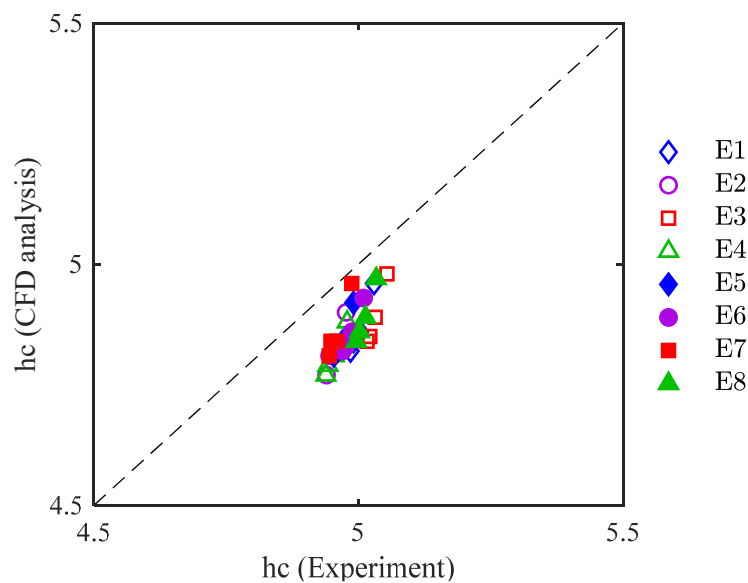


Figure 5-16. The comparison of the radiative heat transfer coefficients based on the CFD analysis and experiment.

Table 5-16. The standard deviation of the difference between the radiative heat transfer coefficient due to experiment and CFD analysis.

	$0.25 \text{ m}\cdot\text{s}^{-1}$	$0.75 \text{ m}\cdot\text{s}^{-1}$	$1.1 \text{ m}\cdot\text{s}^{-1}$	$1.4 \text{ m}\cdot\text{s}^{-1}$
Standard deviation	0.02	0.01	0.02	0.01

Convective heat transfer coefficients for clothing with insulation of 0.5 clo, 1 clo, and 1.5 clo were calculated using CFD analysis. The results showed that the clothing insulation had no effect on the convective heat transfer coefficient for the clothing.

5.5 Conclusions

In this chapter, the convective and radiative heat transfer coefficients of eight sets of clothing ensembles were investigated through manikin experiments and CFD analysis.

The main conclusions arising from this chapter are as follows:

Convective heat transfer coefficient:

- (1) The convective heat transfer coefficients for the clothed manikin were higher than those of the naked manikin, and the maximum difference was 35%. The convective heat transfer coefficients varied between the clothing ensembles, and the maximum difference was 32%.
- (2) The convective heat transfer coefficients for the standing posture were larger than those of the sitting posture. The convective heat transfer coefficients caused by the crosswind were the lowest both in sitting and standing postures.
- (3) The convective heat transfer coefficients for the trunks were smaller than those of limbs, as already has been seen in the convective heat transfer coefficient for the naked manikin. However, the results for pelvis showed a larger value because of the more clothing layers (shirts, pants, and coat).
- (4) The correction factor for the convective heat transfer coefficient calculated by the CFD analysis was presented.

Radiative heat transfer coefficient:

- (5) The radiative heat transfer coefficients for the clothed manikin were marginally lower than those of the naked manikin. The radiative heat transfer coefficients varied slightly between the clothing ensembles. However, these differences were negligible when compared to the convective heat transfer coefficients.
- (6) The clothing radiative heat transfer coefficient for different body segments had the same characteristics as the radiative heat transfer coefficient for the naked manikin.

Clothing affects human thermal comfort significantly because it determines the heat loss from the human body to the environment. The detailed investigation of the convective and radiative heat transfer coefficients will lead to a better understanding of the heat transfer through clothing. The measured convective heat transfer coefficient can be used as input data for several thermal comfort evaluation models and indices such as the PMV index, the standard effective temperature, the two-node model, they will play an important role in accurately simulating the human thermal comfort.

Reference

- [1] J. Colin, Y. Houdas, Experimental determination of coefficient of heat exchanges by convection of human body, *Journal of Applied Physiology*. 22 (1967) 31–38. doi:10.1152/jappl.1967.22.1.31.
- [2] K. Parsons, *Human thermal environments* (Chapter 1), CRC Press, 2014. doi:10.1201/b16750.
- [3] D. Mitchell, Convective heat transfer from man and other animals, in: J.L. Monteith, L.E. Mount (Eds.), *Heat Loss from Animals and Man*, Elsevier, London, 1974: pp. 59–76. <https://linkinghub.elsevier.com/retrieve/pii/B978040870652050010X>.
- [4] R.J. De Dear, E. Arens, Z. Hui, M. Oguro, Convective and radiative heat transfer coefficients for individual human body segments, *International Journal of Biometeorology*. 40 (1997) 141–156. doi:10.1007/s004840050035.
- [5] ISO 9920, *Ergonomics of the thermal environment — Estimation of thermal insulation and water vapour resistance of a clothing ensemble*, (2007). <https://www.iso.org/standard/39257.html>.
- [6] I. Ciesielska-Wrobel, G. De Mey, L. Van Langenhove, Dry heat transfer from the skin surface into textiles: subjective and objective measurement of thermal haptic perception of textiles – preliminary studies, *The Journal of The Textile Institute*. 107 (2016) 445–455. doi:10.1080/00405000.2015.1034938.
- [7] Y. Sun, X. Chen, Z. Cheng, X. Feng, Study of heat transfer through layers of textiles using finite element method, *International Journal of Clothing Science and Technology*. 22 (2010) 161–173. doi:10.1108/09556221011018630.
- [8] A.V.M. Oliveira, A.R. Gaspar, D.A. Quintela, Convective heat transfer from a clothed manikin, in: *Windsor International Conference - Comfort and Energy Use in Buildings: Getting Them Right*, Windsor, UK, 2006. <https://www.researchgate.net/publication/237778232>.
- [9] M. Oguro, E. Arens, R. de Dear, H. Zhang, T. Katayama, Convective heat transfer coefficients and clothing insulation for parts of the clothed human body under airflow conditions, *Journal of Architecture and Planning (Transactions of AIJ)*. 67 (2002) 21–29. doi:10.3130/aija.67.21_5.
- [10] K. Kuwabara, T. Mochida, M. Kondo, K. Matsnaga, Measurement of man's convective heat transfer coefficient by using a thermal manikin in the middle wind velocity region (in Japanese), *Journal of Human and Living Environment*. 8 (2001) 27–32. doi:10.24538/jhesj.8.1-2_27.
- [11] M. Tian, Z. Wang, J. Li, 3D numerical simulation of heat transfer through simplified protective clothing during fire exposure by CFD, *International Journal of Heat and Mass Transfer*. 93 (2016) 314–321. doi:10.1016/j.ijheatmasstransfer.2015.09.027.
- [12] S. Takada, A. Sasaki, R. Kimura, Fundamental study of ventilation in air layer in clothing considering real shape of the human body based on CFD analysis, *Building and Environment*. 99 (2016) 210–220. doi:10.1016/j.buildenv.2016.01.028.
- [13] G. Havenith, *Clothing and thermoregulation*, in: *Textiles and the Skin*, Karger, Basel, 2003: pp.

- 35–49. doi:10.1159/000072236.
- [14] P.O. Fanger, Chapter 2, in: *Thermal Comfort: Analysis and Applications in Environmental Engineering*, Copenhagen: Danish Technical Press, 1970: pp. 32–35.
- [15] K. Sato, T. Kurabuchi, T. Ogasawara, M. Ohba, S. Iwamoto, N. Sahashi, S. Ikehara, A study on the convective heat transfer coefficient and thermal resistance of clothing under cross ventilation, *International Journal of Ventilation*. 10 (2011) 155–162. doi:10.1080/14733315.2011.11683944.
- [16] D. Bechert, M. Bruse, W. Hage, R. Meyer, D. Bechert, M. Bruse, W. Hage, R. Meyer, Biological surfaces and their technological application - Laboratory and flight experiments on drag reduction and separation control, in: *28th Fluid Dynamics Conference, American Institute of Aeronautics and Astronautics*, Reston, Virginia, 1997: pp. 505–507. doi:10.2514/6.1997-1960.
- [17] E. Oguri, Y. Kohama, Drag reduction by micron-sized distributed surface geometry on a flat plate (in Japanese)., *Transactions of the Japan Society of Mechanical Engineers Series B*. 62 (1996) 1754–1761. doi:10.1299/kikaib.62.1754.
- [18] Y.A. Çengel, A.J. Ghajar, External forced convection, in: *Heat and Mass Transfer: Fundamentals and Applications*, McGraw-Hill Education, 2019: pp. 424–472. <https://books.google.co.jp/books?id=RiXCvgEACAAJ>.
- [19] Y. Kamata, T. Kato, A. Ito, N. Yahata, Convective heat transfer from human body. (Part 2. Effect of fabric on heat transfer)., *Sen'i Gakkaishi*. 44 (1988) 78–87. doi:10.2115/fiber.44.2_78.
- [20] Chapter 9, in: *ASHRAE Handbook Fundamentals*, 2017: pp. 9.1–9.30. <https://www.ashrae.org/technical-resources/ashrae-handbook/description-2017-ashrae-handbook-fundamentals>.
- [21] D.N. Sørensen, L.K. Voigt, Modelling flow and heat transfer around a seated human body by computational fluid dynamics, *Building and Environment*. 38 (2003) 753–762. doi:10.1016/S0360-1323(03)00027-1.
- [22] W. Zhang, K. Hiyama, S. Kato, Y. Ishida, Building energy simulation considering spatial temperature distribution for nonuniform indoor environment, *Building and Environment*. 63 (2013) 89–96. doi:10.1016/j.buildenv.2013.02.007.
- [23] H.K. Versteeg, W. Malalasekera, *An introduction to computational fluid dynamics (Chapter 3)*, Prentice Hall, 2007. <https://books.google.co.jp/books?id=RvBZ-UMpGzIC>.
- [24] Y. Kurazumi, L. Rezgals, Convective heat transfer coefficients of the human body under forced convection from ceiling, *Journal of Ergonomics*. 04 (2014) 1–6. doi:10.4172/2165-7556.1000126.

Chapter 6.

Clothing insulation

6.1 *Introduction*

Clothing insulation is one of the six parameters (metabolic rate, clothing insulation, air temperature, mean radiant temperature, airspeed, and relative humidity) to evaluate human thermal comfort. Therefore, it is crucial to have an accurate understanding of the thermal characteristics of clothing insulation. Many studies about the measuring method and the effect factors of clothing insulation have been carried out. Holmer et al. proposed equations determining the reduction in total insulation values as a consequence of wind and walking effects [1]. Havenith et al. conducted experiments on four subjects with three clothing ensembles. They found that all influences (posture, movement, wind, and clothing fit) showed significant effects on the clothing insulation [2]. Besides, there are comprehensive data about clothing insulation values in the literature and standards [3–9]. However, the measurement data on clothing insulation was extremely old. The latest International Organization for Standardization (ISO) database for clothing insulation, ISO 9920, was published in 2007 [3]. The information about various kinds of garments is also limited. Although handbook of American Society of Heating Refrigerating and Air-Conditioning Engineers (ASHRAE) and ISO 9920 provide garment insulation values. However, only some typical clothing types are listed [6]. Furthermore, with the development of material engineering, clothing materials have diversified, such as the windbreaker jacket, the fleece jacket, and clothing made using phase change materials [3,10–12]. Therefore, it is essential to characterize the thermal insulation characteristics of clothing made from such new materials.

Additionally, the clothing insulation databases for ISO 9920, ISO 7730, ASHRAE standard 55–2013, and ASHRAE Handbook only provide clothing insulation for the whole-body [3–6]. The clothing insulation for different body segments is lacking. Many thermophysiological models capable of predicting the thermal sensation for different body parts have been developed over the past few decades. Kaynakli et al. presented a thermal comfort model dividing the body into 16 parts based on the two-node model [13]. Tanabe et al. developed a 65-node thermoregulation model consisting of 16 body segments and a blood compartment, and each body segment has four layers for core, muscle, fat, and skin [14]. In the aforementioned thermal comfort models, the clothing insulations for different body segments were taken as the same. This simplification may not affect the whole-body thermal sensation greatly, but it may have a significant influence on the thermal sensation for different body segments.

In this chapter, the clothing insulations for eight clothing ensembles were measured with a 16-segment thermal manikin. Four different methods to define the clothing insulation were compared. Furthermore, the effects of airspeed, wind direction, and posture on clothing insulation were confirmed.

6.2 The effect of airspeed and wind direction

6.2.1 Experimental setup

The experimental setup is the same as Chapter 5. The experimental conditions are shown in Table 6-1.

Table 6-1. The experimental conditions.

Wind direction	Upwind, crosswind, downwind
Airspeed	0.25, 0.75, 1.1, 1.4 m·s ⁻¹
Manikin surface temperature	10 °C higher than the air temperature
Posture	Standing, sitting

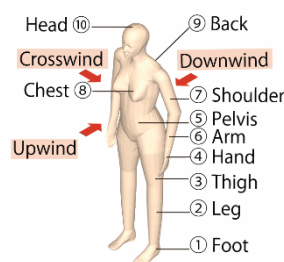


Figure 6-1. Diagram of wind direction.

The information for the clothing ensembles is shown in Section 3.2 in Figure 3-9 and Table 3-2. Two independent tests were conducted on each clothing ensemble, and the mean values for two times were taken. The difference in the results between these two tests was under 4% [15].

6.2.2 Results

6.2.2.1 Whole-body clothing insulation

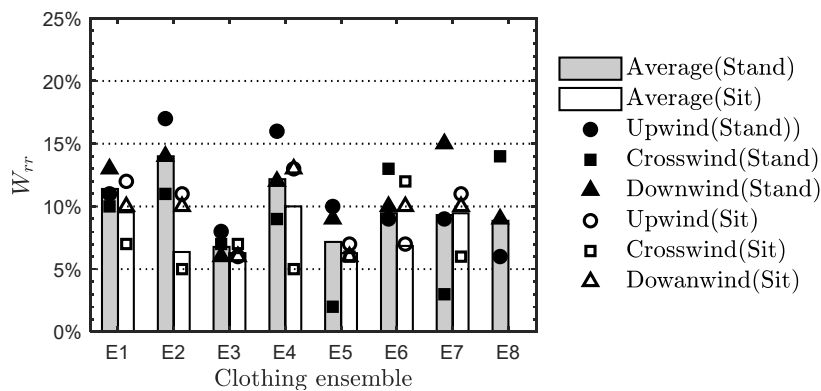
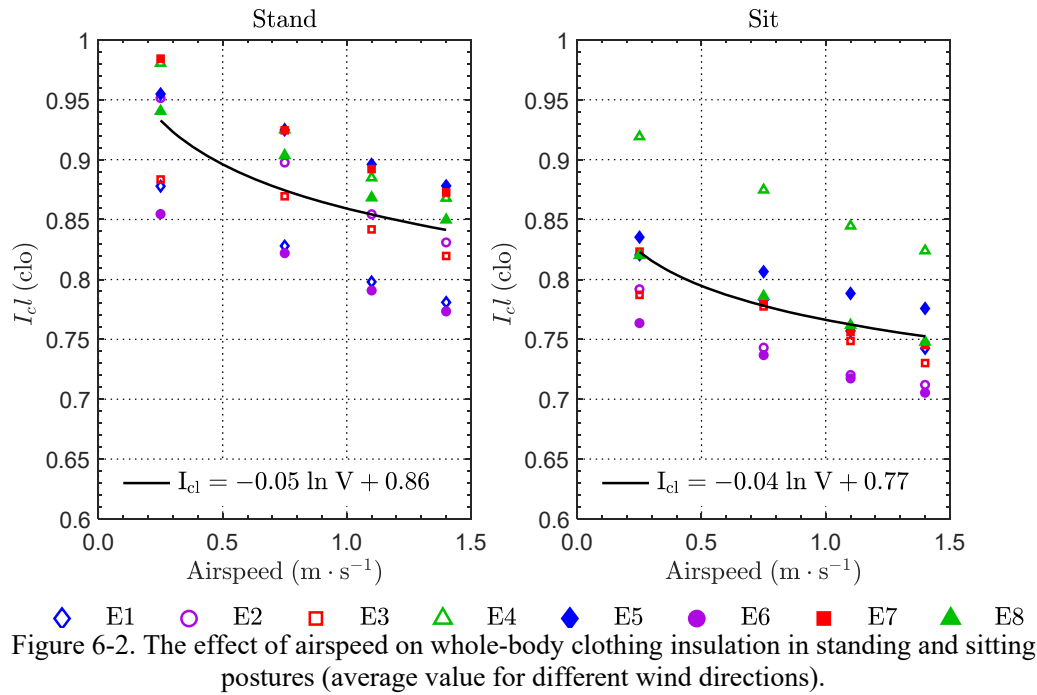
The whole-body clothing insulation is shown in Figure 6-2. The solid black line represents regression line of airspeed and the average value of whole-body clothing insulation for various clothing ensembles.

For all the clothing ensembles, the clothing insulation decreased with airspeed. The clothing insulation for the standing posture was larger than the sitting posture. This is because, in the sitting posture, the clothing on the back and thighs was compressed [3]. Hence, the air layer for the standing posture was thicker than that of the sitting posture. Thus, the basic insulation for the standing posture was higher. For the same reason, the reduction rate of clothing insulation caused by the wind for the standing posture was larger than that for the sitting posture (Figure 6-3). The reduction rate of clothing insulation varied with clothing ensembles. The reduction rate for E3 was the smallest. The top of E3 was a sweater that was easy for the wind to penetrate even under a small airspeed. The clothing insulation for E3 under an airspeed of 0.25 m·s⁻¹ was decreased enough due to the penetration of wind. Therefore, the reduction rate due to wind was low. It was assumed that the reduction rates for E1, E7, and E8 were smaller than other clothing ensembles because their air permeabilities were smaller than other clothing ensembles (Table 3-7 in Section 3.3.4). However, as it is shown in Figure 6-3, the reduction rates for E1, E7, and E8 did not show small values. The

potential reason is that in the airspeed range from $0.25 \text{ m}\cdot\text{s}^{-1}$ to $1.4 \text{ m}\cdot\text{s}^{-1}$, the porosity for the clothing does not have a large effect on the clothing insulation.

Figure 6-4 shows the clothing insulation for different clothing ensembles caused by various wind directions. The clothing insulation caused by the crosswind was the largest. The reason is that the area facing the wind was the smallest under the crosswind. Table 6-2 lists the correction factor for airspeed under different wind directions.

The correction factor for posture under upwind is illustrated in Figure 6-5. The correction factor for wind direction in standing posture and sitting postures are shown in Figure 6-6 and Figure 6-7, respectively.



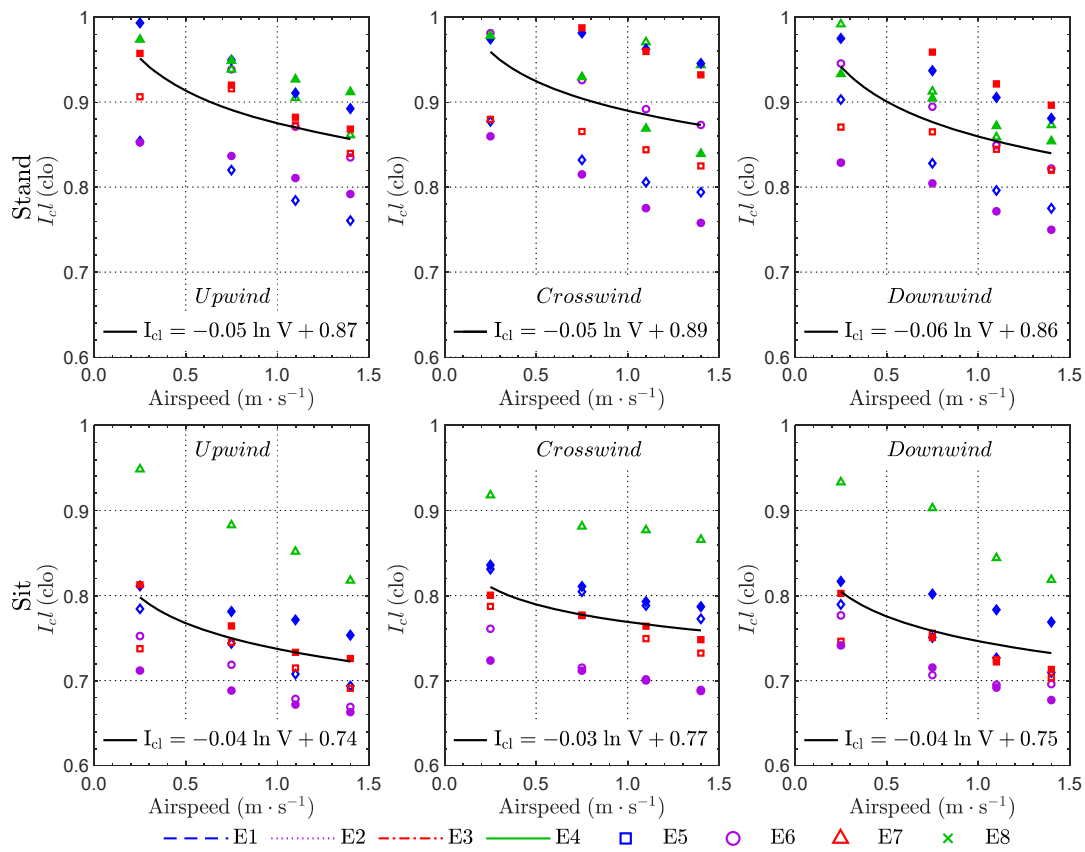


Figure 6-4. Whole-body basic insulation for different clothing ensembles under various wind directions (up: standing posture; down: sitting posture).

Table 6-2. The correction factor for airspeed under different wind directions CFV_{cl} ($CFV_{cl} = I_{cl}/I_{cl-static}$, I_{cl} is the clothing insulation under arbitrary airspeed, $I_{cl-static}$ is the clothing insulation for under an airspeed of $0.25 m \cdot s^{-1}$).

$CFV_{cl} = e^{-a(V-b)}$				
		a	b	R ²
Stand	Upwind	0.10	0.28	0.992
	Crosswind	0.09	0.27	0.994
	Downwind	0.10	0.24	0.995
Sit	Upwind	0.09	0.25	0.997
	Crosswind	0.06	0.23	0.998
	Downwind	0.09	0.25	0.995

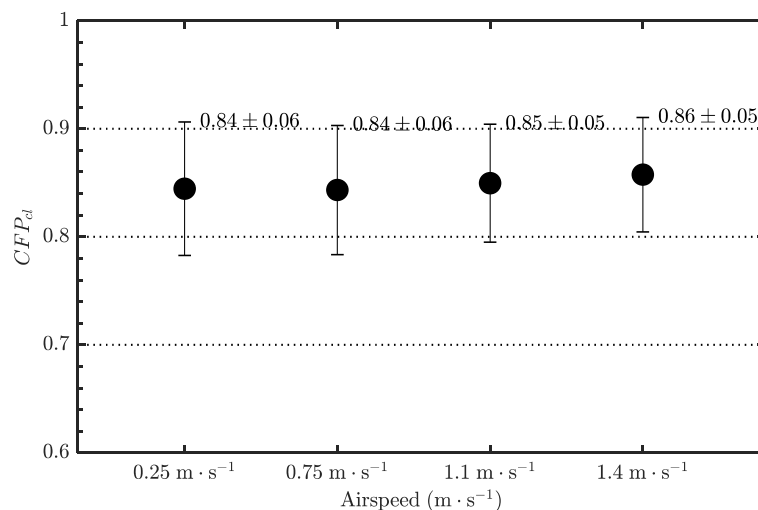


Figure 6-5. The correction factor for posture under upwind CFP_{cl} ($CFP_{cl} = \frac{I_{cl-sit}}{I_{cl-stand}}$, I_{cl-sit} is the clothing insulation for the sitting posture, $I_{cl-stand}$ is the clothing insulation for the standing posture).

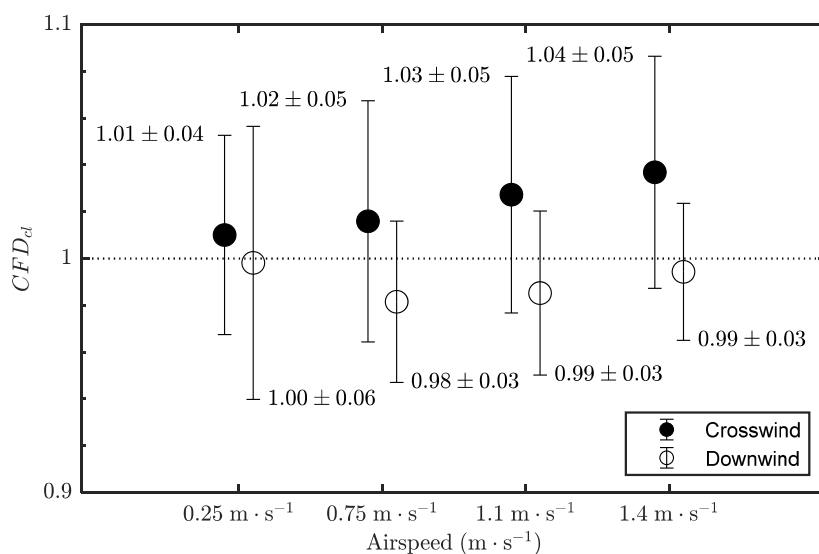


Figure 6-6. The correction factor for wind direction (CFD_{cl}) in standing posture ($CFD_{cl} = [I_{cl-crosswind} \text{ or } I_{cl-downwind}] / I_{cl-upwind}$, $I_{cl-crosswind}$ is the clothing insulation caused by a crosswind, $I_{cl-downwind}$ is the clothing insulation caused by downwind, $I_{cl-upwind}$ is the clothing insulation caused by upwind).

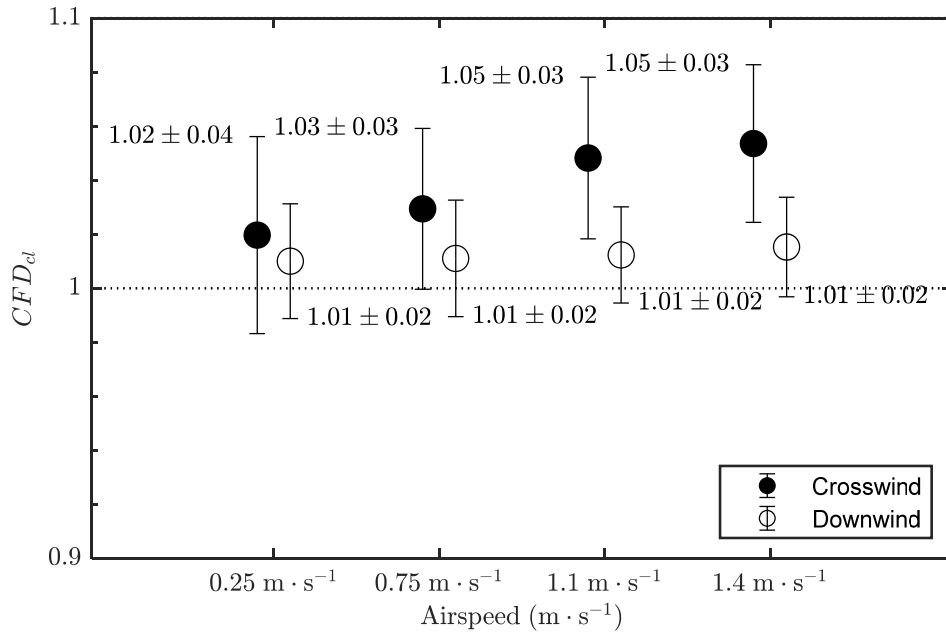


Figure 6-7. The correction factor (CFD_{cl}) for wind direction in sitting posture ($CFD_{cl} = [I_{cl-crosswind} \text{ or } I_{cl-downwind}] / I_{cl-upwind}$, $I_{cl-crosswind}$ is the clothing insulation caused by the crosswind, $I_{cl-downwind}$ is the clothing insulation caused by the downwind, $I_{cl-upwind}$ is the clothing insulation caused by the upwind).

6.2.2.2 The proposal of prediction formula for whole-body clothing insulation considering posture and wind direction

The prediction formula for whole-body clothing insulation considering posture and wind direction was proposed (Equation (6-1)). The calculation procedure for Equation (6-1) is shown in Figure 6-8. This procedure is not only suitable for the clothing insulations measured in the present study, but also for clothing insulation acquired through referring to standards or other studies.

$$I_{cl} = I_{cl-static} CFP_{cl} CFD_{cl} CFV_{cl} \quad (6-1)$$

$I_{cl-static}$, the clothing insulation under an airspeed of $0.25 \text{ m} \cdot \text{s}^{-1}$

CFP_{cl} , the correction factor of posture

CFD_{cl} , the correction factor of wind direction

CFV_{cl} , the correction factor of airspeed

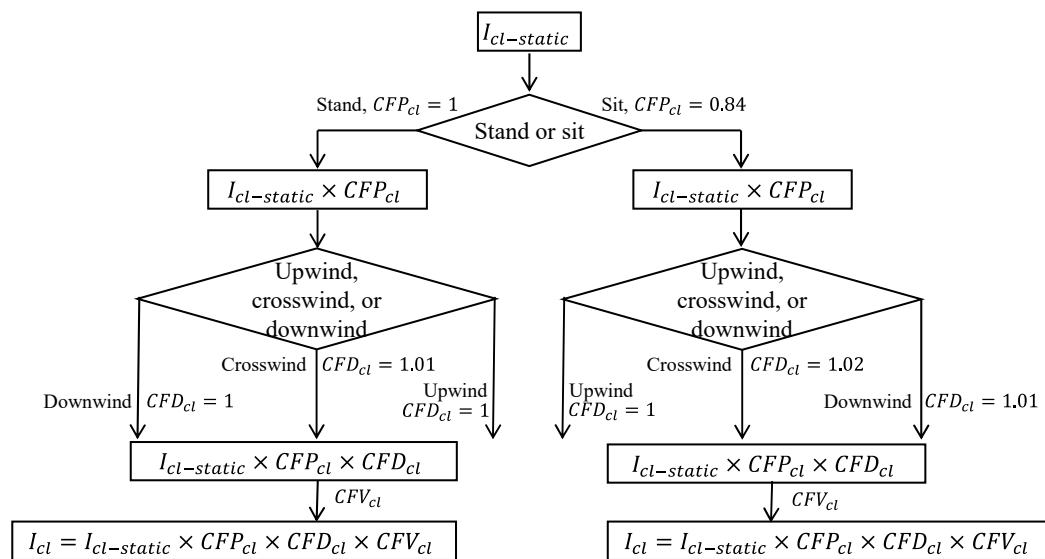


Figure 6-8. The calculation procedure and the determining of correction numbers for Equation (6-1).

6.2.2.3 Local clothing insulation

The local clothing insulations for different clothing ensembles under various airspeeds in standing and sitting postures are shown in Figure 6-9 and Figure 6-10. The solid black line represents the regression line of airspeed and the average clothing insulation for various clothing ensembles. For all the body segments, the clothing insulation decreased with airspeed when looking at the regression line. However, when looking at the clothing insulation for various clothing ensembles, there were some clothing insulation values increased with airspeeds, such as the right leg for E4, and the left foot for E6. The motion of air between the manikin surface and the clothing surface was held responsible for the abnormal pattern of change at the legs. The air layer at the legs was comparatively thick. Hence the motion of the air due to wind pressure was complex. Besides, as the legs and feet were adjacent, the heat transfer at the legs positively affects the feet.

The clothing insulations for the upper body parts were larger than the lower body parts because the upper body parts have two clothing layers, the coat, and the shirt. The finding underlined the importance of considering the unbalanced distribution of clothing insulation between half-bodies when evaluating human thermal comfort [16]. Among the segments for the upper body segments, the clothing insulation for the chest and the pelvis was higher. The higher value for the chest was due to there was underwear beneath the shirt. The higher value for the pelvis was because of the underwear and a part of the shirt tucked into the trousers. Among the body segments of the lower body parts, the legs had higher clothing insulation values because of the thicker air layer between the thermal manikin surface and the clothing.

For most of the body segments, the clothing insulation for the sitting posture was smaller than that of standing posture.

The reduction rate of clothing insulation for the chest, back, and pelvis was the highest. In the low airspeed range, the chest, back, and pelvis were in the developed thermal plume. The thermal plume

was easily broken by the wind [17]. Therefore, the clothing insulation for the chest, back, and pelvis decreased rapidly with airspeed.

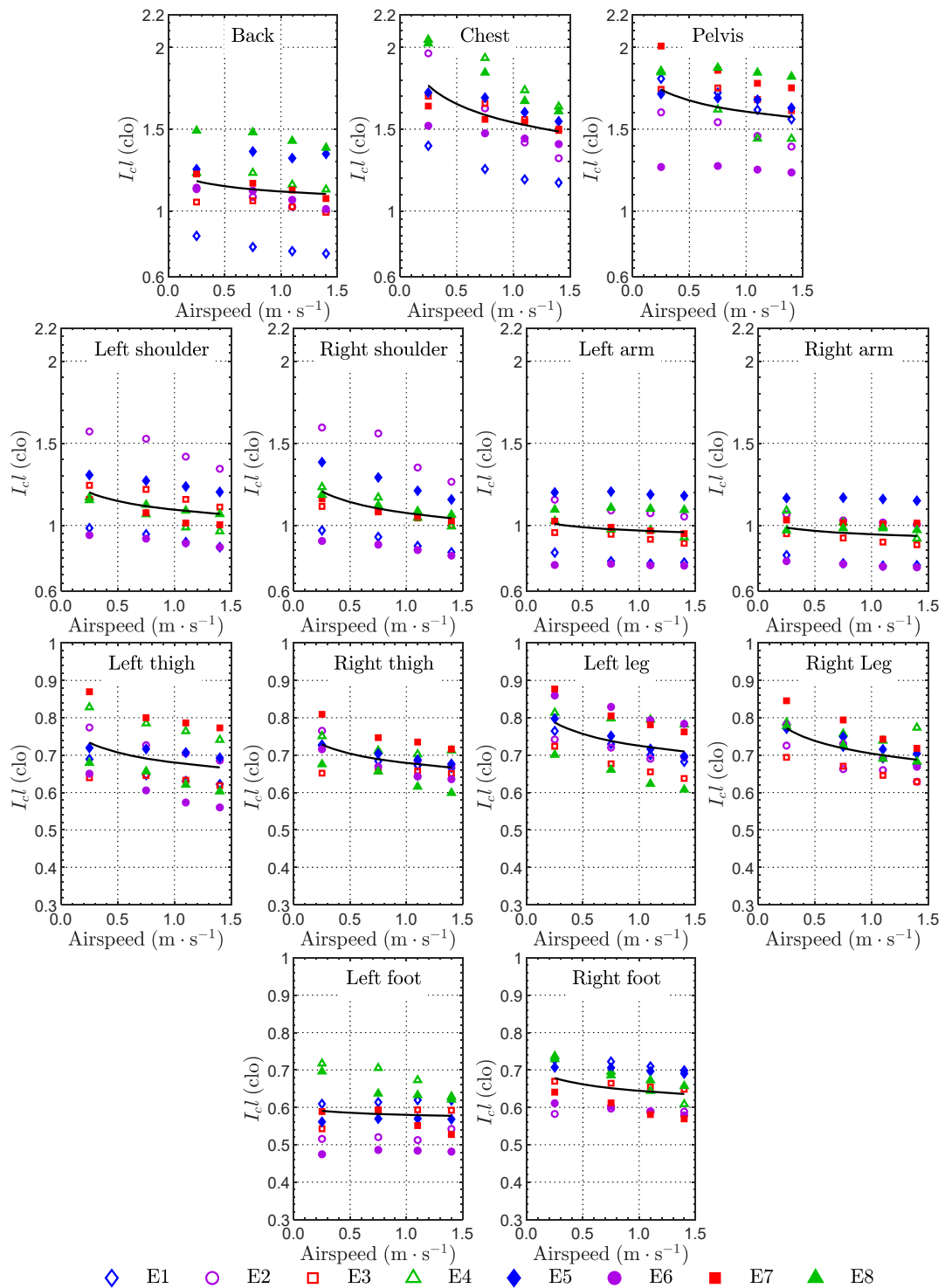


Figure 6-9. The effect of airspeed on local clothing insulation in standing posture (the solid black line represents the regression line of airspeed and the average clothing insulation for various clothing ensembles).

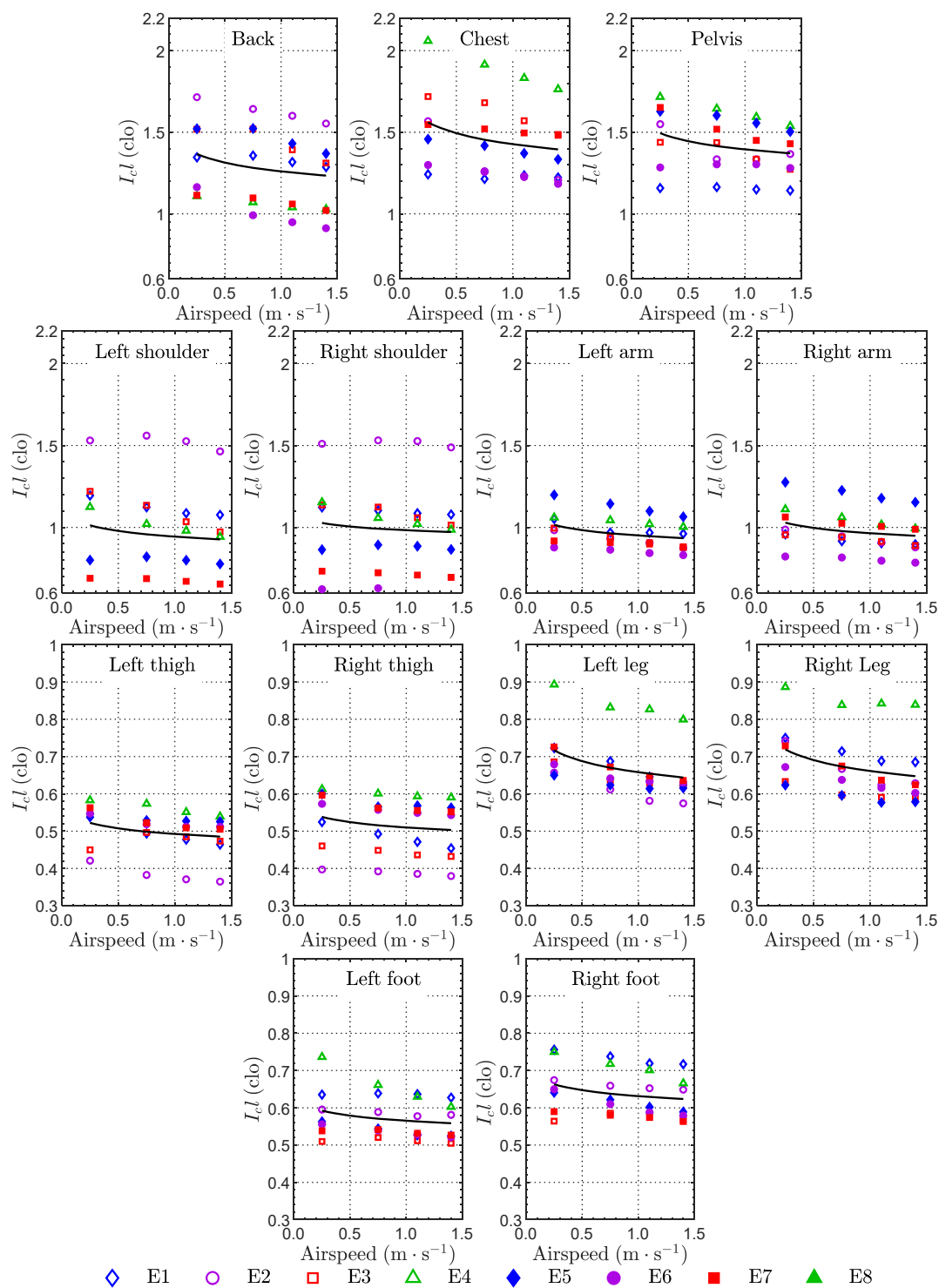


Figure 6-10. The effect of airspeed on local clothing insulation in sitting posture (the solid black line represents the regression line of airspeed and the average clothing insulation for various clothing ensembles).

6.2.2.4 The comparison of various methods of calculating clothing insulation

The clothing insulation calculated by Method A, Method B, Method C, and method D mentioned in Section 2.2 was compared in this section.

① The comparison of Method A and Method B

The comparison of clothing insulation under an airspeed of $0.25 \text{ m}\cdot\text{s}^{-1}$ caused by the upwind calculated with Method A and Method B is listed from Table 6-3 to Table 6-10. The whole-body clothing insulation calculated by the two methods were consistent. However, the difference between clothing insulations for back and legs calculated by Method A and Method B was large (Table 6-10). This result agreed with the opinions of Oguro et al. [18]. They suggested that when there is a large temperature difference between nude and clothed surfaces, the air insulation from the nude manikin I_a should not be used for the clothed manikin. Method B was calculating clothing insulation through subtracting air insulation I_a from total insulation I_t . The temperature difference between nude and clothed surfaces at the back and chest was significant due to the high basic insulation I_{cl} .

Table 6-3. The clothing insulation for Ensemble1 in standing posture under an airspeed of $0.25 \text{ m}\cdot\text{s}^{-1}$ caused by the upwind.

Segments	Method A	Method B
9. Back	0.8	1.24
8 Chest	1.36	1.20
7.Shoulder (L)	0.98	0.94
(R)	0.99	0.89
6.Arm (L)	0.82	0.99
(R)	0.82	0.91
4.Pelvis	2.00	2.01
3.Thigh (L)	0.59	0.62
(R)	0.73	0.68
2.Leg (L)	0.75	0.54
(R)	0.73	0.54
1.Foot (L)	0.60	0.71
(R)	0.75	0.73
Whole-body	0.85	0.84

Method A: clothing insulation calculated by Equation (2-14)

Method B: clothing insulation output by thermal manikin (Equation (2-16))

Table 6-4. The clothing insulation for Ensemble2 in standing posture under an airspeed of $0.25 \text{ m}\cdot\text{s}^{-1}$ caused by the upwind.

Segments	Method A	Method B
9. Back	1.18	1.69
8 Chest	1.92	1.73
7.Shoulder (L)	1.67	1.56
(R)	1.67	1.45
6.Arm (L)	1.24	1.33
(R)	1.02	1.16
4.Pelvis	1.76	2.10
3.Thigh (L)	0.79	0.86
(R)	0.73	0.77
2.Leg (L)	0.86	0.64
(R)	0.80	0.59
1.Foot (L)	0.50	0.73
(R)	0.50	0.63
Whole-body	1.00	1.03

Method A: clothing insulation calculated by Equation (2-14)

Method B: clothing insulation output by thermal manikin (Equation (2-16))

Table 6-5. The clothing insulation for Ensemble3 in standing posture under an airspeed of $0.25 \text{ m}\cdot\text{s}^{-1}$ caused by the upwind.

Segments	Method A	Method B
9. Back	1.09	1.56
8 Chest	1.71	1.47
7.Shoulder (L)	1.40	1.24
(R)	1.07	1.00
6.Arm (L)	0.91	1.06
(R)	0.91	0.95
4.Pelvis	1.98	2.00
3.Thigh (L)	0.59	0.78
(R)	0.69	0.79
2.Leg (L)	0.81	0.62
(R)	0.68	0.57
1.Foot (L)	0.54	0.67
(R)	0.72	0.66
Whole-body	0.91	0.87

Method A: clothing insulation calculated by Equation (2-14)

Method B: clothing insulation output by thermal manikin (Equation (2-16))

Table 6-6. The clothing insulation for Ensemble4 in standing posture under an airspeed of $0.25 \text{ m}\cdot\text{s}^{-1}$ caused by the upwind.

Segments	Method A	Method B
9. Back	1.35	1.71
8 Chest	1.99	1.83
7.Shoulder (L)	0.99	1.07
(R)	1.31	1.13
6.Arm (L)	0.95	1.16
(R)	1.18	1.27
4.Pelvis	2.04	2.29
3.Thigh (L)	0.78	0.80
(R)	0.78	0.87
2.Leg (L)	0.82	0.63
(R)	0.78	0.64
1.Foot (L)	0.64	0.79
(R)	0.67	0.74
Whole-body	1.02	1.04

Method A: clothing insulation calculated by Equation (2-14)

Method B: clothing insulation output by thermal manikin (Equation (2-16))

Table 6-7. The clothing insulation for Ensemble5 in standing posture under an airspeed of $0.25 \text{ m}\cdot\text{s}^{-1}$ caused by the upwind.

Segments	Method A	Method B
9. Back	1.47	2.02
8 Chest	1.76	1.69
7.Shoulder (L)	1.36	1.36
(R)	1.41	1.42
6.Arm (L)	1.27	1.55
(R)	1.22	1.41
4.Pelvis	1.90	2.21
3.Thigh (L)	0.71	0.82
(R)	0.67	0.86
2.Leg (L)	0.85	0.63
(R)	0.77	0.70
1.Foot (L)	0.50	0.72
(R)	0.79	0.72
Whole-body	1.00	1.09

Method A: clothing insulation calculated by Equation (2-14)

Method B: clothing insulation output by thermal manikin (Equation (2-16))

Table 6-8. The clothing insulation for Ensemble6 in standing posture under an airspeed of $0.25 \text{ m}\cdot\text{s}^{-1}$ caused by the upwind.

Segments	Method A	Method B
9. Back	1.13	1.82
8 Chest	1.51	1.36
7.Shoulder (L)	1.01	0.97
(R)	0.89	0.89
6.Arm (L)	0.75	1.01
(R)	0.84	0.93
4.Pelvis	1.36	1.53
3.Thigh (L)	0.62	0.70
(R)	0.75	0.81
2.Leg (L)	0.89	0.67
(R)	0.73	0.65
1.Foot (L)	0.47	0.71
(R)	0.64	0.68
Whole-body	0.87	0.93

Method A: clothing insulation calculated by Equation (2-14)

Method B: clothing insulation output by thermal manikin (Equation (2-16))

Table 6-9. The clothing insulation for Ensemble8 in standing posture under an airspeed of $0.25 \text{ m}\cdot\text{s}^{-1}$ caused by the upwind.

Segments	Method A	Method B
9. Back	1.50	2.20
8 Chest	2.16	1.85
7.Shoulder (L)	1.22	1.15
(R)	1.25	0.97
6.Arm (L)	1.14	1.31
(R)	0.95	1.10
4.Pelvis	2.05	2.15
3.Thigh (L)	0.67	0.73
(R)	0.62	0.73
2.Leg (L)	0.72	0.64
(R)	0.83	0.65
1.Foot (L)	0.67	0.71
(R)	0.73	0.72
Whole-body	0.97	0.99

Method A: clothing insulation calculated by Equation (2-14)

Method B: clothing insulation output by thermal manikin (Equation (2-16))

Table 6-10. The comparison of clothing insulation calculated by Method A and Method B for different clothing ensembles.

	E1	E2	E3	E4	E5	E6	E8	**Average difference②
9. Back	*35%	30%	30%	21%	27%	38%	32%	31%
8 Chest	13%	11%	16%	9%	4%	11%	17%	11%
7.Shoulder	8%	11%	10%	12%	1%	2%	17%	9%
6.Arm	14%	9%	9%	13%	16%	17%	14%	13%
4.Pelvis	0%	16%	1%	11%	14%	11%	4%	8%
3.Thigh	7%	6%	18%	6%	11%	9%	11%	10%
2.Leg	36%	35%	25%	20%	22%	23%	21%	26%
1.Foot	9%	26%	14%	14%	20%	20%	3%	15%
***Average difference①	15%	18%	15%	13%	14%	16%	15%	

$$*|(I_{cl}(\text{Method A}) - I_{cl}(\text{Method B}))/I_{cl}(\text{Method A})|$$

**Average difference①: The average difference of different segments

***Average difference②: The average difference of different clothing ensembles

② The comparison of Method A and Method C

Figure 6-11 shows the clothing insulation for various clothing ensembles according to Method A and Method C (ISO 9920) under different airspeeds. As in ISO 9920, only clothing insulation for the standing posture was provided, results for standing posture were listed in Figure 6-11. The results of Method A were approximately 30% larger than the results based on ISO 9920. For E2 and E3, the results based on Method A and Method C were much more consistent than other clothing ensembles. The E2 consisted of shirts, suit coat, and trousers. The E3 consisted of shirts, sweaters, and trousers. They were both very common types of garments, so it was easy to find the corresponding clothing insulation values in ISO 9920.

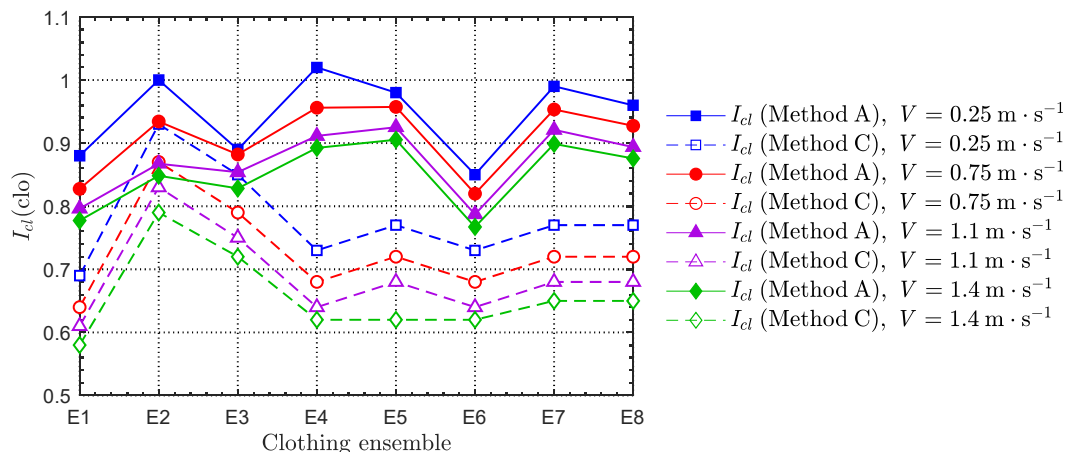


Figure 6-11. Clothing insulation for various clothing ensembles according to Method A and Method C under different airspeeds.

③ The clothing insulation Method D

The clothing insulation defined by Method D, as reported in Section 2.2.4, was 0.96 clo.

6.3 *Conclusions*

In this chapter, both the whole-body clothing insulation and the local clothing insulation of eight sets of clothing ensembles were measured through thermal manikin experiments.

The main conclusions arising from this chapter are as follows:

- (1) The whole-body clothing insulation for the standing posture was larger than that for the sitting posture. Besides, the clothing insulation caused by the crosswind was the highest.
- (2) The reduction rate of basic insulation caused by the wind of various clothing ensembles was different. The reduction rate of basic insulation caused by the crosswind was lower than those of the other wind directions.
- (3) The prediction formula for whole-body clothing insulation considering posture and wind direction was proposed.
- (4) The local clothing insulations for the upper body were larger than those of the lower body. The reduction rates of clothing insulation for the chest, back, and pelvis were higher than other body segments.
- (5) The clothing insulations calculated by Method A and Method B were identical at the whole-body level. The clothing insulations predicted by Method C and Method D were comparable to the experimental data (Method A and Method B) when the type of clothing ensemble was available in the standards (ISO 9920 and ASHRAE Handbook).

This chapter provided local clothing insulation data for kinds of everyday clothing ensembles. The detailed knowledge of local clothing insulation makes the assessment of thermal sensation at different body segments possible. Therefore, the comprehensive information on clothing insulation contributes to the optimal design of heating, ventilating, and air-conditioning (HAVC) systems.

Reference

- [1] I. Holmer, H. Nilsson, G. Havenith, K. Parsons, Clothing convective heat exchange—proposal for improved prediction in standards and models, *The Annals of Occupational Hygiene*. 43 (1999) 329–337. doi:10.1093/annhyg/43.5.329.
- [2] G. Havenith, Clothing Heat Exchange Models for Research and Application, *The 11th International Conference on Environmental Ergonomics*. (2005) 66–73.
- [3] ISO 9920, Ergonomics of the thermal environment — Estimation of thermal insulation and water vapour resistance of a clothing ensemble, (2007).
<https://www.iso.org/standard/39257.html>.
- [4] ISO 7730, Ergonomics of the thermal environment — Analytical determination and interpretation of thermal comfort using calculation of the PMV and PPD indices and local thermal comfort criteria, (2005). <https://www.iso.org/standard/39155.html>.
- [5] ASHRAE Standard 55-2013: Thermal environmental conditions for human occupancy, 2013.
<https://www.ashrae.org/technical-resources/bookstore/standard-55-thermal-environmental-conditions-for-human-occupancy>.
- [6] Chapter 9, in: *ASHRAE Handbook Fundamentals*, 2017: pp. 9.1–9.30.
<https://www.ashrae.org/technical-resources/ashrae-handbook/description-2017-ashrae-handbook-fundamentals>.
- [7] O. Seppanen, Thermal insulating values for typical indoor clothing ensembles, *ASHRAE Trans.* 78 (1972) 120–130.
- [8] B.W. Olesen, R. Nielsen, Thermal insulation of clothing measured on a movable thermal manikin and on human subjects, *ECSC Programme Research*. (1983) 914.
- [9] E.A. McCullough, A comprehensive database for estimating clothing insulation, *ASHRAE Transactions*. 91 (1985) 29–47.
<http://citeseerx.ist.psu.edu/viewdoc/download?doi=10.1.1.258.8876&rep=rep1&type=pdf>.
- [10] D. Bechert, M. Bruse, W. Hage, R. Meyer, D. Bechert, M. Bruse, W. Hage, R. Meyer, Biological surfaces and their technological application - Laboratory and flight experiments on drag reduction and separation control, in: *28th Fluid Dynamics Conference*, American Institute of Aeronautics and Astronautics, Reston, Virginia, 1997: pp. 505–507. doi:10.2514/6.1997-1960.
- [11] Wikipedia, Windbreaker, (n.d.). <https://en.wikipedia.org/wiki/Windbreaker> (accessed January 31, 2020).
- [12] S. Mondal, Phase change materials for smart textiles – An overview, *Applied Thermal Engineering*. 28 (2008) 1536–1550. doi:10.1016/j.applthermaleng.2007.08.009.
- [13] E. Foda, K. Sirén, A new approach using the Pierce two-node model for different body parts, *International Journal of Biometeorology*. 55 (2011) 519–532. doi:10.1007/s00484-010-0375-4.
- [14] S. Tanabe, K. Kobayashi, J. Nakano, Y. Ozeki, M. Konishi, Evaluation of thermal comfort using combined multi-node thermoregulation (65MN) and radiation models and computational

- fluid dynamics (CFD), *Energy and Buildings*. 34 (2002) 637–646. doi:10.1016/S0378-7788(02)00014-2.
- [15] ISO 15831, Clothing — Physiological effects — Measurement of thermal insulation by means of a thermal manikin, (2008). <https://www.iso.org/standard/28720.html>.
- [16] Z. Wang, B. Cao, W. Ji, Y. Zhu, Study on clothing insulation distribution between half-bodies and its effects on thermal comfort in cold environments, *Energy and Buildings*. 211 (2020) 109796. doi:10.1016/j.enbuild.2020.109796.
- [17] M. Oguro, E. Arenz, R. De Dear, H. Zhang, T. Katayama, Evaluation of the effect of air flow on clothing insulation and on dry heat transfer coefficients for each part of the clothed human body, *Journal of Architecture and Planning (Transactions of AIJ)*. 66 (2001) 13–21. doi:10.3130/aija.66.13.
- [18] M. Oguro, E. Arens, R. de Dear, H. Zhang, T. Katayama, Convective heat transfer coefficients and clothing insulation for parts of the clothed human body under airflow conditions, *Journal of Architecture and Planning (Transactions of AIJ)*. 67 (2002) 21–29. doi:10.3130/aija.67.21_5.

Chapter 7.

The effect of clothing on the prediction of thermal comfort

7.1 Introduction

The convective and radiative heat transfer coefficients and the clothing insulation are essential parameters to calculate the thermal comfort indices, such as the (predicted mean vote) PMV index, the (standard effective temperature) SET*, and the (physiological equivalent temperature) PET [1–3].

Concerning the convective heat transfer coefficient for the clothing are estimated through multiplying clothing area factor f_{cl} by the convective heat transfer coefficient for the naked human body. In other words, the clothing convective heat transfer coefficients for different kinds of clothing were considered the same if the clothing insulations are the same. However, with the diversity of garment materials, the heat transfer properties of different garments need to be noted. The results in Chapter 5 have shown that the convective heat transfer coefficients for different clothing may differ significantly, although with similar clothing insulation. Therefore, it is necessary to clarify how the convective heat transfer coefficient affects the prediction of thermal comfort.

Concerning the clothing insulation, it is usually approximated by comparing the studied clothing ensemble with the typical clothing ensembles listed in ISO Standard or ASHRAE Handbook [4,5]. However, the error is significant. For example, the clothing insulation of clothing ensembles in the present study was assumed to 0.96 clo based on the ASHRAE Handbook. While actual measurements were between 0.85 clo to 1.02 clo.

Concerning the radiative heat transfer coefficient, the difference between different clothing ensembles could be neglected as reported in Chapter 5.

The difference between the actual measurements and the estimated value for convective heat transfer coefficient (clothing insulation) emerges a need for investigating how this difference affects the thermal comfort indices.

Therefore, in this chapter, the effect of convective heat transfer coefficient and clothing insulation on the thermal comfort indices (PMV, SET*, and PET) were confirmed by comparing to the results according to the traditional calculation method.

7.2 The effect of clothing on PMV

The PMV model predicts the thermal sensation as a function of activity, clothing, and the four classical thermal environmental parameters: air temperature, mean radiant temperature, air velocity, and humidity [6]. For verification of PMV programs, ISO 7730 provides example output data of PMV at several environmental conditions [1]. Before calculating the actual PMV, the PMV MATLAB code was verified by comparing the example output data of ISO 7730. The results agreed with the example output data of ISO 7730 except the red dot ($M=1.2$ met, $I_{cl}=1.0$ clo, $t_a = t_r = 23.5^\circ\text{C}$, $\text{RH} = 40\%$, $V = 0.1 \text{ m}\cdot\text{s}^{-1}$) as illustrated in Figure 7-1. Therefore, the PMV value for the red dot in Figure 7-1 was verified again by comparing it with the results from the (center for the built environment) CBE thermal comfort tool [7]. The PMV value calculated with the PMV MATLAB

code in this study was identical to that from the CBE thermal comfort tool. So there may be an error in PMV value for the red dots shown in Figure 7-1 provided by ISO 7730.

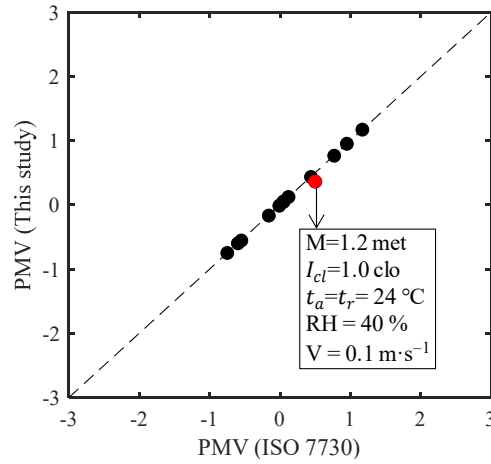


Figure 7-1. The comparison of the PMV values calculates with the PMV MATLAB code in this study and the PMV values from ISO 7730.

7.2.1 The effect of convective heat transfer coefficient and clothing insulation on PMV

When confirming the effect of clothing on the PMV values, the metabolic rate M is assumed to 1.2 met, supposing people are doing office work. The air temperature and mean radiant temperature were both 24 °C. The relative humidity RH was 50%. The airspeeds were $0.25 \text{ m}\cdot\text{s}^{-1}$, $0.75 \text{ m}\cdot\text{s}^{-1}$, $1.1 \text{ m}\cdot\text{s}^{-1}$, and $1.4 \text{ m}\cdot\text{s}^{-1}$. The clothing insulation, convective heat transfer coefficient h_c and radiative heat transfer coefficient h_r are listed in Table 7-1. In Case1, h_c and h_r , were based on ISO 7730, and I_{cl} was based on ISO 9920. In Case2, h_c and h_r , were based on the experimental results of this study, and I_{cl} was from ISO 9920 listed in Figure 6-11 in Section 6.2.2.4. In Case3, h_c , h_r , and I_{cl} were all based on the experimental results of this study.

Table 7-1. Information on input data for PMV program for Case1, Case2, and Case3.

	h_c, h_r	I_{cl}
Case1	ISO 7730	ISO 9920
Case2	the results of this study	ISO 9920
Case3	the results of this study	the results of this study

Figure 7-2 shows the PMV value for various clothing ensembles under different airspeeds in Case1, Case2, and Case3. The first discussion is concerned with standing posture. When comparing the results of Case1 and case2 (i.e., the basic insulation was the same, the convective and radiative heat transfer coefficients were different), there was a difference in the PMV values. This finding indicates that the actual convective heat transfer coefficient for different ensembles should be utilized when calculating the PMV value. When comparing the results of Case2 and Case3 (i.e., the convective and radiative heat transfer coefficients were the same, the basic insulation was different), there was a significant difference in the PMV value except for E2 and E3. This is because the clothing insulation measured in this study (Method A) was larger than the value based on ISO 9920 (Method

C). However, the basic insulations for E2 and E3 measured in this study were well consistent with ISO 9920.

When looking at the results of sitting posture, the difference between Case1 and Case2 was larger than standing posture. This is because the regression model for convective heat transfer coefficient in the PMV program in ISO 7730 is in semi-reclining posture [6]. And it was reported in Chapter 4 that there was a significant difference in the convective heat transfer coefficient between sitting and standing postures. The convective heat transfer coefficient for standing posture was larger than the sitting posture. The unprecise in the convective heat transfer coefficient resulted in a larger difference Case1 and Case2 than the standing posture. This finding indicates that, when calculating the PMV value, the input parameter should match the posture.

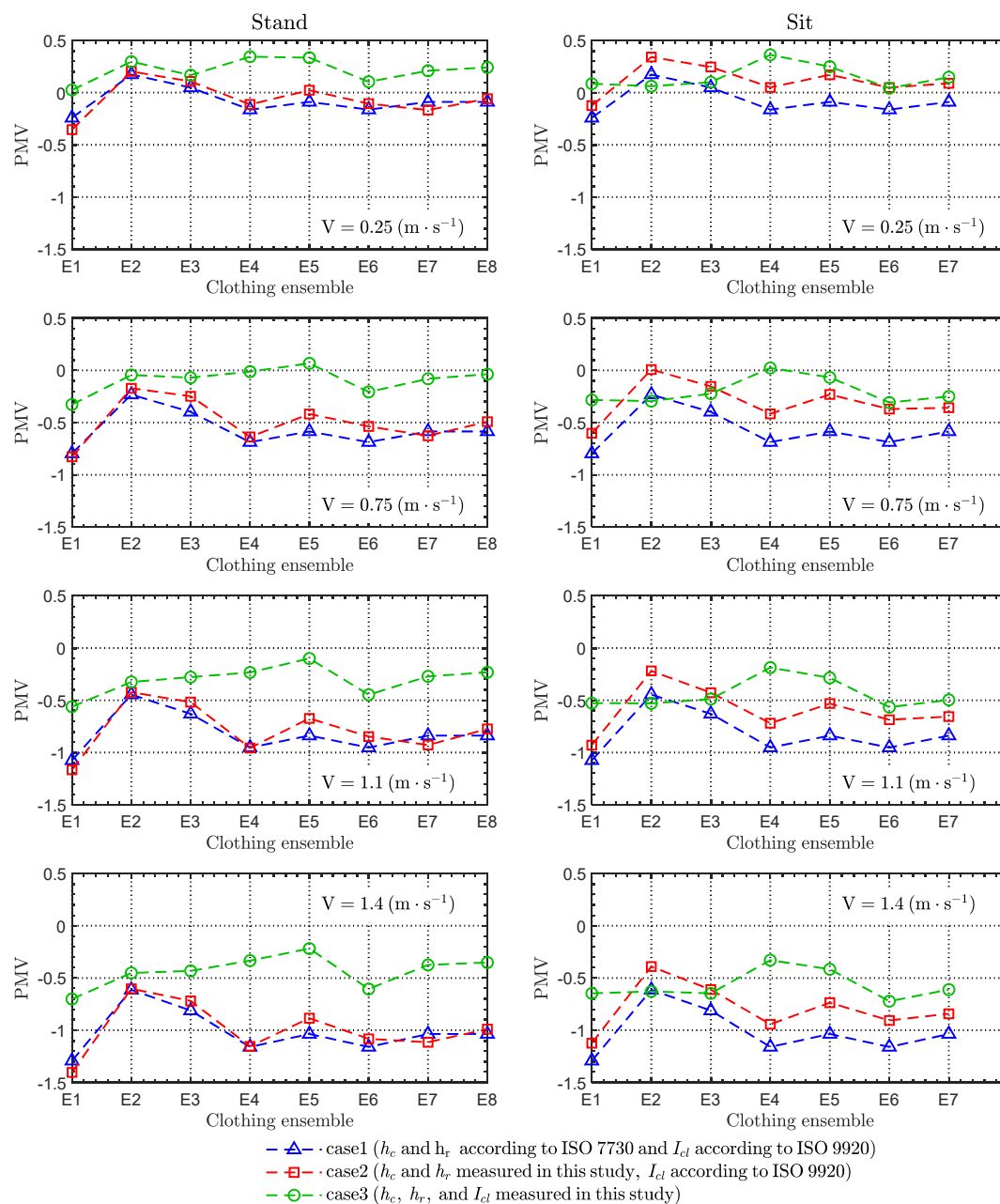


Figure 7-2. PMV for various clothing ensembles under different airspeeds in Case1, Case2, and Case3.

7.2.2 Comparison of PMV values for different clothing ensembles

Figure 7-3 presents the comparison of PMV values for different clothing ensembles under various airspeeds. The input data for the PMV values in Figure 7-3 equaled that in Cases3.

In the standing posture, the PMV value for E5 was the largest. Then was the PMV value for E4. The basic insulation for E5 was not the largest. Hence, the large value of E5 was due to the small value of the convective heat transfer coefficient. The convective heat transfer coefficient for E5 was the smallest in all of the clothing ensembles, so the convective heat loss was the least, which resulted in a higher PMV value. The PMV calculated based on ISO 7730 and ISO 9920 is also shown in Figure 7-3 on the left side. The PMV value based on ISO 7730 and ISO 9920 was larger than all the PMV values based on the h_c , h_r , and I_{cl} of this study. The PMV value based on the results of this study for E1 under the airspeed of $1.4 \text{ m}\cdot\text{s}^{-1}$ was 0.6 smaller than the PMV value based on the results of the ISO standard.

In the sitting posture, the PMV value for E4 was the largest, then was the PMV value for E5. The reason may be that the basic insulation for E4 was larger than other clothing ensembles. The PMV value for E5 was the largest except E4. The reason is the same as the standing posture.

It can also be seen from Figure 7-3 that the PMV values for standing posture were larger than that of sitting posture. This might be due to the higher clothing insulation value for the standing posture. Figure 7-4 shows the PMV value for various clothing ensembles in different wind directions under different airspeeds in Case3. The PMV value caused by the crosswind was the largest. This is because the basic insulation caused by the crosswind was the largest, and the convective heat transfer coefficient caused by the crosswind was the smallest.

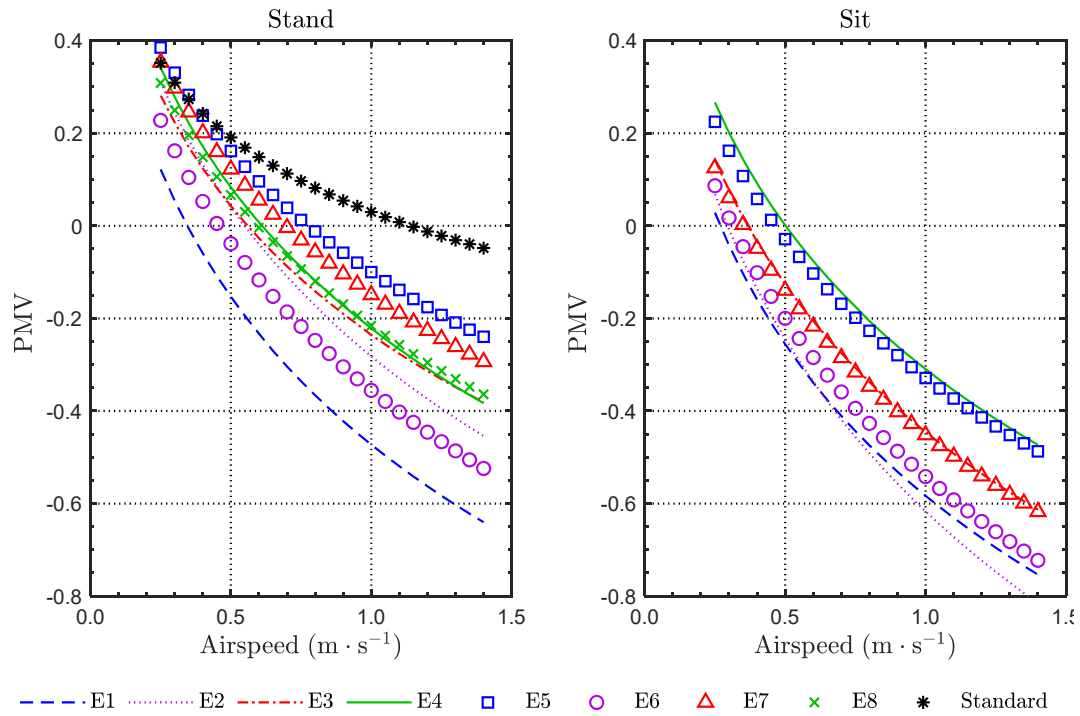


Figure 7-3. PMV for various clothing ensembles under different airspeeds in Case3.

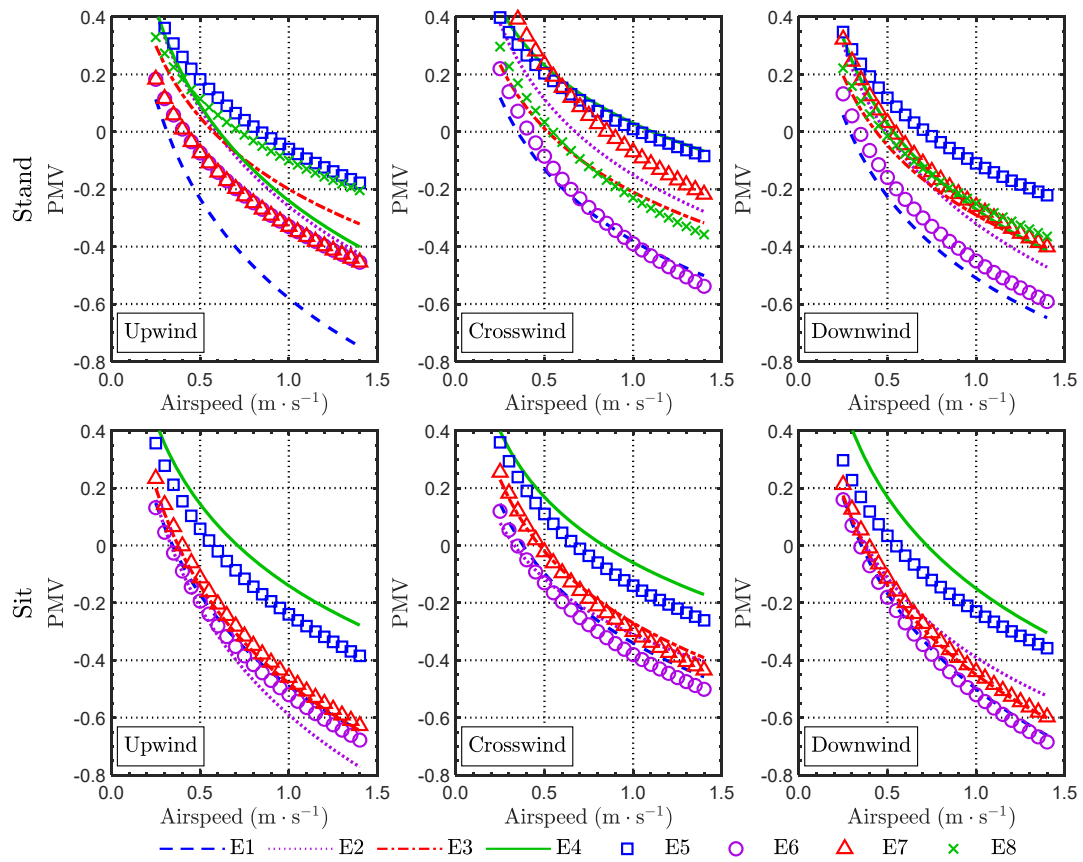


Figure 7-4. PMV for various clothing ensembles in different wind directions under various airspeeds in Case3.

7.3 The effect of clothing on SET^*

7.3.1 The effect of accuracy for clothing insulation on SET^*

Clothing insulation is one of the parameters to calculate SET^* . Usually, the clothing insulation is approximated through referring to the database of clothing insulation, such as the ASHRAE Handbook [5]. As stated in Section 2.2.4, the clothing insulation of clothing ensembles utilized in this research was approximated to 0.96 clo, according to ASHRAE Handbook. The SET^* value calculated with the clothing insulation value of 0.96 clo is shown in red hollow dots in Figure 7-5. In the clothing insulation database, only clothing insulation for the standing posture is provided. Therefore, the SET^* for the sitting posture was approximated the same with standing posture.

The clothing insulation measured with Method A (Section 2.2.1) was in the range of 0.85–1 clo (standing posture) and 0.74–0.95 clo (sitting posture). The range SET^* calculated with the measured clothing insulation is shown in the red area in Figure 7-5.

Other input parameters for the SET^* are summarized in Table 7-2.

Table 7-2. Input variables for SET^* .

Temperature	MRT	Velocity	RH	Met	Clo
24 °C	24 °C	0–1.5 m·s ⁻¹	50%	1.2	0.96 clo or measured value in this study

The maximum difference between the SET^* calculated with clothing insulation usually approximated to 0.96 clo were 1 °C under an airspeed of 0 m·s⁻¹, and 1.4 °C under an airspeed of 1.5 m·s⁻¹ in standing posture. In the sitting posture, the corresponding difference was 1.6 °C and 2.2 °C.

Therefore, it is important to utilize accurate clothing insulation value when calculating SET^* . In the standing posture, the SET^* calculated with the clothing insulation referring to the ASHRAE Handbook (0.96 clo) lies in the range of SET^* calculated with the insulation value measured by Method A. While, in the sitting posture, the SET^* values calculated with $I_{cl} = 0.96$ clo was outside the range of SET^* calculated with the insulation value calculated by Method A. This is because ASHARE Handbook only provides the clothing insulation in standing posture. However, the clothing insulation for sitting posture is 6% to 8% lower than that of the standing posture [4].

The SET^* based on $I_{cl} = 0.96$ clo under an airspeed of 1.5 m·s⁻¹ in standing posture decreased 4 °C compared to that in the calm condition.

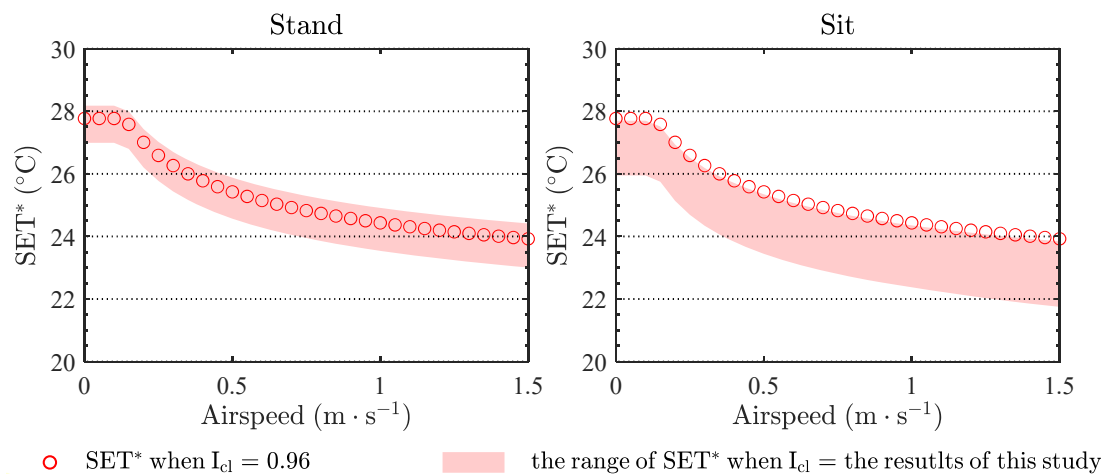


Figure 7-5. The SET^* calculated with clothing insulation based on Method D ($I_{cl} = 0.96$ clo) and Method A (standing posture: 0.85–1 clo, sitting posture: 0.74–0.95 clo).

7.3.2 The effect of reduction of clothing insulation on SET^*

In the calculation of SET^* , the reduction of clothing insulation caused by airspeed is not considered [2,8]. In other words, the clothing insulation at arbitrary airspeed is approximated the same. However, the clothing insulation decreases with airspeed [9]. Figure 7-6 shows the comparison of SET^* considering the reduction of clothing insulation and not based on $I_{cl} = 0.96$. The SET^* under an airspeed of $1.5 \text{ m} \cdot \text{s}^{-1}$ in standing posture decreased 5°C compared to that in the calm condition, larger than the difference when neglecting the reduction of clothing insulation (4°C). Figure 7-7 shows the SET^* considering the reduction of clothing insulation and not based on the measured results of this study in standing and sitting postures.

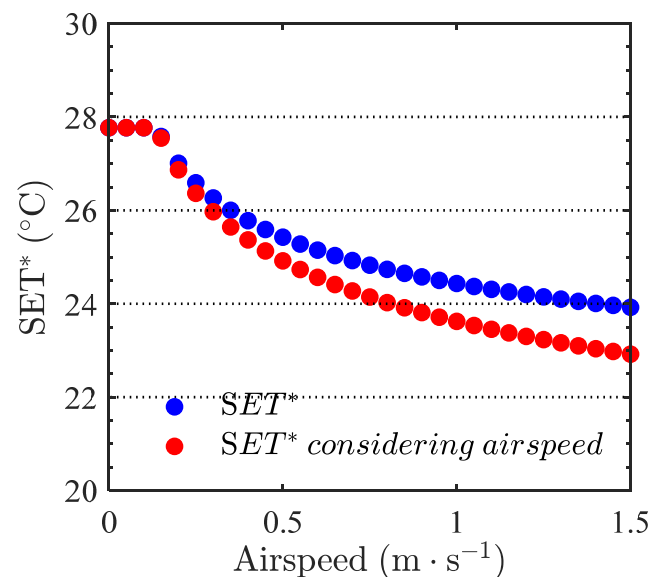


Figure 7-6. The comparison of SET^* considering the reduction of clothing insulation and not based on $I_{cl} = 0.96$.

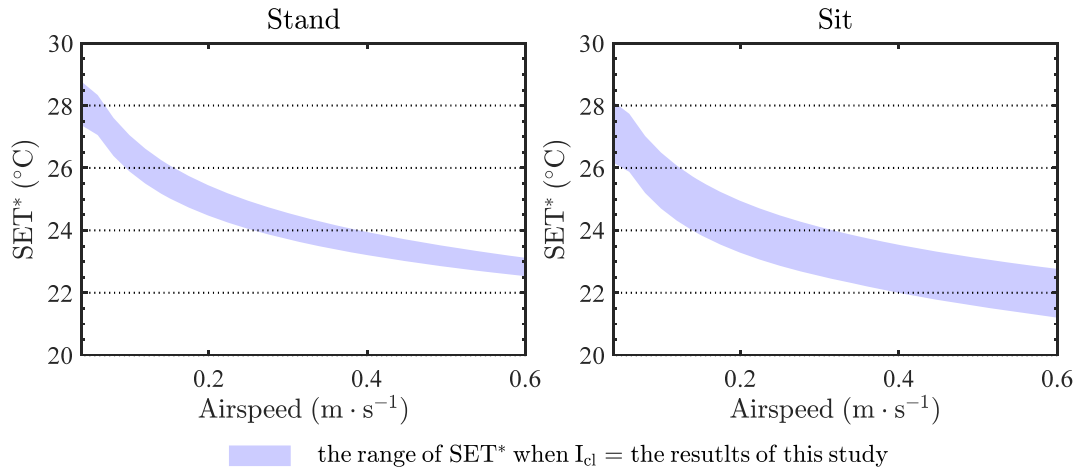


Figure 7-7. The SET^* calculated with measured clothing insulation of this study considering the reduction of clothing insulation caused by airspeed in standing and sitting postures.

As the reduction of clothing insulation caused by airspeed has an effect on the prediction of SET^* . The correction index ΔSET^* is proposed (Figure 7-8 and Table 7-3). ΔSET^* is the difference between SET^* neglecting the reduction of clothing insulation and SET^* considering the reduction of clothing insulation caused by airspeed. Therefore, the correction of SET^* calculated by the traditional method can be corrected by ΔSET^* . Firstly, the SET^* in a calm condition is calculated. Secondly, refer to Figure 7-8 or Table 7-3, and find the corresponding ΔSET^* according to the airspeed and temperature. Lastly, subtract ΔSET^* from the result of the traditional method.

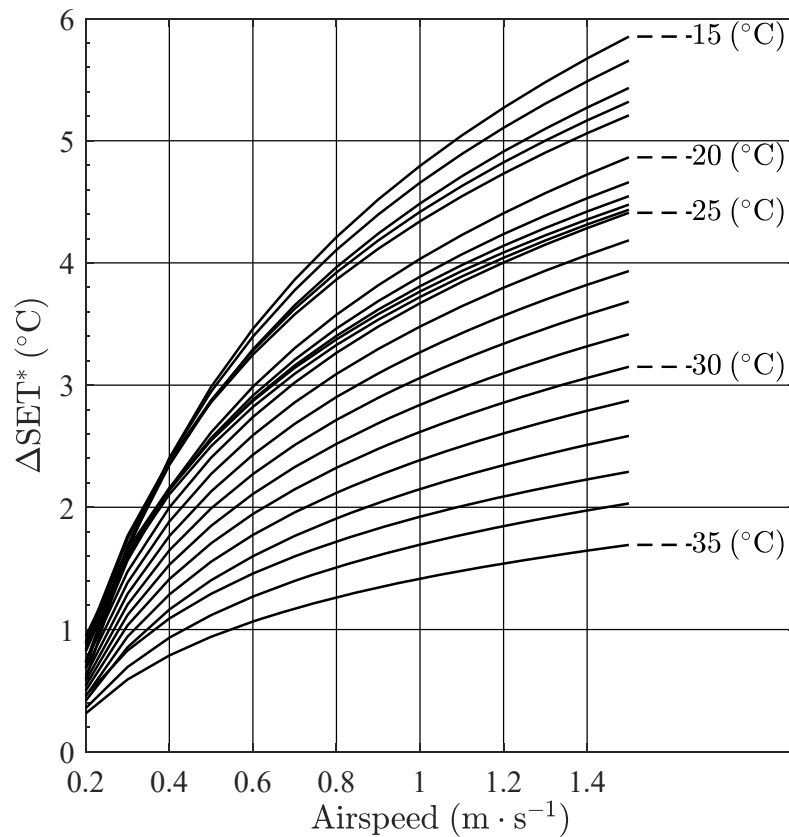


Figure 7-8. The relationship between airspeed and ΔSET^* (ΔSET^* is the difference between SET^* neglecting the reduction of clothing insulation and SET^* considering the reduction of clothing insulation caused by airspeed).

Table 7-3. The regression models for ΔSET^* and airspeed (ΔSET^* is the difference between SET^* neglecting the reduction of clothing insulation and SET^* considering the reduction of clothing insulation caused by airspeed).

$\Delta SET^* = a \ln V + b$ ($^{\circ}\text{C}$)			
$t_a = t_r$ ($^{\circ}\text{C}$)	a	b	R^2
15	2.61	4.79	0.996
16	2.47	4.66	0.995
17	2.34	4.49	0.997
18	2.22	4.42	0.998
19	2.14	4.34	0.999
20	2.05	4.03	1.000
21	1.91	3.89	0.999
22	1.82	3.81	0.999
23	1.75	3.77	0.996
24	1.76	3.72	0.993
25	1.83	3.67	1.000
26	1.74	3.48	1.000
27	1.64	3.27	1.000
28	1.54	3.06	1.000
29	1.43	2.84	1.000
30	1.31	2.62	1.000
31	1.20	2.39	1.000
32	1.08	2.15	1.000
33	0.91	1.92	0.994
34	0.83	1.69	1.000
35	0.68	1.42	0.998

7.4 The effect of clothing on PET

Both the convective heat transfer coefficient and clothing insulation are input parameters for the PET calculation program. The clothing insulation is fixed to 0.9 clo when calculating the PET [10]. Therefore, the effect of convective heat transfer coefficient on the results of PET value was confirmed in this section.

Before the calculation, the (physiological equivalent temperature) PET MATLAB code was verified by comparing the results to those presented by Hoppe [11]. The work metabolism was assumed to 80 W of light activity, added to basic metabolism. The results are listed in Table 7-4.

Figure 7-9 shows the PET values calculated with the convective heat transfer coefficient measured in this study compared to those of Hoppe [7]. Here it can be seen that the results of this study were

smaller than those of Hoppe with 2 °C at an airspeed of 5 m·s⁻¹. Additionally, The different convective heat transfer coefficient for various clothing ensembles caused a 1 °C difference in PET under an airspeed of 5 m·s⁻¹.

Table 7-4. The comparison of the results calculates with the PET calculated with the PET MATLAB code in this study and the PET values from Hoppe.

t_a (°C)	t_{MRT} (°C)	V (m·s ⁻¹)	RH (%)	Work metabolism (W)	Clo (clo)	PET after Hoppe [11] (°C)	PET (this study) (°C)
21	21	0.1	50	80	0.9	21	21
-5	40	0.5	50	80	0.9	10	10
30	60	1.0	50	80	0.9	43	43

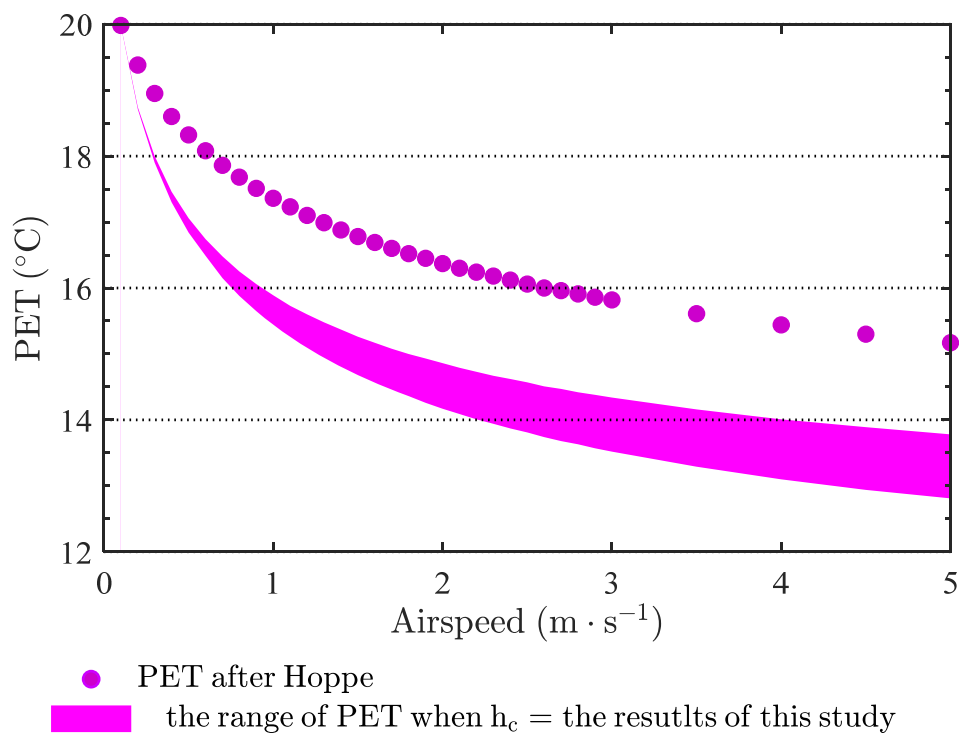


Figure 7-9. The PET value calculated with the convective heat transfer coefficient in this study compared to the results of Hoppe [11] ($t_a = 20^\circ\text{C}$, $t_{MRT} = 20^\circ\text{C}$, $V = 0.1\text{--}5\text{ m}\cdot\text{s}^{-1}$, RH = 50 %, Work metabolism = 80 W, Clo = 0.9 clo).

7.5 *Conclusions*

In this chapter, the effect of clothing insulation and convective heat transfer coefficient on the results of PMV, SET*, and PET was confirmed.

The main conclusions arising from this chapter are as follows:

PMV:

- (1) Both the clothing insulation and the convective heat transfer coefficient affects the results of PMV value.
- (2) The PMV value based on the estimated clothing insulation (0.96 clo) presented a large gap with the PMV value based on the experimental results of clothing insulation.
- (3) The different convective heat transfer coefficient for various clothing ensembles caused a difference in the PMV value.

SET*:

- (4) The maximum difference between the SET* of different clothing ensembles with clothing insulation estimated to 0.96 clo was 1.4 °C.
- (5) The correction index ΔSET^* is proposed. ΔSET^* is the difference between SET* neglecting the reduction of clothing insulation and SET* considering the reduction of clothing insulation caused by airspeed.

PET:

- (6) The different convective heat transfer coefficient for various clothing ensembles caused a maximum difference of 1 °C in PET under an airspeed of 5 m·s⁻¹.

PMV, SET*, and PET are widely accepted as models to predict thermal comfort. Improvements to these models have never stopped. The modification of clothing insulation and clothing convective heat transfer coefficient in these models was executed in this chapter, leading to more accurate predictions of thermal comfort.

Reference

- [1] ISO 7730, Ergonomics of the thermal environment — Analytical determination and interpretation of thermal comfort using calculation of the PMV and PPD indices and local thermal comfort criteria, (2005). <https://www.iso.org/standard/39155.html>.
- [2] A.P. Gagge, A standard predictive index of human response to the thermal environment, ASHRAE Trans. 92 (1986) 709–731. https://www.aivc.org/sites/default/files/airbase_2522.pdf.
- [3] H. Mayer, P. Höppe, Thermal comfort of man in different urban environments, Theoretical and Applied Climatology. 38 (1987) 43–49. doi:10.1007/BF00866252.
- [4] ISO 9920, Ergonomics of the thermal environment — Estimation of thermal insulation and water vapour resistance of a clothing ensemble, (2007). <https://www.iso.org/standard/39257.html>.
- [5] Chapter 9, in: ASHRAE Handbook Fundamentals, 2017: pp. 9.1-9.30. <https://www.ashrae.org/technical-resources/ashrae-handbook/description-2017-ashrae-handbook-fundamentals>.
- [6] P.O. Fanger, Thermal comfort: analysis and applications in environmental engineering, Copenhagen: Danish Technical Press, 1970.
- [7] Tyler Hoyt, Stefano Schiavon, Federico Tartarini, Toby Cheung, Kyle Steinfeld, Alberto Piccioli, and Dustin Moon, CBE Thermal Comfort Tool. Center for the Built Environment, University of California Berkeley, (2019). <https://comfort.cbe.berkeley.edu/> (accessed April 22, 2020).
- [8] ASHRAE Standard 55-2013: Thermal environmental conditions for human occupancy, 2013. <https://www.ashrae.org/technical-resources/bookstore/standard-55-thermal-environmental-conditions-for-human-occupancy>.
- [9] G. Havenith, Clothing heat exchange models for research and Application, The 11th International Conference on Environmental Ergonomics. (2005) 66–73. https://repository.lboro.ac.uk/articles/Clothing_heat_exchange_models_for_research_and_application/9338195.
- [10] E. Walther, Q. Goestchel, The P.E.T. comfort index: Questioning the model, Building and Environment. 137 (2018) 1–10. doi:10.1016/j.buildenv.2018.03.054.
- [11] P. Hoppe, The physiological equivalent temperature - a universal index for the biometeorological assessment of the thermal environment., International Journal of Biometeorology. 43 (1999) 71–75.

Chapter 8.

Conclusions and future studies

8.1 *Conclusions*

In the present research, the heat transfer coefficients and clothing insulation for the human body were discussed. The main achievements are illustrated in Figure 8-1.

Chapter 4 considered the heat transfer coefficients for the naked manikin. As the investigation about convective heat transfer coefficients caused by the vertical airflow was little, the effect of vertical airflow and horizontal airflow on convective heat transfer coefficients were compared. Also, the prediction equations of convective heat transfer coefficients caused by different airspeeds in various wind directions were proposed. Since there not very much data is available on the radiative heat transfer coefficient for different body segments, numerical calculation was conducted to present detailed distribution of radiative heat transfer coefficient on the surface of the thermal manikin in various postures. Furthermore, prediction models for convective heat transfer coefficients considering both environmental temperature and airspeed were proposed making the evaluation of convective heat transfer coefficient under various environmental conditions possible.

Chapter 5 considered the heat transfer coefficients for the clothed manikin. Because there have been few reports about the heat transfer coefficients for the clothed manikin, the convective and radiative heat transfer coefficients for eight sets of clothing ensembles were measured with the thermal manikin. Experimental results indicated that the convective heat transfer coefficients varied with clothing ensembles. While the differences between radiative heat transfer coefficients for various clothing ensembles were negligible. Additionally, the effect of wind direction and airspeed on the clothing convective heat transfer coefficients were confirmed. However, the measurement of convective heat transfer coefficient through experiments was a laborious work, and the thermal manikin is not a very universally available instrument. Therefore, the correction factors for the clothing convective heat transfer coefficient based on CFD analysis were presented.

Chapter 6 considered the clothing insulation. Whole-body clothing insulation and local clothing insulation for eight sets of typical clothing ensembles nowadays were reported. Besides, the calculating procedure for clothing insulation considering posture, wind direction, and airspeed was suggested.

Chapter 7 considered the effect of clothing on the prediction of thermal comfort. To confirm whether the convective heat transfer coefficient and clothing insulation affect the prediction of thermal comfort, the convective heat transfer coefficient and clothing insulation directly measured were introduced to the PMV, SET*, and PET calculation program. The results indicated that the PMV and PET varied with clothing ensembles, although the clothing insulations were almost identical. Moreover, the correction factor ΔSET^* considering the reduction of clothing insulation due to airspeed was proposed.

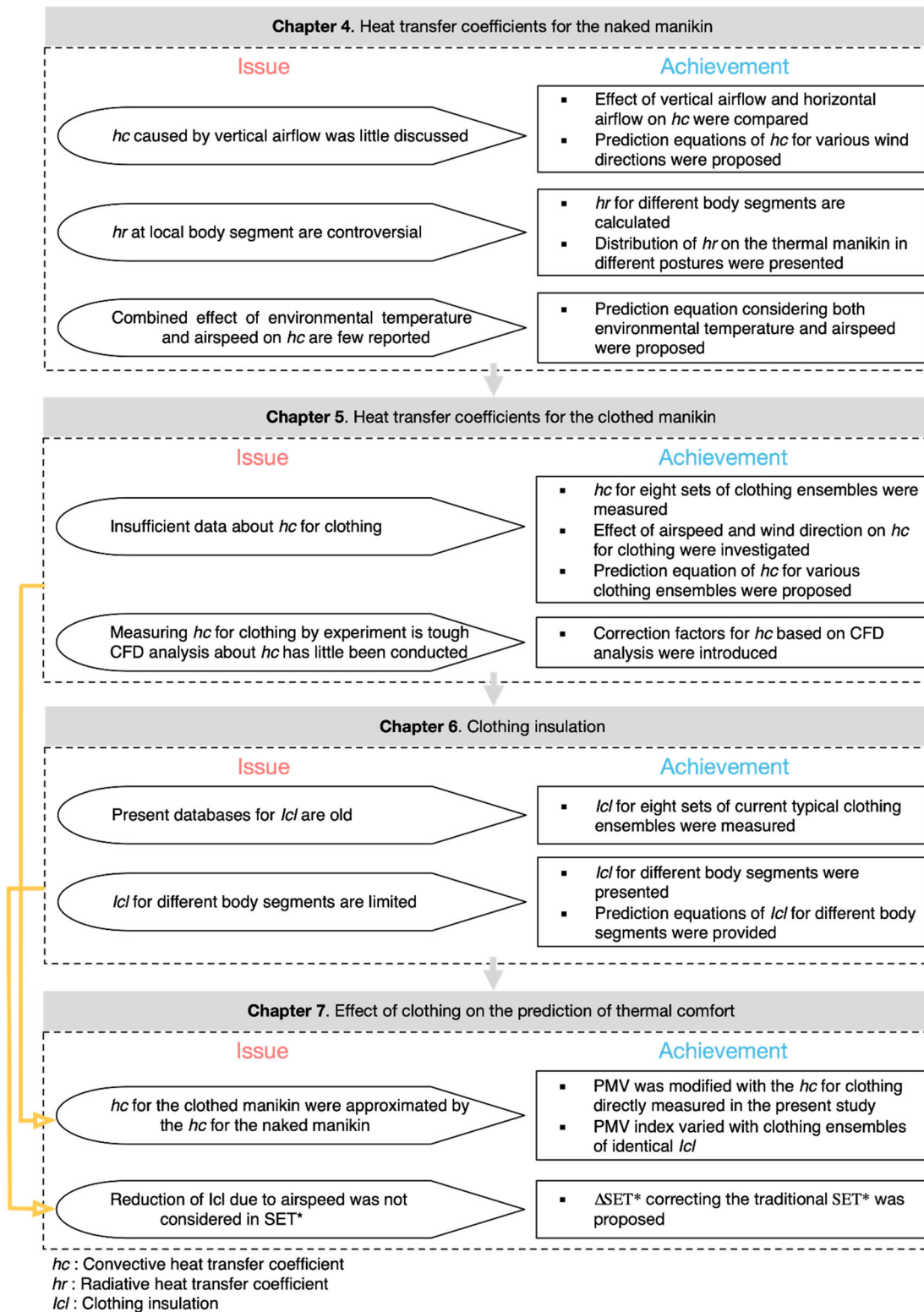


Figure 8-1. Main results of this thesis.

8.2 *Future studies*

The previous section summarized the main results obtained so far through the present study. The following points remain a challenge.

- (1) In the CFD analysis of the clothing convective heat transfer coefficient, the thermal manikin was considered as a whole part. In the future, CFD analysis considering different segments of the thermal manikin needs to be conducted. And the correction factor for different body segments should be presented.
- (2) Although the effects of clothing on several thermal comfort indices were confirmed in Chapter 7, they are all indices for the whole-body. Applying the heat transfer coefficients and clothing insulation for different body segments measured in the present study into the multi-node thermoregulation model remains to be performed.

Appendix

Appendix A. Convective and radiative heat transfer coefficients for the clothed manikin.

Table B-1. Regression models of the convective heat transfer coefficient caused by the upwind for the clothed manikin in standing and sitting postures.

$h_c = aV^b \text{ (W}\cdot\text{m}^{-2}\cdot\text{K}^{-1}\text{)}$						
Ensemble code	Upwind					
	Stand			Sit		
	a	b	R ²	a	b	R ²
E1	13.58	0.68	0.997	11.12	0.54	0.998
E2	12.49	0.66	0.995	11.10	0.65	0.998
E3	10.86	0.65	0.988	10.51	0.71	0.996
E4	12.90	0.71	0.994	10.17	0.62	0.998
E5	9.62	0.59	0.991	9.36	0.71	0.991
E6	10.26	0.61	0.992	9.73	0.66	0.983
E7	14.22	0.52	0.995	10.76	0.63	0.998
E8	11.23	0.60	0.992	—	—	—

Table B-2. Regression models of the convective heat transfer coefficient caused by the crosswind for the clothed manikin in standing and sitting postures.

$h_c = aV^b \text{ (W}\cdot\text{m}^{-2}\cdot\text{K}^{-1}\text{)}$						
Ensemble code	Crosswind					
	Stand			Sit		
	a	b	R ²	a	b	R ²
E1	13.58	0.68	0.997	11.30	0.48	0.986
E2	12.49	0.66	0.995	9.08	0.48	0.986
E3	10.86	0.65	0.988	8.90	0.51	0.988
E4	12.90	0.71	0.994	9.33	0.58	0.995
E5	9.62	0.59	0.991	8.52	0.58	0.995
E6	10.26	0.61	0.992	8.83	0.52	0.989
E7	14.22	0.52	0.995	9.44	0.58	0.995
E8	11.23	0.60	0.992	—	—	—

Table B-3. Regression models of the convective heat transfer coefficient caused by the downwind for the clothed manikin in standing and sitting postures.

$h_c = aV^b \text{ (W}\cdot\text{m}^{-2}\cdot\text{K}^{-1}\text{)}$						
Ensemble code	Downwind					
	Stand			Sit		
	a	b	R ²	a	b	R ²
E1	13.47	0.52	0.976	11.40	0.59	0.993
E2	12.98	0.65	0.995	9.53	0.53	0.970
E3	11.08	0.62	0.987	10.15	0.62	0.997
E4	12.62	0.63	0.995	9.91	0.68	0.993
E5	10.65	0.58	0.997	9.38	0.61	0.990
E6	11.14	0.60	0.994	10.24	0.64	0.994
E7	14.83	0.66	0.997	10.05	0.61	0.989
E8	11.80	0.54	0.996	—	—	—

Table B-4. Regression models of the convective heat transfer coefficient (average value for different wind directions) for the clothed manikin in standing and sitting postures.

$h_c = aV^b \text{ (W}\cdot\text{m}^{-2}\cdot\text{K}^{-1}\text{)}$						
Ensemble code	Average					
	Stand			Sit		
	a	b	R ²	a	b	R ²
E1	12.29	0.55	0.991	11.28	0.52	0.993
E2	11.74	0.61	0.992	9.70	0.54	0.991
E3	10.28	0.59	0.988	9.62	0.59	0.994
E4	11.35	0.59	0.999	9.69	0.61	0.996
E5	10.11	0.59	0.997	8.05	0.62	0.992
E6	10.51	0.61	0.993	9.41	0.59	0.989
E7	13.01	0.54	0.993	9.92	6.60	0.996
E8	11.34	0.60	0.994	—	—	—

Table B-5. Regression models of the convective heat transfer coefficient at each segment (average for different clothing ensembles) of the clothed manikin caused by upwind in standing and sitting postures.

$h_c = aV^b$ ($\text{W}\cdot\text{m}^{-2}\cdot\text{K}^{-1}$)						
Segment	Upwind					
	Stand			Sit		
	a	b	R ²	a	b	R ²
10. Head	11.69	0.58	0.999	10.48	0.62	0.999
9. Back	4.21	0.76	1.000	3.56	0.72	0.987
8. Chest	15.42	0.83	0.997	11.27	0.90	0.993
7. Shoulder (R)	10.48	0.64	0.996	9.02	0.58	0.996
(L)	10.55	0.69	0.994	7.51	0.62	0.998
6. Arm (R)	12.01	0.60	0.998	12.94	0.56	0.996
(L)	11.37	0.53	0.998	11.74	0.65	0.995
5. Pelvis	11.09	0.91	0.998	11.58	0.75	0.997
4. Hand (R)	8.98	0.69	0.996	8.12	0.49	0.987
(L)	7.89	0.63	0.996	7.46	0.45	0.986
3. Thigh (R)	12.12	0.60	0.988	9.45	0.59	0.996
(L)	10.97	0.53	0.991	10.48	0.62	0.999
2. Leg (R)	17.83	0.49	0.990	15.20	0.66	0.989
(L)	19.44	0.43	0.989	15.72	0.58	0.996
1. Foot (R)	13.54	0.56	0.991	11.89	0.45	0.988
(L)	11.24	0.60	0.988	11.03	0.51	0.975
Whole-body	11.91	0.62	0.996	10.40	0.64	0.996

Table B-6. Regression models of the convective heat transfer coefficient at each segment (average for different clothing ensembles) of the clothed manikin caused by crosswind in standing and sitting postures.

$h_c = aV^b$ ($\text{W}\cdot\text{m}^{-2}\cdot\text{K}^{-1}$)						
Segment	Crosswind					
	Stand			Sit		
	a	b	R ²	a	b	R ²
10. Head	11.46	0.67	0.998	9.33	0.62	0.999
9. Back	9.78	0.79	0.982	10.17	0.92	0.993
8. Chest	5.51	0.40	0.969	3.98	0.78	0.996
7. Shoulder (R)	10.19	0.55	0.998	8.41	0.56	0.995
(L)	10.40	0.51	0.987	9.26	0.60	0.996
6. Arm (R)	12.81	0.60	0.994	13.14	0.50	0.992
(L)	13.68	0.54	0.994	13.19	0.56	0.991
5. Pelvis	13.74	0.94	0.997	13.65	0.86	0.994
4. Hand (R)	7.67	0.62	0.997	7.66	0.52	0.973
(L)	8.01	0.64	0.998	6.71	0.52	0.984
3. Thigh (R)	11.20	0.52	0.991	7.43	0.45	0.978
(L)	10.99	0.53	0.996	7.77	0.45	0.988
2. Leg (R)	25.74	0.56	0.987	16.81	0.60	0.993
(L)	22.72	0.55	0.991	14.98	0.52	0.997
1. Foot (R)	12.55	0.42	0.979	13.35	0.46	0.975
(L)	10.39	0.44	0.982	11.39	0.44	0.990
Whole-body	12.32	0.60	0.994	10.10	0.61	0.992

Table B-7. Regression models of the convective heat transfer coefficient at each segment (average for different clothing ensembles) of the clothed manikin caused by downwind in standing and sitting postures.

$h_c = aV^b$ ($\text{W}\cdot\text{m}^{-2}\cdot\text{K}^{-1}$)						
Segment	Downwind					
	Stand			Sit		
	a	b	R ²	a	b	R ²
10. Head	9.54	0.46	1	9.47	0.45	1
9. Back	5.80	0.82	0.999	6.15	0.80	0.999
8. Chest	7.81	0.73	0.999	7.65	0.71	0.997
7. Shoulder (R)	11.58	0.66	0.997	11.31	0.66	0.998
(L)	6.27	0.50	0.998	6.01	0.48	0.998
6. Arm (R)	12.22	0.59	0.989	12.11	0.57	0.984
(L)	7.54	0.49	0.975	7.33	0.52	0.980
5. Pelvis	6.27	0.64	0.992	6.35	0.64	0.988
4. Hand (R)	10.12	0.70	0.999	9.74	0.69	0.999
(L)	5.00	0.57	0.977	5.17	0.57	0.981
3. Thigh (R)	14.67	0.60	0.989	14.83	0.61	0.990
(L)	8.63	0.47	0.960	8.68	0.44	0.955
2. Leg (R)	27.20	0.54	0.999	24.75	0.49	1
(L)	16.63	0.34	0.950	17.53	0.34	0.947
1. Foot (R)	11.12	0.40	0.975	11.32	0.40	0.975
(L)	7.63	0.30	0.949	7.56	0.33	0.971
Whole-body	10.54	0.55	0.994	10.45	0.54	0.994

Table B-8. Regression models of the average convective heat transfer coefficient at each segment (average for different clothing ensembles) of the clothed manikin caused different wind directions in standing and sitting postures.

$h_c = aV^b$ ($\text{W}\cdot\text{m}^{-2}\cdot\text{K}^{-1}$)						
Segment	Average					
	Stand			Sit		
	a	b	R ²	a	b	R ²
10. Head	6.40	0.80	0.998	6.42	0.83	0.999
9. Back	6.40	0.80	0.998	6.42	0.83	0.999
8. Chest	9.16	0.72	0.999	7.02	0.84	0.985
7. Shoulder (R)	9.63	0.59	0.999	8.55	0.57	0.995
(L)	9.71	0.60	0.996	8.39	0.59	0.996
6. Arm (R)	11.15	0.58	0.993	12.83	0.54	0.991
(L)	11.20	0.54	0.993	12.54	0.58	0.993
5. Pelvis	9.36	0.82	0.995	10.58	0.66	0.986
4. Hand (R)	7.94	0.65	0.997	8.61	0.48	0.993
(L)	7.75	0.64	0.997	8.75	0.54	0.993
3. Thigh (R)	11.66	0.56	0.986	8.75	0.53	0.993
(L)	11.32	0.54	0.988	9.10	0.54	0.995
2. Leg (R)	21.87	0.50	0.993	14.95	0.54	0.994
(L)	21.51	0.48	0.992	14.62	0.50	0.996
1. Foot (R)	11.22	0.43	0.980	11.83	0.43	0.980
(L)	10.11	0.44	0.978	11.13	0.44	0.981
Whole-body	11.33	0.58	0.994	9.80	0.58	0.993

Table B-9. Average radiative heat transfer coefficients for different clothing ensembles

Segment	Radiative heat transfer coefficients ($\text{W}\cdot\text{m}^{-2}\cdot\text{K}^{-1}$)
10. Head	5.52
9. Back	5.13
8. Chest	5.01
7. Shoulder (R)	4.86
(L)	4.86
6. Arm (R)	4.68
(L)	4.68
5. Pelvis	5.13
4. Hand (R)	4.57
(L)	4.57
3. Thigh (R)	4.82
(L)	4.82
2. Leg (R)	5.29
(L)	5.29
1. Foot (R)	5.40
(L)	5.41
Whole-body	5.06

Appendix B. MaTLaB code for PMV considering difference in convective heat transfer coefficients for various clothing ensembles.

```

function [answer] = Func_PMV_hc_icl(Met,CLO,Ta, Tmrt, RH, v,W,A,B)
% Met=Metabolic rate, 1Met=58.15W/m2
% CLO=Clothing insulation [clo]
% Ta=Air temperature[centigrade]
% Tmrt=Mean radiant temperature[centigrade]
% RH=relative humidity
% v=airspeed[m/s]
% W=External work,normally around 0
% A,B=Constant for the regressionmodel of convective heat transfer
% coefficient(HC=Av^B)
HR=5;
Tolerance=0.00015;      % Accuracy definition
M=Met*58.15;
pa=RH*10*exp(16.6536-4030.183/(Ta+235)); %Water vapour pressure[Pa]
ICL=CLO*0.155;%Thermal insulation of clothing[m2K/W]
% Calculate surface temperature of clothing TCL
%% First guess for the clothing surface temperature
TAA=Ta+273;
TRA=Tmrt+273;
TCLA=TAA+(35.3-Ta)/(3.5*(ICL+0.1));
XN=TCLA/100; %TCLA=TCL+273
XF=XN;

%% Calculate clothing suafce temperature by iterations
P1=ICL;
P2=P1*3.96;
P3=P1*100;
P4=P1*TAA;
P5=308.7-0.028*(M-W)+P2*(TRA/100)^4;
nIterations=0;
XF=XN;

while((nIterations<150))
    XF=(XF+XN)/2;

```

Appendix

```
%% HC Calculation
HCF=A*v.^B;
HCN=2.38*abs(100*XF-TAA)^0.25;
if(HCF>HCN)
    HC=HCF;      % Convective Heat Transfer Coefficient
else
    HC=HCN;
end

XN=(P5+P4*HC-P2*XF^4)/(100+P3*HC);
nIterations=nIterations+1;
if ((nIterations>1) & (abs(XN-XF)<Tolerance))
    break;
end
end
if(nIterations<150)
    TCL=100*XN-273;    % Surface Temperature of Clothing
    %% Calculate the predicted mean vote (PMV)
    %%HL1 and HL2 are both heat loss from the skin, HL1 is from
    evaporation of
    %moisture diffused through the skin, HL2 is from sweat evaporation
    HL1=3.05*0.001*(5733-6.99*(M-W)-pa);
    HL2=0;
    if(M-W>58.15)
        HL2=0.42*(M-W-58.15);
    end
    %HL3 is latent reapiation heat loss (evaporation)
    HL3=1.7*0.0001*M*(5867-pa);
    %HL4 is dry reapiation heat loss (convection)
    HL4=0.0014*M*(34-Ta);
    %HL5 is heat loss by radiation
    HL5=HR*(TCL-Tmrt);
    %HL6 is heat loss by convection
    HL6=HC*(TCL-Ta);
    % TS is thermal sensation trans coeff
    TS=0.303*exp(-0.036*M)+0.028;
    PMV=TS*(M-W-HL1-HL2-HL3-HL4-HL5-HL6);
    % Calculate the predicted percentage dissatisfied (PPD)
```

```
PPD=100-95*exp(-0.03353*PMV^4-0.2179*PMV^2);  
else  
    PMV1=999;  
    PPD=100;  
end  
answer = PMV;  
HC;  
end
```


Publications

Peer-reviewed journals

- 1) Shan Gao, Ryoza Ooka, Wonseok Oh, Formulation of human body heat transfer coefficient under various ambient temperature, air speed and direction based on experiments and CFD, *Building and Environment*. 160 (2019) 106168. doi:10.1016/j.buildenv.2019.106168.
- 2) Shan Gao, Ryoza Ooka, Wonseok Oh, Experimental analysis of convective and radiative heat transfer coefficients for various clothing ensembles, *Building and Environment* (Under review)

Non-peer-reviewed journals

- 1) Shan Gao, Ryoza Ooka, Wonseok Oh, Qianwen Guo, Study of wall temperature effects on micro-climate around human body with coupled analysis of convection and radiation, *SEISAN KENKYU*, 71 (2019), 35–39

Conference proceeding papers (International)

- 1) Shan Gao, Ryoza Ooka, Wonseok Oh, Effects of ambient temperature, airspeed, and wind direction on heat transfer coefficient for the human body by means of manikin experiments and CFD analysis, *CLIMA 2019, Bucharest (Romania), 2019.5, E3S Web of Conferences*. 111 (2019) 02041. doi:10.1051/e3sconf/201911102041.
- 2) Shan Gao, Ryoza Ooka, Wonseok Oh, Effects of ambient temperature, airspeed, and wind direction on heat transfer coefficient for the human body by means of manikin experiments and CFD analysis (Poster presentation), *Sustainable Built Environment Conference 2019 in Tokyo, Tokyo (Japan), 2019.8*.
- 3) Shan Gao, Ryoza Ooka, Wonseok Oh, Measurement of the convective and radiative heat transfer coefficient for the clothed human body through thermal manikin experiment, *Windsor Conference 2020: Resilient Comfort, Windsor (UK), 2020.4*

Conference proceeding papers (Domestic)

- 1) Shan Gao, Ryoza Ooka, Wonseok Oh, Qianwen Guo, Study of non-uniform wall temperature effects on micro-climate around human body with coupled analysis of convection and radiation (Part1): Cases description and study of skin surface temperature (in Japanese), in: *Proceedings of AIJ Annual Conference at Tohoku University, 2018*: pp. 433–434.
- 2) Qianwen Guo, Ryoza Ooka, Wonseok Oh, Shan Gao, Study of non-uniform wall temperature effects on micro-climate around human body with coupled analysis of convection and radiation (Part2): Study of heat transfer coefficient and heat loss (in Japanese), in: *Proceedings of AIJ annual conference at Tohoku University, 2018*: pp. 435–436.
- 3) Shan Gao, Ryoza Ooka, Wonseok Oh, Hideaki. Nagano, Study on the convective heat transfer coefficients under calm environment with different ambient temperature by using thermal

- manikin (in Japanese), Technical Papers of Annual Meeting, the Society of Heating, Air-Conditioning and Sanitary Engineers of Japan at Daido University, 2018: pp 361–364.
- 4) Shan Gao, Ryoza Ooka, Wonseok Oh, Study on the evaluation of thermal environment around the human body using thermal manikin: Effects of airspeed and wind direction on convective heat transfer coefficient for human body (in Japanese) , in: Proceedings of AIJ annual conference at Kanazawa Institute of Technology, 2019: pp. 527–528.
 - 5) Shan Gao, Ryoza Ooka, Wonseok Oh, Evaluation of the thermal environment around the human body using a thermal manikin: The effect of air speed and direction on convective heat transfer coefficient for the clothing human body (in Japanese), in: Technical papers of annual meeting, the Society of Heating, Air-Conditioning and Sanitary Engineers of Japan at Hokkaido University of Science, 2019: pp. 49–52.
 - 6) Shan Gao, Ryoza Ooka, Wonseok Oh, Evaluation of the thermal environment around the human body using a thermal manikin: Proposal of prediction formula for convective heat transfer coefficient of human body considering environmental temperature and wind speed (in Japanese), in: Proceedings of AIJ annual conference at Chiba University, 2020 (submitted).
 - 7) Yunchen Bu, Ryoza Ooka, Wonseok Oh, Effects of plants on indoor environment and human physiology, psychology and productivity: CFD simulation for distribution of humidity ratio and human perception in a room with plants (in Japanese), in: Proceedings of AIJ annual conference at Chiba University, 2020 (submitted).
 - 8) Shan Gao, Ryoza Ooka, Wonseok Oh, Evaluation of the thermal environment around the human body using a thermal manikin: The effect of the difference in the heat transfer coefficients of clothing on thermal comfort (in Japanese), in: Technical papers of annual meeting, the Society of Heating, Air-Conditioning and Sanitary Engineers of Japan, 2020 (submitted).

Acknowledgments

After sending the four seasons of the campus four times and spending countless morning and night in the laboratory, finally, I finished my Ph.D. thesis. I would like to express my sincere gratitude to people who have supported me a lot here.

Firstly, I would like to thank my supervisor Prof. Ooka Ryozi, he trained and supported me with his insightful questions and immense knowledge during my whole Ph.D. study. His careful consideration of my research topic and strict requirements laid a solid foundation for my future academic research. In addition to that, I really thank him for giving me time and space to grow up. I also would like to thank Prof. Shinsuke Kato. I have been impressed with his in-depth knowledge and insight. Even though he has been retired for two years, I still can't forget his booming voice when he was in a meeting or on the phone.

A debt of gratitude also owed to my subadvisor, Assoc. Prof. Hideki Kikumoto. His research field is a little far from mine, so he was always able to give me advice from the point of view that I never thought about. I will never forget that he helped me test the temperature control function of the wind tunnel and made much effort to make my experiment go smoothly.

I extend my deepest appreciation to my advising committee members, Prof. Shinichi Sakamoto, Assoc. Prof. Junta Nakano, and Assoc. Prof. Masayuki Mae for giving their precious time. They provided excellent comments and suggestions from different perspectives enabling me to improve my research.

I am grateful to thank Dr. Wonjun Choi. I will never forget he provided me with his help on using MATLAB to solve the heat transfer problem. I was impressed by his enthusiasm and knowledge of his research.

My sincere thanks also go to Prof. Arsen Krikor Melokov. He listened to my research report and gave a lot of pertinent suggestions. Also, his comments on my first journal paper helped me a lot.

I wish to thank Prof. Rijal Hom Bahadur. I have made several presentations in front of him, and he has given me beneficial suggestions. I learned a lot from him.

I owe a deep sense of gratitude to Dr. Wonseok Oh. He helped me build the foundation of my knowledge about thermal comfort. He set up all the experimental equipment when I carried out my first experiment. I also learned from him about troubleshooting and academic writing. He provided many useful insights to improve my research.

I am grateful to Dr. Mengtao Han, for his help and guidance in the last four years. His advice both on my research and life helped me a lot. He climbed to the roof of the wind tunnel for many times to help me to fasten the thermal manikin. I will remember forever.

I am also grateful to Mr. Christopher O' Malley, for providing a helping hand to revise my English paper.

I wish to thank members for our study group on CFD, Dr. Mengtao Han, Mr. Mingzhe Liu, Mr.

Acknowledgments

Honyuan Jia, Mr. Chao Lin, and Ms. Hong Hu. I enjoyed the discussion with them.

I am grateful to Mr. Qi Zhou, Mr. Bingchao Zhang, and Mr. Ke Wen. I cannot accomplish the experiments without their help.

I would especially like to thank Ms. Doyun Lee, Ms. Qianwen Guo, and Ms. Yunchen Bu. We talked to each other about our research and life so many times. Thank you very much for your words and encouragement.

I want to say thanks to Mr. Noto Uchida, Mr. Chaoyi Hu, Ms. Shuyuan Hu, Mr. Ken Takahashi, Ms. Mayuka Nakai, Ms. Sorana Ozaki, Mr. Toshiki Nakamura, Mr. Eki Sakamoto, and Mr. Rongmao Li. It is because of the excellent laboratory atmosphere you have provided that I was able to accomplish this thesis.

And many thanks to the seniors in the laboratory who have already graduated. They provided extensive support for this research.

I would like to express my appreciation to Ms. Ono Seika, Ms. Takeuchi, Ms. Dei, Ms. Izumi Nobuko, and Ms. Homma Ruiko for their extensive support for not only my research activities but also my daily life.

Thanks are also extended to the Japanese government scholarship program. It provided me an opportunity to go abroad for further study and make communications with people holding different world views.

Very special appreciation goes to Prof. Xiaoming Zhang, who was my supervisor on my undergraduate course. His encouragement brings me to here.

Last but not least, I would like to thank my family for supporting me, spiritually and financially.

June 2020

Shan Gao